Defining the early cellular response to mitochondrial stress: implications for Parkinson's

Thomas Anthony Ryan

Submitted in accordance with the requirements for the degree of
Doctor of Philosophy

The University of Leeds
Leeds Institute of Biomedical and Clinical Sciences

July 2016

The candidate confirms that the work submitted is his own and that appropriate credit has been given where reference has been made to the work of others.

ACKNOWLEDGEMENTS

I would like to thank my supervisors in Leeds, Dr Ewan Morrison, Dr Sandra Bell and Dr Jacquelyn Bond, and my supervisor in York, Dr Sean Sweeney, for giving me the opportunity to study for my PhD at the University of Leeds and for their endless support over the past few years. I would also like to say a huge thank you to the members the Level 8 labs in the Wellcome Trust Brenner Building. There are too many to mention who have helped me out. I've met some of the best people I know and made so many great friends during my time here. Thank you for all of your help.

I greatly appreciate the funding from the White Rose Scholarship for my PhD studies. I have been lucky enough to gain great insight into exciting new neurodegenerative research through meetings with The White Rose Parkinson's Consortium.

Finally, I'd like to say thank you to all of my friends and family. I greatly appreciate so many of my friends sticking with me through thick and thin. A special thank you must go to my parents, Gary and Anne, and my brother, Liam. They have had to put up with my stresses and moans for far too long and they were always there to support me when I felt like banging my head against a brick wall. This PhD is as much yours as it is mine, so thanks for believing I could do it!

ABSTRACT

Parkinson's disease (PD) is characterised by loss of dopaminergic neurons within the substantia nigra pars compacta. Mitochondrial dysfunction and oxidative stress are pathological characteristics of PD. It is not fully understood how neurons respond to these stresses, though adaptive responses involving the activity of PD-associated proteins such as Parkin may play a critical role. When these adaptive responses are overcome neurons are lost through apoptotic mechanisms aimed at minimising further tissue damage.

AP-1 transcription factors are encoded by immediate early genes (IEGs) such as *FOS* and *JUN*. They regulate early cellular responses to stress. Mitogen-associated protein kinases (MAPKs), such as JNK and ERK, regulate AP-1 function. Previous studies have implicated MAPK/AP-1 signalling in the progression of PD. The aim of this thesis was to elucidate whether the AP-1 system was involved in the response to mitochondrial stress in neurons and to dissect the signalling pathways by which this was regulated.

SH-SY5Y neuroblastoma cells were used as a model system. CCCP-induced mitochondrial uncoupling induced oxidative stress in this cell line. In response to this AP-1 levels were modulated at both the mRNA and protein levels. SH-SY5Y differentiation or Parkin overexpression altered AP-1 protein response profiles. Treatment with c-Jun siRNA lead to an increase in cell death induced by lower levels of mitochondrial coupling, but a decrease under higher levels of uncoupling. Additionally, a novel link between Parkin and the AP-1 response was observed and investigated.

Further work indicated that both JNK and ERK could regulate c-Jun function. Critically, this was dependent on both cell differentiation and the level of stress. Notably, JNK signalling was the primary promoter of apoptosis in response to high levels of mitochondrial stress in differentiated cells.

This study suggests that the JNK/c-Jun pathway is differentially regulated by the level of mitochondrial stress, contributing to both adaptive and apoptotic

responses and thereby playing a central role in deciding neuronal fate. It further suggests that enhancing adaptive cytoprotective pathways represent a better approach than inhibiting apoptotic pathways when developing therapeutics for the neurodegenerative progression observed in PD.

CONTENTS

LIST OF FIGURES

LIST OF TABLES

ABBREVIATIONS

6-OHDA	6-hydroxydopamine
AD	Alzheimer's disease
ALS	Amyotrophic lateral sclerosis
AMBRA1	Beclin-1-regulated autophagy 1
AP-1	Activating protein 1
AR-JP	Autosomal-recessive juvenile Parkinson's disease
ASK1	Apoptosis signal-regulating kinase
ATF	Activating transcription factor
ATG	Autophagy-related gene
ATP	Adenosine triphosphate
BDNF	Brain-derived neurotrophic factor
BSE	Bovine spongiform encephalopathy
cAMP	Cyclic adenosine monophosphate
CCCP	Carbonyl cyanide m-chlorophenyl hydrazone
CJD	Creautzfeldt-Jakob disease
CNS	Central nervous system
COMT	Catechol-)-methyltransferase
CRE	cAMP responsive element
DARPP-32	Dopamine and cAMP-regulated phosphoprotein 32kDa
DAT	Dopamine transporter
DBD	DNA binding domain
DBS	Deep brain stimulation
DRP1	Dynamin-related protein 1
DUB	Deubiquitinating enzyme
DUSP	Dual specificity phosphatase
EOPD	Early-onset Parkinson's disease
ER	Endoplasmic reticulum
ERK	Extracellular regulated kinase
FIS1	Mitochondrial fission 1 protein

FTD	Frontotemporal dementia
GPCR	G-protein coupled receptor
GWAS	Genome-wide association study
HD	Huntington's disease
H_2O_2	Hydrogen peroxide
HECT	Homologous to the E6AP carboxyl terminus
HTT	Huntingtin
IBR	In-between-RING
IEG	Immediate early gene
IF	Immunofluorescence
JDP	Jun dimerisation protein
JIP	JNK interacting protein
JNK	c-Jun N-terminal kinase
KHC	Kinesin heavy chain
LC3	Light chain 3
LIR	LC3-interacting region
LRRK2	Leucine-rich repeat kinase 2
MAPK	Mitogen-associated protein kinase
MAPKK	MAPK kinase
MAPKKK	MAPK kinase kinase
MEF	Mouse embryonic fibroblast
MFN	Mitofusin
MLK	Mixed-lineage kinase
MND	Motor neurone disease
MOM	Mitochondrial outer membrane
MPP^+	1-methyl-4-phenyl-pyridium ion
MPTP	1-methyl-4-phenyl-1,2,3,6-tetrahydropyridine
mt-KR	Mitochondrial KillerRed
mTOR	Mammalian target of rapamycin
NAC	*N*-actetylcysteine
NES	Nuclear export signal
NGF	Nerve growth factor

NLK	Nemo-like kinase
NLS	Nuclear localisation signal
PBS	Phosphate buffered saline
PD	Parkinson's disease
PERK	Protein kinase-like ER kinase
PINK1	PTEN-induced putative kinase 1
PKA	Protein kinase A
PLF	Primary ling fibroblast
PPN	Pedunculopontine nucleus
RA	Retinoic acid
RING	Really interesting new gene
RIPA	Radioimmunoprecipitation assay buffer
ROS	Reactive oxygen species
RSK	Ribsomal S6 kinase
SDS-PAGE	Sodium dodecyl sulphate-polyacrylamide gel electrophoresis
SD	Standard deviation
SEM	Standard error of the mean
SNpc	Substantia nigra pars compacta
SRE	Serum response element
STN	Subthalamic nucleus
TAD	Transactivation domain
TNF	Tumour necrosis factor
TPA	12-*O*-tetradecanoylphorbol-13-acetate
TRE	TPA responsive element
Ub	Ubiquitin
UBC	Ubiquitin conjugating enzyme
UBL	Ubiquitin-like domain
UCHL1	Ubiquitin C-terminal hydrolase isozyme L1
UPR	Unfolded protein response
UPS	Ubiquitin-proteasome system
VDAC1	Voltage-dependent anion channel 1
WT	Wild-type

CHAPTER 1
INTRODUCTION

1.1 NEURODEGENERATION

Neurodegenerative diseases are complex, multifactorial debilitating conditions affecting millions worldwide. The wide range of these diseases, such as Alzheimer's disease (AD), Parkinson's disease (PD), Huntington's disease (HD), motor neurone disease (MND), prion diseases (e.g. Creutztfeldt-Jakob disease (CJD)) and amyotrophic lateral sclerosis (ALS), demonstrate both distinct and common characteristics. These neurodegenerative disorders pose a major socioeconomic burden, one that is set to greatly increase with an ever-ageing population. With an estimated cost of €798 billion in Europe for 2010 alone (Gustavsson et al., 2011), these diseases have the potential to become unmanageable or even cripple worldwide economies with effective treatments remaining elusive. In the UK there are an estimated 45 million cases of brain disorders, costing around €134 billion per annum, although this includes disorders such as, headaches, sleep disorders, brain tumours, addiction and anxiety as well as typical neurodegenerative diseases. The cost of treating PD alone is over €2 billion (Fineberg et al., 2013).

Over the past few decades, there has been a huge investment into research to understand the enigmatic basis of neurodegeneration. It has become apparent that novel and successful therapies are likely to be borne of a greater knowledge of the molecular and cellular mechanisms underlying the death of post-mitotic neurons. Despite varying characteristics between these diseases, they also share some common features such as protein misfolding (Selkoe, 2004) and mitochondrial dysfunction (Streck et al., 2013, Itoh et al., 2013). By determining the causative mechanisms of conditions such as AD and PD it may be possible to determine new therapeutic targets or create practical screens to assess high-risk individuals in the general population.

The identification of pathogenic genetic mutations in patients with inherited forms of these diseases has been key to our increased knowledge of the mechanisms underlying the neurodegenerative process. The most common neurodegenerative disease is AD, accounting for around 70% of dementia cases (Ott et al., 1995). Although most cases of AD are sporadic, the identification of mutations in genes causing familial early-onset forms of the

disease have allowed the elucidation of pathways central to the condition (Bertram and Tanzi, 2008). The identification of genetic mutations in the amyloid precursor protein (APP) leading to plaques in the brains of familial AD patients (Levy et al., 1990, Van Broeckhoven et al., 1990) allowed the generation of the 'amyloid cascade hypothesis' (Hardy and Allsop, 1991, Hardy and Higgins, 1992). Pathogenic processing of APP leads to the accumulation of plaques largely made up of Aβ oligomers, which is part of the cascade resulting in the AD phenotype, although there has been some debate on the validity of this hypothesis (Hardy, 2009, Karran and Hardy, 2014). Nevertheless, the focus of research directed by this hypothesis has allowed the identification of genes, pathways and cellular events involved in AD pathogenicity (Bertram and Tanzi, 2008, Selkoe, 2004, Hardy, 2009).

Unlike AD, HD is a purely genetic condition that has autosomal dominant inheritance, making it different to other neurodegenerative diseases such as PD and ALS, which are largely sporadic. HD is caused by the expansion of a polyglutamine region (CAG triplet repeat) in the Huntingtin (HTT) protein, generating a mutant form of this protein, mutant HTT (mHTT) (HD Collaborative Group, 1993), which leads to intracellular accumulation of mHTT aggregates. HD prevalence is far lower than that of AD or PD, with around 4-10 cases per 100,000 people (Ross and Tabrizi, 2011). Despite differences between these diseases, they are all often classed as protein misfolding diseases along with other conditions such as prion diseases like Creutzfeldt-Jakob disease, which is caused by transmissible infectious prion protein particles from bovine spongiform encephalopathy (BSE) (Selkoe, 2004, Lin and Beal, 2006, Reynaud, 2010). Similarities can allow for research on one disease to be applicable to others (Figure 1.1). A comparison of several genome-wide association studies (GWAS) identified shared genetic pathways between AD, PD and ALS (Shang et al., 2015), highlighting how knowledge of one disorder is likely to be transferable. It is likely that future clinical advances, whether it is in terms of predictive screenings, preventative treatments or even cures, will be driven by our knowledge of the molecular and cellular basis of these conditions, making understanding these mechanisms of paramount importance.

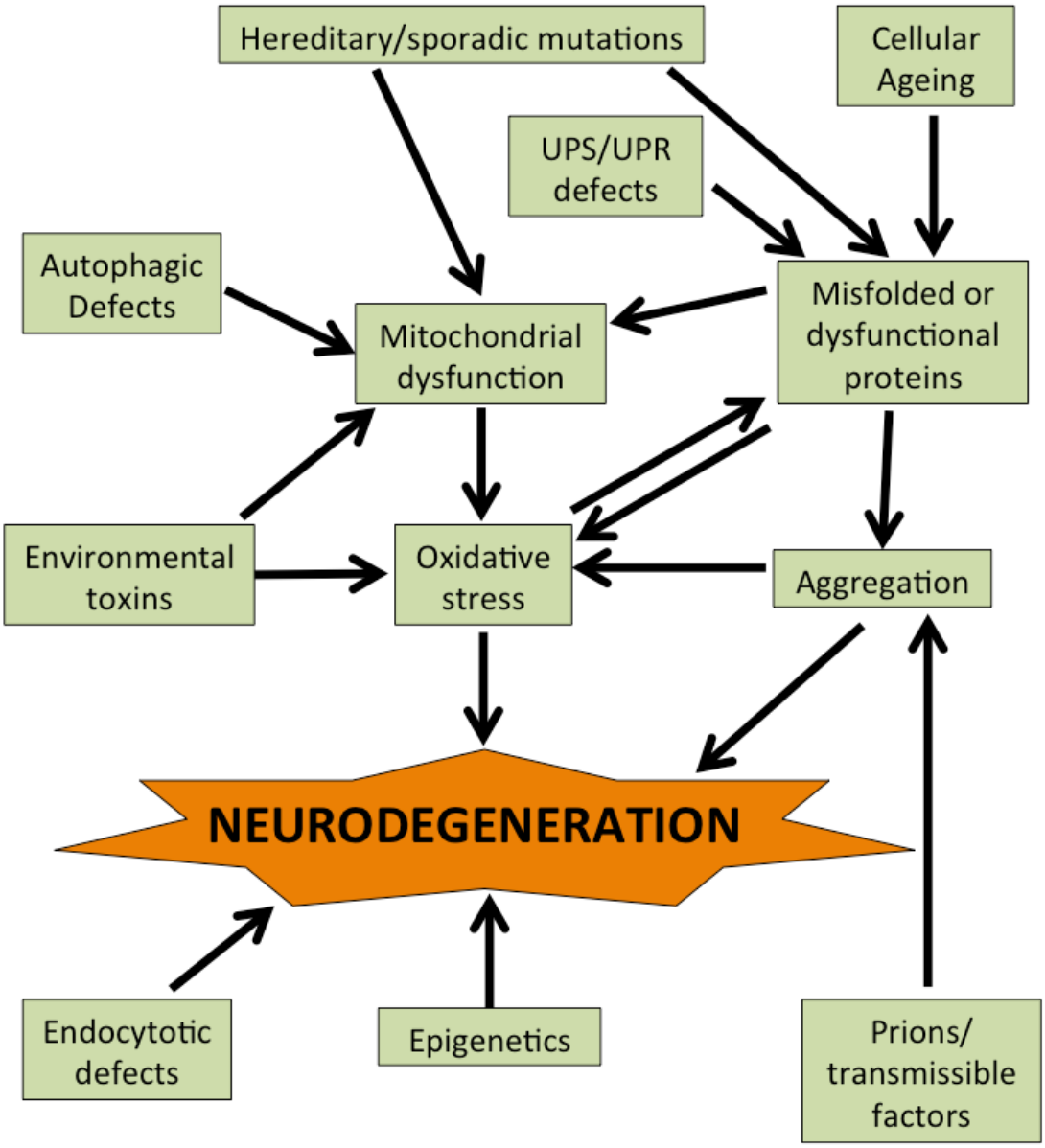

Figure 1.1: Cellular pathways to neurodegeneration. Oxidative stress is central to many of these pathways. Both acute and chronic perturbation or dysregulation of these processes can lead to synaptic dysfunction and neuronal cell death.

1.2 PARKINSON'S DISEASE

Parkinson's is a neurodegenerative disorder characterised by the loss of dopaminergic neurons in the substantia nigra pars compacta (SNpc) of the midbrain. As the second most common neurodegenerative disease, it represents a major socioeconomic burden on ever ageing populations throughout the world. The precise molecular mechanisms behind the disease's pathology are not currently fully understood. However, oxidative stress and

mechanisms such as autophagy/mitophagy and apoptosis are strongly suspected to play a role.

PD was first described in 1817 with a detailed analysis of the characteristic resting tremor, rigidity and bradykinesia (slow movement) of this malady being given (Parkinson, 1817). PD can be considered, like many other diseases, an individual condition, with different patients experiencing differing symptoms and pathologies. There are a wide range of other physical complications that can be associated with PD such as bladder and bowel problems, eye problems, pain (e.g. muscle cramps and headaches) and sleep problems amongst others. Furthermore, a patient's mental health can also be affected, with cases of anxiety, dementia, hallucinations, memory problems and depression also being reported (www.parkinsons.org.uk).

1.2.1 PD Pathology

PD is a condition in which dopaminergic neurons within the SNpc die. The primary role of these cells, which comprise about 3-5% of the substantia nigra, is to synthesise dopamine (Figure 1.2). These neurons play a significant role in a wide and varied range of processes such as movement and drug addiction. Selective nigral cell loss leads to the development of Parkinsonism, although the mechanisms driving this are not understood (Chinta and Andersen, 2005). The age-related loss of these neurons is evident in humans, with the number of dopaminergic cells within the midbrain being around 590,000 in the fourth decade of life but dropping to about 350,000 by the sixth decade (Bogerts et al., 1983, German and Manaye, 1993).

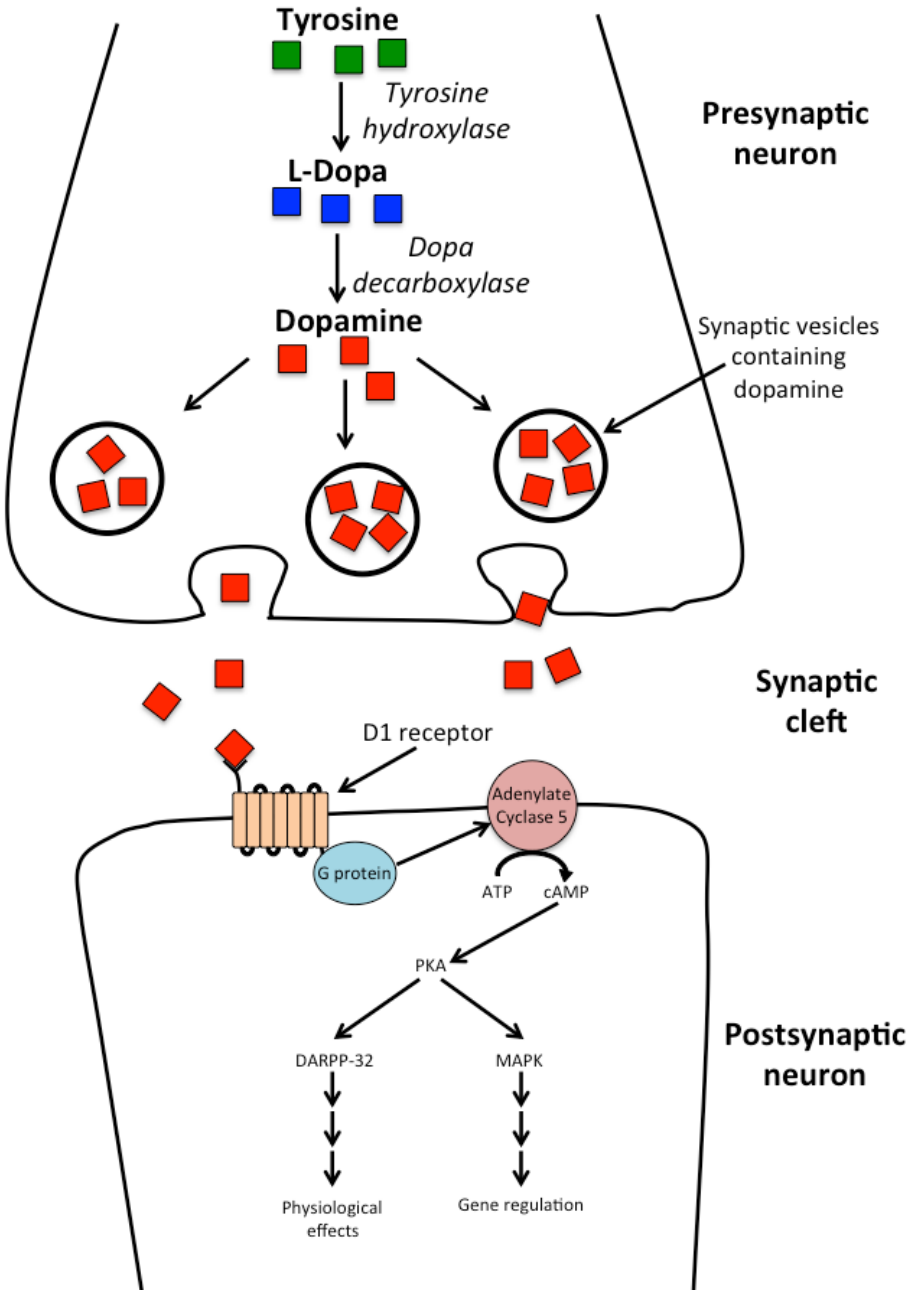

Figure 1.2: Dopamine signalling in neurons. Dopamine is produced from tyrosine, packaged in vesicles then exocytosed into the synaptic cleft. It then binds to a dopamine receptor resulting in a conformational shift in the GPCR in order to transduce the signal across the postsynaptic membrane, thus modulating a multitude of signalling pathways.

There have been 11 dopaminergic cell groups identified to date (A8-16, Aaq and Telencephalic), with 4 major pathways originating from the A8 (tuberoinfundibular pathway), A9 (nigrostriatal pathway) and A10 (mesolimbic and mesocortical pathways) dopaminergic cell groups (Beaulieu and

Gainetdinov, 2011). In Parkinsonisms, A9 dopaminergic neurons progressively degenerate. These cells have multiple characteristics that leave them susceptible to the progressive degeneration observed in PD (Lu, 2011). These are highly polarised cells with excessive amounts of dendritic and axonal branching, thus the soma accounts for less than 1% of the total cellular volume (Sulzer, 2007). In particular, the nigral A9 dopaminergic neurons are inherently sensitive to dysfunction and degeneration of their mitochondrial network, discussed later in this chapter (section 1.4.1.1).

Dopaminergic neurons are of relativity low abundance, making up less than 1/100,000 of our neurons. Progressive degeneration of these neurons is seen in PD whereas blocking dopamine receptors has therapeutic applications in the treatment of psychosis (Girault and Greengard, 2004). Dopamine receptors can differ in their localisation and density depending on the neuron and can be found both pre- and postsynaptically (Missale et al., 1998). There are 2 dopamine receptor families, both of which are G protein coupled receptors (GPCRs). The D1-like receptor family are made up of D1 and D5 receptors, which act via G_s-proteins in order to activate adenylate cyclase in order to upregulate cAMP production (Figure 1.2) (Lee et al., 2000, Vallone et al., 2000). The D2-like receptor family, comprising of D2, D3 and D4 receptors reduce adenylate cyclase activity, thus reducing cAMP, acting via G_i-proteins (Missale et al., 1998, Lee et al., 2000). As well as regulating physiological functions such as movement, dopamine signalling is critical in regulating pathways such as mitogen-associated protein kinase (MAPK) cascades (Luo et al., 1999, Neve et al., 2004).

The activation of the protein kinase A (PKA) substrate Dopamine- and cAMP-regulated phosphoprotein 32kDa (DARPP-32) is involved in the signal transduction for multiple neurotransmitters and also results in the activation of extracellular signal-regulated kinase (ERK) signalling (Hisahara and Shimohama, 2011). MAPKs, such as ERK, are critical in the regulation of synaptic plasticity (Berhow et al., 1996). Mice lacking D2 receptors show Parkinsonian-like locomotor dysfunction (Baik et al., 1995) with D1-deficient mice also showing symptoms consistent with neurodegenerative conditions (Xu

et al., 1994, Drago et al., 1994, Gantois et al., 2007, Hisahara and Shimohama, 2011). Using positron emission tomography, it has been shown that the dopamine binding capacity of D3 receptors in early-stage Parkinson's patients is decreased and that this correlates with locomotor defects (Boileau et al., 2009). This suggests that the ability of dopamine receptors to bind their ligands, and thus transduce their signalling, may decrease as PD progresses.

1.2.2 Causes of PD

Parkinson's is mainly considered a sporadic disease, with less than 10% of cases being classified at familial (Thomas and Beal, 2007). Head injury and exposure to pesticides are 2 environmental risk factors that positively correlate with PD (Dick et al., 2007). Interestingly, smoking appears to guard against PD, which may suggest a neuroprotective capability for tobacco (De Palma et al., 1998, Benedetti et al., 2000, Dick et al., 2007). Over recent decades, 18 chromosomal loci with a link to PD have been identified (Table 1.1), which are named *PARK1-18* in order of their original identification.

Although 18 loci have been named, *PARK1* and *PARK4* represent the same locus (Klein and Westenberger, 2012). It must also be noted that the disease gene of some of these 18 loci is still to be determined in some cases. Mutations in some of these genes, such as *PARK10*, do not directly cause a form of Parkinsonism, but are instead considered risk factors. Only 6 of these genes are linked to monogenic hereditary PD, with mutations in the α-synuclein gene (*SNCA, PARK1*) and the gene encoding Leucine-rich repeat kinase 2 (*LRRK2, PARK2*) mutations causing autosomal-dominant forms of the disease. Autosomal recessive PD results from mutations in *PARKIN*, *PINK1*, *DJ-1* and *ATP13A2* genes. Mutations in *SNCA* are probably the most studied of these 6 genes, with individuals who have one of the 3 mutations currently identified (A53T, A30P and E46K) resulting in the development of early-onset PD (Klein and Westenberger, 2012). Duplications of this gene have been identified in a number of families, as well as in several sporadic cases (Chartier-Harlin et al., 2004, Ahn et al., 2008, Ibanez et al., 2009, Klein and Westenberger, 2012).

Triplication of the *SNCA* gene has also been reported in three different families (Farrer et al., 1998, Singleton et al., 2003, Ibanez et al., 2009).

The locus encoding the *SNCA* gene (α-synuclein) was the first to be identified as a causative agent in familial PD (Polymeropoulos et al., 1996). Mutations in the *SNCA* gene usually result in early-onset PD (EOPD) with initial symptoms occurring before the patient is 50 years old and progressing rapidly, often presenting with symptoms such as dementia. A classic pathological characteristic of this form of the disease is the presence of intracellular inclusions called Lewy bodies (containing α-synuclein aggregates) throughout several areas of the brain, including the SNpc (Polymeropoulos et al., 1996, Klein and Westenberger, 2012). PD-causing mutations within the *SNCA* gene are relatively rare with only 3 missense mutations reported to date. Furthermore, duplications and triplications of the entire gene have been reported in some families (Klein and Schlossmacher, 2006). There has been some debate as to whether α-synuclein adopts a natively unfolded structure or exists as a helically folded tetramer within cells (Weinreb et al., 1996, Bartels et al., 2011, Burre et al., 2013, Bartels and Selkoe, 2013). A recent study concluded that α-synuclein exists in dynamic equilibrium between unfolded monomers and metastable helical tetramers (Selkoe et al., 2014). Interestingly, tetramers were found to be more resistant to aggregation often seen in PD patient brains compared to the monomeric form of α-synuclein.

The most common causative mutations of autosomal-recessive forms of PD are found in *PARK2*, which encodes the E3 ubiquitin ligase Parkin (Kitada et al., 1998, Scarffe et al., 2014). Parkin, along with PTEN-induced putative kinase 1 (PINK1), encoded by *PARK6*, plays a major role in maintaining the mitochondrial network by eliminating damaged mitochondria (Narendra et al., 2008, Narendra et al., 2010b, Matsuda et al., 2010, Vives-Bauza et al., 2010). Mutations in either gene can result in autosomal recessive PD (Deas et al., 2011), indicating the importance of these regulatory proteins.

Despite 18 loci being identified to date, not all of the PD causative genes have been identified (Table 1.1). Furthermore, there have been several studies published that disagree on the causative genes within certain loci. One study concluded that the *UCHL1* gene, encoding the neuronal ubiquitin *C*-terminal hydrolase isozyme L1 (UCHL1), was not a susceptibility factor in PD (Healy et al., 2006). This study found that the S18Y mutant did not decrease susceptibility to PD. However, a more recent study found that the I93M mutant, associated with increased risk of PD, was structurally disruptive leading to the exposure of hydrophobic residues (Andersson et al., 2011). Although *OMI/HTRA2* (*PARK13*) was reported to be PD-linked gene (Strauss et al., 2005), several other studies have disputed this and found no major association with the disease (Kruger et al., 2011, Simon-Sanchez and Singleton, 2008).

These genes are all part of complex, multi-tiered cascades and it must therefore be taken into consideration that there will be crossover and interactions between PD-associated genetic pathways and proteins. For example, the F-box domain-containing protein Fbxo7 (*PARK15*) has been shown to interact with both Parkin (*PARK2*) and PINK1 (*PARK6*) in order to regulate the turnover of damaged mitochondria via the process of mitophagy (Burchell et al., 2013). Interestingly, PD-associated mutations in Fbxo7 appear to disrupt this interaction. Mutations in the *LRRK2* gene are the most common cause of familial and sporadic PD (Kumari and Tan, 2009). The most common PD-causing mutation in this gene is the missense G2019S mutation, which has recently been shown to impair dopamine release and the expression of dopaminergic genes such as tyrosine hydroxylase in the neurons of transgenic mice (Liu et al., 2015). A separate study demonstrated that RAB7L1 (*PARK16*) interacts with LRRK2 (*PARK8*) to regulate retromer and lysosomal pathways in neuronal cells (MacLeod et al., 2013). Defects in the regulation of these processes may contribute to the progression of PD.

Symbol	Gene	Locus	Function	Resultant disorder	References
PARK1	*SNCA*	4q21-22	Not fully understood.	AD-EOPD	(Polymeropoulos et al., 1996, Polymeropoulos et al., 1997, Singleton et al., 2003)
PARK2	*PARKIN*	6q25.2-q27	E3 ubiquitin ligase	AR-EOPD	(Matsumine et al., 1997, Kitada et al., 1998)
PARK3	Unknown	2p13	-	AD-PD	(Gasser et al., 1998, DeStefano et al., 2002)
PARK4	*SNCA*	4q21-q23	Same as *PARK1*	AD-EOPD	Same as *PARK1*
PARK5	*UCHL1*	4p13	De-ubiquitinating enzyme	AD-PD	(Leroy et al., 1998)
PARK6	*PINK1*	1p35-p36	Mitochondrial kinase	AR-EOPD	(Valente et al., 2002, Valente et al., 2004, Rogaeva et al., 2004)
PARK7	*DJ-1*	1p36	Oxidative stress response	AR-EOPD	(van Duijn et al., 2001, Bonifati et al., 2003)
PARK8	*LRRK2*	12p11.2-q13.1	Serine/threonine kinase	AD-PD	(Funayama et al., 2002, Paisan-Ruiz et al., 2004, Zimprich et al., 2004a, Zimprich et al., 2004b)
PARK9	*ATP13A2*	1p36	Intracellular trafficking	AR-PD/Kufor-Rakeb syndrome	(Ramirez et al., 2006)
PARK10	Unknown	1p32	-	Risk factor for classical PD	(Farrer et al., 2006, Hicks et al., 2002, Li et al., 2007)
PARK11	Unknown	2q36-27	-	AD-PD	(Bonifati, 2009, Pankratz et al., 2003)
PARK12	Unknown	Xq21-q25	-	Risk factor for classical PD	(Pankratz et al., 2002)
PARK13	*HTRA2*	2p12	Serine peptidase	AD-PD or risk factor for classical PD	(Strauss et al., 2005, Simon-Sanchez and Singleton, 2008, Kruger et al., 2011)
PARK14	*PLA2G6*	22q13.1	Phospholipase	AR-EO dystonia-parkinsonism	(Paisan-Ruiz et al., 2009, Sina et al., 2009)
PARK15	*FBX07*	22q12-q13	Mediates ubiquitination	AR-EO parkinsonian-pyramidal syndrome	(Di Fonzo et al., 2009, Shojaee et al., 2008)
PARK16	*RAB7L1*	1q32	Lysosome function	Risk factor for classical PD	(Chang et al., 2013, Tucci et al., 2010)
PARK17	*VPS35*	16q11.2	Retromer complex	AD-PD	(Wider et al., 2008, Zimprich et al., 2011)
PARK18	*EIF4G1*	3q27.1	Scaffold protein	AD-PD	(Chartier-Harlin et al., 2011, Deng et al., 2015)

Table 1.1: PD-associated genes. To date 18 loci have been identified to play a role causative role in PD, although *PARK1* and *PARK4* are in fact the same locus, encoding *SNCA*. Not all genes within these loci have been identified so far and it is likely more PD loci will be identified in the future.

1.2.3 Treatment of PD

Currently no cure is available for PD. However, there are treatments aimed at alleviating symptoms, with this being tailored to the individual (Jankovic and Aguilar, 2008). A wide range of treatments are currently being used and/or developed from oral drugs, patches, surgery and deep brain stimulation (DBS). Most current therapies are based around the dopamine replacement strategy and use L-DOPA, a dopamine precursor. Unfortunately, long-term treatment usually results in the development of motor defects (Olanow and Schapira, 2013).

Parkinson's does not just involve the degeneration of the SNpc, with pathology extending to serotinergic, choloinergic and norepinephrinergic neurons (Olanow and Schapira, 2013). It has been reported that the bilateral DBS of two neuronal regions, the pedunculopontine nucleus (PPN) and the subthalamic nucleus (STN), improved patient gait and day-to-day living (Stefani et al., 2007), although this is yet to be fully confirmed. Dementia is a commonly seen, nondopaminergic, feature of PD with around 80% of patients going on to develop it. Unfortunately, no current therapies exist to significantly halt or reverse cognitive decline in patients (Olanow and Schapira, 2013).

Although mutations in *LRRK2* are the most common genetic cause of PD no clinical trials have been undertaken to specifically target defects in this gene. Mutations in *PARKIN* and *PINK1* are common causes of autosomal-recessive PD and are known to lead to mitochondrial defects and oxidative stress. A small study involving 80 patients in the early stages of PD suggested the potent antioxidant coenzyme Q10, which is reduced in mitochondria isolated from PD patients, may slow disease progression (Shults et al., 2002). Coenzyme Q10 also reduced the loss of dopaminergic axons in mice treated with the mitochondrial poison 1-methyl-4-phenyl-1,2,3,6-tetrahydropyridine (MPTP) (Beal et al., 1998). However, in a large-scale double-blind trial this treatment failed (Investigators, 2007).

Despite the fact we are part of an ever-ageing population, an effective treatment for PD is yet to be found. It is therefore critical that new and effective treatments

to eradicate symptoms or halt/reverse the progressive neurodegeneration are developed. The effect of cellular stress, in particular mitochondrial and oxidative stress, in the development of the Parkinsonism pathology can be highlighted by cases presented several decades ago in which 4 drug users intravenously injecting impure batches of what they believed to be synthetic heroin developed PD-like symptoms. These batches contained traces of the mitochondrial poison, MPTP, which led to the selective destruction of dopaminergic neurons within the SNpc (Langston et al., 1983). This highlights how subcellular stress can lead to PD-associated neurodegeneration. Importantly, how neurons respond to cellular stress and dysfunction is not fully understood and warrants further investigation.

1.3 THE CELLULAR RESPONSE TO STRESS AND DYSFUNCTION

In both *in vivo* and *in vitro* conditions, cells experience changing conditions and thus are subject to 'stress'. Undergoing any degree of stress or insult will evoke a range of cellular responses, some of which are not stressor-specific and some that are, although even specific response mechanisms will share common elements or be activated in parallel with other response arms (Kultz, 2005). Furthermore, cells may initiate either a protective, destructive or even apoptotic response depending on factors such as the level or duration of stress. Initially a cell will look to respond with the aim of recovering from the insult and maintaining homeostasis. The capacity of this initial response is what dictates the eventual outcome (Fulda et al., 2010).

Both the type and level of stress is key in determining what defensive and adaptive mechanisms the cell mounts. If these are overcome or insufficient, apoptotic mechanisms may be triggered in order to limit damage to the organism or surrounding tissues (Figure 1.3) (Fulda et al., 2010). The programmed cell death, termed apoptosis, has been recognised as an essential regulated process for a long time (Vogt, 1842, Lockshin and Williams, 1965, Kerr et al., 1972, Vaux, 2002, Kultz, 2005). In short, a cell will initially look to counter stress by containing and reversing it, however, apoptosis is a mechanism by which a cell may sacrifice itself for the preservation or development of the organism.

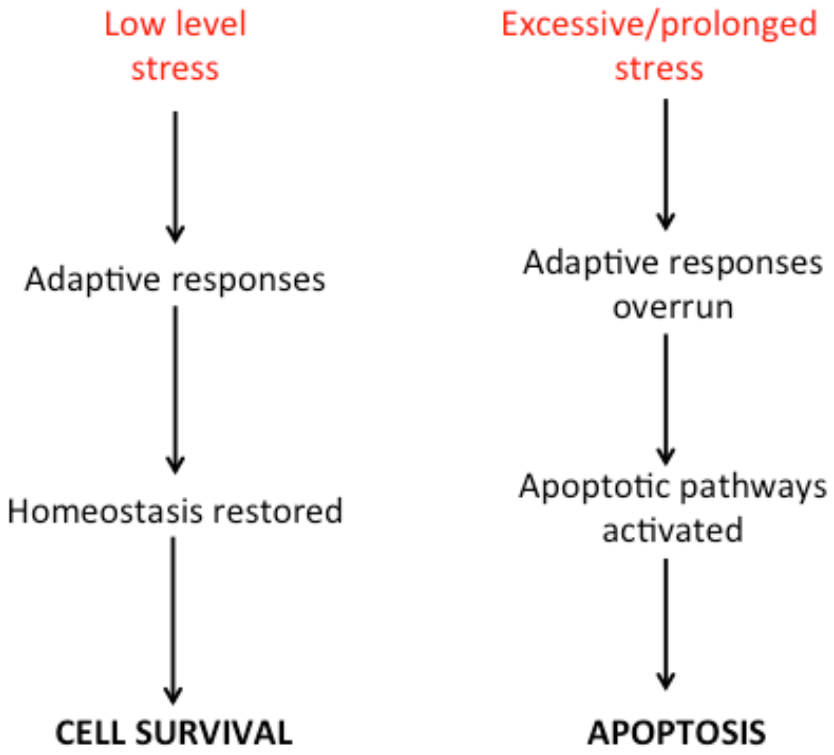

Figure 1.3: The cell stress response can be divided into 2 arms. These are governed by the level of stress that a cell experiences. The apoptotic response is activated if the initial adaptive response is unable to cope with the level of stress. Due to the constitutive metabolic activity of cells, it is likely they are constantly adapting to stress by the initial response and only when the stress has become too high or prolonged will pro-apoptotic signalling begin.

1.3.1 Immediate early gene signalling

In cellular biology, stress refers to an individual cell's response to specific stimuli which is often the rapid transcription of a particular set of genes (Senba and Ueyama, 1997) defined as immediate early genes (IEGs). Stress can be used to describe many cellular events such as excessive reactive oxygen species (ROS) production, heat shock or DNA damage, which can result in rapid IEG protein modulation (Curran and Morgan, 1995, Cochran et al., 1983). IEGs are also expressed in response to stimuli such as growth factors, implicating their protein products in cellular processes such as cell differentiation and growth (Sheng and Greenberg, 1990, Okuno, 2011).

To date there are dozens of known IEGs, some of which are implicated in disease. Many of these are transcriptional regulators such as members of the Fos and Jun families, which dimerise to form the AP-1 transcription factor. Jun proteins can heterodimerise with Fos proteins, or homodimerise with other Jun proteins. Fos proteins, on the other hand, can only form heterodimers. One of the most extensively studied IEGs is the *c-fos* proto-oncogene, the cellular homologue of the viral *v-fos* oncogene (Curran et al., 1984). Jun and Fos families are also capable of forming heterodimers with some members of the activating transcription factor (ATF) and Jun dimerisation protein (JDP) families (reviewed by Hess et al., 2004).

IEG expression varies between cell type, with some being constitutively expressed and some expressed in response to extracellular stimuli (Senba and Ueyama, 1997, Sheng and Greenberg, 1990). Members of the *FOS* and *JUN* families are constitutively expressed at relatively low basal levels in many cell types, although their expression can be transiently upregulated in response to extracellular stimuli (Curran, 1992). Furthermore, the protein products of these IEG families all share similar affinity for each other which may suggest the proportion of different dimer complexes is governed by the cellular concentrations of the individual subunits (Kovary and Bravo, 1991).

1.3.1.1 The AP-1 transcription factor complex

Transcription factors are sequence-specific DNA-binding proteins that control the rate of mRNA synthesis, regulating gene expression. AP-1 is a homo- or heterodimeric transcription factor complex capable of regulating both the basal and inducible expression levels of genes containing the 12-*O*-tetradecanoylphorbol-13-acetate (TPA) responsive element (TRE) consensus sequence (5’-TGA(G/C)TCA-3’) in their promoter regions (Hess et al., 2004). As well as TREs, these dimeric transcription factors can also bind cAMP responsive element (CRE) sequences (5'-TGACGTCA-3') (Ryseck and Bravo, 1991). Although many gene promoters contain the AP-1 binding sites, comparatively few have actually been shown to be directly regulated by these IEG-encoded transcription factors (Okuno, 2011).

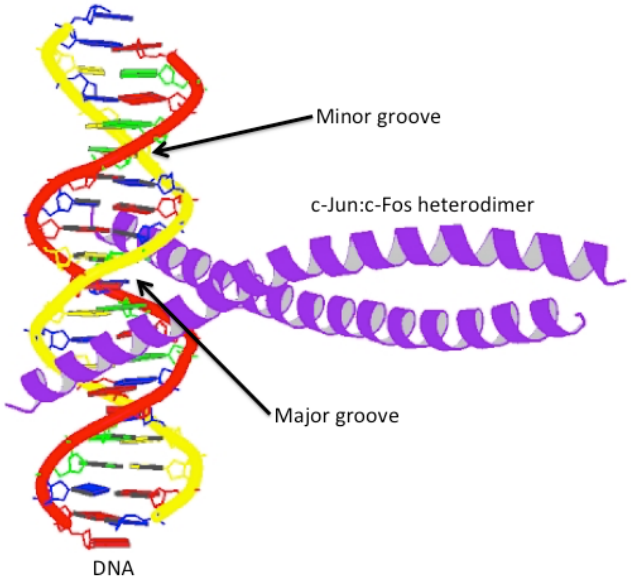

Figure 1.4: DNA binding of the heterodimeric AP-1 transcription factor complex. Adapted from RCSB Protein Data Bank (PDB 1FOS) (RCSB, Glover and Harrison, 1995). The x-ray crystal structure of a c-Jun:c-Fos:DNA complex at 3.05Å resolution. The AP-1 heterodimer grips the major grove like forceps, bending it towards the coiled coil region (Glover and Harrison, 1995).

Several types of DNA-binding structures have been observed in eukaryotic and prokaryotic cells. AP-1 is part of the basic-leucine zipper, or bZIP, protein class. This complex consists of a pair of α-helices (Figure 1.4), which form a coiled-coil structure with each other stabilised by the intermolecular interactions of hydrophobic amino acid side chains (usually leucine residues). Thus, this structure is often termed a 'leucine zipper' (Berg et al., 2007, Alberts et al., 2008). The charged residues within the coiled-coil region of the Fos proteins at positions 'e' and 'g' (Figure 1.5) are likely to result in the destabilisation of a Fos-Fos homodimer, thus favouring Fos-Jun or Jun-Jun dimerisation (Glover and Harrison, 1995, O'Shea et al., 1992). These acidic residues in the coiled-coil region of the Fos family proteins makes their homodimerisation thermodynamically unfavourable (O'Shea et al., 1992).

Fos and Jun proteins induce DNA bending upon interaction, a common characteristic transcription factors. However, Jun homodimers and Jun-Fos heterodimers induce bending in opposite orientations, bending towards the

minor groove or the major groove, respectively (Kerppola and Curran, 1991b, Kerppola and Curran, 1991a). A c-Jun homodimer binds to the AP-1 DNA site with much less efficiency than a c-Fos:c-Jun heterodimer (Halazonetis et al., 1988). A range of bZIP family proteins bind to the AP-1 site and induce DNA bending, although bZIP proteins CREB and ATF1 dimers did not induce a significant bend (Kerppola and Curran, 1993). Therefore, variation in the leucine zipper dimer subunits can result in topologically different DNA-protein complex structures, which may play a part in determining selectivity and specificity of co-operative initiation complex assembly. Furthermore, the flexure of DNA allows the factor-induced bend, which in turn facilitates a reduction in the thermodynamic barrier that is preventing interactions between proteins bound at different DNA sites (Kerppola and Curran, 1991b).

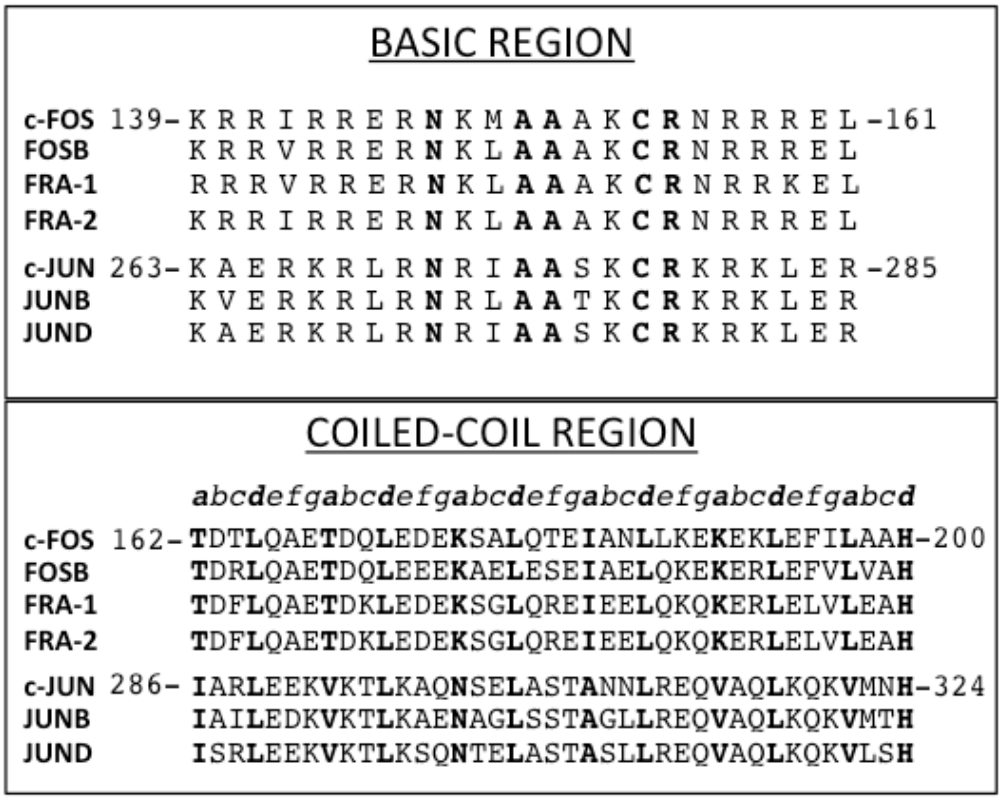

Figure 1.5: The amino acid sequences of the basic and coiled-coil regions of the AP-1 proteins. Conserved homology is demonstrated between the proteins and families (Glover and Harrison, 1995). Residues within the basic region in bold contact the DNA upon binding. The heptad repeat in the coiled-coil domain is demonstrated by the ‘a-g’ motif highlighted above the sequences. Residues ‘a’ and ‘d’ (bold) form the hydrophobic interface of the coiled-coil.

Transactivation activity and stability of the AP-1 subunits can be regulated by their phosphorylation status. MAPKs, such as c-Jun amino N-terminal kinases (JNKs), ERKs, p90 ribosomal S6 kinases (RSKs) and a variety of p38 isoforms, play a major role in mediating stimuli into a cellular response via the phosphorylation of transcription factors such as Jun and Fos (Cargnello and Roux, 2011). In terms of transactivation potential, individual Jun and Fos proteins differ considerably. c-Jun, c-Fos and FosB are considered strong activators, whereas JunB, JunD, Fra-1 and Fra-2 display weaker potential (Hess et al., 2004). Weaker transactivators may even repress AP-1 activity by forming inactive dimers or competing with more active complexes for the binding site.

The subcellular localisation of AP-1 subunits, as well as the control of this localisation, is a poorly studied area. Although these DNA-binding proteins must be located in the nucleus to affect the transcription of their target genes, they do not solely reside here, with some having functions outside the nucleus. As well as intracellular localisation regulating AP-1 activity, their stability is also key to their regulation. The Fos proteins, c-Fos, Fra-2 and FosB have been shown to be present in both nuclear and cytosolic fractions of murine hippocampus cells, in which their half-lives differ significantly (Manabe et al., 2000, Manabe et al., 2001). Both c-Fos and Fra-1, whose transient expression can be induced by extracellular stimuli within 15 minutes and 2 hours, respectively (Basbous et al., 2008), share destabilising domains (Ferrara et al., 2003, Bossis et al., 2003). Fra-1 contains only one of the two ‘destabilisers’, located within its *C*-terminal region (Ferrara et al., 2003). This *C*-terminal destabilising domain sequence is highly conserved in both Fra-2 and FosB (Basbous et al., 2008). RSK1/2 and ERK1/2 reduce the activity of the c-Fos *C*-terminal destabiliser upon phosphorylation of the serine residues S363 and S374, respectively (Ferrara et al., 2003). Although c-Fos undergoes proteasomal degradation, much of this is ubiquitylation-independent (Bossis et al., 2003), as is the case for Fra-1 (Basbous et al., 2008).

Despite being one of the most extensively studied IEGs, the dynamic intracellular distribution of c-Fos is poorly understood. c-Fos has predominantly

been reported to accumulate in the nucleus (Roux et al., 1990, Vriz et al., 1992, Malnou et al., 2007), which may largely be attributed to its nuclear localisation signals (NLSs) residing within the DNA-binding domain (DBD) and *N*-terminal region (Malnou et al., 2007). c-Fos can also be cytoplasmically localised (Roux et al., 1990, Vriz et al., 1992, Sasaki et al., 2006) and associates with the ER to activate phospholipid synthesis (Bussolino et al., 2001, Gil et al., 2004), as well as being present in the nucleus and cytoplasm of differentiated PC12 cells (Figure 1.6).

c-Fos undergoes nucleocytoplasmic shuttling, with the nuclear membrane transporter Transportin 1 mediating its nuclear import via the *N*-terminal NLS. Deletion of either the N-terminal or DBD NLS only leads to partial cytoplasmic redistribution, indicating quantitative nuclear accumulation is dependent on the synergistic action of both NLSs (Malnou et al., 2007). The half-life of c-Fos in HeLa cells is approximately 2.5 hours (Bossis et al., 2003), and although it is more unstable in the cytoplasm (Roux et al., 1990), the estimated c-Fos half-return to the cytoplasm (Malnou et al., 2007) suggests it may undergo multiple rounds of nucleocytoplasmic shuffling during its lifetime.

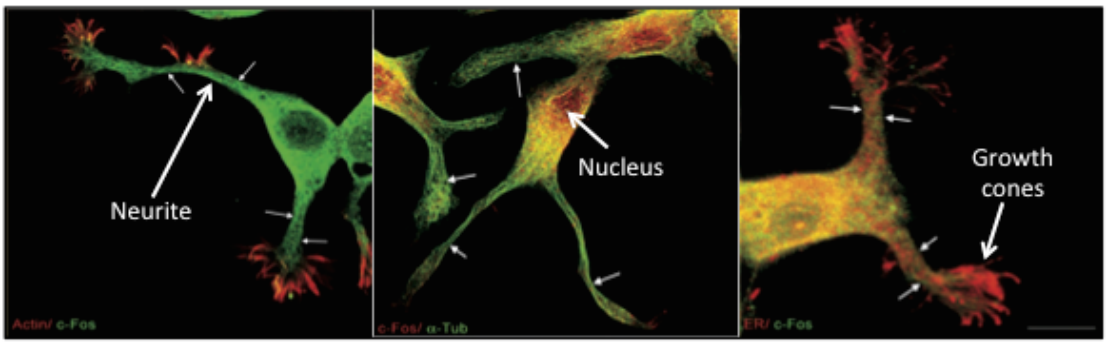

Figure 1.6: Confocal microscopy images of NGF-differentiated PC12 cells demonstrating both cytoplasmic and nuclear c-Fos (adapted from Gil et al., 2004). Small arrows denote how c-Fos is spread throughout neurites as well as the main cell body. Furthermore, c-Fos shows greater colocalisation with the ER marker, calnexin, in the cell body compared to in the growth cones. Left image shows c-Fos (green) and actin (red). Middle image shows c-Fos (red) and α–tubulin (green). Right image shows c-Fos (green) and the calnexin (red). Copyright permission in Appendix A.

Cytoplasmic retention of c-Fos in HEK293 cells is reversed upon UV-induced stress activation of the p38 MAPK pathway, by which c-Fos is phosphorylated (Tanos et al., 2005). Nuclear accumulation of c-Fos is also enhanced by heterodimerisation with c-Jun by reducing the efficiency of their nuclear export (Malnou et al., 2007). c-Fos and c-Jun undergo rapid dissociation and association cycles (Kovary and Bravo, 1991). Using a 'tethered dimer' to stabilise c-Fos:c-Jun dimerisation by a peptide linker, nucleocytoplasmic transport was further reduced, indicating dimer formation is critical for shuttling inhibition.

Despite being a similar molecular weight, monomeric c-Jun undergoes nucleocytoplasmic shuffling with less efficiency than c-Fos (Malnou et al., 2007). Interestingly, it appears that the nuclear accumulation of ATF2, which is enhanced by dimerisation with c-Jun, is essential for the activation of its target genes, one of which is *c-JUN* (Liu et al., 2006). Other Jun proteins appear to also undergo nucleocytoplasmic shuffling. JunB is present in both the nucleus and cytoplasm of skeletal muscle cells (Raffaello et al., 2010).

A host of AP-1-like transcription factors have also been identified in yeast cells (reviewed by Toone and Jones, 1999). Furthermore, the subcellular localisation of some of these yAP-1 proteins can be influenced and regulated by oxidative stress. The subcellular distribution of Yap1p shifts from predominantly cytoplasmic to nuclear under oxidative stress conditions, a key step in the cell's stress response (Kuge et al., 1997). This is not due to the oxidative stress-induced effects on Yap1p's nuclear import, but instead the down-regulation of its Crm1p-dependent nuclear export (Isoyama et al., 2001), resulting from the inhibition of the interaction between Crm1p and protein's cysteine-rich *C*-terminal domain around the NES (Kuge et al., 1998, Yan et al., 1998, Isoyama et al., 2001, Kuge et al., 2001). Thus, these cysteine residues appear essential in sensing the redox state of the cell in order to regulate the transcription factor's activity by maintaining its nuclear accumulation (Kuge et al., 1997).

As previously discussed, members of the Fos and Jun families have been observed in both cytosolic and nuclear fractions, suggesting their intracellular

localisation is dynamically regulated. It is possible that the subcellular state, such as ROS levels, is partially responsible for the transcription factor's location within the cell. This may be regulated by the protein's phosphorylation state or whether is part of a dimeric complex, amongst other things. Subcellular localisation of these proteins may also be dependent on cell type.

1.3.1.2 AP-1 transcription factors and MAPKs

MAPKs are serine/threonine kinases that play a major role in the conversion of extracellular stimuli into a cellular response via signal transduction pathways. MAPKs can be considered conventional and atypical (Figure 1.7). JNK1/2/3, ERK1/2/5 and p38 isoforms (α, β, γ and δ) are classed as conventional MAPKs as they contain a conserved Thr-X-Tyr motif within their activation loop. These conventional MAPKs are part of a 3-tier signal transduction pathway involving 3 sequentially acting kinases; a MAPK, a MAPK kinase (MAPKK) and a MAPKK kinase (MAPKK). The activation of the MAPKKK leads to MAPKK phosphorylation and activation, which in turn results in the phosphorylation of the Thr and Tyr residues within the activation loop motif of the MAPK, which is essential for its enzymatic activity. Atypical MAPKs, such as ERK3/4/7, are not part of these 3-tiered cascades and usually lack the Thr-X-Tyr motif (the tyrosine residue is often substituted). Although ERK7 contains the Thr-X-Tyr motif, its bisphosphorylation appears to be catalysed not by an upstream MAPKK, but by ERK7 itself (reviewed by Cargnello and Roux, 2011). Scaffold proteins, such as JNK interacting proteins (JIPs), provide docking sites for MAPKs and their upstream kinases, are generally non-catalytic, provide another level of regulation to incur MAPK activation selectivity by different stimuli, and can even bind other proteins such as kinesins (Morrison and Davis, 2003, Johnson and Nakamura, 2007). JIP-1 mediates JNK activation by the mixed-lineage kinase (MLK) class of MAPKKKs, but not signalling conducted via the MEK kinase (MEKK) class (Whitmarsh et al., 1998). However, overexpression of JIPs leads to cytoplasmic retention of JNK, thus inhibiting JNK-mediated activation of gene expression (Davis, 2000, Peng and Andersen, 2003).

There are 3 JNK genes encoded in the human genome (*JNK1, JNK2* and *JNK3*), all with alternatively spliced isoforms (Gupta et al., 1996). Although

JNK1 and 2 have broad tissue distribution, JNK3 is primarily expressed in CNS neurons. The recognition that JNK3 may have an important pathological role in several neurodegenerative conditions has led to its crystal structure being determined (Xie et al., 1998).

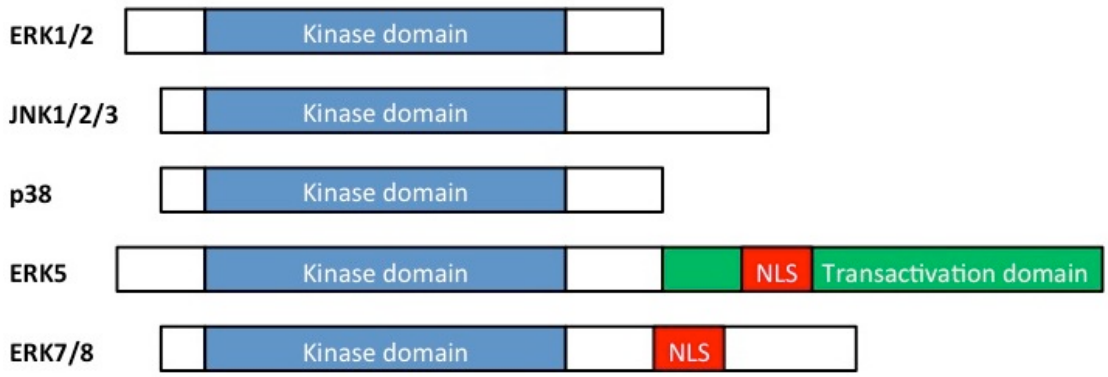

Figure 1.7: Schematic diagram of some MAPKs. Their activation motifs are located within the kinase domain of the protein. Certain MAPKs have extra domains such as a nuclear localisation signal (NLS) or a transactivation domain (TAD). Some atypical MAPKs, such as the Nemo-like kinase (NLK) contain domains rich in Ala, His and Glu residues.

JNKs are activated by the bisphosphorylation of threonine and tyrosine residues in their activation loop by upstream activator kinases, such as MKK4 or MKK7 (Resnick and Fennell, 2004, Cargnello and Roux, 2011). Monophosphorylation of the JNK3α1 Thr residue by MKK4 only triggers low levels of activation whereas bisphosphorylation by both MKK4 and MKK7 induces maximal enzymatic activity. Moreover, activation appears to be achieved by a 'processive mechanism' by which Thr 221 phosphorylation by MKK7 is required for MKK4 to phosphorylate Tyr 223 (Lisnock et al., 2000). Furthermore, most extracellular stimuli that activate the MAPK p38 isoforms, also activate JNK isoforms (Cargnello and Roux, 2011). Importantly, in mice lacking all 3 *Jnk* genes the activating phosphorylation of c-Jun Ser63 does not occur (Xu et al., 2011).

JunB lacks the phosphorylation sites for JNK activity and is therefore not under control of this class of MAPK. On the other hand, JunD contains a

phosphoacceptor site but lacks a docking site for JNK. However, upon heterodimerisation with c-Jun, JunD can be phosphorylated by JNK as c-Jun can provide a docking site to recruit JNK (Kallunki et al., 1996). This would indicate how specific heterodimers might play a role in modulating specific cascades. Furthermore, c-Jun has been shown to localise to the nucleus independently of phosphorylation by JNK (Schreck et al., 2011). The authors also proposed that JNK nuclear translocation is promoted by c-Jun. However, only JNK2 was studied and it is unclear whether this would be the case for all JNK isoforms.

ERK1, which shares 83% amino acid identity with ERK2, was the first MAPK to be characterised, with alternatively spliced isoforms being described later. They are activated by growth factors, heterotrimeric G protein coupled receptor (GPCR) ligands, cellular stress, amongst other stimuli. As conventional MAPKs, ERK1/2 are activated by the sequential action of a MAPKKK (e.g. Raf-1) and a MAPKK (e.g. MEK1/2), whereas ERK5, another conventional MAPK, is stimulated by a different pathway (Cargnello and Roux, 2011). ERK has been shown to activate the Elk-1 transcription factor by phosphorylation of residues with its *C*-terminal domain, resulting in increased expression of *c-Fos* (Gille et al., 1995). c-Fos is stabilised by ERK1/2-mediated phosphorylation (Murphy et al., 2002), thus allowing c-Fos to accumulate and dimerise with c-Jun (Shaulian and Karin, 2001, Cargnello and Roux, 2011). As well as being activated by ERK1/2 phosphorylation (Murphy and Blenis, 2006), Fra-1 and c-Fos are also phosphorylated, activated and stabilised upon MEK5-induced activation of ERK5 (Terasawa et al., 2003). It is possible that c-Fos acts as a form of 'sensor' for the dynamic activation of ERK as *Fra-1* gene expression, a target of c-Fos, is only activated in NIH 3T3 fibroblasts upon sustained c-Fos expression (Murphy et al., 2004). The ability for ERK-mediated phosphorylation of c-Fos to stabilise this otherwise highly unstable protein may allow the cell to distinguish between sustained and transient ERK signalling and initiate an appropriate response (Murphy and Blenis, 2006). ERK/c-Jun signalling can also contribute to the anti-apoptotic activity of Bcl-2, which activates the Ras-Raf-ERK cascade leading to the phosphorylation of c-Jun (Schwarz et al., 2002). Considerable

cross-talk between MAPK pathways also adds further levels of regulation and complexity.

The regulation of AP-1 proteins by MAPKs can, in turn, then influence the rate at which AP-1 genes are expressed. The AP-1 proteins c-Jun, Fra-2 and JunD have been shown to play a role in the up-regulation of *FRA-1* expression, by interaction with the TRE located within the genes promoter region at -318bp (Adiseshaiah et al., 2003). However, the TRE (-318) alone is insufficient to mediate TPA-induced *FRA-1* expression thus a bipartite enhancer is formed in conjunction with a downstream serum response element (SRE) and ATF site (Adiseshaiah et al., 2005). Mutations within the TRE (Adiseshaiah et al., 2003), or the ATF and SRE site (Adiseshaiah et al., 2005) abolish promoter activity. Additionally, in response to TPA stimulation ERK1/2 signalling, but not JNK1/2 or p38, is critical for the recruitment of c-Jun and Fra-2 to the *FRA-1* promoter (Adiseshaiah et al., 2008). It seems likely that the range of MAPKs allow the cell to differentiate between a variety of extracellular stimuli and stressors. For example, depending on the stimulus, the IEG transcription factor ATF2 is activated through the phosphorylation of its *N*-terminal activation domain by either JNK, ERK or p38 (Yang et al., 2013).

Further complexity is added to these signalling modules by the fact that MAPKs not only regulate downstream targets such as AP-1 proteins, but they also regulate other MAPK pathways, as well as self-regulating their own cascade via feedback loops (Fey et al., 2012). In mouse fibroblasts, JNK supressed tumour necrosis factor (TNF)-induced apoptosis. However, JNK also potentiated ROS production under these conditions, which in turn activates JNK and induces necrosis (Ventura et al., 2004). A similar observation has also been made in mouse B lymphoma cells, where JNK activity produced H_2O_2, leading to the activation of apoptosis signal-regulating kinase 1 (ASK1), a kinase upstream of JNK (Furuhata et al., 2009). Interestingly, ERK has been shown to negatively regulate JNK activity by stabilising and activating dual specificity phosphatases (DUSP) 4 and 16, which dephosphorylate JNK, thus reducing its activity (Paumelle et al., 2000, Monick et al., 2006). Conversely, in human melanoma ERK signalling may upregulate and activate the JNK/c-Jun pathway (Lopez-

Bergami et al., 2007). A combination of crosstalk, positive and negative feedback loops and multiple response thresholds allows MAPK pathways to dictate cell fate decisions, such as stress-induced apoptosis, by switching between transient and sustained activation (Fey et al., 2012).

Several studies have shown that pathways other than MAPK signalling modules regulate AP-1 transcription factor activity. The inducible transactivation activity of the c-Fos/c-Jun AP-1 complex has also been shown to be reversibly down-regulated by sumoylation (Muller et al., 2000, Bossis et al., 2005). Modification of c-Jun at K229 by the post-translational modifier SUMO-1 moderately reduces transcription factor activity (Muller et al., 2000). Conjugation of c-Fos or c-Jun, at K265 or K257 respectively, by SUMO-1, SUMO-2 or SUMO-3 significantly reduces their transactivation activity. A single sumoylation at any of these 3 lysine acceptor sites within the heterodimer will substantially reduce its activity (Bossis et al., 2005). Interestingly, JNK activation decreases SUMO-1 dependent sumoylation of the K229 residue of c-Jun (Muller et al., 2000).

Overall, MAPK cascades play an important regulatory role in AP-1 signalling, despite not being the lone modulator of their activity. The entire signalling module, from the stimuli, via the MAPK cascade and through to the AP-1 activation or expression is critical in regulating a dynamic cellular response.

1.3.1.2.1 AP-1/MAPK signalling in differentiation

Differentiation of a cell line is common practice in cell biology and allows a more specialised cell type to be obtained compared to an undifferentiated population. Upon differentiation, cells cease proliferating and become a stable population, often with different morphological characteristics, such as extensive neurite outgrowth. Several neuronal cell lines, such as SH-SY5Y and PC12 cells, have been differentiated to obtain a functionally mature neuronal phenotype (Gil et al., 2004, Xie et al., 2010). A range of differentiating protocols utilising varying reagents exist and can direct these cells towards different neuronal phenotypes. Several differentiation-inducing reagents can be used, such as retinoic acid (RA), TPA, brain-derived neurotrophic factor (BDNF) and nerve growth factor (NGF), all of which result in a different phenotype (Xie et al., 2010).

Often more than one differentiating reagent is used sequentially. RA treatment of SH-SY5Y cells followed by BDNF treatment is a common and effective method of differentiation, yielding an almost homogenous population of neuronal-like cells (Encinas et al., 2000). Neurotrophins, such as NGF and BDNF, bind and activate 2 classes of cell surface receptors, the Trk tyrosine kinases and the p75 neurotrophin receptor. NGF preferentially activates TrkA, whereas BDNF preferentially activates TrkB (Kaplan and Miller, 2000). RA has been shown to upregulate neurotrophin receptors, including TrkB, which is critical step in the cell's differentiation (Cernaianu et al., 2008, Esposito et al., 2008).

Expression of *c-Fos* is induced in both *Trkb* transfected fibroblasts (Klein et al., 1991) and primary hippocampal pyramidal neurons (Marsh et al., 1993) by BDNF. In the latter, c-Fos levels peak at around 30-60 minutes after BDNF treatment and return to near basal levels at around 2 hours. Another neurotrophin, NGF, rapidly induces *c-Fos* expression in PC12 cells (Milbrandt, 1986) and activates the ERK cascade in PC12 cells to promote differentiation (Leppa et al., 1998). ERK acts to phosphorylate c-Jun (Ser63 and Ser73 residues) as well as induce its expression, whereas JNK only phosphorylates the transcription factor (Figure 1.8). The fact that ERK appears to play a more prominent role in this c-Jun mediated differentiation is counterintuitive as JNKs are considered a more efficient activator of c-Jun activity. This may again demonstrate how the dynamic capability of IEGs allows for a range of signalling interpretations. Furthermore, c-Jun/AP-1 activity also appears to play a critical role in NGF-induced differentiation in SH-SY5Y cells (Feng et al., 2002).

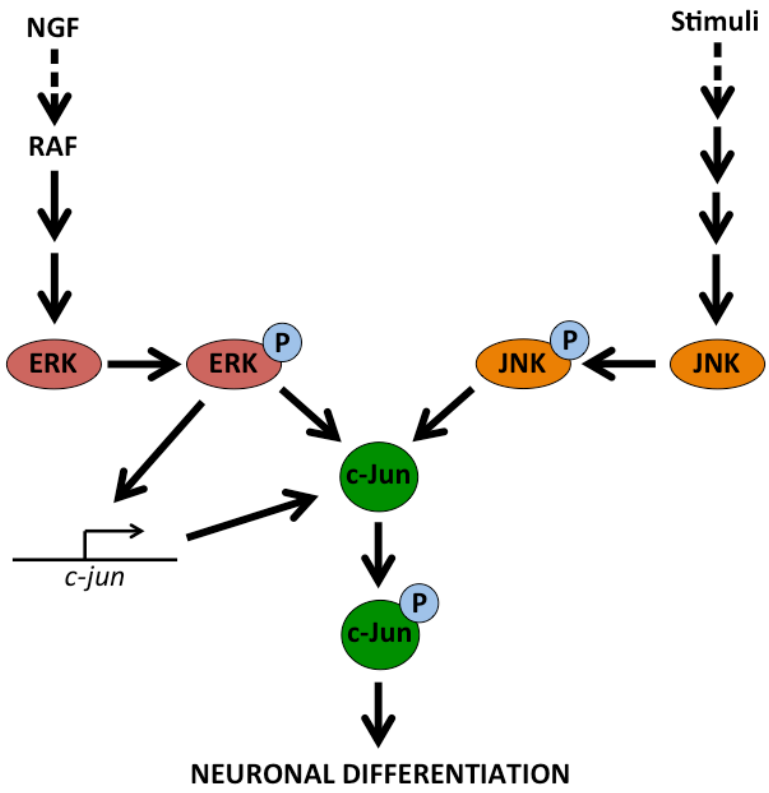

Figure 1.8: Proposed model of JNK/ERK-mediated regulation of c-Jun in PC12 cell differentiation. Based on a model from Leppa et al., 1998. This figure shows how 2 signalling cascades converge upon a common transcription factor. Although both cascades appear to play a role in PC12 differentiation, the ERK pathway seems to play a more prominent part. However, their synergistic effect may also be critical.

c-Jun has opposite functions in undifferentiated and differentiated PC12 cells. In undifferentiated PC12 cells c-Jun protects against MEKK1- and ATF2-mediated apoptosis. The balance between the two AP-1 proteins, c-Jun and ATF2, may be critical in determining whether the cell enters a differentiation or apoptotic program. Conversely, in differentiated PC12 cells apoptotic JNK signalling is mediated by c-Jun. In its differentiation-mediating capacity c-Jun appears to acts as a conventional AP-1 transcription factor. However, c-Jun's interaction with another bZip protein, DNA or JNK is not required for its anti-apoptotic potential in undifferentiated PC12 cells (Leppa et al., 2001).

Cytoplasmic c-Fos has also been shown to play a part in phospholipid synthesis in NIH 3T3 fibroblasts (Bussolino et al., 2001) and PC12 cells (Gil et al., 2004). This cytoplasmic regulatory role is independent of AP-1 activity. c-Fos also

plays a critical role in PC12 differentiation as part of its AP-1 transactivation capability. Gil and colleagues suggest this dual function occurs by c-Fos firstly activating the genomic differentiation program, and then associating with the ER to activate phospholipid synthesis required to sustain the genomically activated neuritogenesis (Gil et al., 2004).

1.3.1.3 The ubiquitin-proteasome system (UPS)

The ubiquitin-proteasome system (UPS) is an essential system by which the cell disposes of proteins. It has a role in a wide-range of processes. The UPS allows the cell to dispose of proteins that may be misfolded, damaged, mutated, mislocated, over-accumulated or simply not required at that particular time (Figure 1.9). The rapid proteolytic degradation controlled by this system provides highly effective cytoprotection, as well as allowing it to act as a rapid molecular switch in a range of signalling pathways.

The elucidation of the multistep process of ubiquitination (or ubiquitylation) won Ciechanover, Hershko and Rose the Nobel Prize in Chemistry in 2004. Ubiquitin is an 8.5kDa protein, which is covalently attached by a peptide bond to a lysine residue within the protein to be degraded by a series of enzymatic reactions (reviewed by McNaught et al., 2001, Lehman, 2009). The polyubiquitin tagging of substrates allows for specificity within this system, thus only selected proteins are degraded (Ravid and Hochstrasser, 2008). There are essentially 2 successive pathways involved in degradation via the UPS. Firstly, the substrate is tagged by multiple ubiquitin molecules. Secondly, ubiquitin is released and recycled and the substrate is degraded by the 26S proteasome.

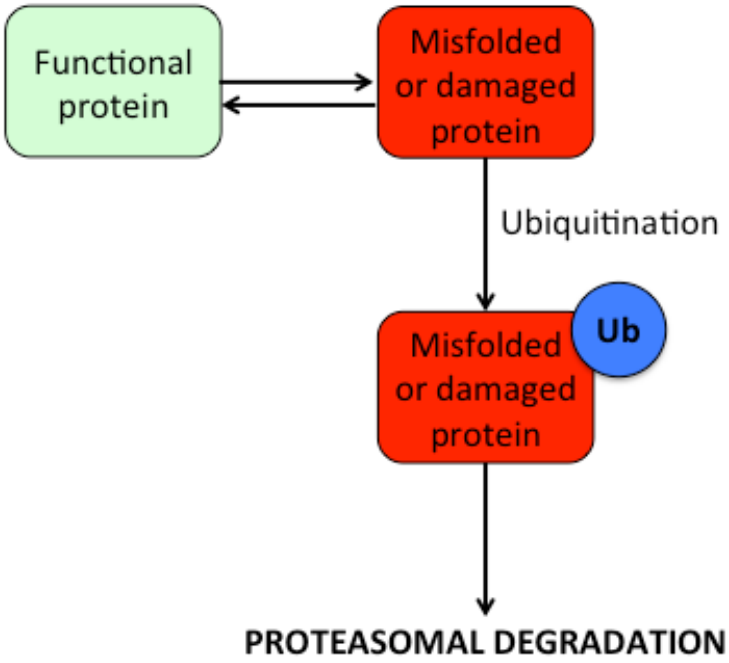

Figure 1.9: Basic overview of the UPS-directed degradation of dysfunctional proteins. This occurs in order to prevent their accumulation. Chaperones may act to "repair" a protein and fold it into its native and functional state.

The process of ubiquitination requires the sequential action of several classes of enzymes called ubiquitin ligases (Figure 1.10). The initial step in this multi-tier cascade involves the activation of ubiquitin by an E1 ubiquitin ligase. This reaction utilises ATP to generate a high-energy thiol ester intermediate in which the ubiquitin molecule is transiently adenylated then bound by its *C*-terminal to the sulfhydryl group of a cysteine residue within the E1 ligase (Haas et al., 1982, Ciechanover and Brundin, 2003, Lehman, 2009). There are only two E1 isoforms (E1a and E1b) of differing molecular weights (110kDa and 117kDa), thus offering limited substrate specificity (Cook and Chock, 1992). Following this, ubiquitin is transferred to the substrate via an E2 ligase (ubiquitin conjugating enzyme (UBC)), by associating with the E3 ligase specifically bound to target protein. However, if the substrate is bound to a HECT domain E3 ligase, a high energy thiol ester E3-ubiquitin moiety intermediate is created prior to the activated ubiquitin being transferred to the target protein.

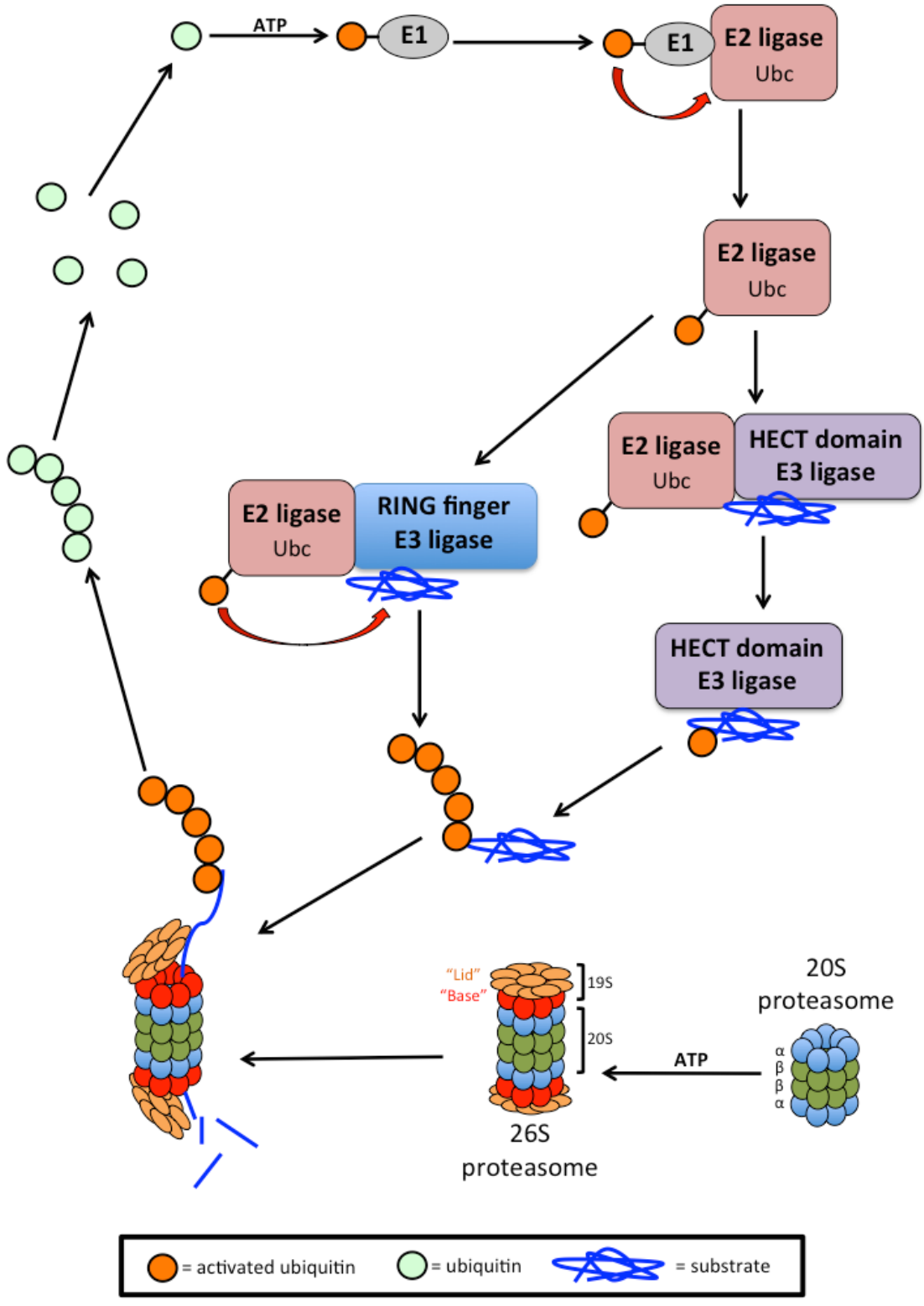

Figure 1.10: The UPS is a multi-faceted system whereby 'labelled' proteins are specifically degraded by the proteasome. Ubiquitin is firstly activated by an E1 ubiquitin ligase and then transferred to a cysteine residue of an E2 ubiquitin conjugating enzyme (Ubc). Phosphorylation is often required for substrate recognition by an E3 protein.

For substrate recognition by the E3 ubiquitin ligase, the target protein is often phosphorylated by a kinase prior to the E3-dependent catalysis of the isopeptide bond between a glycine residue of ubiquitin and a lysine within the substrate. Post-translational modification of the target is generally required as the E3 ligase will not constitutively recognise and label the protein (Ciechanover and Brundin, 2003, Lehman, 2009). Whilst E2 ligases have some specificity (around 50 different E2s identified), E3 ligases are by far the most variable and substrate-specific with over 500 E3s identified to date (Chen et al., 2006, Lehman, 2009). E4 ligases are then responsible for the formation of polyubiquitin chains, which determine the fate of the substrate.

The 19S proteasomal cap recognises the ubiquitin labelled protein and functions to act like a door opening to allow the substrate into the cylindrical chamber of the 20S catalytic core. Furthermore, it is believed that the 19S recognition particle unfolds the substrate to allow it to fit into the 20S core particle, where it is degraded into small peptides. Deubiquitination enzymes (DUBs) function to remove and recycle the ubiquitin monomers used to label the substrate prior to its degradation in the proteasomal core (Koegl et al., 1999, Lehman, 2009, Kirkin et al., 2009).

The multiubiquitination of substrates required for efficient proteasomal targeting is dependent on E4 ubiquitin ligases (Koegl et al., 1999). The type of lysine linkage of these polyubiquitin chains is important in determining the type of degradation a substrate undergoes, with 7 linkages possible within a ubiquitin monomer (K6, K11, K27, K33, K48 and K63) (Ikeda and Dikic, 2008). Proteins labelled with K48 linkages are, in general, degraded by the proteasome, whereas K63 polyubiquitination labels the substrate for lysosomal (autophagic) degradation (Welchman et al., 2005, Tan et al., 2008, Kirkin et al., 2009), although the proteasome has been shown to degrade K63 labelled proteins *in vitro* (Saeki et al., 2009). Excessive protein labelling by K48-linkages may overload the UPS, which leads to the aggregation of ubiquitinated proteins. However, these polyubiquitin chains can be remodelled by the combined action of deubiquitinating enzymes (DUBs) and E3 activity, thus forming K63-linked chains. Through the recognition of these chains by the p62, a polyubiquitin

binding protein, these aggregates are targeted to inclusion bodies called aggresomes, which can be degraded by proteasomal or lysosomal means (Shaid et al., 2013). This occurs via the interaction of the p62 LC3-interacting region (LIR) motif with light chain 3 (LC3), an autophagosomal component marker (Pankiv et al., 2007). Nevertheless, the accumulation of ubiquitinated protein aggregates, a common characteristic of neurodegenerative conditions, can result in the inhibition of the UPS (Bence et al., 2001).

The proteasome is a large protease complex made up of a 20S core particle (2,100 kDa) and a 19S regulatory particle (700 kDa). Usually, the 26S proteasome is comprised of 2 19S subcomplexes capping each end of the barrel-like 20S particle. In general, the 26S proteasome, which is localised to the nucleus, cytosol and perinuclear regions of eukaryotic cells, only recognises modified substrates that have been ubiquitinated. The removal of ubiquitin molecules from the substrate precedes the unfolding of the protein and entry into the proteasome. The 20S complex is the proteolytically active part of the 26S proteasome and is composed of 4 heptameric rings (2 α-rings and 2 β-rings) to form a hollow cylindrical structure. Each of these rings comprises of 7 distinct subunits, each encoded by separate genes. The α-rings cap either side of both of the 2 β-rings, which provide the 3 types of catalytic sites on the inner surface of the cylinder-like structure. These provide the hydrolytic activity for the carboxyl terminus of hydrophobic, acidic and basic amino acids within proteins targeted to the proteasome. The α-rings provide an anchor for the 19S complex to bind to the 20S proteasome. The 19S complex is comprised of at least 17 subunits with 6 of these being ATPases. The addition of the 19S cap facilitates the opening of a channel through the proteolytic core, as well as allowing the ATPase-dependent unfolding of ubiquitinated proteins by the 19S complex in order for them to pass into the 20S catalytic centre. Two of the subunits within the 19S regulatory particle have been identified as ubiquitin binding proteins, which allow the recognition of substrates labelled for degradation (reviewed by McNaught et al., 2001, Ciechanover and Brundin, 2003, Lehman, 2009).

1.3.1.4 Autophagy

Proteasomal and autophagic degradation are two processes that can be linked. Furthermore, both are highly regulated systems that can result in specific pathogenic phenotypes when perturbed or deregulated. Autophagy is a catabolic process by which cellular components are engulfed by double membrane structure called an autophagosome. This then fuses with a lysosome, resulting in the degradation of cargo and inner membrane. Both non-selective and selective autophagy occurs. Furthermore, 3 forms have been identified that differ in terms of their cellular function and cargo delivered to the lysosome for degradation. These forms are chaperone-mediated autophagy, microautophagy and macroautophagy. During starvation, cells can gain metabolic precursors by the non-selective degradation of cytosolic contents via autophagy. However, cargo-specific autophagy occurs under nutrient-rich conditions to remove potentially cytotoxic components, such as protein aggregates or damaged organelles (Youle and Narendra, 2011).

Autophagy occurs at basal levels in nearly all cells to maintain homestasis in a number of respects. It can also be rapidly upregulated or downregulated by multiple signalling pathways. The process of autophagy can be broken down and summarised into 4 sequential stages: vesicle nucleation, vesicle elongation and closure, docking and fusion of the autophagosome with the lysosome and finally degradation of the contents within the autolysosome (Levine and Kroemer, 2008). The correct function of these steps is key for roles such as neuroprotection, making it a highly studied process in neurodegenerative research (Nedelsky et al., 2008). The initial step involves the formation of the isolation membrane or phagophore. This then proceeds to become elongated and eventually fuses to form a double membrane vesicle known as an autophagosome, which contains the cargo to be degraded. A lysosome, a membrane-bound organelle containing hydrolytic enzymes, then fuses with the autophagosome and lyses the inner membrane and the contents within the vesicle.

The process of autophagy is often considered an adaptive process by which the cell attempts to resolve stress, thus supressing apoptosis. However, the reality

is likely to be more complex than this. Under certain conditions autophagy may act as a separate cell death pathway (Maiuri et al., 2007), so in certain paradigms the inhibition of autophagy induces apoptosis. An example of this can be seen from the knockout of the autophagy-essential gene *Atg7* in mice, which results in neuronal loss and eventual death due to autophagy deficiency within the brain (Komatsu et al., 2006). The neuronal accumulation of intracellular protein inclusions observed in the *Atg7* knockouts also occurs in *Atg5*-deficient mice (Hara et al., 2006) suggesting any perturbation of autophagy may lead to neurodegeneration. Conversely, autophagy can essentially kill a cell by either inducing pro-apoptotic signalling or by excessive autophagy resulting in irreversible cellular atrophy. These are termed type I or II cell death, respectively (Maiuri et al., 2007). Transgenic overexpression of *atg1* in *Drosophila* led to excessive autophagic activity followed by caspase-dependent cell death that could be rescued by *atg3* or *atg8a* deletion (Scott et al., 2007). This represented the first *in vivo* example of autophagy as an apoptotic trigger.

AP-1 transcription factors are major regulators of a number of key cellular processes, yet to date very little data has been presented on their role in autophagy. However, MAPKs are a much more studied area, although their role in signalling via certain AP-1s remains relatively unclear. Although the mammalian target of rapamycin (mTOR) is considered a major regulator of autophagy, by acting as a potent inhibitor, there are multiple pathways by which autophagy is controlled (Meijer and Codogno, 2006). It is therefore likely that further study of MAPK/AP-1 pathways in autophagic regulation could provide insightful and novel information into autophagy under stress conditions.

During starvation, JNK1, but not JNK2, is capable of inducing autophagy, independent of AP-1 signalling via phosphorylation of Bcl2, thus dissociating it from Beclin 1 (Wei et al., 2008). Both c-Jun and JunB act as autophagic inhibitors, thus their expression is decreased upon low nutrient conditions to allow the induction of starvation-induced autophagy. Moreover, c-Jun acts independent of JNK activity to inhibit autophagy (Yogev et al., 2010). The mitochondrial outer membrane (MOM) contributes to autophagosomal

membrane biogenesis during starvation, but not ER stress (Hailey et al., 2010). It is yet to be determined whether the MOM is involved in other forms of stress-induced autophagy. In contrast, in mice the ablation of all three *Jnk* genes demonstrates that JNK acts to suppress FoxO-dependent autophagy in neurons (Xu et al., 2011). Here it appears JNK acts not only to inhibit FoxO-induced autophagy-related gene expression but also to induce expression of proapoptotic genes. Therefore, JNK inhibition may offer neuroprotection and increased autophagy. However, another study found that oxidative stress activates JNK/AP-1 signalling in pre- and postsynaptic compartments along with autophagy in *Drosophila* (Milton et al., 2011). Although autophagy acts as a protective mechanism to degrade damaged proteins and organelles, it was also found to be required, along with JNK/AP-1 signalling, to induce synaptic overgrowth.

1.3.1.5 Mitophagy

Mitochondria are the major intracellular source of ROS, with the production of this cytotoxic by-product increasing exponentially if a mitochondrion is dysfunctional (Wallace, 2005). Mitophagy is the regulated and selective autophagic removal of damaged mitochondria in order to prevent their accumulation and resulting cytotoxic ROS production. Under normal conditions, PTEN-induced kinase 1 (PINK1), a serine/threonine kinase, is constitutively imported into mitochondria and degraded by mitochondrial proteases, thus undergoing voltage-dependent proteolysis. Upon mitochondrial depolarisation, rapid MOM accumulation of PINK1 is observed (Narendra et al., 2010b). Following mitochondrial damage, the E3 ubiquitin ligase, Parkin, is recruited to these mitochondria in a PINK1-dependent manner (Narendra et al., 2008).

The E3 ubiquitin ligase activity of Parkin is supressed in the cytoplasm under conditions of proper mitochondrial function. However, the stabilisation of PINK1 on the MOM leads to the recruitment of Parkin and its subsequent activation (Matsuda et al., 2010) (Figure 1.11). Upon their interaction Ser65 on Parkin is phosphorylated by PINK1, a critical step to activate Parkin's E3 activity and induce its mitochondrial translocation (Kondapalli et al., 2012, Okatsu et al., 2012, Shiba-Fukushima et al., 2012). Furthermore, a more recent study found

that PINK1 directly phosphorylates ubiquitin, which in turn activates Parkin, thus suggesting PINK-dependent phosphorylation of both ubiquitin and Parkin may be required for complete activation of E3 ligase activity (Koyano et al., 2014). This PINK1/Parkin activity leads to the collapse of the normal mitochondrial network and the modulation of mitochondrial trafficking to the perinuclear region (Vives-Bauza et al., 2010).

In recent years the structure of the 465-residue protein Parkin has been elucidated. Parkin contains 2 RING motifs linked together by a cysteine-rich in-between-RING (IBR) motif. At the *N*-terminal region is a ubiquitin-like domain (UBL) followed by a Zn^{2+} coordinating motif (RING0) (Hristova et al., 2009) that interacts with PINK1 (Xiong et al., 2009) (Figure 1.12a). The UBL domain shares 30% sequence identity with human ubiquitin and functions to inhibit Parkin autoubiquitination (Chaugule et al., 2011). A recent study to determine the crystal structure of a proportion of inactive Parkin has allowed for a hypothetical explanation of the autoinhibition of Parkin activity (Wauer and Komander, 2013). The authors propose a two-fold autoinhibitory mechanism whereby E2 ligase access to RING1 and RING2 regions is blocked by the linker helix between the IBR and RING2 and the RING0 region, respectively (Figure 1.12b). In the autoinhibited conformation, the active Cys85 residue of the E2 enzyme and the active Cys431 residue within the RING2 domain of Parkin is separated by 54Å. In order for full Parkin activation to occur both interactions must be released.

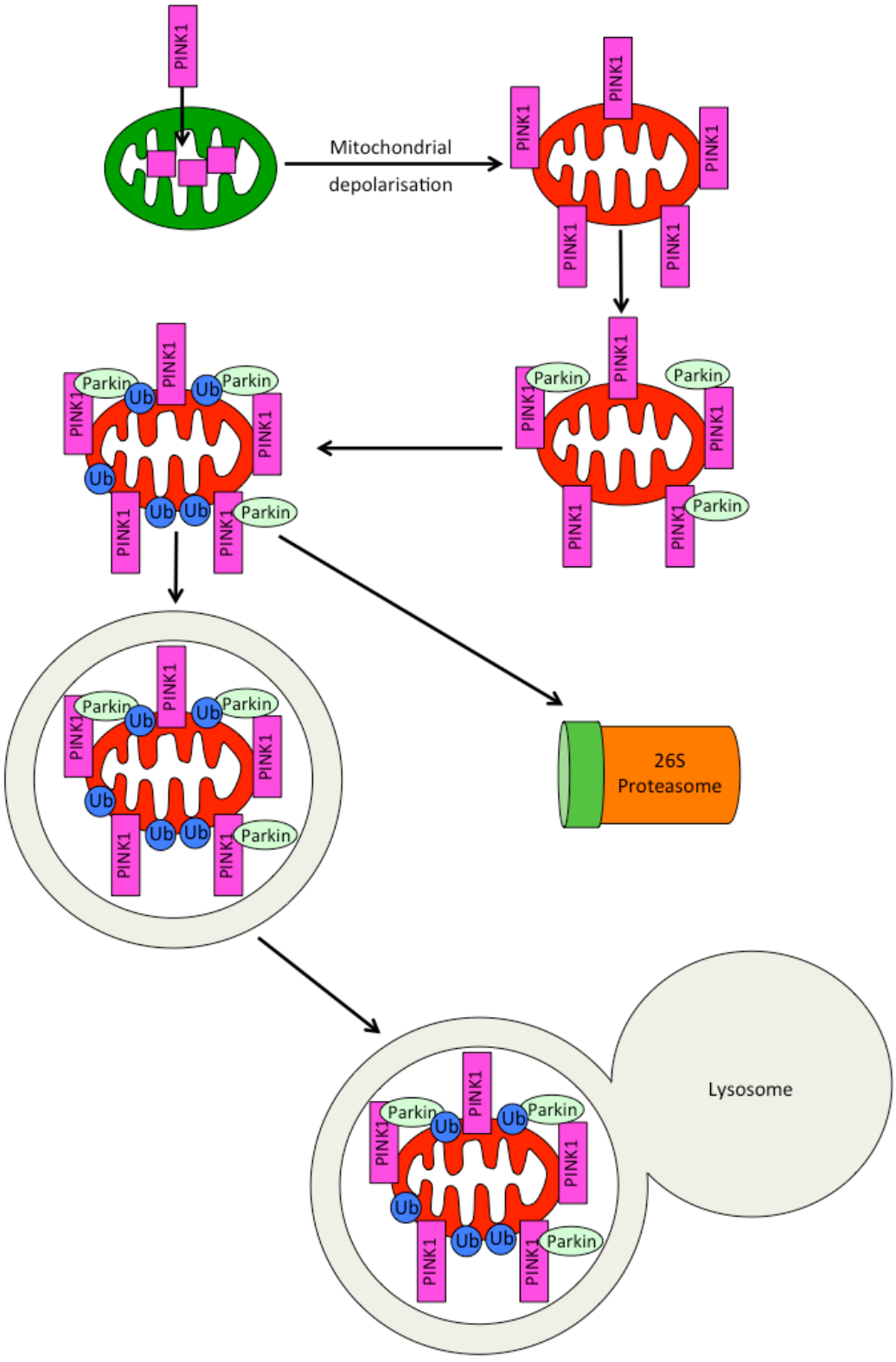

Figure 1.11: **An overview of mitophagy.** Mitophagy is a highly regulated process by which the cell removes dysfunctional mitochondria to prevent their accumulation. Both proteasomal and autophagic degradation play key roles in mitophagy.

Interactions between Parkin and several E2 ligases have been shown to occur, with the interaction with the UbcH13/Uev1a E2 heterodimer believed to catalyse the formation of K63-lined polyubiquitin chains (Olzmann et al., 2007). Parkin activation subsequently leads to the polyubiquitination of multiple MOM proteins leading to the recruitment of p62/SQSTM1, a ubiquitin-binding autophagy adaptor protein, to these damaged organelles. Although one study found p62/SQSTM1 to be required for PINK1/Parkin-directed mitophagy in both neuronal and non-neuronal cells, with PD-linked mutations perturbing this (Geisler et al., 2010), other data has inferred that this protein is only required for Parkin-dependent mitochondrial perinuclear clustering but not mitochondrial degradation (Narendra et al., 2010a, Okatsu et al., 2010). It appears that the p62/SQSTM1-mediated aggregation of damaged mitochondria occurs via the protein's *N*-terminal PB1 domain, a process abolished in mouse embryonic fibroblasts (MEFs) expressing a mutation within this domain (Narendra et al., 2010a). The MOM voltage-dependent anion channel 1 (VDAC1) was identified as a target for Parkin-dependent Lys27 polyubiquitination and suspected as being critical for mitophagy (Geisler et al., 2010).

Many model systems have been used to study mitophagy. In SH-SY5Y neuroblastoma cells, mitofusin (MFN) 1 and 2 are rapidly ubiquitinated in a PINK1/Parkin-dependent manner following CCCP-induced mitochondrial depolarisation (Gegg et al., 2010). In mice Mfn2, but not Mfn1, is phosphorylated by PINK1 and acts as a receptor for Parkin to translocate from the cytosol to a damaged mitochondrion in order to initiate mitophagy (Chen and Dorn, 2013). Furthermore, PINK1 activity is also required to phosphorylate ubiquitin (Ser65) in order to activate Parkin E3 ligase activity (Kane et al., 2014, Koyano et al., 2014), making PINK1 the first ubiquitin kinase identified to date.

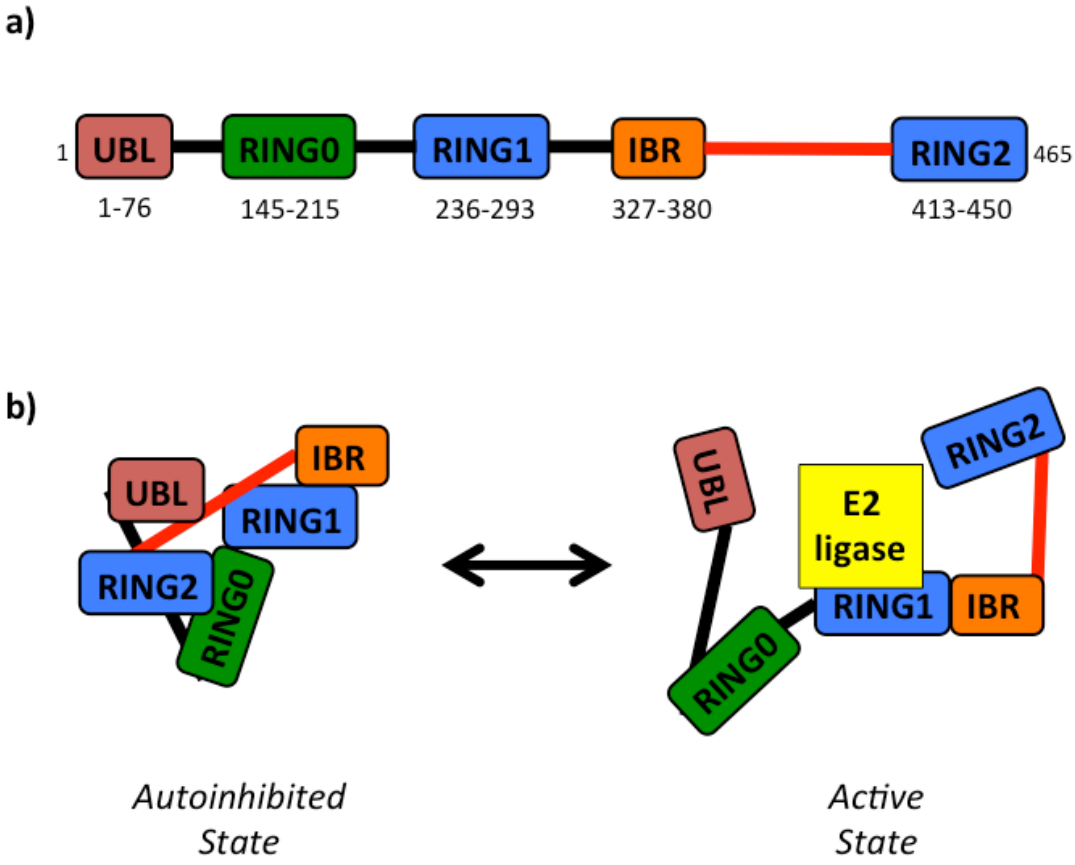

Figure 1.12: The structure of Parkin. (a) Schematic of Parkin domain structure. (b) A schematic representation combining two hypothetical models suggesting how Parkin activity is regulated at the structural level. The UBL domain acts as an autoinhibitory module by occluding the ubiquitin binding site in the *C*-terminal region (Chaugule et al., 2011). The linker helix (red) blocks E2 ligase access to the catalytic residue (Cys431) within the RING2 domain (Wauer and Komander, 2013).

Mitochondria are mobile organelles, a process critical to neurons in which they must move along long axons and dendrites to ensure energy production occurs where required. This dynamic regulation allows for changing energy requirements of a specific cell region to be met, albeit limited by the speed of mitochondrial transport. It has long been established that mitochondrial motility is vigorous in both axons and dendrites, although to a much greater degree in the former (Overly et al., 1996). Mitochondrial transport is highly dynamic, with motility in both directions and arrest regularly occurring (Hollenbeck and Saxton, 2005, Chang et al., 2006). Movement along microtubules is facilitated by both kinesin (anterograde transport towards the (+) end of microtubules at the cell

periphery) and dynein (retrograde transport towards the (-) end of microtubules in the cell body) motors, whereas translocation observed along actin filaments is likely to be driven by myosin V (Hollenbeck and Saxton, 2005).

Kinesin-1 is the major anterograde motor for mitochondrial translocation and is dependent on the formation of a motor/adaptor complex comprised of the kinesin heavy chain (KHC) binding to Milton, which is linked to the mitochondrion via Miro, a transmembrane MOM protein (Glater et al., 2006). Ca^{2+} signalling is one regulatory mechanism for mitochondrial transport, with the two Ca^{2+}-binding EF-hand motifs of Miro mediating the arrest of a mitochondrion by the motor domain of kinesin-1 binding to Miro, thus preventing its interaction with the microtubule (Wang and Schwarz, 2009).

Unlike in other cells, neuronal mitochondria largely reside along axons and dendrites far from the cell body where lysosomes localise. Although some studies have suggested damaged mitochondrial undergo retrograde transport towards lysosome in the soma (Miller and Sheetz, 2004, Cai et al., 2012) it would be counterintuitive to move a dysfunctional mitochondrion producing cytotoxic ROS along a neurite. Another study reported mitochondrial damage in hippocampal neurons leads to PINK1-dependent phosphorylation of Miro, which is then ubiquitinated by Parkin and degraded by the proteasome (Wang et al., 2011). This in turn results in the arrest of mitochondrial motility. Although this arrest occurs within minutes of damage along with the Parkin-dependent Lys27 ubiquitination of Miro, the proteasomal degradation of Miro occurs 2-3 hours later (Birsa et al., 2014). This may suggest that the ubiquitination, and not the degradation of Miro, is responsible for mitochondrial *in situ* arrest. A recent breakthrough study using hippocampal cells demonstrated the local PINK1/Parkin-dependent degradation of damaged mitochondrial within distal neuronal axons (Ashrafi et al., 2014). By inducing damage selectively in a subset of mitochondria using the light-induced activation of mitochondrial-targeted mitochondrial KillerRed (mt-KR) the rest of the mitochondrial network could be maintained. Activation of mt-KR by a laser resulted in ROS-mediated damage of the mitochondrion in which it was activated and induced the rapid recruitment of Parkin in a PINK1-dependent fashion. Interestingly, damaged

mitochondria underwent arrest and LC3-positive autophagosomes formed locally to engulf them. Furthermore, axonal lysosomes were recruited to mitochondrion-containing autophagosomes in order to mediate mitochondrial degradation. This study provided a step forward in our understanding of mitophagy and indicated a much more efficient process occurring compared to the transport of damaged mitochondria back to the soma for degradation.

As well as regulating mitophagy, Parkin has other functions independent of this process, such as MAPK regulation. Parkin is capable of binding microtubules via any of 3 domains (linker region, RING1 or RING2) (Yang et al., 2005). Each of these domains acts to attenuate JNK, ERK and p38 activation in response to microtubule destabilising agents, such as colchicine, although this ability is lost in cells derived from PD patients with *PARKIN* mutations resulting in the deletion of exon 4 (Ren et al., 2009).

1.4 PARKINSON'S AND CELLULAR DYSUNCTION

1.4.1 Subcellular stress in PD

PD, like many other neurodegenerative conditions, is associated with multiple forms of stress and the failure of both intra- and intercellular regulatory/cytoprotective mechanisms. Importantly, PD is a progressive disorder thus the pathological development observed in patients occurs over a number of years. Therefore, the accumulation of stress over this period indicates how the failure and/or inability of the cytoprotective neuronal responses to deal with these problems is a chronic occurrence. PD is characterised by the loss of dopaminergic neurons. Nevertheless, this is a highly complex, multi-faceted disease with a wide range of causes, many of which are yet to be identified or properly characterised, and so it is likely that many of the pathological intracellular signalling pathways modulated are unique to specific forms of PD. This makes it vital to identify shared pathologies between these forms, and if possible any crossover between other neurodegenerative conditions.

1.4.1.1 Oxidative stress and mitochondrial dysfunction in PD

Mitochondria are the main source of intracellular oxidative stress. As excessive ROS can damage the mitochondria these 2 forms of stress are heavily linked. To maintain mitochondrial homeostasis within a cell both mitochondrial dynamics and mitophagy are critical, with the perturbation of these processes leading to diseases such as PD. Mitochondrial dynamics refers to a balance between the processes of fusion and fission. In mammals, mitochondrial fusion is largely mediated by the MOM proteins MFN1, MFN2 and OPA1 whereas fission is mediated by DRP1, FIS1 and MTP18 (reviewed by Liesa et al., 2009). In neurons, the mitochondrial network will be constantly experiencing fusion and fission. Fusion of a damaged mitochondrion with a healthy mitochondrion may serve to 'dilute' the damage and prevent any excessive cytotoxic species production. On the other hand, a depolarised mitochondrion is a target for mitophagy, thus will be permanently removed from the mitochondrial network (Twig and Shirihai, 2011). In neurons it may be that a partly damaged mitochondrion will undergo fusion or fission but a heavily damaged one will be mitophagically removed. In this way the cell only loses the valuable organelle if absolutely necessary. The perturbation of mitophagy is heavily linked with PD; however, breakdown in the interplay between mitophagy and mitochondrial dynamics may play just as much of an important role in the pathogenesis of the disease.

The overall makeup of A9 dopaminergic neurons ensure these cells not only require massive amounts of mitochondrial activity, but they are also more susceptible and less equipped to deal with the cytotoxicity brought about by dysfunctional mitochondria (Figure 1.13) (Lu, 2011). Nigral dopaminergic neurons demonstrate massive arborisation compared to other neurons (Matsuda et al., 2009). Further characteristics such as higher basal levels of oxidative stress and oxidative phosphorylation, as well as greater axonal mitochondrial density, all due to increased bioenergetics demands, provides an explanation for the specific neurodegeneration of dopaminergic cells in the SNpc witnessed in PD (Pacelli et al., 2015). Intriguingly, Pacelli et al show that by reducing axonal arborisation the bioenergetic demands of these neurons is decreased, thus reducing oxidative phosphorylation. This in turn reduces their

sensitivity to both 1-methyl-4-phenyl-pyridium ion (MPP^+) and rotenone, both of which induce cellular oxidative stress.

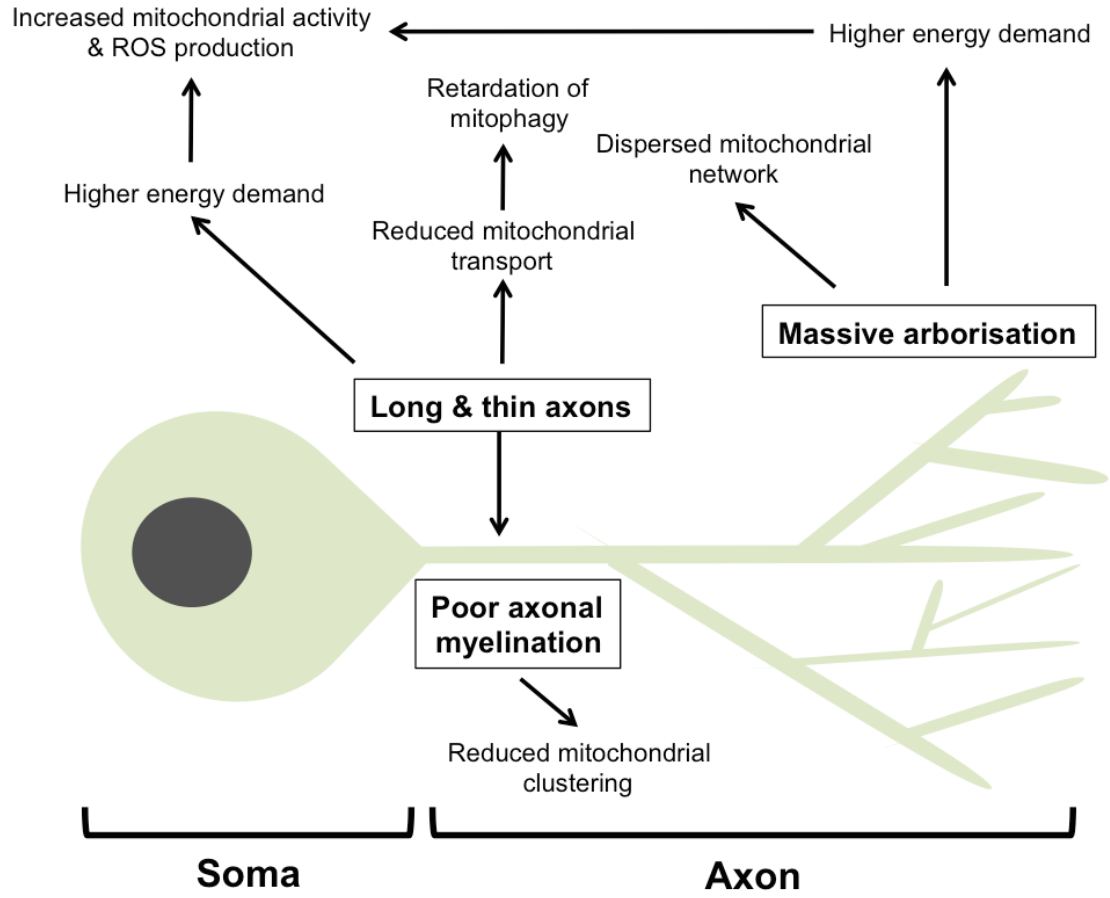

Figure 1.13: A9 dopaminergic neurons – "the perfect storm" for disruptions in mitochondrial dynamics, motility and mitophagy. The characteristics of these neurons make them inherently susceptible to mitochondrial dysfunction and aberrant ROS production.

1.4.1.2 PINK1/Parkin-mediated mitophagy in PD

Parkin mutations are the most common cause of autosomal-recessive forms of Parkinsonism (Kitada et al., 1998, Scarffe et al., 2014). It has also recently been implicated in the response to stress observed in AD (Ye et al., 2015). Despite mitophagy still being far from fully understood, the requirement of PINK1 and Parkin for the maintenance of a fully functional mitochondrial network has been appreciated for over a decade and has been studied in a range of models. Much work has been done using *Drosophila* to model *pink1/parkin* deficiencies and mutations. *Drosophila parkin* null mutants exhibit apoptotic muscular

degeneration leading to locomotor defects and male sterility (Greene et al., 2003). The authors found mitochondrial defects, such as cristae disintegration, to be a common characteristic across the different cell types. The loss of a specific set of dopaminergic neurons in *Drosophila* can be rescued by the overexpression of glutathione-*S*-transferase, an enzyme implicated in the oxidative stress response (Whitworth et al., 2005), suggesting excessive ROS production by unregulated mitochondria may cause this neuronal loss. The translocation of parkin from the cytosol to mitochondria in *Drosophila* is dependent on pink1 (Ziviani et al., 2010), with loss-of-function *pink1* mutants displaying similar phenotypes to *parkin* mutants, such as dopaminergic degeneration and locomotive defects (Park et al., 2006). Loss of pink1 function results in a similar phenotype to *parkin* mutants, although attenuation of pink1 function can be rescued by the overexpression of human *PARKIN* and its *Drosophila* orthologue, but not DJ-1 (Clark et al., 2006, Yang et al., 2006).

In PD patient-derived fibroblasts with *PARKIN* mutations, ATP synthesis was reduced (Grunewald et al., 2010), with decreased complex I activity and greater mitochondrial branching also being observed relative to controls (Mortiboys et al., 2008). Moreover, *parkin* knockdown zebrafish (*Danio rerio*) also demonstrate reduced mitochondrial complex I activity (Flinn et al., 2009). *Pink1*$^{-/-}$ mice show a decrease in mitochondrial respiration within the cerebral cortex at 2 years old and are more sensitive to H_2O_2 induced- oxidative stress (Gautier et al., 2008). RNAi has demonstrated that *PINK1* is required for long-term viability of human dopaminergic neurons. These cells display hallmarks of both oxidative and mitochondrial stress and enter apoptosis (Wood-Kaczmar et al., 2008). It is clear from studies in multiple models that the role of Parkin and PINK1 in maintaining mitochondrial integrity and certain antioxidant capabilities is highly conserved, explaining why the perturbation of their function can lead to degenerative diseases.

The p62/SQSTM-dependent aggregation of dysfunctional mitochondria requires Parkin activity as the pathogenic mutant R275W, found in some PD patients, does not promote this clustering in HeLa cells treated with CCCP (Narendra et al., 2010a). Other PD-linked mutations also failed to initiate any significant

mitophagic degradation in MEFs treated with CCCP. However, the 4 mutants observed had distinct phenotypes upon mitochondrial depolarisation in terms of where mitophagy is perturbed. The UBL-domain mutant, R42P, is not recruited to damaged mitochondria. The E3 ubiquitin ligase-deficient mutants T240R (RING1 domain) and T415N (RING2 domain) are recruited and induce mitochondrial aggregation but not mitochondrial degradation whereas R275W (RING1 domain), although localised to dysfunctional mitochondria, did not mediate aggregation (Lee et al., 2010).

It has been suggested that poor mitochondrial transport along A9 dopaminergic neuron axons perturbs efficient mitophagy of damaged mitochondria thus contributing towards PD pathogenesis (Lu, 2011). However, with more recent evidence suggesting that mitophagy can occur *in situ* within axons and does not require transport back to a somal lysosome this hypothesis may not hold as much sway as originally suggested (Ashrafi et al., 2014). Nevertheless, compromised lysosomal capacity in A9 dopaminergic neurons suggested by vesicles containing high levels of lipofuscin and neuromalinin, a consequence of high ROS levels from mitochondria and dopamine metabolism (Lu, 2011), may offer some explanation to the sensitivity of these cells to mitochondrial dysfunction. Functional lysosomes are critical for effective mitophagy (Figure 1.11) and so the fact these cells inherently exhibit reduced lysosomal capacity will no doubt contribute to the ineffective clearance of autophagosomes containing dysfunctional mitochondria.

Several studies suggest interplay between Parkin and the 26S proteasome. Proteasomal activity is required for Parkin-mediated mitophagy with proteasomal subunits colocalising with mitochondria upon CCCP treatment (Chan et al., 2011). Furthermore, the *N*-terminal UBL domain of Parkin is required for the activation of the proteasome, but this is independent of Parkin's E3 ubiquitin ligase activity (Um et al., 2010). The R42P Parkin mutant, a PD-linked mutation, abrogates its ability to activate the proteasome. Parkin activity is also modulated by post-translational modification. The tyrosine kinase, c-ABL, phosphorylates Parkin in order to inhibit its E3 ubiquitin ligase activity (Imam et al., 2011, Ko et al., 2010). We have recently shown that the proteasome can

regulate Parkin activity through a feedback loop via the c-ABL-mediated phosphorylation and inactivation of Parkin at Tyr143 (Roper, 2015). In addition, AP-1 can be both activated and itself activate c-ABL and the JNK pathway (Barila et al., 2000). However, the regulation of mitophagy is further complicated by the recent demonstration that the activating molecule in Beclin-1-regulated autophagy 1 (AMBRA1) can interact with the autophagosome adapter LC3 and induce mitophagy independent of Parkin (Strappazzon et al., 2015). The dysregulation of any of these pathways or processes may therefore result in the aberrant mitophagic clearance of damaged mitochondria observed in PD.

As previously described, Parkin function encompasses cellular processes other than mitophagy. Under stress conditions sufficient to induce apoptosis, the proapoptotic protein Bax translocates from the cytosol to mitochondria in order to induce cytochrome *c* release (Gross et al., 1998). Parkin increases the threshold at which cytochrome *c* is released from mitochondria (Berger et al., 2009), probably by its ability to prevent the stress-induced recruitment of Bax to mitochondria (Charan et al., 2014).

Parkin is generally considered a cytoprotective protein and to promote neuronal survival. However, more recent data has suggested that PINK1/Parkin signalling can promote apoptosis under conditions of excessive mitochondrial depolarisation (Carroll et al., 2014). This suggests Parkin may act as a sensor of cell stress and that its role in the mitochondrial stress response may be more complex than originally thought. Further study by this group has also revealed that pro- and antiapoptotic factors regulate Parkin function in mitophagy (Hollville et al., 2014). The authors demonstrate that the translocation of Parkin to mitochondria is inhibited by prosurvival Bcl-2 proteins. These proteins bind to PINK1/Parkin in order to prevent MOM protein ubiquitination and initiation of mitophagy. Moreover, apoptotic BH3-only proteins (BIM, PUMA, BAD and NOXA), as well as the BH3-only mimetic ABT-737, enhance recruitment of Parkin to mitochondria post-CCCP treatment. This could suggest that Bcl-2 proteins regulate the threshold of mitochondrial stress by which Parkin targets dysfunctional mitochondria for removal. However, in cases where excessive/irreversible damage to the mitochondrial network or other parts of the

cell has occurred, Parkin may assist in the induction of apoptosis alongside BH3-only proteins.

Other data has suggested a similar hypothesis in which Parkin acts as 'molecular switch' or sensor in order to mediate cell fate decisions between repair, mitophagy or apoptosis. Although different levels and types of stress were shown to activate the PINK1-Parkin pathway, apoptotic induction from this pathway only occurred upon Parkin-dependent ubiquitination of the antiapoptotic protein MCL-1 and the activation of the caspase cascade in response to an apoptotic insult (Zhang et al., 2014a). This apparent apoptotic capability of Parkin may therefore offer some explanation as to why the overexpression of WT Parkin, but not non-functional mutants, results in increased sensitivity to mitochondrial depolarisation (Morrison et al., 2011).

1.4.1.3 Protein aggregation and Lewy bodies

The accumulation of ubiquitin-positive inclusions is a common pathological characteristic of several neurodegenerative diseases such as Parkinson's, Alzheimer's and frontotemporal dementia (FTD) (Ramanan and Saykin, 2013). In PD α-synuclein can form highly insoluble cytoplasmic aggregates called Lewy bodies, as well as forming accumulations in neuronal extensions called Lewy neurites. Furthermore, these inclusions contain high levels of phosphorylated and ubiquitinated α-synuclein and are associated with the neuronal loss observed in PD (Kuzuhara et al., 1988, Spillantini, 1999, Galvin et al., 2001, Fujiwara et al., 2002, Hasegawa et al., 2002, Wakabayashi et al., 2007).

The dominant mutations in *SNCA* causing early-onset PD, A30P and A53T accelerate aggregation compared to the WT form (Narhi et al., 1999). However, despite having similar abilities to oligomerise in living cells, different mutations have different propensities to form inclusions (Lazaro et al., 2014). The UPS and autophagy pathways are responsible for the removal of these aggregates (Rubinsztein, 2006). However, α-synuclein aggregates are highly stable and perturb autophagosome maturation, thus preventing their autophagic degradation (Tanik et al., 2013).

1.4.1.4 AP-1 and MAPK signalling in PD

AP-1 proteins are key regulators of many cellular processes, including stress response pathways. This AP-1 signalling was initially implicated in the response to neuronal injury nearly 3 decades ago when *c-Fos* expression was rapidly and transiently induced *in* vivo in neurons after treatment with the convulsant Metrazole. However, pre-treatment with anti-convulsant compounds abolished this induction (Morgan et al., 1987). Furthermore, meta-analysis revealed AP-1 to be associated with AD- and PD-associated genes (Ramanan and Saykin, 2013).

In both post-mortem brain samples from human PD patients and mice treated with MPTP, increased activation of c-Jun has been detected (Hunot et al., 2004). Adenoviral-mediated expression of a dominant negative form of c-Jun attenuates both c-Jun phosphorylation and axotomy-induced dopaminergic neuronal death *in vivo* (Crocker et al., 2001). CEP11004, a MLK inhibitor, suppressed the increased expression and Ser73-phosphorylation of c-Jun associated with the 6-hydroxydopamine (6-OHDA) PD rat model. This inhibition resulted in the suppression of dopaminergic neuron apoptosis in the SNpc (Ganguly et al., 2004).

In *Drosophila* JNK/AP-1 signalling appears to play a major role in the cellular response to oxidative stress (Milton et al., 2011). ROS-activated JNK signalling protects *Drosophila* from oxidative stress by inducing autophagy via transcriptionally regulating (autophagy-related genes) ATGs (Wang et al., 2003, Wu et al., 2009). The *Drosophila* homologue of Fos, D-fos, appears to mediate oxidative stress-induced synaptic overgrowth, a phenotype of lysosomal storage disease, together with JNK signalling (Milton et al., 2011). Interestingly, D-fos is able to homodimerise unlike its mammalian homologue (Collins et al., 2006), suggesting their signalling and transactivation capacities may differ significantly. This must therefore be taken into account when applying “read-across” between different models in order to develop a hypothesis based around MAPK/AP-1 signalling.

JNK cascades have been extensively linked to stress signalling in PD (Peng and Andersen, 2003). To date there is some limited evidence for crossover between Parkin activity and JNK/AP-1 signalling. Parkin E3 activity has been shown to inhibit the phosphotransferase activity of JNK in both dopaminergic neurons of *Drosophila* and the COS1 mammalian cell line (Cha et al., 2005) although no direct interaction was demonstrated. Increased JNK activity in Parkin mutants may therefore be due to increased dysfunction within the mitochondrial network. Critically, this study did not assess which specific JNK isoform(s) the Parkin mutant affects and whether other mutations can have an agonistic or antagonistic effect on JNK activity. A later study found that mRNA levels of *bsk*, a *Drosophila* JNK homologue, were reduced in *parkin* overexpressing animals, which in turn reduced JNK signalling (Hwang et al., 2010). Furthermore, the expression of the kinesin motor *Eg5* is repressed by Parkin-mediated inactivation of the JNK/c-Jun pathway (Liu et al., 2008). Parkin acts to block c-Jun binding to the *Eg5* promoter along with inactivating JNK, thus reducing c-Jun phosphorylation.

PARKIN expression is induced by both ER and mitochondrial stress with this upregulation being mediated by the transcription factor ATF4 (Bouman et al., 2011) which provides cytoprotection in PD models via the increased expression of *PARKIN* (Sun et al., 2013). Interestingly, Sun et al. show that despite *PARKIN* mRNA levels increasing after treatment with 6-OHDA or MPP+, protein levels decrease. Furthermore, c-Jun can bind the CREB site within the *PARKIN* promoter region that ATF4 binds to in order to competitively inhibit ATF4-mediated upregulation of *PARKIN*, thus acting as a transcriptional repressor (Bouman et al., 2011). Importantly, it was also shown that the JNK pathway negatively regulates *PARKIN*, with this repression being reversed, even under stress conditions, by JNK inhibition. Bouman et al. propose a model (Figure 1.14) by which *PARKIN* is upregulated under stress conditions. However, upon excessive or prolonged stress JNK/c-Jun signalling gains the upper hand, represses *PARKIN* expression, thus preventing its cytoprotective capabilities, and pushes an irreversibly damaged cell towards apoptosis.

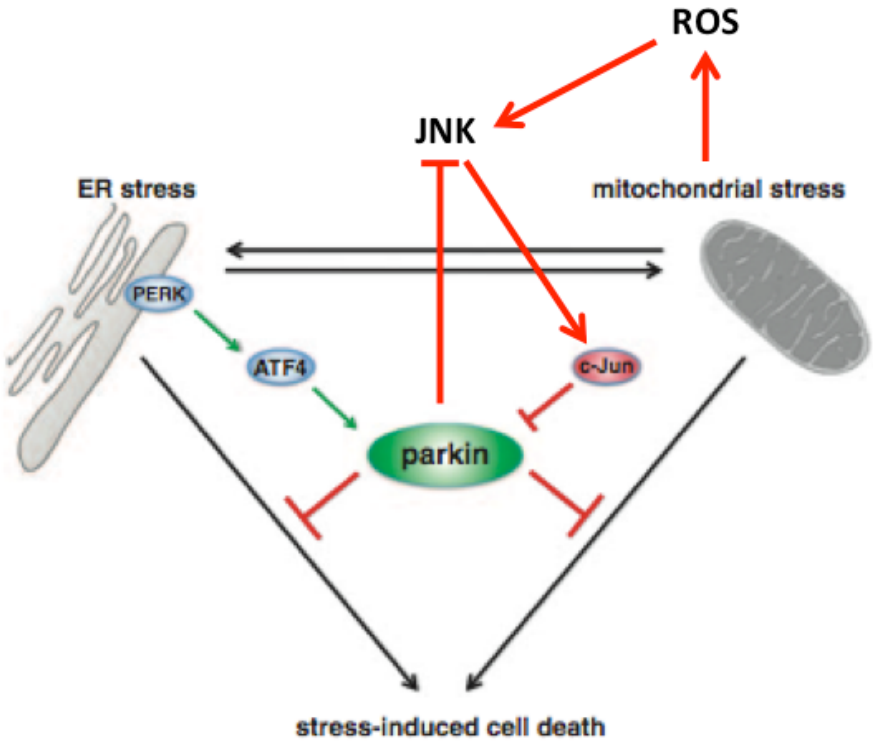

Figure 1.14: A link between Parkin and JNK/c-Jun? Several studies have suggested a link between JNK and Parkin; however, this is the first demonstration of c-Jun directly regulating *PARKIN* expression. There has been previous evidence to demonstrate that Parkin can attenuate JNK activity under certain conditions. This may therefore play a pivotal role in any feedback loop between these proteins and if any threshold exists at which a neuron switches between cytoprotective pathways and apoptosis. Adapted from Bouman et al., 2011. Copyright permission in Appendix B.

1.5 AIMS

On a cellular level Parkinson's is characterised by multiple forms of stress. The accumulation of damaged mitochondria and ROS are commonly observed characteristics, with the perturbation of adaptive processes such as mitophagy and the UPS allowing these stresses to progressively increase over time. The aim of this PhD project was to determine the cell signalling pathways (specifically involving AP-1 transcription factors) that are modulated in response to mitochondrial depolarisation in neuronal cells. Importantly, elucidating how these regulate the mitophagic and apoptotic responses. By characterising these pathways, it may provide more clarity to how neurons attempt to adapt to mitochondrial dysfunction and oxidative stress and why they enter apoptosis when these responses are overcome.

CHAPTER 2
MATERIALS AND METHODS

2.1 MATERIALS

2.1.1 Chemicals

DMEM/F12 GlutaMAX™ medium (31331-093) and non-essential amino acids (NEAA) (100X) (11140-035) were purchased from Gibco (Paisley, UK). Hygromycin B was supplied by Invitrogen (Paisley, UK). Blasticidin (ant-bl-1) and Zeocin (ant-zn-1) were purchased from InvivoGen (Toulouse, France). DMEM (D6429), foetal calf serum (FCS; F7524), PBS (D8537), Trypsin/EDTA (T4174), penicillin/streptomycin (P/S; P0781), retinoic acid (R2625) and 12-*O*-tetradecanoylphorbol 13-acetate (TPA; P1585) were supplied by Sigma (Dorset, UK). Brain-derived neurotrophic factor (BDNF) was supplied by PeproTech (London, UK).

Compounds used for stressor/inhibitor assays were obtained from multiple sources. Carbonyl cyanide 3-chlorophenylhydrazone (CCCP) (C2759), hydrogen peroxide (323381), FR180204 (SML0320), rotenone (477737) and tunicamycin (T7765) were all supplied by Sigma. The small molecule inhibitors, SP600125 (sc-200635) and epoxomicin (2190-50), were supplied by Santa Cruz Biotechnology (CA, USA) and BioVision (CA, USA), respectively.

Halt™ protease and phosphatase inhibitor cocktail (100X) (78444), Restore ™ PLUS western blot stripping buffer (46428), Super Signal West Pico (34095) and Femto (34078) kits, CellROX® Green reagent (C10444) and Dithiothreitol (DTT; R0861) were supplied by Thermo Fisher Scientific (Epsom, UK). Milk powder used for blocking protein-protein interactions was Marvel Original dried skimmed milk powder. The 30% acrylamide, 37:5:1 (2.6% C) solution (161-0158) was supplied by Bio-Rad (Hertfordshire, UK). PBS tablets (P4417), bovine serum albumin (BSA; A2153), Tween20 (P1379), Triton X-100 (X-100), ammonium persulphate (A3678) and tetramethylethylenediamine (TEMED; T7014) were supplied by Sigma. Nitrocellulose, 0.45μm pore size, was sourced from Amersham (Buckinghamshire, UK).

Lipofecatine 2000 (11668027) and RNAiMax (13778-075), TRIzol® reagent (15596-026, 10nM dNTP mix (18427-088) and the Supercript III reverse transcriptase kit (18080-044) were supplied by Invitrogen. The Turbo DNA-free™ kit (AM1907) and glycogen (AM9510) were sourced from Ambion (TX, USA). The TaqMan® Gene Expression master mix (4369016) was supplied by Applied Biosystems (Warrington, UK).

2.1.2 Cell lines

Wild type (WT) and Parkin overexpressing SH-SY5Y neuroblastoma cell lines were obtained from Dr. Phil Robinson (Pennington et al., 2010). The latter cell line was created by stable transfection of a pcDNA3.1/Hygro(+) vector (Invitrogen, Paisley, UK) containing *PARK2* cDNA into SH-SY5Y cells followed by selection using hygromycin B. The T-REx SH-SY5Y host cell line (SH-TR) was kindly supplied by Dr. Buee (INSERM U422, IMPRT, Place de Verdun, France) (Hamdane et al., 2003). Briefly, these serve as host cell lines for a tetracycline-regulated mammalian expression (T-REx) system. These cells were transfected with a pcDNA6/TR vector purchased from Invitrogen using ExGen500 (Euromedex, France) to create a stable line constitutively expressing the tetracycline repressor.

Flp-In™ T-REx™ HEK293 cells stably expressing tetracycline (Tet) inducible Parkin constructs were previously generated and characterised by Dr Phil Robinson, Miss Penelope La-Borde and Dr Katherine Roper, some of which have been previously published (Morrison et al., 2011). In brief, Flp-In™ Hek293 cells provided by Invitrogen were co-transfected with a pOG44 plasmid (expressing the Flp recombinase) and a pcDNA/FRT vector containing full-length Parkin WT or mutant cDNA. Successfully transfected clones were selected with hygromicin B (100μg/ml) and blasticidin (10μg/ml).

2.1.3 Antibodies

Antibodies specific for c-Jun (5B1, ab119944), JunD (EPR6520, ab134067), JunB (EPR6518, ab128878), c-Fos (2G2, ab129361), FosB (83B1138, ab11959), Fra-1 (EP4711, ab124722), Fra-2 (EPR4713(2), ab124830), anti-

mitochondria [MTCO2] (ab3298) and Histone H3 (1791, ab1791) were obtained from Abcam (Cambridge, UK). An anti-Parkin (Prk8) (4211) mouse monoclonal antibody along with antibodies raised in rabbit specific to c-Fos (9F6, 2250) and phosphorylated c-Jun (Ser63) II (9261) were obtained from Cell Signalling Technology (New England Biolabs Ltd., Hertfordshire, UK). An antibody specific to *β*-actin (A5441) was obtained from Signma. Horseradish-peroxidase anti-mouse (P0260) and anti-rabbit (P0448) secondary antibodies for western blot analysis were supplied by Dako (Stockport, UK). Highly-cross adsorbed (H+L) Alexa Fluor 488 anti-mouse (A11029) and Alexa Fluor 594 anti-rabbit (A11037) secondary antibodies for immunofluorescence were purchased from Molecular Probes (Invitrogen, Paisley, UK). The details of dilutions used for different techniques can be found below in Table 2.1.

Antibody	Cat.No.	Type	Dilution	
			Western blotting	Immunofluorescence
c-Jun	ab119944	Ms mono	1:1000	1:1000
JunB	ab128878	Rb mono	1:1000	1:1000
JunD	ab134067	Rb mono	1:1000	1:1000
Phos c-Jun (S63)	9261	Rb poly	1:500	
c-Fos	ab129361	Ms mono		1:1000
c-Fos	2250	Rb mono	1:1000	
FosB	ab11959	Ms mono	1:1000	1:1000
Fra-1	ab124722	Rb mono	1:1000	1:1000
Fra-2	ab124830	Rb mono	1:1000	1:1000
MTCO2	ab3298	Ms mono	1:500	1:500
Parkin	4211	Ms mono	1:1000	1:1000
Histone H3	ab1791	Rb poly	1:2000	
***β*-actin**	A5441	Ms mono	1:2000	

Table 2.1: Antibody dilution summary table. Antibodies were diluted in 5% milk for western blotting and 1% for immunofluorescence, except the antibody specific to phosphorylated c-Jun (S63), which was diluted in 5% BSA. Secondary antibody concentrations were 1:2000 for western blotting and 1:500 for immunofluorescence.

2.1.4 siRNAs

siRNA smartpools were obtained from Dharmacon. Smartpools specific to JUN (c-JUN) (M-003268-03-0005), JUNB (M-003269-01-00), JUND (M-003900-05-

0005), FOS (c-FOS) (M-003265-01-0005), FOSB (M-010086-03-0005), FOSL1 (FRA-2) (M-004341-04-0005), FOSL2 (FRA-2) (M-004110-00-0005) and PARK2 (PARKIN) (M-003603-00-0005) were all utilised in siRNA-based studies. siRNA specific to non-targeting 1 (NT1) and polo-like kinase 1 (PLK1) were used as negative and positive controls, respectively. A BLAST search was performed (http://blast.ncbi.nlm.nih.gov/Blast.cgi) for each individual siRNA used, to predict for off-target effects. The details for each specific siRNA can be found in Appendix C of this thesis.

2.1.5 Primers for qRT-PCR

All primer/probe sets were sourced from Invitrogen. The following TaqMan© Assay On Demand primer/probe sets were used:

c-Jun (Hs00277190_s1), JunB (Hs00357891_s1), JunD (Hs04187679_s1), c-Fos (Hs01119266_g1), FosB (Hs00171851_g1), Fra-1 (FOSL1) (Hs04187685_m1), Fra-2 (FOSL2) (Hs01050117_m1), Parkin (PARK2) (Hs01038325_m1), Rab8a (Hs00180479_m1) and Bim (BCL2L11) (Hs01076940_m1).

2.1.6 Mammalian expression vectors

The SH-TR, supplied by Dr. Buee (INSERM U422, IMPRT, Place de Verdun, France)(Hamdane et al., 2003), had previously been stably transfected with the pcDNA6/TR plasmid (Appendix D). The expression vectors for WT and T240R Parkin had been previously generated for another PhD project (Hung, 2007) and supplied by Dr Phil Robinson. Briefly, *Hind* III and *Apa* I restriction endonucleases were used to digest the pcDNA4/TO/*myc*-His A vector (Appendix E), which was then purified by agarose gel electrophoresis. Again, *Hind* III and *Apa* I restriction endonucleases were used to digest the cDNAs for WT and T240R from a pcDNA5/FRT/TO vector used to transfect HEK293 cells in the aforementioned PhD thesis. Initially, *PARKIN* cDNA was isolated from *myc-PARKIN* constructs generated in a study prior to the thesis (Ardley et al., 2003). These *PARKIN* cDNAs were then subcloned into the pcDNA4/TO/*myc*-His A vector used here. After clonal selection, plasmids were purified and sequenced. These plasmids were stored at -20°C and used in this study.

2.2 METHODS

2.2.1 Cell culture

2.2.1.1 Maintenance of cell lines

SH-SY5Y cells were grown in DMEM/F12 GlutaMAX™ (Gibco, Paisley, UK) media supplemented with 10% FCS, 100µg/ml penicillin, 100µg/ml streptomycin (P/S) and minimum essential media non-essential amino acids (MEM NEAA) (Gibco, Paisley, UK) at 37°C and 5% CO_2. Media for Parkin overexpressing cells contained 100mg/ml hygromycin B. SH-TR host cells were maintained in the same media containing 5µg/ml blasticidin. SH-TR cells transfected with the pcDNA4/TO expression vector were selected for and maintained in DMEM/F12 GlutaMAX™ (10% FCS, P/S, MEM NEAA) containing 5µg/ml blasticidin and 100µg/ml zeocin.

Flp-In™ T-REx™ HEK293 cells stably expressing tetracycline (Tet) inducible Parkin constructs were previously generated and characterised by Dr Phil Robinson, Miss Penelope La-Borde and Dr Katherine Roper, some of which have been previously published (Morrison et al., 2011, Roper, 2012). In brief, Flp-In™ Hek293 cells provided by Invitrogen were co-transfected with a pOG44 plasmid (expressing the Flp recombinase) and a pcDNA/FRT vector containing full-length Parkin WT or mutant cDNA. Successfully transfected clones were selected with hygromicin B (100µg/ml) and blasticidin (10µg/ml).

2.2.1.2 Passage of cells and preparing frozen aliquots

Cell media was carefully removed and cells gently washed with phosphate buffered saline (PBS). To detach cells from plastic, trypsin in PBS (10% (v/v)) was applied to cells, which were then incubated with the enzyme for 5 minutes at 37°C and 5% CO_2. Trypsin activity was inhibited by the addition of appropriate media containing 10% FCS, in which cells were resuspended. An appropriate volume of cell suspension was used to seed cells in flasks (25cm^2, 75cm^2 or 150cm^2) or culture dishes (6-well, 12-well or 96-well), as required for the experiment being carried out.

If required, cells were counted using a Countess™ instrument (Invitrogen). After cells were incubated with trypsin and thoroughly resuspended, a 10μl aliquot was taken from the suspension and mixed with an equal volume of trypan blue. Live cells were then counted on the Countess™ by the trypan blue exclusion method to obtain cell suspensions of required density.

To create frozen stocks, cells were grown to near confluence in 75cm^2 flasks then trypsinised as usual. The resulting cell suspension was pelleted at 200xg for 5 minutes at room temperature and the supernatant decanted. The pellet was then resuspended in 3ml of freezing media (10% DMSO, 90% FCS) and aliquots of 1ml frozen at -80°C (-1°C/minute) for 16 hours before being transferred to liquid nitrogen for long-term storage.

2.2.1.1 Recovering cell lines from frozen stocks

Frozen aliquots of cells (1ml volumes) were removed from liquid nitrogen and transferred to cell culture facilities on dry ice. Aliquots were rapidly thawed at 37°C and transferred to 25cm^2 flasks containing 5ml of media with no selection antibiotics. Cells were then incubated at 37°C until near confluence.

2.2.1.4 Differentiation of SH-SY5Y cells

WT and *PARKIN* overexpressing cells underwent one of 3 differentiation protocols based on previous studies (Mastroeni et al., 2009, Pennington et al., 2010, Presgraves et al., 2004a). Cells were differentiated over 7 days by sequential retinoic acid (RA) treatment (RA/RA); RA followed by brain derived neurotrophic factor (BDNF) (RA/BDNF); or RA followed by 12-*O*-tetradecanoyl-phorbol-12-acetate (TPA) (RA/TPA). Cells were plated in standard culture medium for 24 hours, then in standard medium containing 10μM RA for 3 days. Medium was removed and cells washed with PBS. RA/RA differentiated cells were then given 10μM RA-containing medium with 0.5% FCS for another 3 days. Serum-free medium containing 50ng/ml BDNF was given to RA/BDNF cells for 3 days. RA/TPA cells received medium containing 0.5% FCS and 80nM TPA for 3 days.

2.2.1.5 siRNA experiments

siRNA studies were carried out in either 6-well or 96-well plate formats. For Operetta studies, these siRNA-based experiments occurred in 96-well plates. Final siRNA concentration for knockdowns was 50nM. Firstly, 2.5μl of the required siRNA at 2μM in 1X siRNA buffer was applied to each well. Each condition was carried out in duplicate on a plate. Transfection reagent mix was made up using 17.5μl of Opti-MEM serum free medium plus 0.1μl RNAiMax per well. This was briefly vortexed, incubated at room temperature (RT; approximately 20°C) for 5 minutes then 17.5μl applied to each well. The plate was then incubated at RT for 45 minutes on a shaker. After 45 minutes, cells were seeded in an 80μl volume of antibiotic-free media at 4,000 cells/well using a Fluid-X Xrd-384 dispenser, then incubated for 48 hours at 37°C. Cells were then treated as described in section 2.2.3 and were fixed and stained as described below (2.2.5.3).

For western blot or qRT-PCR analysis, cells were seeded in 6-well plates and all volumes and cell numbers multiplied by 15 in relation to siRNA experiment in 96-well plates. Incubation times and reagent concentrations remained unchanged. Protein or RNA extractions were then carried out as described below (sections 2.2.4 and 2.2.6, respectively).

2.2.1.6 Growing cells on methanol-sterilised cover slips

Glass coverslips were sterilised by complete immersion in ice-cold 100% methanol and allowed to dry in 6-well plates by evaporation for approximately 5 minutes. A 2ml suspension of cells at the required density was then added to each well and incubated at 37°C for the appropriate time.

2.2.2 Creating inducible SH-SY5Y cell lines

2.2.2.1 SH-TR host cell selection

The SH-TR cell line supplied by Dr Luc Buee had been previously transfected with pcDNA6/TR conferring blastcidin resistance. To show that these cells were not resistant to Zeocin, the selection antibiotic to be used when host cells are

transfected with the second vector containing the gene of interest, a kill curve was set up. Using the Countess™, 40,000 cells in 2ml of standard media containing 5μg/ml blasticidin were seeded into standard 6-well plates and incubated for 48 hours at 37°C. Media was then removed and fresh media also containing Zeocin at a range of concentrations was added to appropriate wells. Cells were then incubated at 37°C for 72 hours in Zeocin selection.

After 72 hours, media was removed, cells gently washed with 1ml PBS then 150μl trypsin added and incubated for 5 minutes at 37°C. Trypsin activity was then quenched with the addition of 850μl of media and cells were resuspended as a single cell solution and live cells counted using the Countess™ as previously described.

2.2.2.2 Measuring plasmid concentrations

Vectors had been previously generated by Dr Chao-Chun Hung for her PhD thesis (Hung, 2007) and stored at -20°C. Plasmid stocks were thawed and a Qubit™ Fluorometer (Invitrogen, Q32857) was used to ascertain the concentration of vector DNA according to the manufacturer's instructions. Solutions and standards required were supplied with the Qubit™.

A Quant-iT™ Working Solution was made up by diluting the Quant-iT™ reagent 1:200 in the Quant-iT™ buffer. The two standards and plasmid samples were then prepared as detailed above (Table 2.2) in 500ml PCR tubes. Samples were then briefly vortexed and incubated at RT for 2 minutes. Tubes were then read using the Qubit™ fluorometer and the concentrations of the plasmid samples calculated via multiplication of the dilution factor (i.e. 100). Plasmids were then stored at -20°C.

	Volume (μl)	
	Standard assay tubes	**Plasmid assay tubes**
Working solution	190	198
Standards	10	-
Plasmid	-	2
Total volume	200	200

Table 2.2: **Set up for assessment of plasmid concentrations.** Volumes used were taken from the Quibit™ recommended protocol.

2.2.2.3 Transfection

The general Lipofectamine® 2000 Reagent Protocol 2013 (Life Technologies) was followed for transfection of the SH-TR cell line. Cells were grown to approximately 80% confluence in 6-well plates in 2ml of media containing 5μg/ml blasticidin. The recommended protocol suggests that 4 different concentrations of Lipofectamine® 2000 reagent is used. However, here I used 3 concentrations. Firstly, 9, 12 or 15μl of Lipofectamine® 2000 were added to 150μl aliquots of Opti-MEM® medium in 1.5ml nuclease-free centrifuge tubes. A second set of solutions were then made by diluting 14μg of either Parkin Par1 (WT) or T240R (mutant) plasmids in 700μl of Opti-MEM®. DNA:lipid complex solutions were then made up by adding 150μl of the diluted DNA solution to the 150μl of diluted Lipofectamine® 2000 reagent, creating 3 solutions with different transfection reagent concentrations for each plasmid. These were then incubated for 5 minutes at RT.

In total 6 wells were set up to allow one well for each Lipofectamine® 2000 concentration for both *PARKIN* constructs. Media was removed from all wells and 250μl of DNA:lipid solutions added to each well, thus a final DNA amount of 1400ng/well. Cells were then incubated for 24 hours at 37°C. Media was then removed and wells washed gently with PBS to remove dead cells. Selection media containing 5μg/ml blastcidin and 100μg/ml Zeocin was then added and cells incubated for 72 hours at 37°C. Media was then removed, fresh selection media added and cells incubated for a further 72 hours.

2.2.2.4 Obtaining monoclonal cultures

After selection, cells in each well were trypsinised and counted using the Countess™ as described above (section 2.2.1.2). To obtain monoclonal cultures, 40ml suspensions (10 cells/ml) in media containing 5μg/ml blastcidin and 100μg/ml Zeocin were made up from each well of the 6-well transfection plate. To create single cell colonies, 100μl of cell suspension was added to wells in 2x 96-well plates or to wells in a 48-well plate already containing 100μl media per well for each of the 6 polyclonal cultures. This would, in theory, seed 1 cell per well to establish a monoclonal colony. Furthermore, for each of the polyclonal cultures a separate 6-well plate was set up whereby 400μl of cell suspension was added to all of the wells in the plate, which already contained 2ml of selection media. All 24 plates were then incubated at 37°C.

Cells were given 1 week to grow and then monitored on a daily basis to observe if monoclonal colonies were established. The 48 and 96-well well plates were also checked to ensure that only colony was established per well. If it appeared more than 1 colony was growing in a well then that well was not considered for further use. Once colonies appeared to have approximately 500 cells or greater, media was removed from these wells and cells gently washed with PBS. In the 48 and 96-well plates, 50μl or 100μl of trypsin was added to the appropriate wells, respectively, and incubated at 37°C for 5 minutes. In the 6-well plates, where approximately 4 cells per well were seeded, individual colonies were isolated using cloning rings (Sigma) before 50μl of trypsin was added to cells within the ring. After incubation, trypsin was gently pipetted up and down to resuspend cells. Cells were then transferred to individual wells in 12-well plates containing 1ml of selection media and incubated at 37°C. Once near confluence, media was removed, cells washed and 100μl trypsin added to wells and cells incubated for 5 minutes at 37°C. Cells were then resuspended in media then added to 5ml of selection media in 25cm^2 flasks and incubated at 37°C. From here cells could be cultured as normal.

2.2.2.5 Polyclonal cultures

After making up 40ml suspensions in previous section, remaining cells from each well were used to seed separate 25cm^2 flasks containing 5ml selection media and incubated at 37°C until cells were nearly fully confluent. Polyclonal cultures were labelled Par1 or T240R 1, 2 and 3 depending on volume of transfection reagent used in section 2.2.2.3 (1 = 9μl, 2 = 12μl and 3 = 15μl). Cells were then passed as usual into 75cm^2 flasks and grown to near confluence before splitting and aliquoting for storage in liquid nitrogen as described above (section 2.2.1.2).

2.2.2.6 Characterising monoclones

Monoclones were characterised by both immunofluorescence (IF) and western blotting. For IF analysis cells were grown on MeOH-sterilised coverslips in 6-well plates (2 wells/monoclone) for 24 hours at 37°C as previously described (section 2.2.1.6). Media was then removed and fresh media added containing 1μg/ml Tet or ethanol (vehicle). Cells were incubated for 24 hours at 37°C then fixed and stained for DAPI and Parkin prior to analysis, as described below (2.2.5.2).

For western blot analysis, 2ml of cells (50,000 cells/ml) were added to 6-well plates (2 wells/monoclone) in media containing 5μg/ml blastcidin and 100μg/ml Zeocin and incubated at 37°C for 24 hours. Media was then removed and fresh media added containing 1μg/ml Tet or ethanol (vehicle). Cells were incubated for 24 hours at 37°C before media was removed and PBS added. Cells were then scraped into PBS and pelleted at 200xg for 5 minutes at RT. Supernatant was removed and pellet stored at -80°C until required for protein extraction and western blotting (section 2.2.4).

2.2.3 Inducing cellular stress

2.2.3.1 Carbonyl cyanide m-chlorophenyl hydrazine (CCCP) assays

Cells treated with CCCP were either scraped for protein extraction followed by SDS-PAGE and western blotting, fixed for IF or RNA extracted for qRT-PCR

analysis. All are described in detail below. Where required, 100μg/ml TPA was used as a positive control due to its ability to induce the expression of AP-1 genes. The same protocol was used as CCCP with cells being incubated with TPA containing media for 2 hours at 37°C.

To analyse protein level modulation by western blotting, CCCP assays were conducted in either 25cm^2 or 75cm^2 flasks. Undifferentiated cells were grown to around 70% confluence then media removed 24 hours prior to beginning of CCCP assay. Fresh media (5ml in 25cm^2 or 15ml in 75cm^2 flasks) was added and cells incubated for 24 hours at 37°C to ensure cells were at basal conditions and starvation was not a factor in the assay. CCCP was made up in media such that a 0.5ml (25cm^2) or 1.5ml (75cm^2) volume added to flasks resulted in the required final concentration (e.g. media with 55μM CCCP made up so 0.5ml added to the 5ml volume in 25cm^2 flask resulted in a final concentration of 5μM). Cells were then incubated at 37°C. At appropriate time points media was removed and cells scraped into PBS and pelleted at 200xg for 5 minutes. For differentiated CCCP assays, WT cells were subjected to the differentiation protocol described above (section 2.2.1.4) in 25cm^2 flasks with a final media volume of 5ml. A 0.5ml volume of 55μM CCCP media containing 0% FCS and 50ng/ml BDNF (to ensure a decrease in BDNF concentration was not the cause of any stress response) was added to flasks and incubated at 37°C for required time. Cells were then scraped into PBS and pelleted at 200xg. Supernatant was removed and all pellets stored at -80°C.

For mRNA analysis cells were grown in 75cm^2 flasks. Upon reaching approximately 60% confluence media was removed and 15ml fresh media added. Cells were then incubated for 24 hours prior to CCCP addition. CCCP or TPA containing media was added to cells as described above and cells incubated for required time points. RNA was then extracted as described below (2.2.6.1).

For cells in 96-well Operetta plates to be analysed by high-throughput IF, volumes used depended on what assay was being conducted. For inhibition of

MAPK signalling or the 26S proteasome prior to CCCP treatment, see below (2.2.3.3/4). Experiments using siRNA for 48 hours were conducted as described above (2.2.1.5) with cells being in 100μl of media. After this, 50μl volumes of CCCP (or DMSO as vehicle) were applied to wells using a multi-channel pipette and cells incubated for 24 hours at 37°C.

2.2.3.2 CellROX® assay

For IF analysis cells were grown in 6-well plates on MeOH-sterilised cover slips (see 2.2.1.6) in 2ml of standard media for 24 hours. Media was then removed and fresh media containing 5μM CCCP or 0.5μM rotenone and cells incubated for up to 24 hours. At 30 minutes prior to fixation, CellROX® Green Reagent was applied to all wells at a final concentration of 5μM and incubated at 37°C. As CellROX® is a photosensitive reagent, all steps from here were conducted in dark, with well plates being covered in tinfoil for incubation steps. At required time points media was removed and cells fixed for 15 minutes in 4% paraformaldehyde (PFA) at RT. Cells were washed twice in PBS then permeabilised in 0.1% Triton X-100 in PBS for 5 minutes at RT. Cells were washed twice again then blocked in 0.1% milk in PBS for 5 minutes. DAPI was diluted at 1:1000 in blocking solution and applied to all wells for 1 hour at RT. Cells were then imaged as described below (2.2.5.2).

2.2.3.3 MAPK inhibition

For analysis of MAPK inhibition in stress induced-cell death in undifferentiated SH-SY5Y cells, a Fluid-X Xrd-384 dispenser was used to seed cells (5,000/well) in 96-well plates (80μl/well), which were then incubated for 24 hours at 37°C. Cells were then treated with 40μl of standard media containing SP600125 (JNK inhibitor), FR180204 (ERK inhibitor) or DMSO (vehicle control) to obtain the desired final concentration prior to incubation for 2 hours at 37°C. After this, cells were treated with 40μl of media containing either CCCP, hydrogen peroxide or tunicamycin at the required concentration. Cells were then incubated for either 24 or 48 hours at 37°C before fixation, staining and Operetta analysis (see 2.2.5.3).

For analysis of MAPK inhibition in stress induced cell death and mitochondrial clustering in differentiated SH-SY5Y cells, cells were seeded by the dispenser (7,000/well) in 96-well plates (80μl/well) and incubated for 24 hours at 37°C. These cells would undergo RA/BDNF differentiation, as described above (2.2.1.4). Media was then removed and 80μl of fresh media containing 10μM RA was added and cells incubated for 72 hours at 37°C. After 72 hours, RA media was removed, cells gently washed with PBS to remove remaining serum and 80μl of media (0% FCS, 50ng/ml BDNF) added and plates incubated for 72 hours at 37°C. MAPK inhibitors were added in 40μl volumes per well in media (0% FCS) containing 50ng/ml BDNF and cells incubated for 2 hours at 37°C prior to CCCP treatment. CCCP (DMSO as vehicle control) was made up in media (0% FCS, 50ng/ml BDNF) to 4X the final concentration so that after 2 hours incubation with a MAPK inhibitor 40μl gave desired final concentration. Cells were then incubated for either 3 or 24 hours at 37°C before fixation, staining and Operetta analysis (see 2.2.5.3). For treatment of differentiated cells with MAPK and proteasomal inhibitors together see next section.

2.2.3.4 Proteasomal inhibition

Epoxomicin, an irreversible proteasome inhibitor, was used at a final concentration of 100nM for both differentiated and undifferentiated SH-SY5Y cells. In order to inhibit the proteasome prior to 5μM CCCP treatment to produce extracts for western blotting undifferentiated WT cells were grown in 25cm^2 flasks to approximately 70% confluence before media was removed, 5ml of fresh media added and cells incubated for 24 hours at 37°C. To irreversibly inhibit the 26S proteasome, 0.5ml of media containing 1.1μM epoxomicin was added to flasks and cells incubated for 1 hour at 37°C. After 1 hour, 0.5ml of media containing 60μM CCCP was added and cells in flasks incubated at 37°C. Cells were scraped and pelleted for protein extraction and western blotting at required time points as described in section 2.2.3.1.

For proteasomal inhibition in differentiated SH-SY5Y cells in 96-well plates, fully differentiated cells were treated with MAPK inhibitors, or DMSO as vehicle control, as described in section 2.2.3.3. After 1 hour with MAPK inhibitors, 20μl

of media (0% FCS, 50ng/ml BDNF) containing 700nM epoxomicin (DMSO as vehicle control) was added and cells incubated for a further hour. Cells were then treated with 20μl of media (0% FCS, 50ng/ml BDNF) containing CCCP at 8X the desired final concentration and incubated for either 3 or 24 hours at 37°C. Fixation, staining and Operetta analysis was carried out as described in 2.2.5.3.

2.2.4 Western blot analysis

2.2.4.1 Protein extraction and Bradford assays

All cell pellets were generated by scraping cells into PBS and pelleting at 200xg. Pellets were always stored at -80°C prior to protein extraction. Cell pellets were resuspended in 30-60μl (depending on pellet size) of ice cold ice cold RIPA buffer (1% Nonidet-P-40, 0.5% sodium deoxycholate and 0.1% SDS in PBS) containing 1X Halt Protease and Phosphatase Inhibitor Cocktail (Pierce, Northumberland, UK), then left on ice for 30 min. Samples were then spun at 14800xg for 10 min at 4°C and 5μl of the supernatant used to determine total protein concentration. The remaining supernatant was removed, mixed with an equal volume of 2X SDS loading buffer containing 0.2M DTT and stored at -20°C until required for western blot analysis.

Protein concentrations were determined using a 96-well plate based Bradford assay format according to the manufacturer's instructions (BioRad, Hertfordshire, UK). Protein standards between were made up to create a calibration curve. The 5μl of protein supernatant was mixed with 45μl dH_2O and 5μl volumes of this aliquoted in triplicate per sample to wells. Following this, 25μl of solution SA and 200μl solution B was added to each well and the plate gently shaken then left for 15 minutes at room temperature. Protein concentrations were then calculated using a plate reader at 690nm.

2.2.3.2 Western blotting

Extracts were subjected to Sodium Dodecyl Sulphate Polyacrylamide Gel Electrophoresis (SDS-PAGE) (Table 2.3). Sample gels were run in a Mini-

Protean II electrophoresis cell (Bio-Rad, Hertfordshire, UK) at 100V in running buffer (25mM Tris base, 250mM glycine, 0.1% SDS). Protein was transferred to a Hybond-C extra nitrocellulose membrane (Amersham, Buckinghamshire, UK) using the Mini-Protean II transfer system at 100V for 90 min in transfer buffer (25mM Tris base, 192mM glycine, 20% methanol, 0.01% SDS).

For blocking and antibody incubations, nitrocellulose membranes were put in 50ml centrifuge tubes and left on rollers to ensure equal application across the membrane. These membranes were blocked in 5% (w/v) milk in PBS for one hour at room temperature then incubated with primary antibody solutions prepared at 1:1000 dilutions in 5% milk in PBS containing 0.1% Tween 20 (PBS-T) overnight at 4°C. For phosphorylation-specific antibodies, blocking was performed using 5% (w/v) BSA in PBS for one hour. These primary antibodies were prepared at 1:1000 dilution in 5% BSA in PBS-T and incubated with the membrane overnight at 4°C. Antibody solutions were removed and membranes washed 6 times in PBS-T (5 minutes each), then incubated with a horseradish peroxidase (HRP)-conjugated secondary antibody, diluted in 5% milk PBS-T, for 1 hour at room temperature. Membranes were washed 6 times in PBS-T then once in PBS. Target antigens were detected using enhanced chemiluminescence Super Signal West Pico or Femto reagents. A ChemiDoc MP Imaging System in association with Image Lab 4.0.1 (Bio-Rad, Hertforshire, UK) was used to image and analyse the membranes by densitometry.

	Volume Added (mL)	
	Stacking Gel (5%)	**Resolving Gel (12%)**
H_2O	6.8	6.6
30% acrylamide	1.7	8
1M Tris-HCl (pH 6.8)	1.25	-
1.5M Tris- HCl (pH 8.8)	-	5
10% SDS	0.1	0.2
10% ammonium persulphate	0.1	0.2
TEMED	0.01	0.012

Table 2.3: Volumes used for SDS-PAGE size-fractionation. Water saturated 1-butanol was used to remove bubbles that formed on top of the resolving gel after pouring.

2.2.3.3 Stripping and reprobing of nitrocellulose membranes

If nitrocellulose was reprobed for a second protein the membrane was incubated with Restore PLUS Stripping Buffer for 8 minutes at RT on a shaker. Membranes were then washed twice with PBS then blocked and probed as described above. For loading controls, membranes were stripped and blocked as previously described then incubated with an anti-β-actin antibody (1:2000 in 5% milk in PBS-T) for one hour at RT. Membranes were washed with PBS-T (3 x 5 minutes) then incubated with an anti-mouse HRP secondary as described above. Membranes were then washed in PBS-T (3 x 5 minutes) and imaged on the ChemiDoc MP Imaging System sing enhanced chemiluminescence Super Signal West Pico reagent.

2.2.3.4 Quantification of protein bands

Densitometric analysis was conducted to quantify relative protein levels from western blots. This was performed using Bio-Rad Image Lab software. Initially, individual lanes were isolated by software. Protein bands were then detected and detection field narrowed to the edges of each of these bands. Image lab software then calculated the density of each band relative to the control band. The density of each individual band for the protein of interest was normalised to the corresponding protein band of the loading control in each well. Background was automatically subtracted by Image Lab software using the 'rolling disc' function at 10mm, which accounted for the background of each individual lane.

2.2.5 Microscopy

2.2.5.1 Bright-field microscopy

Bright-field microscopy was conducted using an Olympus CKX41 microscope. Photographs from bright-field microscopy were taken using an Olympus 7.1 megapixel Camedia C-7070 Wide Zoom digital camera connected to the microscope with an Olympus C5060-ADU ED Wide Zoom Lens.

2.2.5.2 Immunofluorescence

Cells grown on MeOH-sterilised coverslips (2.2.1.6) were analysed by immunofluorescence microscopy. Media was removed and cells washed once

in PBS. Cells were incubated at RT for 15 minutes in 4% paraformaldehyde, washed 3 times in PBS then permeabilised with PBS-0.1% Triton X-100 for 5 minutes. Cells were washed 3 times in PBS then blocked in 0.1% milk powder in PBS for 10 minutes. Primary antibody solutions were prepared at 1:1000 dilutions (unless stated otherwise) in blocking solution and spun at 13,000 rpm on an Eppendorf 5415D centrifuge for 5 minutes before use. Coverslips were incubated with 200µl of primary antibody solutions for 1 hour at room temperature then washed 3 times in PBS. Secondary antibodies were prepared at 1:500 dilutions in blocking solution and centrifuged at 13,000 rpm for 5 min. DAPI was prepared with secondary antibodies at a dilution of 1:1000. Coverslips were incubated in the dark with 200µl secondary antibody solutions for 1 hour, after which they were washed 3 times with PBS. Stained coverslips were mounted on glass slides using Mowiol and allowed to set for 24 hours in the dark. Immunostaining was observed using an Olympus BX61 upright microscope supported by Cell^P software or a Zeiss Imager Z1 fluorescent microscope utilising AxioVision software.

2.2.5.3 High-throughput immunofluorescent analysis

2.2.5.3.1 Fixation and staining

Cells were seeded in 96-well plates at the required density as previously described. Cells were then treated as required then media was removed from the well plate by inverting it and gently tapping the plate onto tissue paper. To fix cells, 80µl of 4% PFA was gently added to each well using a multi-channel pipette and incubated at RT for 15 minutes. Cells were then washed twice with 80µl PBS then permeabilised with 80µl 0.1% Triton X-100 (v/v) in PBS for 5 minutes. Cells were then washed twice again with PBS prior to blocking in 80µl of 1% milk in PBS for 15 minutes at RT.

Primary antibodies were prepared at the required concentration (Table 2.1) in 1% milk PBS. Antibody solutions were briefly spun then 80µl applied to each well and incubated at RT for 1 hour. Cells were then gently washed 3 times in 80µl PBS (5 minutes each). Secondary antibody solutions were also prepared in 1% milk PBS with fluorescent stains at dilutions previously stated (Table 2.1),

then briefly spun. Cells were incubated with 80µl/well of secondary antibody solution for 1 hour at RT in the dark. Cells were again given 3x 5 minute washes with PBS. After washes, 160µl of PBS was added to each well and plate stored at 4°C until high-throughput image capture.

2.2.5.3.2 High-content/high-throughput (HC/HT) imaging

Plates were processed using the Operetta HC/HT wide-field fluorescence imaging system with Harmony software (PerkinElmer). Plates were individually loaded onto the Operetta and wells imaged using either 20X or 40X objective lenses (10 or 17 fields of view per well, respectively) capable of detecting up to 3 channels. Optimal focal planes were determined at the start of each experiment for every plate for individual channels to ensure the highest possible quality images were obtained for all stains. Focal planes were relative to the Operetta infrared focusing laser, which automatically detected the base of each well.

2.2.5.3.3 Image analysis

Images obtained from the Operetta were analysed using Columbus software (PerkinElmer). Analysis was conducted using algorithms (Appendices F and G) and data exported into Microsoft Excel. Objects around the border regions of fields of view were excluded in order to ensure only whole cells were analysed. DAPI was used to detect nuclei using UV illumination (>30µm^2 with contrast of over 0.10). TOTO3 was imaged using far-red illumination and used to detect the cytoplasmic area of cells. Mitochondria were detected using in Alexa Fluor 488 compatible (FITC; green) filersets.

2.2.6 Assessing relative gene expression

2.2.6.1 RNA extraction

Cells were sampled at approximately 70-80% confluence. For a 150cm^2 flask, 4ml of Trizol was added and cells incubated at RT for 5 minutes. The cell suspension was then divided into 4x1ml aliquots, 200µl of chloroform was added to each tube and shaken for 15 seconds. Samples were incubated at RT for 3 minutes then centrifuged at 12,000xg for 15 minutes at 4°C. The upper

aqueous phase containing the RNA was then carefully removed and decanted into a fresh centrifuge tube.

To act as a carrier, 1µl of RNase-free glycogen was then added to each sample, followed by 500µl of 100% isopropanol. The samples were incubated at RT for 10 minutes then spun at 12,000xg for 15 minutes at 4°C. The supernatant was removed leaving only the pellet of RNA, which was washed with 1ml of 75% ethanol. This sample wash was briefly vortexed then pelleted at 7,500xg for 5 minutes at 4°C. Supernatant was then discarded and pellet resuspended in 30µl of RNase-free water.

To remove any DNA, 3µl of 10X TURBO DNase buffer was added to each sample, along with 1µl of TURBO DNase. Samples were then incubated at 37°C for 30 minutes before adding 3µl DNase inactivation reagent and incubating for a further 5 minutes at RT, mixing occasionally. These samples were then spun at 10,000xg for 90 seconds at RT and the supernatant containing the RNA was transferred to a fresh tube. RNA was stored at -80°C until required.

2.2.6.2 Calculating concentration of RNA

To calculate the yield of RNA from the extraction process, a NanoDrop® ND-1000 Spectrophotometer (Thermo Scientific, Loughborough, UK) was used. After calibrating the instrument with RNase-free water as a 'blank', a 1µl volume of the sample was added to the spectrophotometer sensor according to the manufacturer's instructions and the absorbance at 260nm used to calculate the concentration of RNA in the sample.

2.2.6.3 cDNA synthesis

cDNA was synthesised in 20µl aliquots from RNA samples. Firstly, a 500ng dilution of RNA was made up on 5µl of RNase-free water. Samples were then heated to 65°C for 5 minutes after the addition of 1µl random hexamers, 1µl dNTP mix (10mM dA, dC, dG and dT) and a further 7µl of RNase water. Tubes were placed on ice for 2 minutes then quickly centrifuged to ensure full volume was at the bottom of the tube. After this, 4µl of the 5X 1st strand buffer, 1µl 0.1M

DTT and 1µl of SuperScript III reverse transcriptase (200U/µl) were added and tubes incubated at RT for 5 minutes. Samples were then heated to 50°C for 50 minutes, followed by 70°C for 15 minutes before being cooled on ice for 2 minutes and stored at -20°C.

2.2.6.4 qRT-PCR analysis

Reactions were run in duplicate in a MicroAmp® Optical 96-well Reaction Plate (Applied Biosystems, Warrington, UK) with a 20µl final volume in each well. The basic recommended protocol from Invitrogen was adjusted accordingly. The details of each reaction are shown in Table 2.4.

The 2µl volume of cDNA was added directly to the 96-well plate and not the reaction mixes. A 1:10 dilution of cDNA synthesised from section 2.2.5.3 was used, unless stated otherwise. Reaction mixes were made up in individual nuclease-free 0.5ml centrifuge tubes for each primer, with an excess of around 20% to allow for volume loss during pipetting. After adding cDNA to the appropriate wells, reaction mixes were briefly vortexed then centrifuged and 18µl volumes applied to each well. RNase-free water was used a negative control.

PCR reaction mix component	Volume per 20µl reaction (µl)
20X Taqman® Gene Expression Assay (Primer)	1.0
2X Taqman® Gene Expression Mater Mix	10.0
RNase-free water	7.0
cDNA (added directly to well prior to master mix)	2.0

Table 2.4: **TaqMan® master mix set up.** Individual master mixes for each primer were made up (18µl per well) with approximately 20% excess to compensate for volume loss during pipetting. These were applied to the required wells containing the cDNA template.

The 96-well plate was run using the TaqMan recommended qPCR cycle (50°C for 2 minutes, denaturation at 95°C for 10 minutes, then; 95°C for 15 seconds and annealing/extension at 60°C for 1 minute repeated for 40 cycles) on the ABI 7500 Real Time PCR System (Applied Biosystems) using 7500 SDS software.

2.2.6.5 Determining relative expression levels

The qRT-PCR analysis produced cycle threshold (Ct) values for each of the primer targets. To calculate the relative expression level of a gene of interest (GOI), the "Delta Delta Ct" (ΔΔCt) method (sometimes referred to as the Livak method) was used. Because the pre-optimised Assay On Demand primers were used, amplification efficiency was approximately 100% (-/+10%), which is an assumption of the ΔΔCT method. A 100% efficient reaction would mean that each cycle of PCR would double the cDNA for the specific primer within that reaction. To calculate the ΔCt of each sample:

GOI = Gene targeted by primer
Housekeeping gene = Primers targeting β-actin was used

$$\Delta Ct_{(sample)} = Ct_{(GOI)} - Ct_{(housekeeping\ gene)}$$

Therefore:

$$\Delta Ct_{(untreated\ sample)} = Ct_{(GOI\ in\ untreated\ sample)} - Ct_{(housekeeping\ gene\ in\ untreated\ sample)}$$

$$\Delta Ct_{(treated\ sample)} = Ct_{(GOI\ in\ treated\ sample)} - Ct_{(housekeeping\ gene\ in\ treated\ sample)}$$

This could then be used to calculate the ΔΔCt of the target:

$$\Delta\Delta Ct_{(target\ gene)} = \Delta Ct_{(treated\ sample)} - \Delta Ct_{(untreated\ sample)}$$

The ΔΔCt was then used to calculate the ratio of the GOI in the untreated sample relative to the untreated sample. The value of $2^{\Delta\Delta Ct}$ gives the mRNA

level of the GOI post-treatment relative to the untreated, negative control sample.

For example, a $\Delta\Delta$Ct value of 2.345:

$2^{2.345} = 5.0806039302$

Therefore, the expression level of the GOI has increased 5.081 times relative to the control sample.

The efficiency of each primer/probe set was calculated using serial dilutions of cDNA to ensure results were accurate. The efficiency of a primer refers to the doubling of its amplicon after each PCR cycle. This would mean that an efficiency of 100% dictates an amplification factor of 2. On the other hand, an efficiency of 75% would have an amplification factor of 1.75.

Amplification efficiency can be determined using serial dilutions of cDNA in a qPCR reaction set up. This allows the rate at which the accumulation of the product (i.e. amplicon) occurs to be calculated by fitting the results to a standard curve. A range of cDNA serial dilutions in water, between neat and 1 in 1000, were used. It should be noted that not all concentrations were used for every gene analysed and that the expression of some genes was too low to be detectable by qPCR reactions to be detectable at the lower concentrations of cDNA.

The Ct values for the individual genes analysed were plotted against the Log_{10}(cDNA template concentration) and linear standard curve fitted to these values in order to calculate the y value (y = -mx + b) of the line. Amplification efficiency, and then % efficiency of amplification, was then calculated. An example for the β-actin primer/probe set is shown below:

The trendline value for the β-actin primer/probe set was 'y = -3.2863 + 17.68' (see Appendix H). To calculate the percentage efficiency, the following equation was used:

$$\% \textit{ efficiency} = 10^{((-1/-3.2863)-1)\times 100)} = 101.508598$$

The efficiency of amplicon doubling was calculated in this manner for all genes to be analysed. From this, the change in expression was then calculated using the following formula:

$$\textit{Relative expression} = \frac{\text{Efficiency(GOI)}^{\text{CT(GOI,untreated)-CT(GOI,treated)}}}{\text{Efficiency(housekeeping)}^{\text{CT(housekeeping,untreated)-CT(housekeeping,treated)}}}$$

2.2.7 Statistical analysis

Statistical testing was performed as required throughout thesis. Unpaired two-tailed t-tests were performed in order to analyse statistically significant differences between two data points. For multiple comparisons, a 2way ANOVA with *post-hoc* testing (95% confidence interval) was used to reduce the chance of false positives. As multiple comparisons increase the chance of 'false-discovery', the application of *post-hoc* testing was critical. The type of statistical test used is stated in individual figure legends. All statistical analyses were conducted using Graph Pad Prism 6 software.

Where data is combined from 2 experiments, the mean of each experiment was used to calculate the overall mean and the standard error of the mean (SEM). Where data from individual experiments is shown, error bars represent standard deviation (SD).

CHAPTER 3
UTILISING THE SH-SY5Y CELL LINE AS A MODEL FOR PARKINSON'S DISEASE AND MITOCHONDRIAL DYSFUNCTION

3.1 INTRODUCTION

3.1.1 SH-SY5Y Cells

SH-SY5Y human neuroblastoma cells are a subline derived from the SK-N-SH cell line, originally established from a neuroblastoma patient in December 1970 (Biedler et al., 1973, Biedler et al., 1978). This cell line is widely utilised as a neuronal model because it possesses a wide range of neuronal-like properties, both biochemical and functional (Xie et al., 2010). Examples of these neuronal-like properties include neurite outgrowth and the expression of tyrosine hydroxlase (TH).

3.1.2 SH-SY5Y Cells in Neurodegenerative Research

Over the past few decades the SH-SY5Y cell line has been a widely utilised model in PD research. Their accurate representation of a wide range of neuronal properties has made the cell line a highly useful tool in many aspects of neurodegenerative research. Interestingly, the constitution of the media in which the cells are grown can heavily influence the characteristics and behaviour of SH-SY5Y cells (Buttiglione et al., 2007). The SH-SY5Y cell line can exist in either differentiated or undifferentiated forms. However, with no gold standard currently in place in PD research, the available literature utilises both forms of this cell line despite significant phenotypic variation and different tolerances to neurotoxins (Xie et al., 2010).

Several reagents can be used to differentiate SH-SY5Y cells. However, it must be carefully considered which reagent, or combination, to use as the resulting phenotype of the differentiated cell will be determined by this selection. For example, treatment with retinoic acid (RA) results in differentiation towards the cholinergic phenotype (Pahlman et al., 1984, Xie et al., 2010). Nevertheless, RA used sequentially with 12-0-tetradecanoyl-phorbol-13-acetate (TPA) can induce a dopaminergic phenotype, with D_2 and D_3 dopamine receptors expression levels elevated (Presgraves et al., 2004a). The relevance of the differentiated phenotype in terms of PD research is apparent here as agonists of these receptors have no neuroprotective effects on SH-SY5Y cells that are undifferentiated (Presgraves et al., 2004b). SH-SY5Y cells are often

differentiated using RA to achieve more neuronal-like properties, such as neurite outgrowth. However, RA-mediated differentiation can confer a higher tolerance to the neurotoxins 6-hydroxydopamine (6-OHDA) and 1-methyl-4-phenyl-pyridium ion (MPP^+) compared to undifferentiated SH-SY5Y cells (Cheung et al., 2009). This could suggest that undifferentiated SH-SY5Y cells are a better model to use in studies on neurotoxicity in PD than RA differentiated cells.

When differentiated correctly, the SH-SY5Y cell line shares many features with dopaminergic neurons, such as the ability to synthesise the neurotransmitter dopamine (Oyarce and Fleming, 1991) and expression of the dopamine transporter (*DAT*), found only in dopaminergic neurons (Takahashi et al., 1994). DAT is required for MPP^+ uptake, thus its expression has enabled the SH-SY5Y cell line to be used to study MPP^+-induced toxicity in PD models (Xie et al., 2010).

Neuronal cells are non-dividing. However, undifferentiated SH-SY5Y cells are mitotically active. This ongoing mitotic activity brings another problem in that the increasing cell number throughout an experiment can make it difficult to determine the influence an treatment has on cell death or proliferation (Xie et al., 2010). It must also be considered whether a proliferating cell line accurately represents *in vivo* neuronal cells, as mitotically active genes may influence an agent's neurotoxic or neuroprotective properties.

In particular, oxidative stress has been shown to elicit different cellular responses in SH-SY5Y cells upon differentiation (Schneider et al., 2011). Differentiated neurons rely on mitochondria for their bioenergetic needs, whereas mitotically active cells (i.e. undifferentiated SH-SY5Y cells) employ glycolysis as their primary energy source (Malkus et al., 2009). Upon RA-induced differentiation, SH-SY5Y cells have increased mitochondrial membrane potential but do not alter their mitochondrial number. Furthermore, differentiation appears to result in a greater resistance to compounds such as the ROS-generating 2,3-dimethoxy-1,4-napthoquinone and the electrophilic 4-hydroxy-2-nonenal (Schneider et al., 2011). An increased bioenergetic reserve

capacity was observed in the differentiated cells, which may be due to induced changes in complex IV of their mitochondria which become more widely distributed upon differentiation. This may suggest that approaches to selectively increase mitochondrial reserve capacity in dopaminergic cells may offer a therapeutic route.

Overall, SH-SY5Y cells have been shown to be representative of other model systems, both *in vivo* and *in vitro*, for neurodegenerative research. However, many variables must also be taken into consideration when using this cellular model. Firstly, differentiated and undifferentiated cells, despite sharing many characteristics, will have major differences. Also, many studies utilising cell models, as well as many animal models, for neurodegenerative study are not able to replicate the long-term and highly complex progression of a disease and must therefore mimic much more acute and perhaps intense conditions. Therefore, it is vitally important that this is considered when drawing conclusions from data generated in this manner. Nonetheless, to generate a tractable *in vitro* model to examine the neuronal response to mitochondrial dysfunction and oxidative stress, in particular cells resembling neurons, the use of differentiated cells where possible will be crucial.

3.2 AIMS

Previous reports suggest differences between undifferentiated and differentiated SH-SY5Y cells, some of which may have a direct effect on research related to PD, therefore both differentiated and undifferentiated cell types were utilised where possible. The first aim of this research project was to validate SH-SY5Y cells as a suitable model for studying mitochondrial damage in relation to PD. Parkin regulates the major cellular response to mitochondrial damage by coordinating mitophagy, therefore a SH-SY5Y cell line constitutively overexpressing Parkin was characterised and a cell line inducibly overexpressing the E3 ubiquitin ligase was created.

3.3 RESULTS

3.3.1 Parkin overexpression in SH-SY5Y cells

The 2 cell lines mainly utilised in this project were a WT SH-SY5Y line and a Parkin overexpressing SH-SY5Y line, both provided by Dr Phil Robinson (Leeds Institute of Biological and Clinical Sciences, Leeds, UK). Therefore, *PARKIN* overexpression was confirmed in this cell line (Figure 3a). To ensure *PARKIN* overexpression would be maintained after differentiated, cells were differentiated by sequential treatment with RA in media with 10% serum (3 days) then media lacking serum containing BDNF (3 days). As the undifferentiated form of this cell line was to be used regularly, it was determined if *PARKIN* overexpression affected the rate at which these cells proliferate. WT and *PARKIN* overexpressing cells were incubated for 72 hours before cell counts were obtained (Figure 3.1). No significant difference was found in the proliferation rates of the two cell lines ($p = 0.4768$) over a 72-hour period.

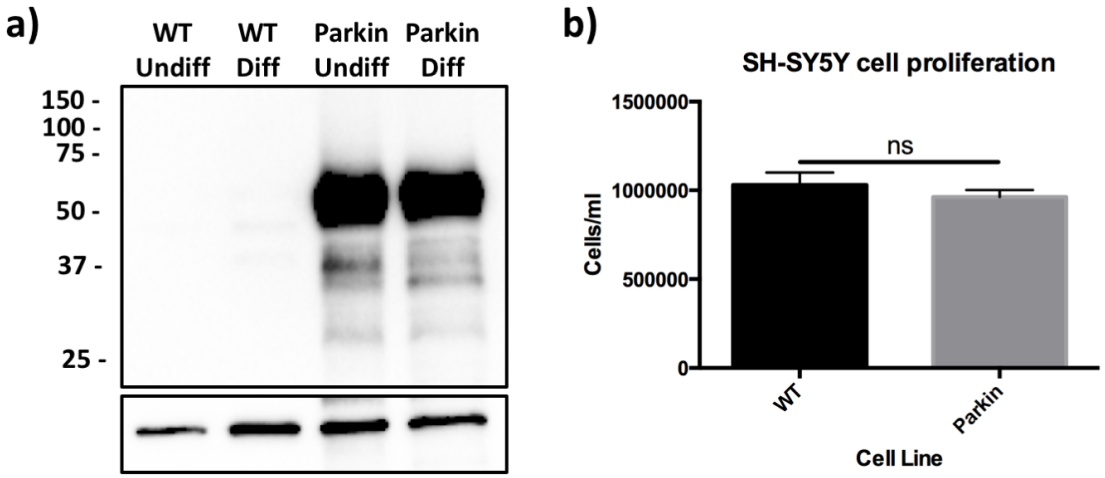

Figure 3.1: *PARKIN* expression does not affect the proliferation of SH-SY5Y cells. (a) *PARKIN* overexpression is maintained post-RA/BDNF differentiation. Western blot shows Parkin (top block) and β–actin (bottom block) as a loading control. (b) Undifferentiated WT and *PARKIN* overexpressing SH-SY5Y cell counts were performed in duplicate wells per experiment. Two fully independent experiments were conducted on separate occasions (n = 2). Data shown is from the mean value of each individual biological replicate for each cell line. Statistical analysis was performed using an unpaired student's t test. Error bars represent standard error of the mean (SEM).

As only 2 biological replicates were performed, a small difference in proliferation may not be detected as statistically significant. Therefore, greater statistical power may be required to properly determine if any difference in proliferation rate exists. Moreover, it should be acknowledged that WT and Parkin lines used here are non-matched cell lines and thus other factors (e.g. selection antibiotics in media) may have an effect.

3.3.2 Differentiation of the SH-SY5Y cell line

In previous neurodegenerative studies both undifferentiated and differentiated SH-SY5Y cells have been used. Importantly, the method of differentiation used must be taken into consideration as these can result in phenotypic differences in this resulting differentiated cells (Xie et al., 2010). Cells were subjected to three different differentiation protocols (RA/RA, RA/BDNF and RA/TPA). All three protocols lasted a total of 7 days and resulted in a population of non-dividing cells (Figure 3.2).

The sequential treatment of RA and BDNF was the method that appeared to yield differentiated cells with the greatest neurite outgrowth (Figure 3.2a). It was for this reason that all studies in differentiated SH-SY5Ys herein used this protocol instead of the other methods. Furthermore, the RA/BDNF protocol has been previously shown to produce the most dopaminergic phenotype, such as increased *DAT* expression (Xie et al., 2010). Importantly, western blot analysis showed that constitutive *PARKIN* overexpression was maintained post-differentiation (Figure 3.1a). However, this overexpression also resulted in significantly fewer cells being present post-differentiation (Figure 3.2b), indicating these Parkin SH-SY5Y cells were more sensitive to this process.

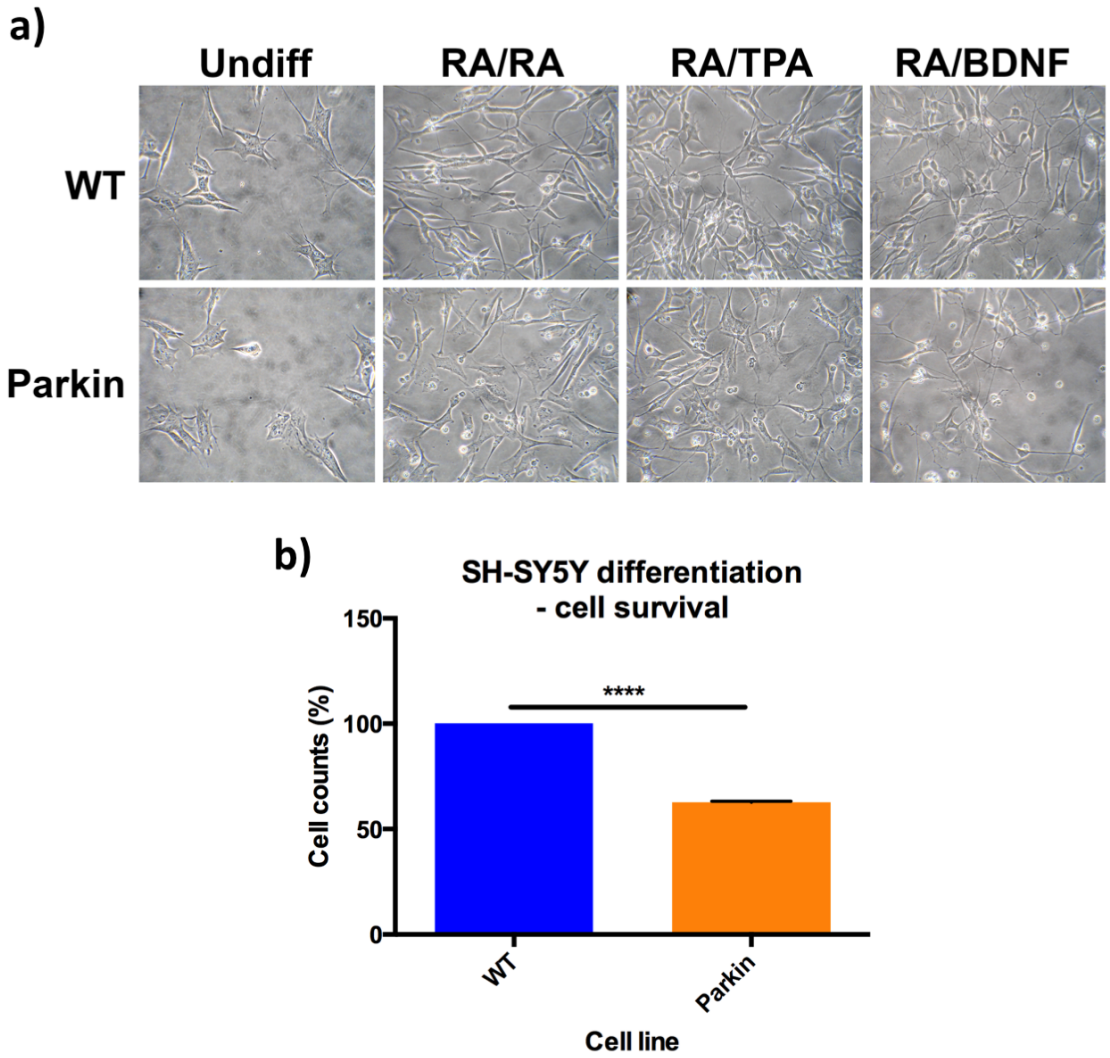

Figure 3.2: The differentiation of SH-SY5Y neuroblastoma cells using RA/BDNF produced the most observable neurite outgrowth. (a) Photos taken by bright-field microscopy at 40X magnification demonstrating the morphological differences between cells differentiated by the 3 separate methods. (b) The overexpression of *PARKIN* resulted in significantly greater sensitivity to RA/BDNF differentiation assessed using an unpaired two-tailed t-test (****$p < 0.001$). Counts were performed in duplicate wells for each experiment. Two fully independent replicate experiments were performed at different times, whereby cells were seeded, differentiated, fixed and counted ($n = 2$). Error bars represent SEM calculated from the mean of each individual experiment.

3.3.3 Inducing mitochondrial dysfunction and oxidative stress

The aim of this study was to dissect the cell signalling pathways modulated in response to mitochondrial damage. The protonophore CCCP is known to induce mitochondrial damage by uncoupling the proton gradient. However, it is

unclear whether this then induces cellular oxidative stress. CellROX® Green Reagent, a dye that fluoresces upon oxidation, was used to determine how ROS levels accumulate over a 24 hour period post-CCCP treatment in undifferentiated WT SH-SY5Y cells (Figure 3.3).

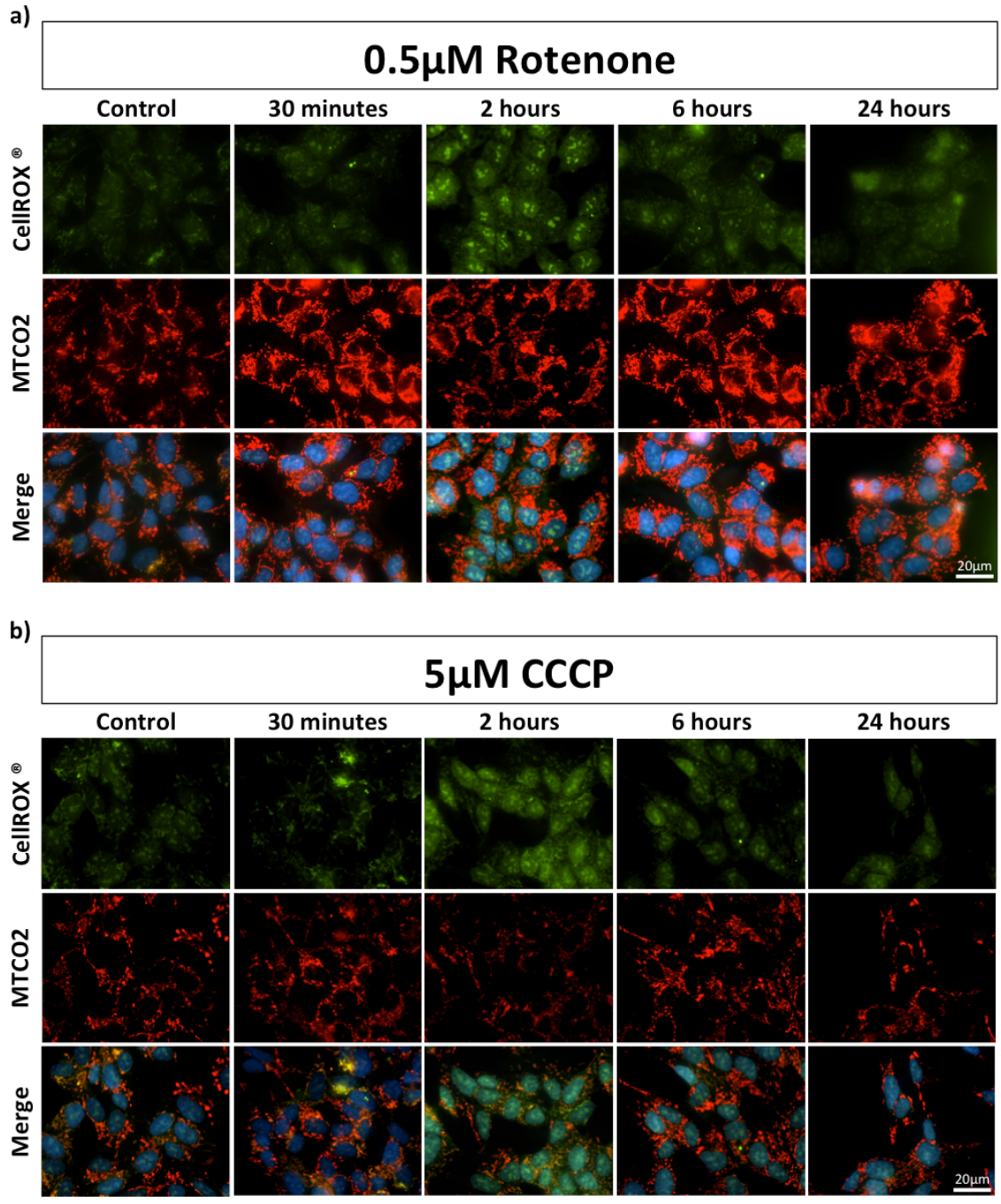

Figure 3.3: Treatment of SH-SY5Y cells with 5µM CCCP induces oxidative stress. Cells were stained with the mitochondrial marker MTCO2 (red), CellROX® (green) and DAPI (blue). (a) CellROX® Green Reagent detects oxidative stress induced by 0.5µM rotenone in undifferentiated SH-SY5Y cells. (b) CellROX® Green was used to show that ROS levels peak around 2 hours post-CCCP treatment.

Rotenone is proposed to damage mitochondria by inhibition of complex I and has previously been shown to induce oxidative stress in SH-SY5Y cells (Dal-Cim et al., 2012). This was therefore used as a positive control (Figure 3.3a). Treatment of cells with 5μM CCCP induces oxidative stress, with ROS levels peaking at around 2 hours post-treatment and resolving back to basal levels by 24 hours (Figure 3.3b). The use of 5μM CCCP is cytotoxic but does not result in the outright killing of the entire population of SH-SY5Y cells, thus providing a good concentration to study cell death whilst leaving cells to study after 24 hours of treatment.

3.3.4 Parkin overexpression alters sensitivity to stress

To determine if the sensitivity of SH-SY5Y cells constitutively overexpressing *PARKIN* differed from the WT line, the cell survival of these 2 cell lines after exposure to a range of cellular stressors was determined (Figure 3.4).

Cells were treated with 5μM CCCP, 10μM H_2O_2, 0.1μM rotenone or 100nM epoxomicin, an irreversible 26S proteasomal inhibitor, for 24 hours and surviving cells counted (Figure 3.4). Although Parkin is widely considered a protective protein, its overexpression resulted in greater sensitivity to CCCP-induced mitochondrial depolarisation ($p = 0.0063$). no statistically significant difference between the two SH-SY5Y lines was determined for the other stressors. This suggests that *PARKIN* overexpression may differentially alter the cellular responses to various forms of stress and confirms that it sensitises SH-SY5Y cells to mitochondrial insult caused by CCCP. As only a low number of replicates were performed, if a small rescue/increase in sensitivity from *PARKIN* overexpression exists for the other stressors used here, it is unlikely it will be seen as statistically significant. Therefore, greater statistical power is required to fully confirm these data.

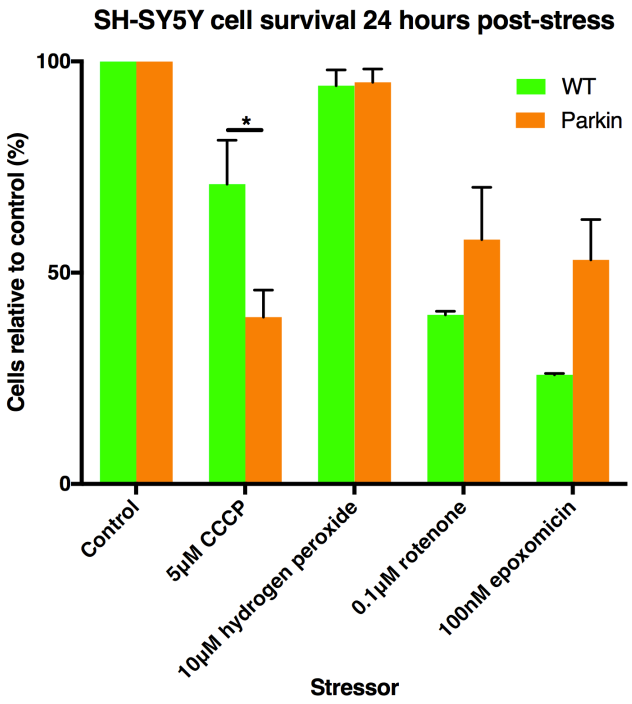

Figure 3.4: Cells expressing *PARKIN* are more sensitive to mitochondrial uncoupling than other stresses. Undifferentiated WT and *PARKIN* overexpressing SH-SY5Y cells exposed to multiple cellular stressors over a 24-hour period. Cell counts were performed in duplicate wells per experiment on the Operetta immunofluorescence microscope. Two fully independent replicate experiments were performed at different times, whereby cells were seeded, differentiated, fixed and counted (n = 2). Data shown is from the mean value of each individual biological replicate. Statistical significance was ascertained using an 2way ANOVA test (Bonferroni's) (*$p < 0.05$). Error bars represent SEM calculated from the mean of each individual experiment.

3.3.5 AP-1 proteins in SH-SY5Y cells

AP-1 proteins are transcription factors that play a major role in the stress response (Hess et al., 2004). Evidence has recently shown that the *Nrf2* expression is epigenetically repressed in neurons (Bell et al., 2015), thus suggesting antioxidant defences dependent on this pathway may be ineffective. In turn, this may suggest that AP-1-regulated defences could play a more prominent role in perturbing neuronal oxidative stress. To firstly test antibodies and look at the expression of the Jun (c-Jun, JunB and JunD) and Fos (c-Fos, FosB, Fra-1 and Fra-2) AP-1 transcription factors in SH-SY5Y cells, before and after differentiation, in both WT and Parkin lines immunofluorescence was employed. (Figures 3.4, 3.5, 3.6 and 3.7). Cells were co-stained for two different

AP-1 proteins at a time, thus both FITC (488 – green) and TRITC (594 - red) channels were used to visualise AP-1 localisation, along with DAPI.

Although not all antibodies have been previously validated for immunofluorescence, some of them had. All antibodies used for this analysis (Figures 3.4 - 3.7) were sourced from Abcam, who supply images for previously validated antibodies by this technique on their website. The antibody specific specific for c-Jun has been validated in PC-2 cells (human pancreatic cancer cell line), showing nuclear staining. Antibodies raised against JunB and JunD have also been shown to stain the nucleus in MCF-7 (human breast cancer cell line) and HeLa cells (human cervical cancer cell line), respectively. No previous data is available for antibodies specific to c-Fos or Fra-2 for immunofluorescence. However, both antibodies used for FosB and Fra-1 have been utilised previously to show nuclear staining in the mouse brain cortex and A-431 cells (human epidermoid carcinoma), respectively, by this technique.

No discernible differences in the expression or subcellular localisation of any of the AP-1 proteins were observed between WT and Parkin overexpressing cells using this method. Interestingly, despite being transcription factors it appears that not all Fos and Jun proteins localise solely to the nucleus under basal conditions. This was demonstrated by c-Jun and c-Fos being present in the nucleus and cytoplasm, whereas Fra-2 was solely localised to the cytoplasm in all 4 different cell lines.

The presence of JunB was not detected in all 4 lines assessed, which may suggest its expression is very low under normal conditions, thus below the detection level by this method. Unlike c-Jun and c-Fos, both JunD and Fra-1 showed no cytoplasmic localisation and appeared to be completely nuclear. Unfortunately, staining for FosB in the differentiated *PARKIN* overexpressing line did not work and, due to time constraints, this was not pursued further. However, overall nearly all of the AP-1 proteins assessed here were expressed in the different forms of the SH-SY5Y cell line.

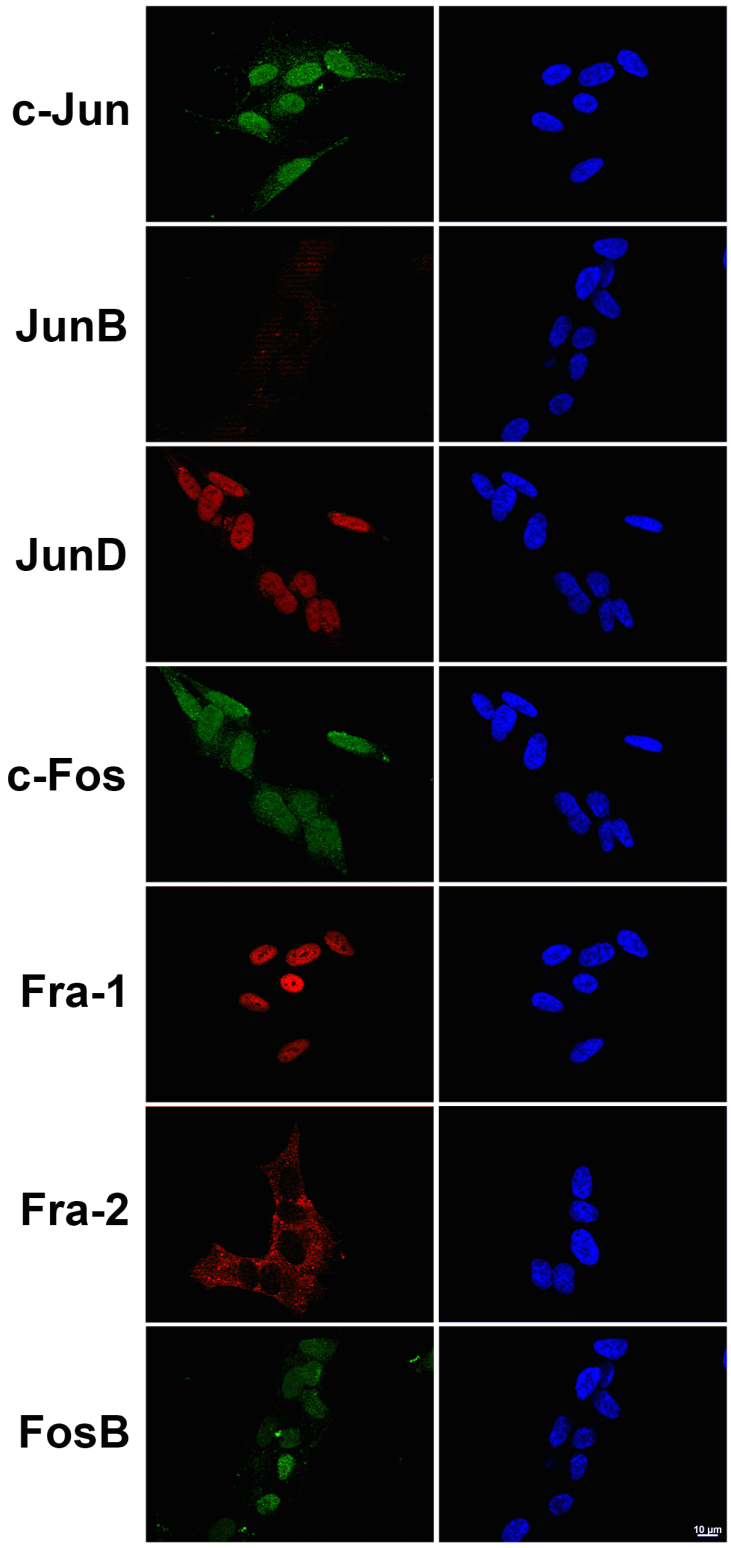

Figure 3.5: In undifferentiated WT SH-SY5Y cells most AP-1 proteins are detectable by immunofluorescence. Cell nuclei were stained with DAPI (blue) and AP-1 proteins visualised as red or green. Images were captured at 100X magnification using a Zeiss Imager Z1 fluorescent microscope coupled to AxioVision software (scale bar – 10µm).

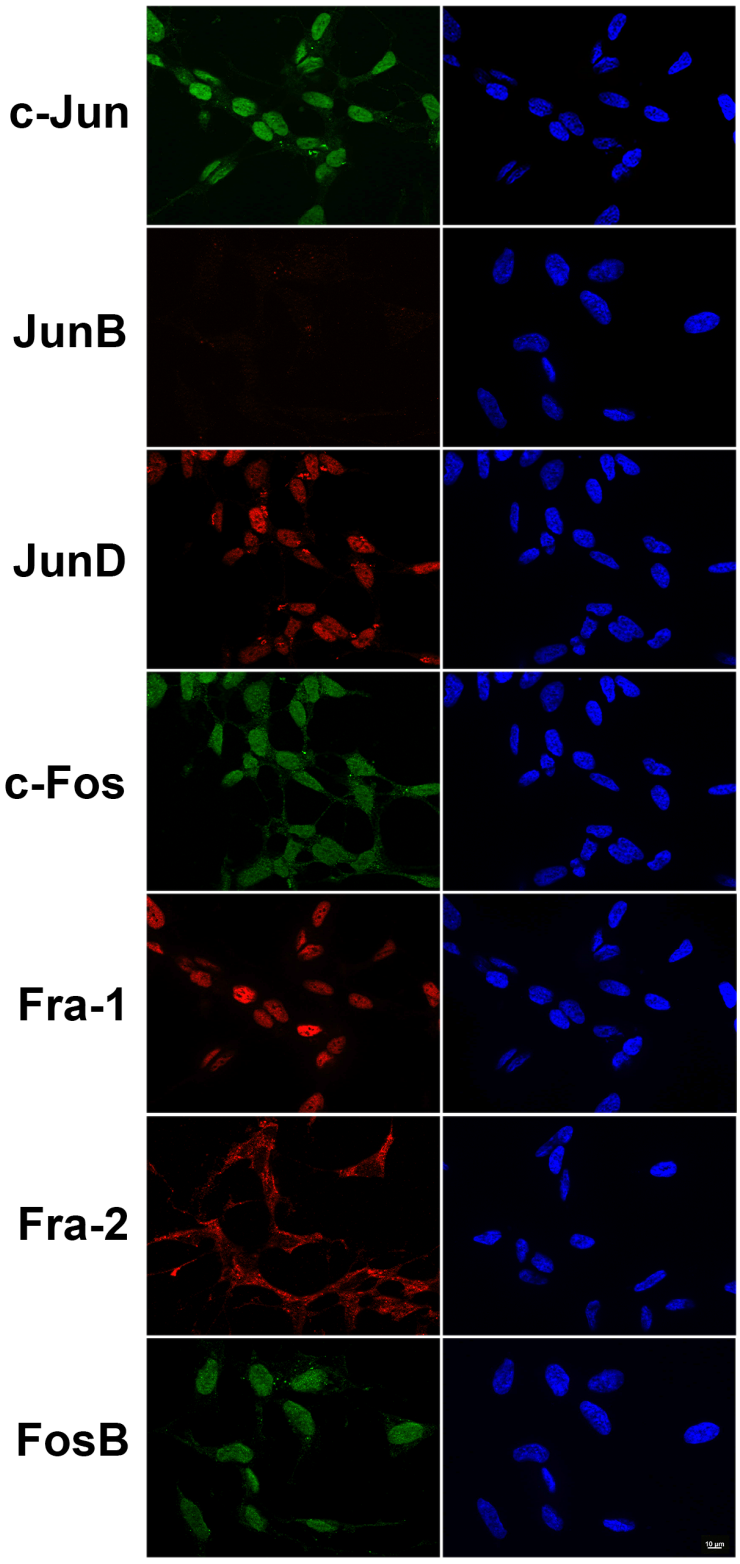

Figure 3.6: In differentiated WT SH-SY5Y cells most AP-1 proteins are detectable by immunofluorescence. Cell nuclei were stained with DAPI (blue) and AP-1 proteins visualised as red or green. Images were captured at 100X magnification using a Zeiss Imager Z1 fluorescent microscope coupled to AxioVision software (scale bar – 10μm).

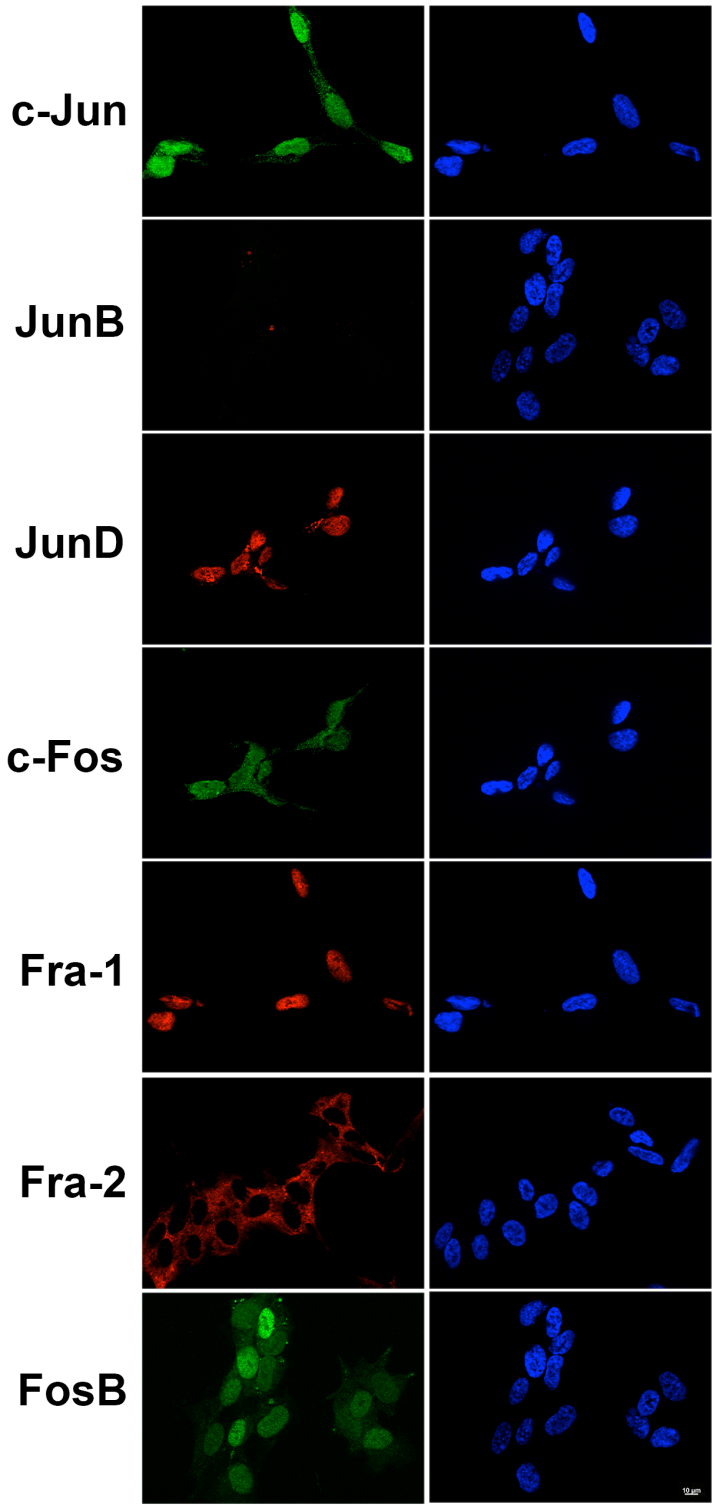

Figure 3.7: In undifferentiated Parkin SH-SY5Y cells most AP-1 proteins are detectable by immunofluorescence. Cell nuclei were stained with DAPI (blue) and AP-1 proteins visualised as red or green. Images were captured at 100X magnification using a Zeiss Imager Z1 fluorescent microscope coupled to AxioVision software (scale bar – 10μm).

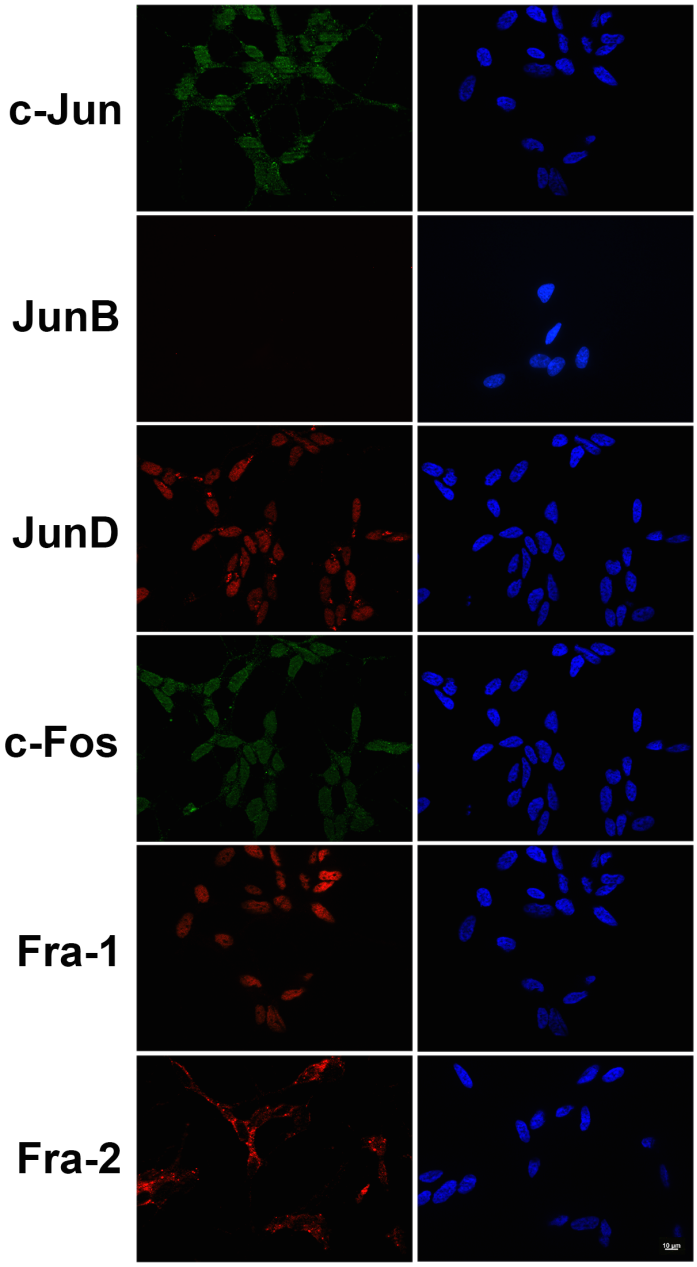

Figure 3.8: In differentiated Parkin SH-SY5Y cells most AP-1 proteins are detectable by immunofluorescence. Cell nuclei were stained with DAPI (blue) and AP-1 proteins visualised as red or green. Images were captured at 100X magnification using a Zeiss Imager Z1 fluorescent microscope coupled to AxioVision software (scale bar – 10μm).

3.3.6 Creating an inducible Parkin overexpression system in the SH-SY5Y cell line

Using the SH-SY5Y line constitutively expressing *PARKIN* can provide insight into the function of the E3 ligase and in the case of this study, how this protein

links in with AP-1/MAPK signalling. However, the use of a cell line that can inducibly overexpress *PARKIN* may be more advantageous. Few examples exist of successful inducible overexpression systems in SH-SY5Y cells and previous attempts to create an inducible system in these cells in this lab were unsuccessful (Hung, 2007).

The host cell line used (SH-TR) was kindly provided by Dr Luc Buee (INSERNM U422, IMPRT, Place de Vernun, France). These cells had been transfected with a pcDNA6/TR plasmid containing the tetracycline repressor element of the T-REx system and conferring blasticidine resistance (Hamdane et al., 2003). The preparation of pcDNA4/TO-*myc*-His expression vectors containing WT or T240R Parkin cDNA had been previously generated and sequenced as part of a prior PhD project (Hung, 2007). The pcDNA4/TO-*myc*-His expression vector contains a resistance gene to the antibiotic zeocin to allow for clonal selection. Prior to transfection with this vector the sensitivity of the SH-TR host cell line to zeocin was tested in order to allow for successful selection of transfected clones at a later date (Figure 3.8).

a)

SH-TR Zeocin Treatment		
Conc. (µg/ml)	**Cells/ml**	**% of control**
0 (control)	1.7×10^6	100
10	9.2×10^5	54.1
50	2.9×10^5	17.1
100	1.4×10^5	8.2
500	$2.0 \times 10^{4*}$	1.2
1000	Dead	0
* = Below accurate range		

b)

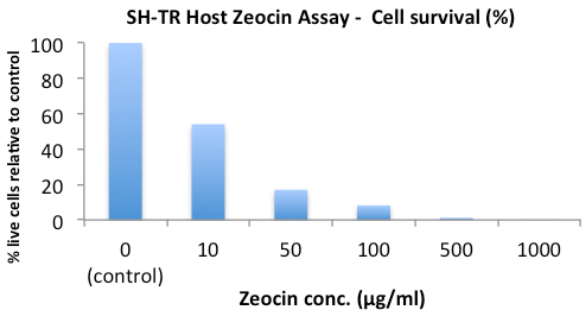

Figure 3.9: A kill curve demonstrating the range of cytotoxic Zeocin concentrations for SH-TR host cells (n =1). Host cells were set up at 20,000 cells/ml, 2ml/well of cell suspension applied to 6-well plates and incubated for 24 hours. Media was then removed and cells incubated in fresh media containing different zeocin concentrations for 72 hours. Live cell counts were performed on the Countess™ 72 hours after treatment with Zeocin.

To help dissect the role of Parkin using the SH-TR system, the aim was to transfect cells with either WT *PARKIN* (Par1) or the non-functional (lacks E3 ubiquitin ligase activity) *PARKIN* containing the PD-associated T240R mutation. The successful creation of a T-REx SH-SY5Y cell line should result in little to no expression of the exogenous *PARKIN* gene. Upon incubation with 1µg/ml tetracycline, the Tet repressor (TetR) contained in the pcDNA6/TR integrated into the SH-TR host genome is bound by tetracycline. This causes a conformational change in the TetR, which in turn allows the expression of the gene of interest. In this case, the gene of interest will be either WT or T240R Parkin, integrated as part of the pcDNA4/TO-*myc*-His vector.

Initially, the success of Par1 and T240R transfections was assessed by immunofluorescence. Monoclonal lines were treated with 1µg/ml Tet (or ethanol as vehicle control) the intensity of Parkin staining used to determine if overexpression was induced by incubation with Tet (Figures 3.9 and 3.10). All images were captured using the same exposure times to allow for quantitative analysis if required.

These immunofluorescence images shown here in figures 3.9 and 3.10 provide examples of some of the monoclonal lines generated. The images firstly suggest that expression of the T240R mutant was generally greater than WT Parkin, hence why many of the mutant images are overexposed. Furthermore, nearly all monoclones overexpressed their Parkin construct even prior to tetracycline induction.

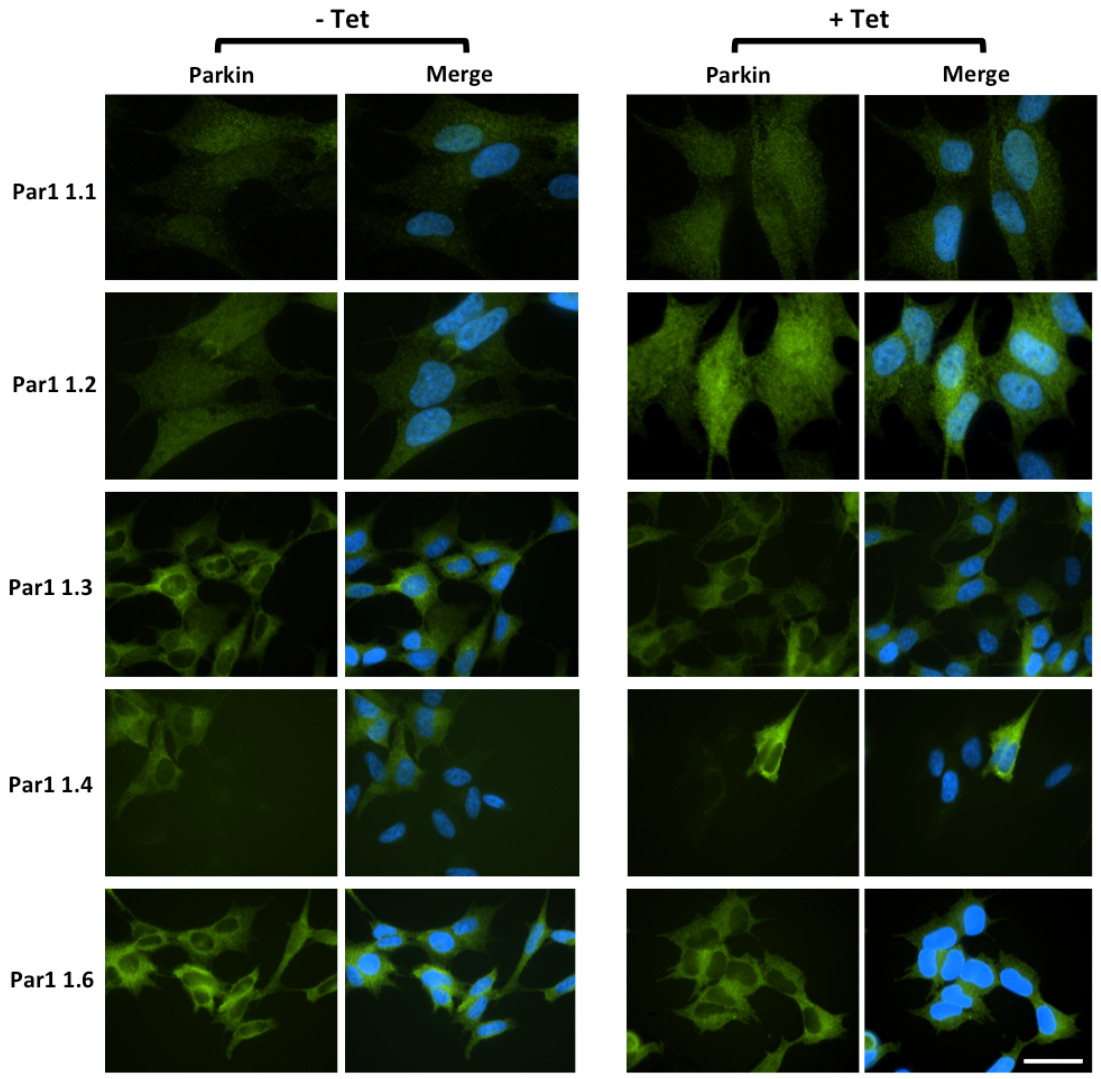

Figure 3.10: SH-TR Par1 show no discernible induction of *PARKIN* expression. Cells were viewed at 100X magnification. Monoclonal cell lines that had been transfected with the WT Parkin plasmid were treated with tetracycline or ethanol (vehicle), fixed then stained for DAPI and Parkin (green). Scale bar – 50μm.

The Par1.4 cell line (Figure 3.9) did not appear to be monoclonal since a proportion of cells in this culture, although clearly resistant to zeocin, did not express the transfected Parkin construct before or after tetracycline treatment. Interestingly, an inducible mutant cell line, SH-TR T240R 3.3, was successfully produced (Figure 3.10), as Parkin levels were very low without tetracycline treatment but clearly induced upon incubation with Tet media. Unfortunately, bacterial contamination in some of the cultures, including T240R 3.3, resulted in several lines being lost.

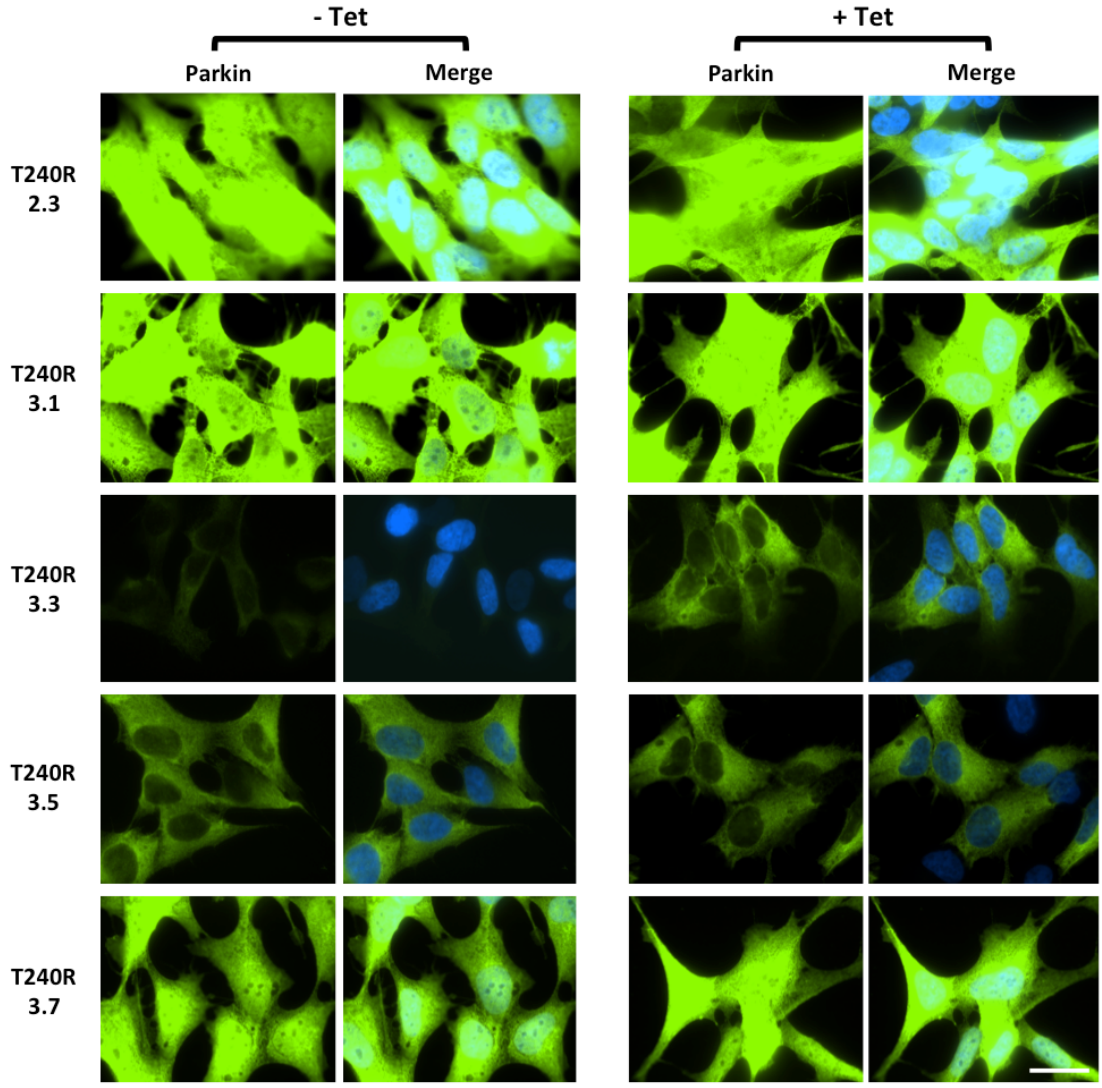

Figure 3.11: SH-TR T240R cells viewed at 100X magnification showing one successfully established inducible cell line. Monoclonal cell lines that had been transfected with the T240R mutant Parkin plasmid were treated with tetracycline or ethanol (vehicle), fixed then stained for DAPI and Parkin (green). Scale bar - 50μm.

Later monoclonal cultures were assessed using western blotting analysis to ascertain Parkin protein levels (Figure 3.11), Parkin was undetectable by western blotting in the host cell line. However, all transfected monoclones showed elevated levels of Parkin relative to the host even prior to tetracycline treatment. This concurred with observations made from IF analysis (Figures 3.9 and 3.10).

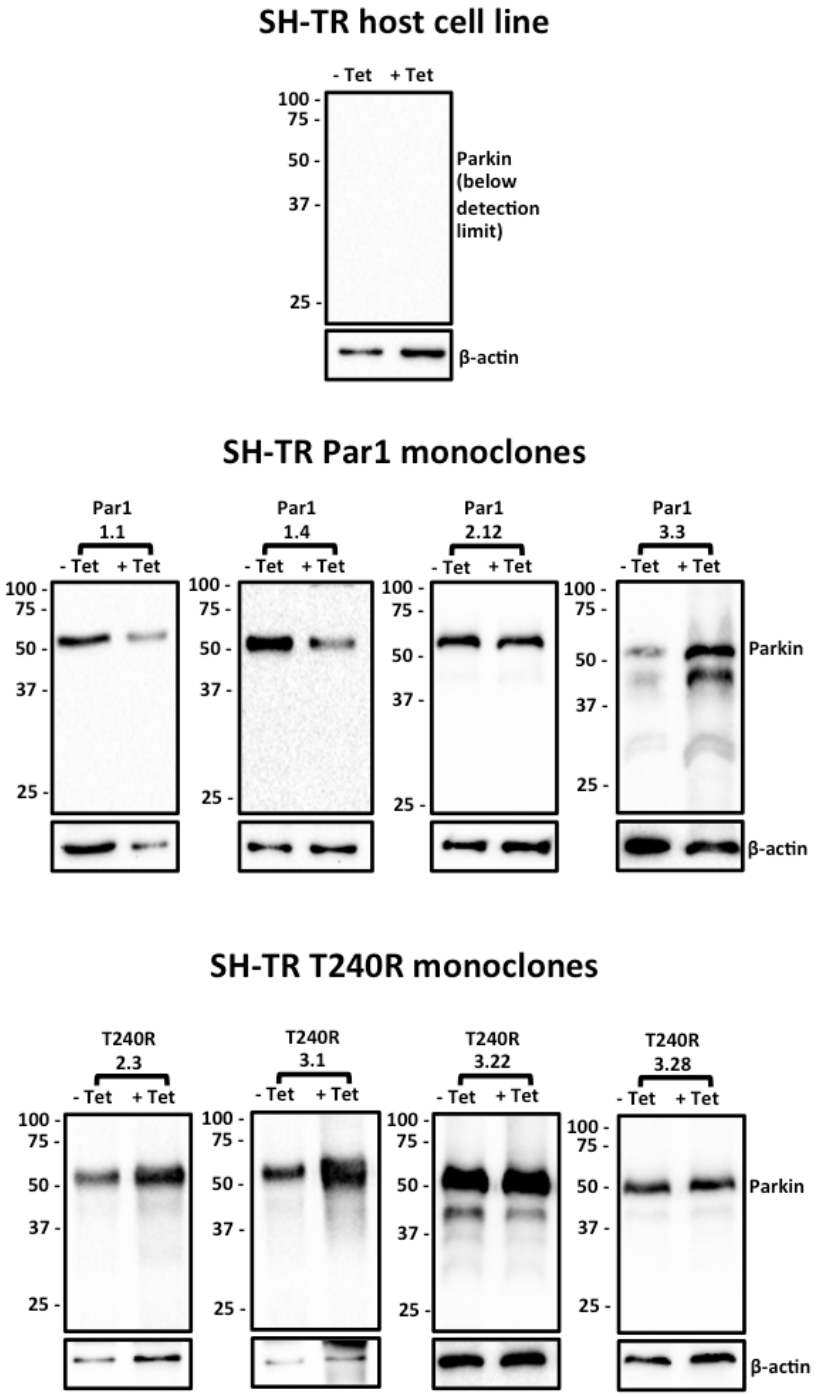

Figure 3.12: Detection of inducible Parkin in SH-SY5Y T-REx monoclonal cell lines with and without tetracycline treatment. After Parkin immunoblotting membranes were stripped and re-probed for β-actin as a loading control.

Although all monoclones assessed appeared to have 'leaky' expression (i.e. *PARKIN* overexpression was occurring prior to Tet induction), the SH-TR Par1 3.3 did appear to show some induction (Figure 3.11). To quantitatively assess

this, densitometric analysis was performed using Bio-Rad Image Lab software (Figure 3.12). The fold change in Parkin protein levels 24 hours after incubation with 1µg/ml tetracycline relative to the vehicle control (EtOH) was calculated and normalised to β-actin.

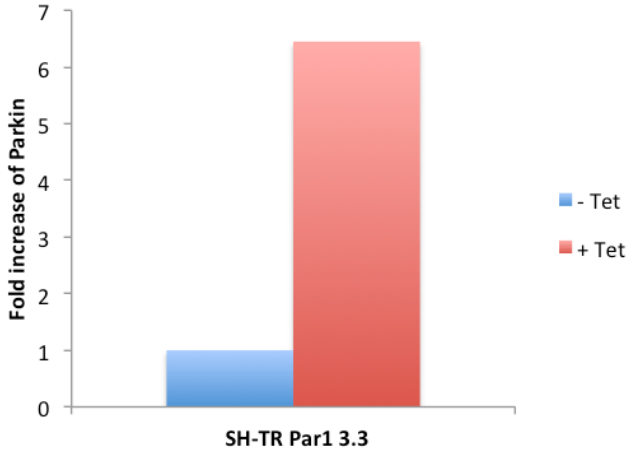

Figure 3.13: The tetracycline-induced expression of Parkin. The level of Parkin in clone SH-TR Par1 3.3 detected by western blot (Figure 3.11) was analysed by densitometry and the fold change in Parkin protein levels relative to β–actin calculated (n = 1).

A clear induction in the expression of the integrated *PARKIN* construct can be seen from this, with around 6-fold increase relative to the uninduced cells. However, 'leaky' expression was still observed (Figure 3.11), thus Parkin levels were still significantly higher without Tet induction than in the host cell line. Nevertheless, the fact that this cell line provides a platform by which to induce relative overexpression of Parkin may prove useful.

3.4 CONCLUSIONS

The initial aim of the project was to show the SH-SY5Y cell line would be suitable for studying mitochondrial dysfunction and oxidative stress. The CellROX® Green Reagent allowed confirmation of this, showing that CCCP-induced mitochondrial uncoupling leads to cellular oxidative stress. Furthermore, the overexpression of Parkin, a key protein in the response to mitochondrial stress, was maintained post-differentiation using RA/BDNF. This

was important as both differentiated and undifferentiated SH-SY5Y cells will be utilised in this project. The creation of a cell line that could inducibly overexpress *PARKIN*, WT or mutant, could be advantageous. However, despite the SH-R Par1 3.3 line showing inducible expression of WT *PARKIN*, 'leaky' expression was still observed prior to tetracycline induction. A single Par1 inducible cell line (clone 3.3) was successfully established for potential use in future experiments. As the WT and Parkin SH-SY5Y cell lines used in this study were non-matched lines, other factors may have an effect, thus making any differences that are observed between these cells difficult to attribute to Parkin overexpression. This is why the establishment of an inducible Parkin overexpressing model that did not have 'leaky' expression of the construct would have been advantageous.

Overall, data presented here suggest the WT and Parkin SH-SY5Y lines will provide a usual model for studying AP-1 modulation in response to mitochondrial dysfunction and oxidative stress in relation to PD. As both undifferentiated and differentiated SH-SY5Y cells have been used in the past, the use of both forms in studies presented in this thesis may give greater insight into neuronal responses to mitochondrial stress.

CHAPTER 4
THE AP-1 RESPONSE TO MITOCHONDRIAL DAMAGE AND OXIDATIVE STRESS

4.1 INTRODUCTION

The AP-1 transcription factor complex is a key regulator of the immediate cellular response to stress (Hess et al., 2004). Mitochondrial and oxidative stress are key features of PD pathology, thus the response of neurons undergoing these forms of stress is likely to play a key role in the progression of the disease, thus understanding this response will be critical in the development of future therapeutics. Furthermore, as mitochondria are the primary source of intracellular ROS (Wallace, 2005), these two forms of stress will often be linked.

MAPK/AP-1 pathways have previously been linked to mitochondrial dysfunction and oxidative stress in PD (Crocker et al., 2001, Peng and Andersen, 2003, Ganguly et al., 2004, Hunot et al., 2004, Milton et al., 2011, Bouman et al., 2011). By dissecting these signalling pathways and understanding how they are modulated in response to neuronal insults associated with dopaminergic neurodegeneration, it may be possible to understand how the cellular adaptive responses are overcome and apoptotic pathways are then initiated. How AP-1 transcription factors fit into this is still currently unclear. It is likely that the individual Jun (c-Jun, JunB and JunD) and Fos (c-Fos, FosB, Fra-1 and Fra-2) proteins will play different roles in these responses. Moreover, not all of these will have any function whatsoever under the conditions focused on in this study.

Data from Chapter 3 shows that the SH-SY5Y cell line provides a suitable model to study mitochondrial and oxidative stress in relation to PD. Furthermore, many of the AP-1 proteins were readily observed by immunofluorescence under basal conditions (Figures 3.4 – 3.7). Importantly, it is possible to differentiate this cell line to develop a neuronal-like phenotype, thus giving a more accurate representation of dopaminergic neurons. The use of cells overexpressing Parkin may also help elucidate the role of defined AP-1 proteins in the response to mitochondrial stress. Parkin is critical in the mitophagic response initiated by CCCP-induced mitochondrial depolarisation (Narendra et al., 2008, Gegg et al., 2010, Narendra et al., 2010a, Vives-Bauza et al., 2010) and mutations in the *PARKIN* gene are the most common cause of autosomal-recessive juvenile PD (AR-JP) (Kitada et al., 1998, Scarffe et al., 2014). Previous data has already shown that *PARKIN* expression is repressed

by the AP-1 protein, c-Jun (Bouman et al., 2011). Therefore, comparing the AP-1 response to CCCP between WT and Parkin overexpressing SH-SY5Y cells may provide insight into how defined Jun or Fos proteins fit into the mitochondrial stress response in neurons.

4.2 AIMS

The use of the SH-SY5Ys provides a model to study mitochondrial dysfunction in a neuronal-like cell line. The purpose of this was to recapitulate cellular events that are strongly associated with the PD phenotype. By inducing mitochondrial depolarisation in SH-SY5Y cells, the aim was to monitor how individual AP-1 proteins are modulated in response to the uncoupling of mitochondria. This was achieved by western blot and RT-qPCR analysis. Furthermore, this thesis looked to determine the role of these proteins in CCCP-induced apoptosis by utilising siRNA and high-throughput immunofluorescence techniques. The overall aim of this was to identify which AP-1 transcription factor(s) play a role in the response to mitochondrial stress and would therefore warrant further investigation.

4.3 RESULTS

4.3.1 AP-1 protein levels are modulated in response to mitochondrial damage

To determine how the protein levels of the individual AP-1 transcription factors vary upon mitochondrial uncoupling, western blotting was used to monitor changes in protein levels relative to β-actin at specific time points in response to 5μM CCCP treatment (Figures 4.1 – 4.14). Both Jun and Fos protein families were observed in this manner. The initial aim was to determine their modulation over a 6-hour period after CCCP treatment to look at the immediate response to mitochondrial damage. After this, the resulting changes in AP-1 protein levels from CCCP over a 24-hour period after treatment was then observed by the same method.

PARKIN overexpressing SH-SY5Y cells were more sensitive to both differentiation and CCCP treatment compared to WT cells, and consequently a substantially lower amount of protein was obtained from extractions. This made it unrealistic to thoroughly assess all 7 AP-1 transcription factors by this method. Furthermore, differentiation of WT SH-SY5Ys led to an increased sensitivity to CCCP-induced mitochondrial depolarisation when compared with undifferentiated cells. Therefore, only the first 6 hours post-CCCP was assessed here (some data for differentiated cells over a 24-hour period of uncoupling can be found in the next chapter). The promoter regions of AP-1 genes contain TREs (Hess et al., 2004) and so AP-1 expression is upregulated in response to TPA. Therefore, protein extracts obtained from SH-SY5Y cells that had been treated with 100μg/ml TPA for 2 hours were utilised as positive control, when required.

4.3.1.1 The Jun family proteins

4.3.1.1.1 c-Jun

c-Jun, a Jun protein family member, is one of the most extensively investigated AP-1 transcription factors. It has the ability to homodimerise or heterodimerise

with other Jun or Fos proteins in order to form an AP-1 transcription factor complex (Hess et al., 2004) and has been linked to PD in several studies (Crocker et al., 2001, Hunot et al., 2004, Ganguly et al., 2004, Bouman et al., 2011).

To investigate the initial response of c-Jun, protein extracts obtained at time points between 0 and 6 hours post-5μM CCCP were analysed by western blotting. Over the first 6 hours after treatment with 5μM CCCP, c-Jun protein levels underwent significant changes in the SH-SY5Y lines examined (Figure 4.1). A significant initial drop was observed in the undifferentiated WT cell line. In the differentiated cell line, protein levels were elevated relative to basal conditions by 2 hours post-uncoupling and this was sustained. This may suggest that RA/BDNF differentiation of these cells could result in the c-Jun response being exaggerated and sustained. Parkin overexpression also led to increased elevation of c-Jun levels after uncoupling, which continue to rise up to the 6-hour cut off point.

In WT cells, c-Jun levels were elevated relative to starting conditions by 2 hours post-uncoupling (Figure 4.2). This was maintained at the 12, 18 and 24 hour time points as well. In the Parkin overexpressing line, a small continual increase was seen up until 24 hours, by which time the levels of c-Jun were around 7 times higher than prior to CCCP treatment.

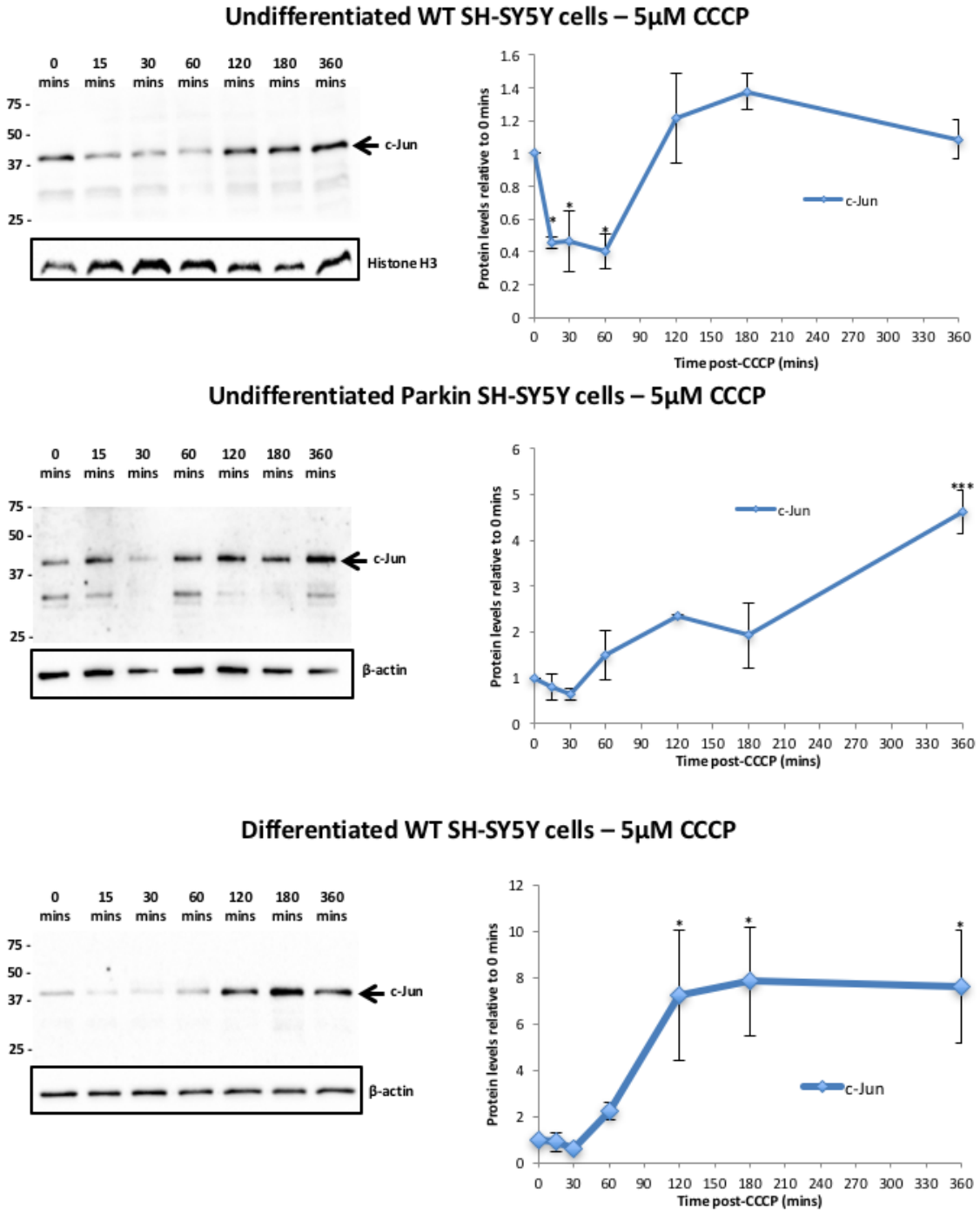

Figure 4.1: c-Jun protein levels are rapidly modulated during the first 6 hours post-5µM CCCP. c-Jun (36kDa) was assessed in undifferentiated WT and Parkin overexpressing cells (n = 2), as well as in differentiated SH-SY5Ys (n = 3). Protein extracts were obtained at specific time points and analysed by western blotting and densitometry relative to β–actin. 'n' values refer to independent biological replicates, where cells were seeded, treated, protein extracted, western blot analysis and quantification performed per individual replicate. Statistical significance was assessed using a 2way ANOVA (Dunnett's). (*$p < 0.05$, ***$p < 0.005$). Error bars represent SEM.

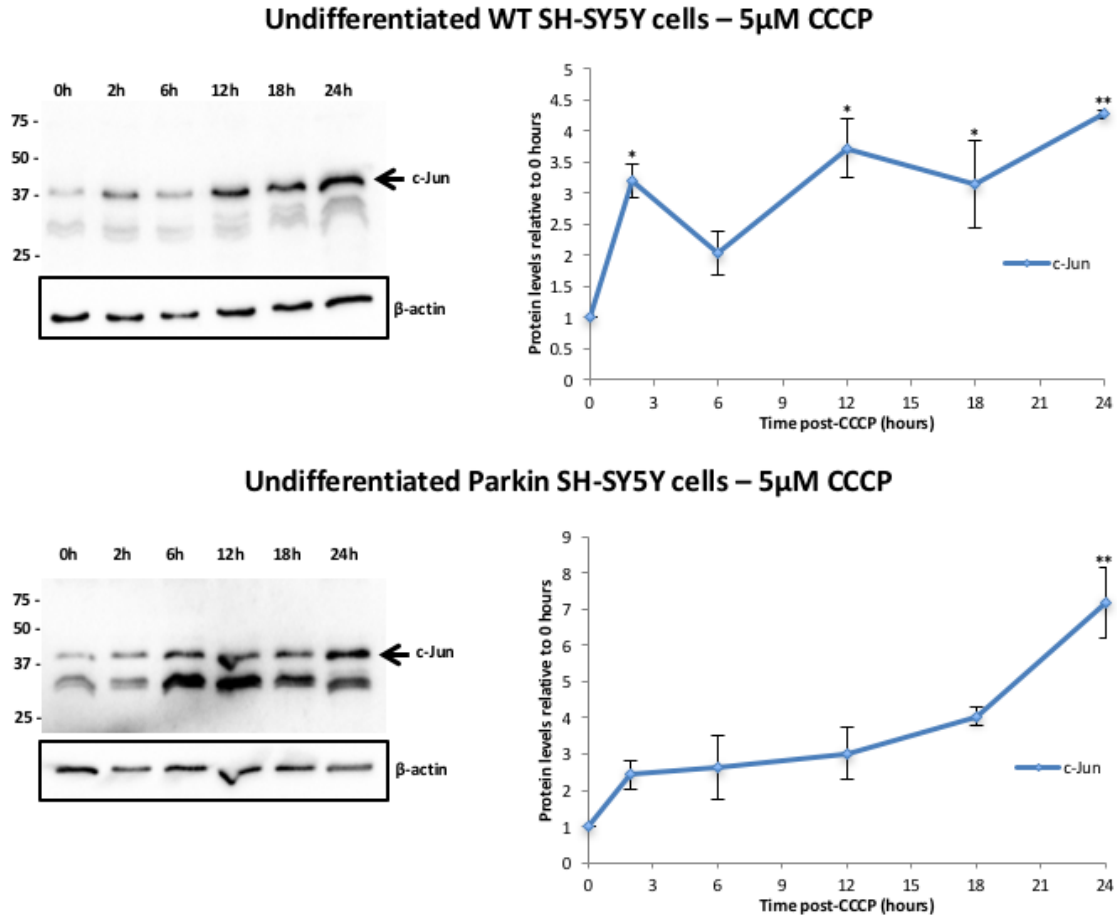

Figure 4.2: c-Jun protein levels become elevated over the period of 24 hours after 5µM CCCP exposure in undifferentiated WT and Parkin SH-SY5Y cells (n = 2). Protein extracts were obtained at specific time points and analysed by western blotting and densitometry relative to β–actin. An increase in c-Jun protein levels occured in WT cells and in the Parkin overexpressing line. 'n' values refer to independent biological replicates, where cells were seeded, treated, protein extracted, western blot analysis and quantification performed per individual replicate. Statistical significance was assessed using a 2way ANOVA (Dunnett's). (*$p < 0.05$, **$p < 0.01$). Error bars represent SEM.

Although a significant increase was observed 2 hour post-uncoupling in undifferentiated WT cells in the 24 hour assay (Figure 4.2), it was not observed in the 6 hour assay at this same time point (Figure 4.1). This lack of reproducibility, along with a low number of replicates, makes it difficult to properly conclude exactly how c-Jun is modulated in these initial 2 hours. The conclusive determination of this would be critical in determining the validity of a 2 phase c-Jun response to mitochondrial uncoupling.

4.3.1.1.2 JunB

JunB is another Jun protein, but is generally considered to have weaker transactivation potential compared to c-Jun (Hess et al., 2004). JunB was not detectable by IF under basal conditions in any of the SH-SY5Y lines tested (Figures 3.4 – 3.7), but was detectable by western blotting utilising the same antibody (Figures 4.3 and 4.4).

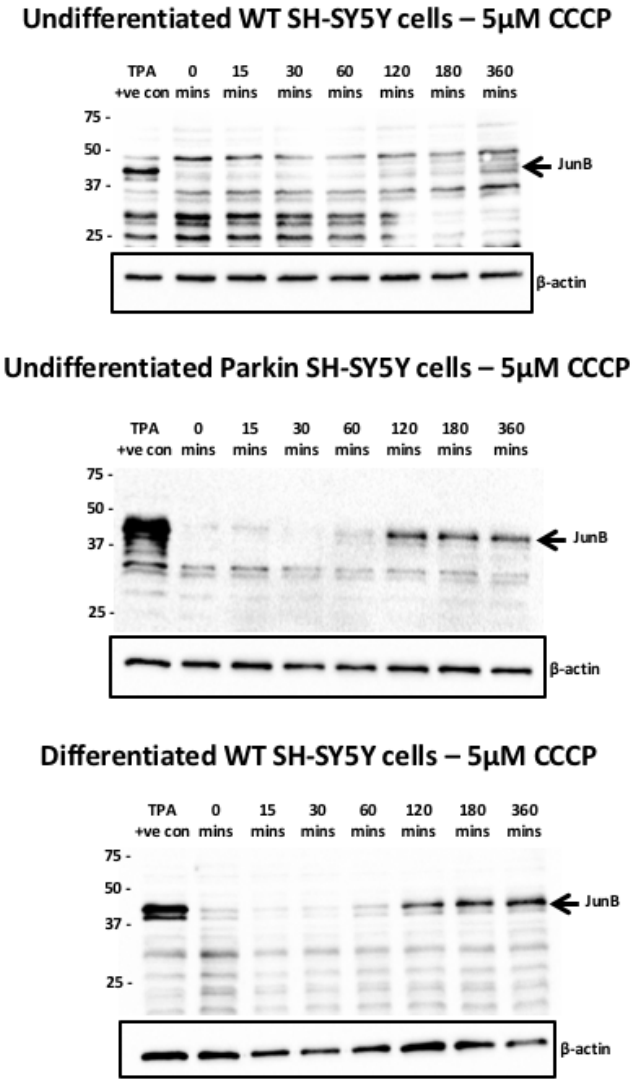

Figure 4.3: JunB protein levels rapidly rise during the first 6 hours of 5µM CCCP treatment. Undifferentiated WT and Parkin cells (n = 2) both saw increased levels of JunB (36kDa) towards 6 hours. JunB levels in differentiated WT cells (n = 1) also rapidly increased all the way up until the 6 hour time point. TPA induction was used as a positive control. 'n' values refer to independent biological replicates, where cells were seeded, treated, protein extracted, western blot analysis and quantification performed per individual replicate.

The treatment of cells with TPA for 2 hours strongly induced the expression of JunB(Figure 4.3). As multiple bands were observed, as well as several blots showing non-uniform levels of background, densitometric analysis was not applied to quantify changes in JunB protein levels. Nevertheless, it does appear that JunB protein levels do rise during the first 6 hours of CCCP treatment. In differentiated WT cells (Figure 4.3) JunB was strongly induced. However, upon repeating this experiment several times, the antibody did not work. Due to time constraints this experiment was not repeated again. If extra time was available this assay would have been repeated to confirm JunB modulation in this cell line.

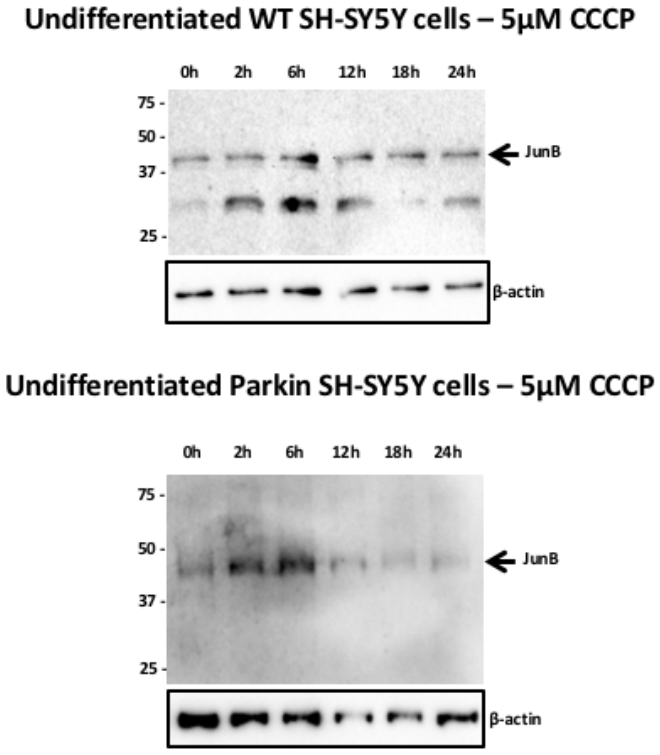

Figure 4.4: JunB protein levels increase and then reduce by 24 hours in response to 5µM CCCP. Protein levels were assessed by western blotting and densitometry for both undifferentiated WT and Parkin SH-SY5Y cells (n = 2). 'n' values refer to independent biological replicates, where cells were seeded, treated, protein extracted, western blot analysis and quantification performed per individual replicate.

4.3.1.1.3 JunD

In all 3 cell lines treated, no large increases in either of the JunD isoforms (37kDa (blue line) and 41kDa (red line)) was observed over the first 6 hours of

uncoupling (Figure 4.5). In the undifferentiated WT cells, only small changes in the levels of the JunD proteins were observed during the first 6 hours. It was only in the undifferentiated WT cells that a significant increase in JunD levels was observed during this period.

Large SEM values in the WT cells make it difficult to assess the validity of any apparent increase (Figure 4.6), thus highlighting the need for further replicates to be performed to properly determine this. Significant elevation in JunD levels is observed in the WT cells by 24 hours post-CCCP, which may be supressed by *PARKIN* overexpression.

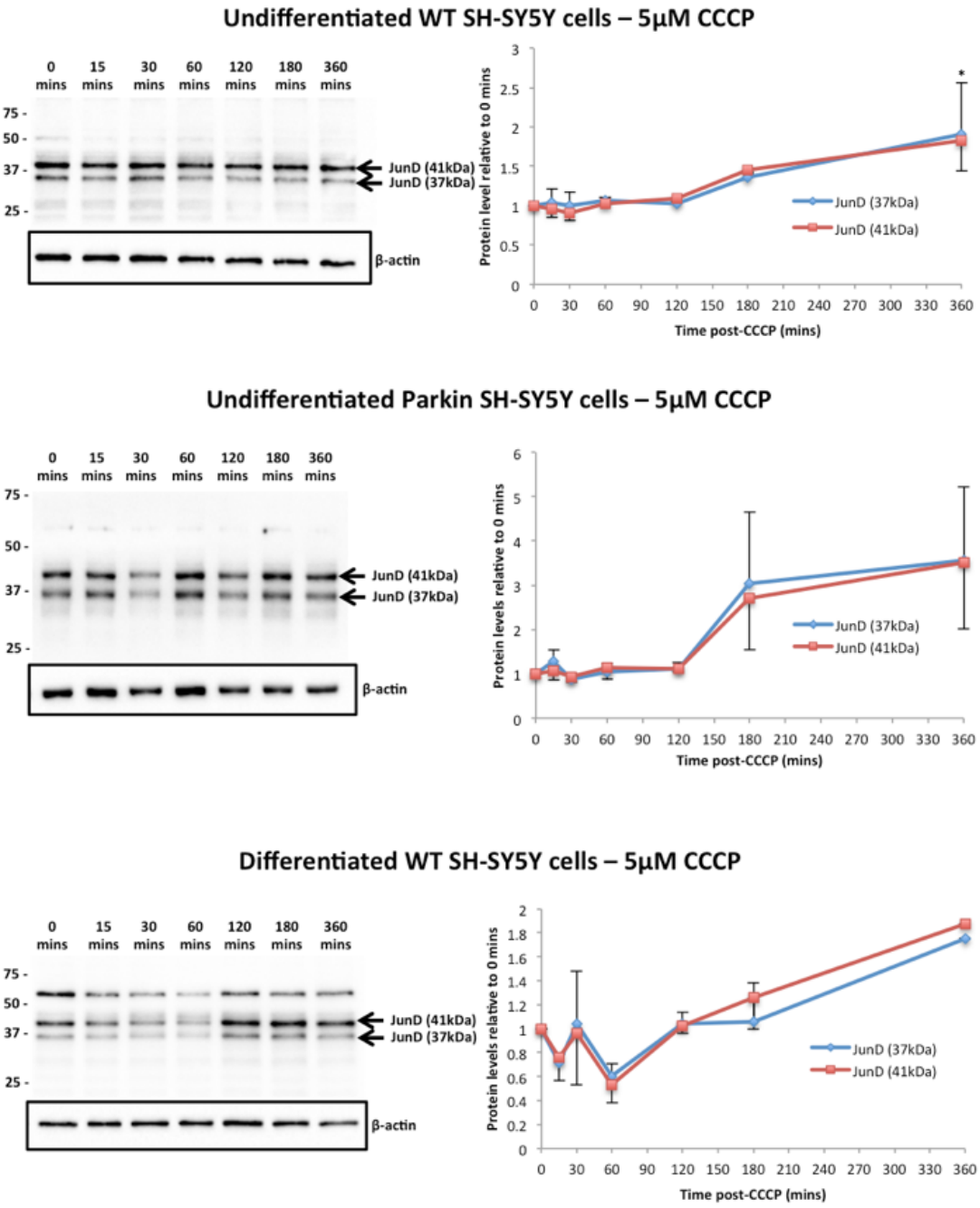

Figure 4.5: JunD protein levels during the initial 6 hours post-5µM CCCP show no significant modulation for either isoform. The 37kDa (blue) and 41kDa (red) isoform levels appear to mirror one another for all 3 cell lines. Both isoforms were individually assessed from undifferentiated WT (n = 2) and Parkin overexpressing lines (n = 3), as well as in differentiated WT SH-SH5Ys (n = 2). 'n' values refer to independent biological replicates, where cells were seeded, treated, protein extracted, western blot analysis and quantification performed per individual replicate. Statistical significance was assessed using a 2way ANOVA (Dunnett's). (*p < 0.05). Error bars represent SEM.

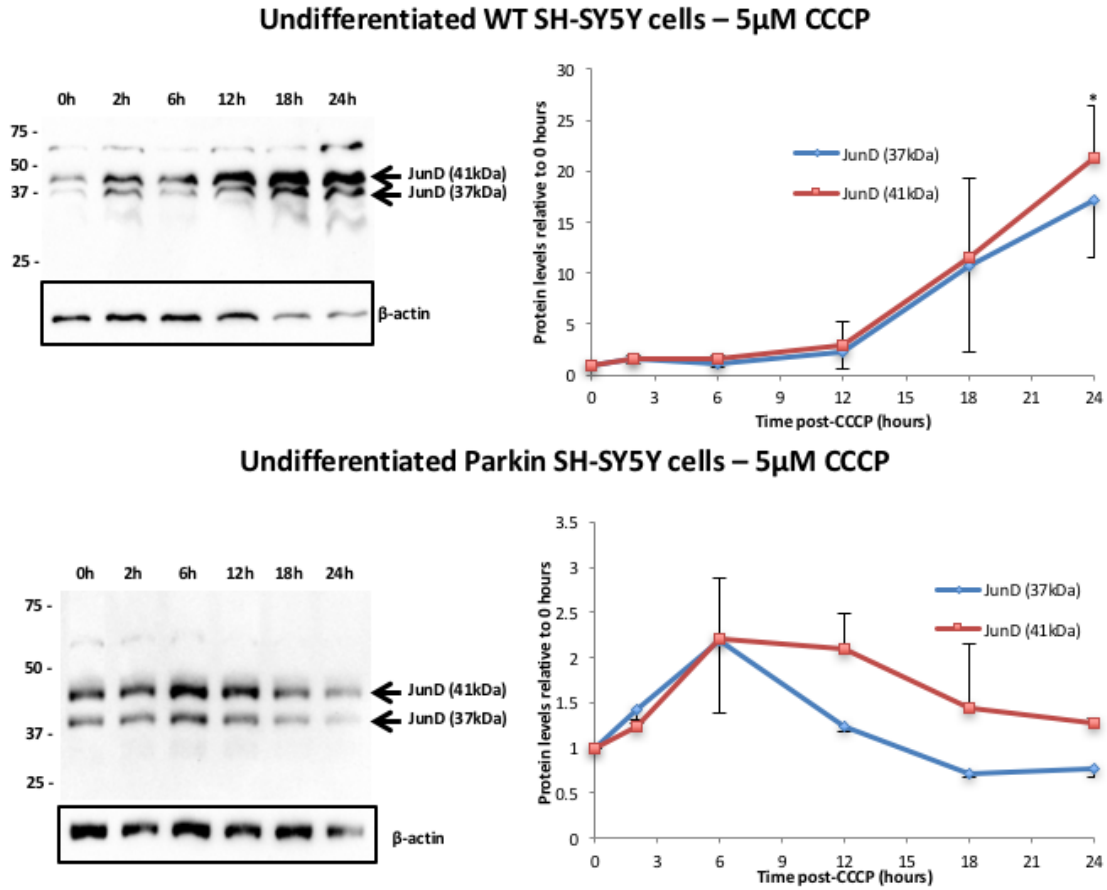

Figure 4.6: The 24 hour JunD protein response to 5µM CCCP treatment may be suppressed by Parkin overexpression. Both the 37kDa (blue) and 41kDa (red) isoforms were modulated in the WT and Parkin cell lines (n = 2). Protein extracts were obtained at specific time points and analysed by western blotting and densitometry relative to β–actin. 'n' values refer to independent biological replicates, where cells were seeded, treated, protein extracted, western blot analysis and quantification performed per individual replicate. Statistical significance was assessed using a 2way ANOVA (Dunnett's). (*$p < 0.05$). Error bars represent SEM.

4.3.1.2 The Fos family proteins

4.3.1.2.1 c-Fos

Like c-Jun, c-Fos has been one of the more extensively studied AP-1 proteins. The expression of *c-FOS* can be induced rapidly, within a 15 minute period post-stimulus (Basbous et al., 2008). The anti-c-Fos antibody (ab129361) raised in mouse that was utilised in the previous results chapter for immunofluorescence (Figures 3.4 – 3.7) was initially tried for western blotting.

However, no band corresponding to c-Fos (MW = 55kDa) was observed upon multiple attempts, even in TPA treated cells. An alternative antibody was therefore sourced (Cell Signaling 2250). This antibody raised in rabbit, was proficient at detecting the c-Fos protein band in the TPA-induced positive control (Figure 4.7).

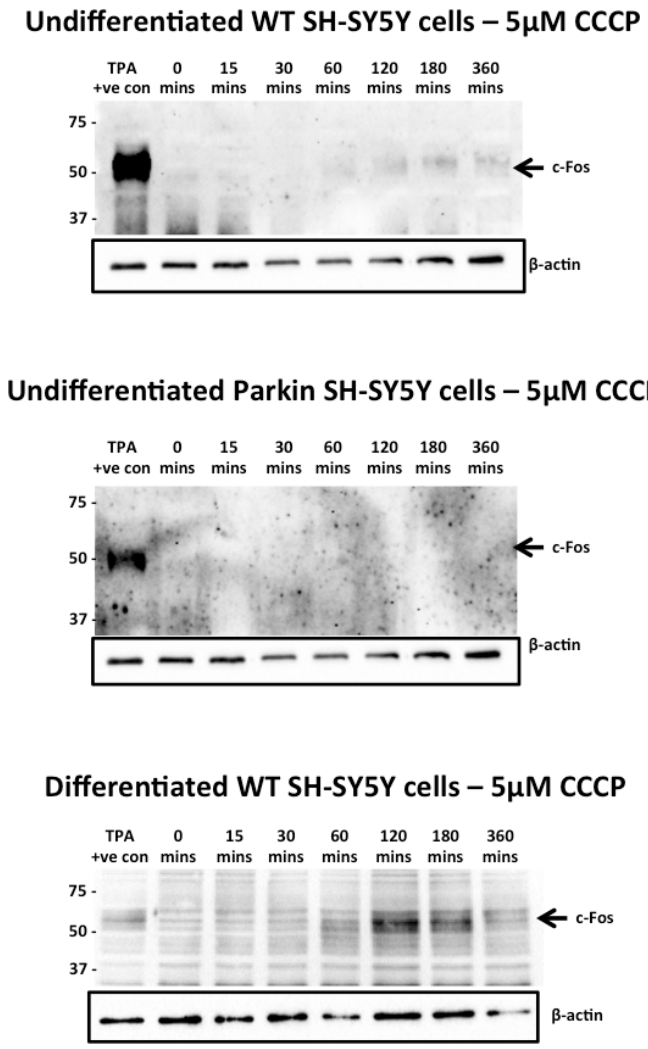

Figure 4.7: c-Fos expression can be induced by 5µM CCCP. Under normal conditions c-Fos (41kDa) levels were below detection by western blotting. Treating cells with 100µg/ml TPA for 2 hours induced c-Fos expression to provide a positive control for undifferentiated WT and Parkin and differentiated WT cells (n = 2). 'n' values refer to independent biological replicates, where cells were seeded, treated, protein extracted, western blot analysis and quantification performed per individual replicate.

In undifferentiated WT cells c-Fos became detectable at around 120 minutes post-CCCP (Figure 4.7), although the bands observed were faint, even after prolonged exposure, suggesting protein levels were still very low once induced. However, this was not able to detect any c-Fos protein, other than in the TPA positive control when performing the 24 hour CCCP assay (Figure 4.8). As c-Fos for the 6 hour assay was probably at the lower limit of detection it is possible that the c-Fos expression was still induced under these conditions but was just below the detection capacity of this technique. Differentiation of these cells did not abolish c-Fos induction during the first 6 hours of CCCP treatment (Figure 4.7).

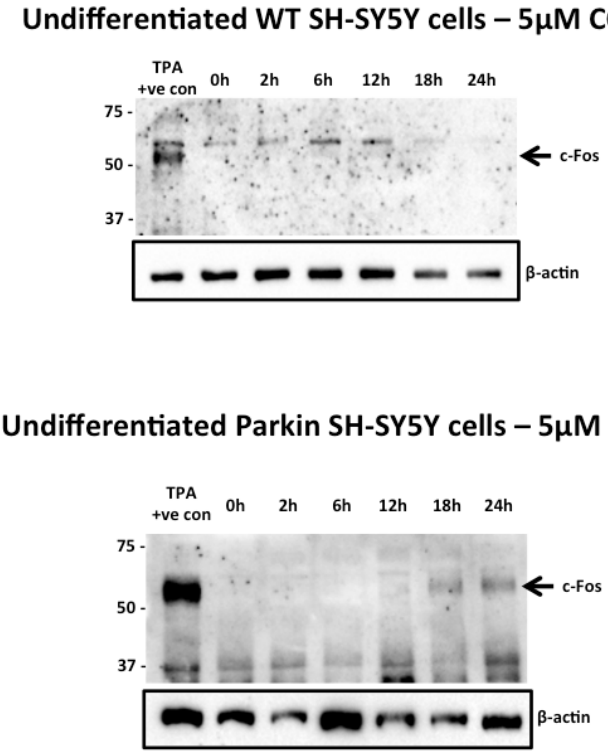

Figure 4.8: c-Fos protein levels for 24 hours post-5µM CCCP. The expression of c-Fos was induced by CCCP between 12-18 hours after treatment in Parkin overexpressing cells. Protein extracts were obtained at specific time points and analysed by western blotting and densitometry relative to β–actin. Cells were incubated with media containing 100µg/ml TPA for 2 hours in order to induce c-Fos expression in undifferentiated WT and Parkin cells (n = 2). 'n' values refer to independent biological replicates, where cells were seeded, treated, protein extracted, western blot analysis and quantification performed per individual replicate.

In the Parkin overexpressing SH-SY5Y cells no c-Fos protein was detected during the first 6 hours of CCCP-induced mitochondrial depolarisation (Figure 4.7). However, the induction of c-Fos was detectable by 18 hours post-CCCP suggesting a delay in the expression of this protein (Figure 4.8).

4.3.1.2.2 FosB

FosB exists as 2 isoforms, the full-length transcript, FosB, and the smaller isoform, ΔFosB (Hess et al., 2004). Like c-Fos, FosB was not detectable under normal conditions in any of the 3 cell lines. However, its expression, in the same manner as c-Fos, was induced by incubation with TPA allowing both FosB and ΔFosB, its truncated form, to be easily detectable by western blot.

In undifferentiated WT cells, FosB protein levels became visible at 3 hours post-CCCP (Figure 4.9). After FosB induction protein levels appeared to be maintained until around 12 hours post-CCCP before dropping off (Figure 4.10). Furthermore, unlike the other 2 cells lines, a clear band was observed at around 30kDa. Due to its molecular weight it is likely that this is a non-specific band. Upon differentiation, the FosB response was detectable 6 hours after CCCP (Figure 4.9). This was similar to in the undifferentiated cell line and again was only visible as very faint bands.

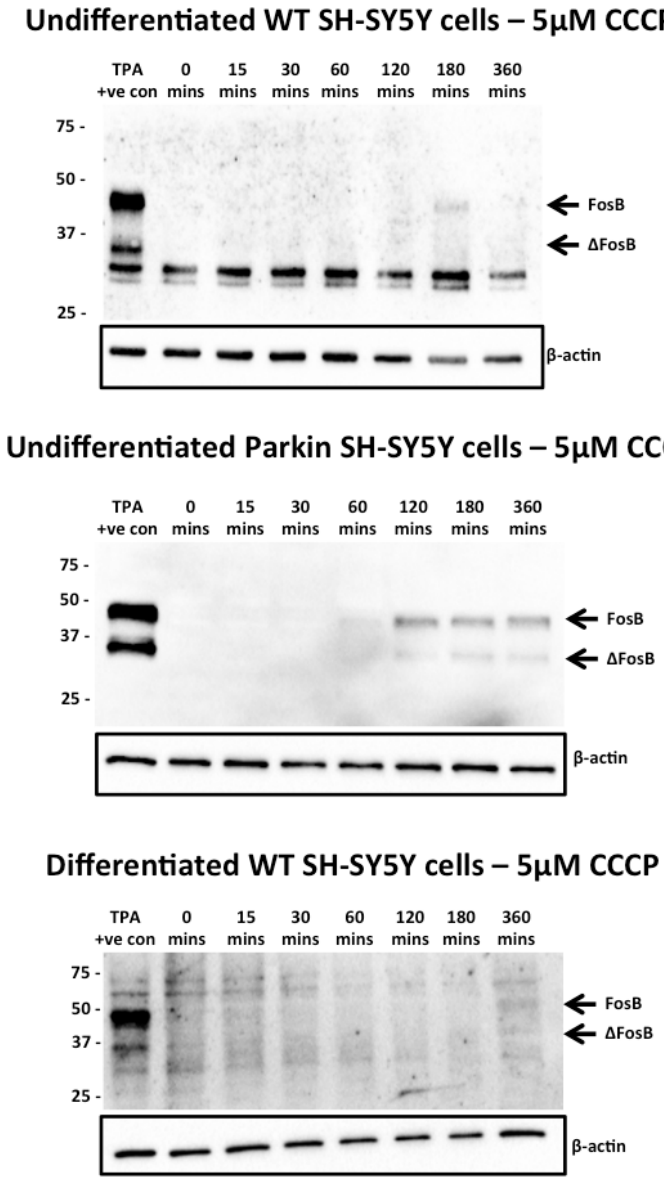

Figure 4.9: FosB expression is induced by 5µM CCCP application in SH-SY5Y cells. Upon mitochondrial depolarisation, FosB (46kDa) and ΔFosB (35-37kDa) became detectable in undifferentiated and differentiated cell lines examined (n = 2). Protein extracts were obtained at specific time points and analysed by western blotting and densitometry relative to β–actin. 'n' values refer to independent biological replicates, where cells were seeded, treated, protein extracted, western blot analysis and quantification performed per individual replicate. TPA induction of FosB expression was used as a positive control.

In the undifferentiated Parkin overexpressing cells, both FosB and ΔFosB were clearly detectable just 2 hours after administration of CCCP (Figure 4.9). This

appeared to a more rapid and prominent induction of FosB expression compared to WT cells. In comparison, FosB was not detected at any time point during the 24 hour CCCP experiment in this cell line (Figure 4.10). Why this happened was unclear as according to the 6 hour CCCP assay, FosB bands should have been observed at the 2 and 6 hour time points at least.

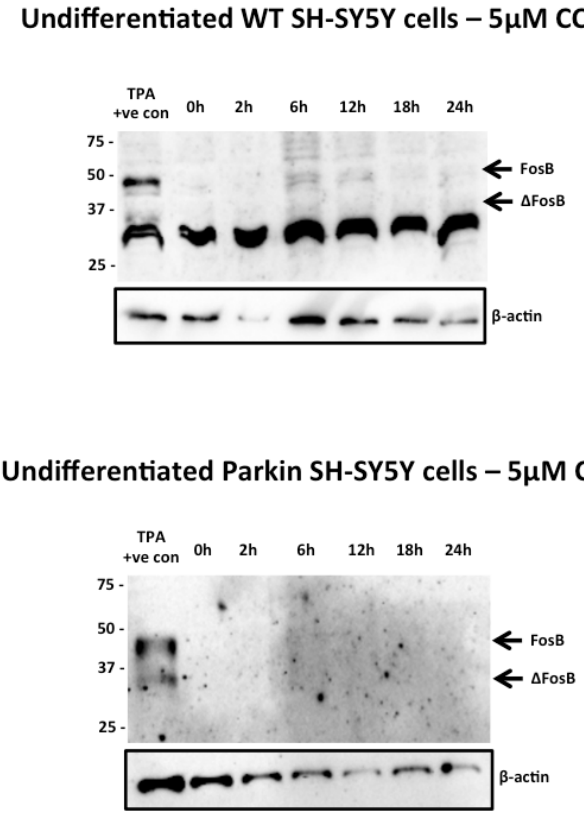

Figure 4.10: FosB protein levels for 24 hours post-5µM CCCP. Both undifferentiated WT and Parkin overexpressing SH-SY5Y cells were treated with CCCP for 24 hours and FosB protein levels assessed by western blotting (n = 2). Protein extracts were obtained at specific time points and analysed by western blotting and densitometry relative to β–actin. 'n' values refer to independent biological replicates, where cells were seeded, treated, protein extracted, western blot analysis and quantification performed per individual replicate. TPA induction was used as a positive control.

4.3.1.2.3 Fra-1

Initial experiments to assess Fra-1 abundance during the first 6 hours after CCCP treatment showed no significant change in the protein levels over this time period in all 3 lines (Figure 4.11). However, a drop in Fra-1 levels may

occur in the differentiated cells, although this result is unclear due to the high standard deviation observed between replicate experiments. Again, this highlights the need for further replicates.

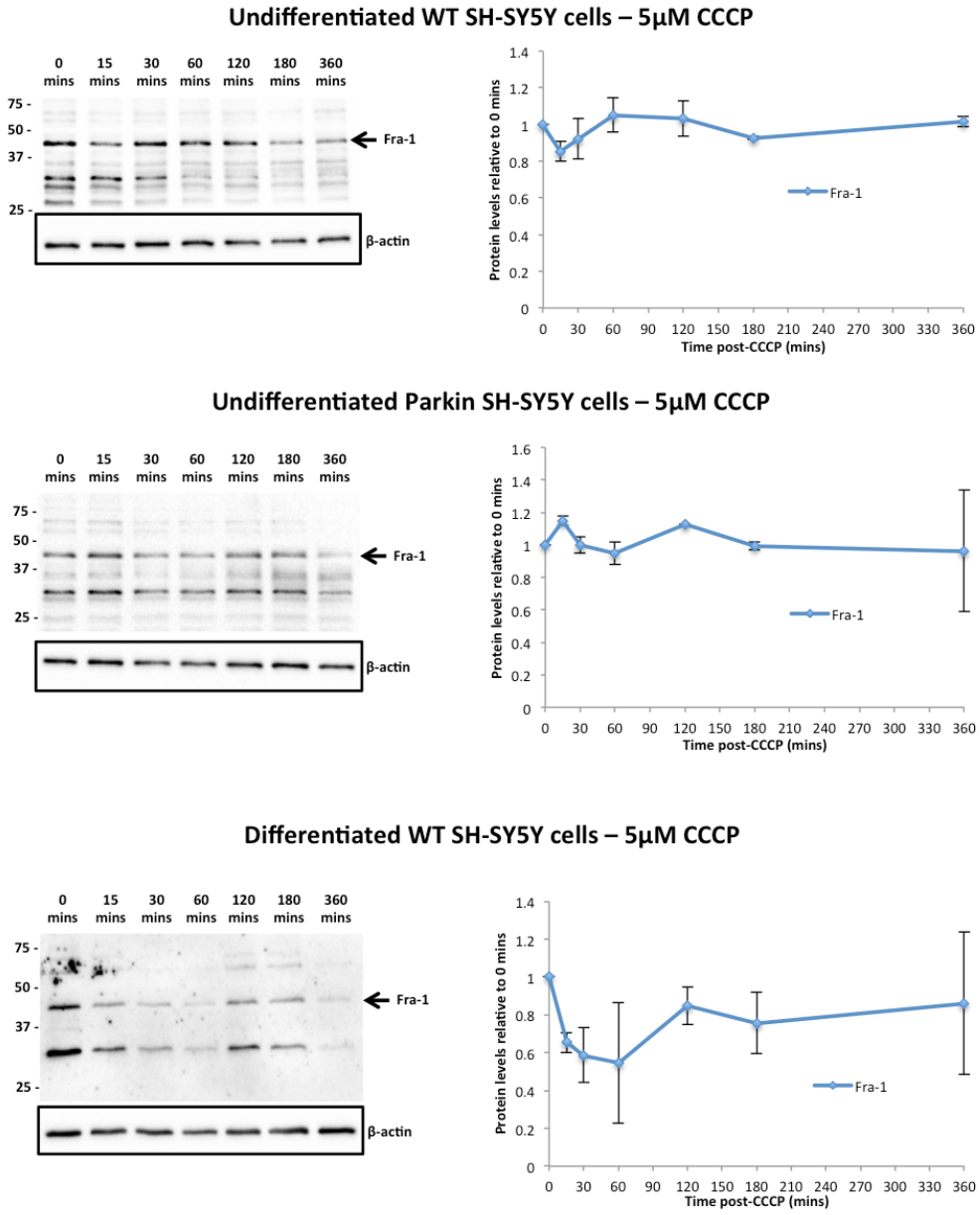

Figure 4.11: No increase in Fra-1 protein levels for 6 hours post-5µM CCCP occurs in SH-SY5Y cells. Western blot analysis of protein extracts for all 3 lines indicated that Fra-1 (41kDa) expression was not significantly induced during the first 6 hours after mitochondrial uncoupling in undifferentiated WT or *PARKIN* overexpressing cells (n = 2) and differentiated SH-SY5Y cells (n = 3). 'n' values refer to independent biological replicates, where cells were seeded, treated, protein extracted, western blot analysis and quantification performed per individual replicate. Statistical significance was assessed using a 2way ANOVA (Dunnett's). Error bars represent SEM.

Nevertheless, it did appear clear that Fra-1 expression was not induced by CCCP treatment in a manner similar to some other AP-1 transcription factors. Western blot analysis of the undifferentiated WT and Parkin SH-SY5Y lines for the 24 hour time period post-CCCP again showed no significant change in Fra-1 protein levels (Figure 4.12).

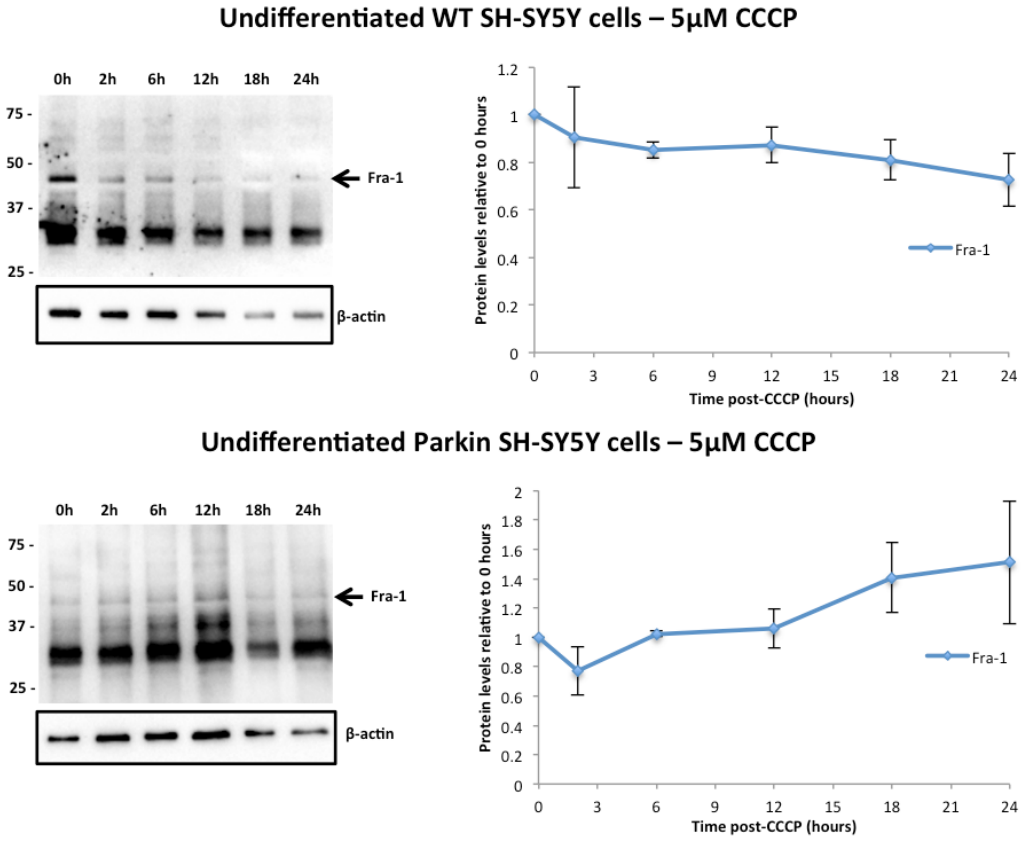

Figure 4.12: Fra-1 protein levels remain relatively constant for 24 hours post-5µM CCCP in undifferentiated WT and Parkin overexpressing cell lines. Protein extracts from both cell lines were assessed by western blotting (n = 2). Statistical significance was assessed using a 2way ANOVA (Dunnett's). 'n' values refer to independent biological replicates, where cells were seeded, treated, protein extracted, western blot analysis and quantification performed per individual replicate. Error bars represent SEM.

4.3.1.2.4 Fra-2

In all 3 cell lines assessed, a double band for Fra-2 was observed in all western blots (Figures 4.13 and 4.14). This has been previously reported, with the 2 bands determined to be phosphorylated (upper band) and unphosphorylated

(lower band) forms of the Fra-2 protein (Alli et al., 2013). In order to assess the total levels of Fra-2, densitometry was performed to include both bands.

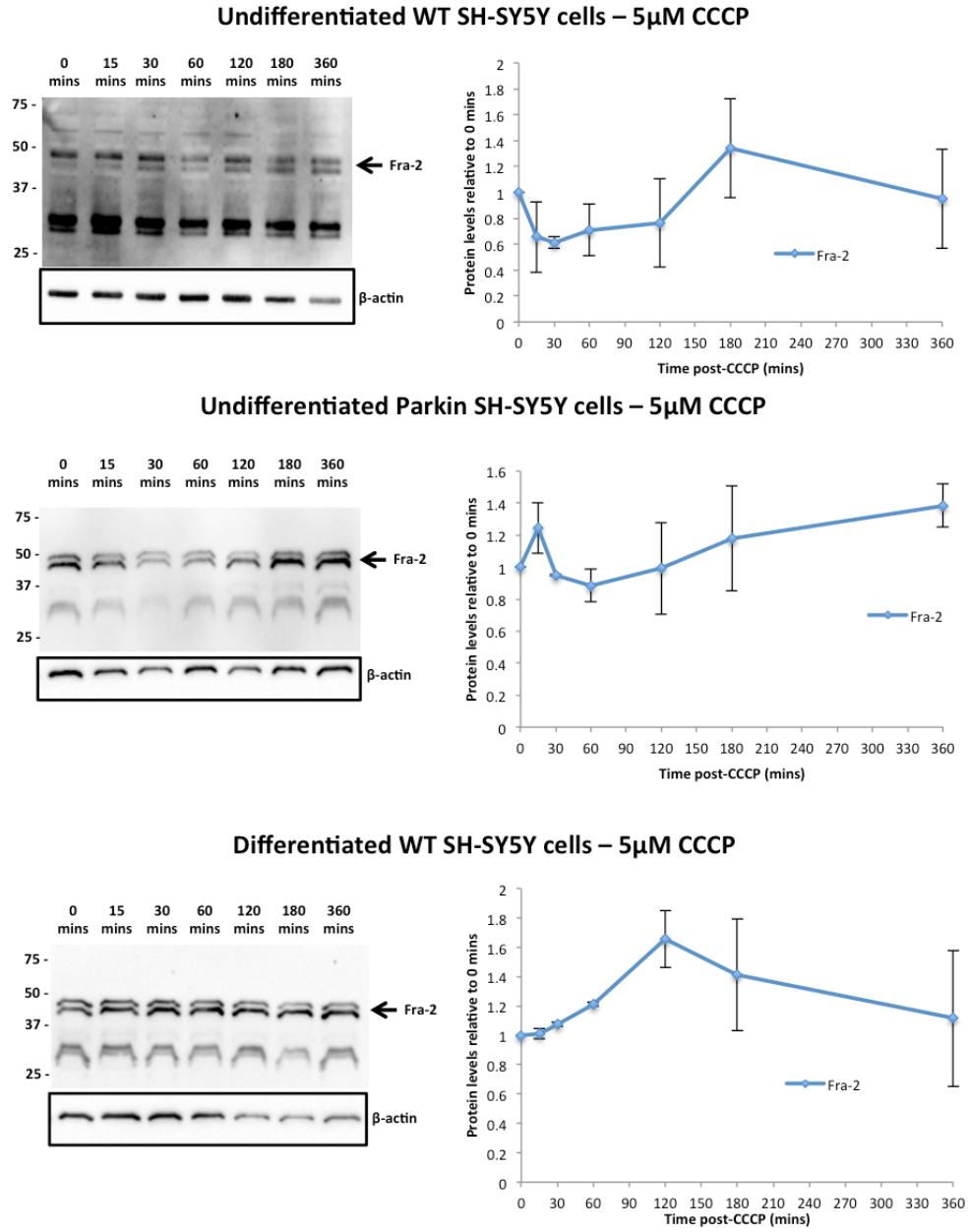

Figure 4.13: Fra-2 protein levels for 6 hours post-5µM CCCP remained relatively stable in SH-SY5Y cells. Protein extracts obtained at specific time points post-CCCP treatment were analysed by western blotting. An initial minor decrease in Fra-2 (35kDa) levels may occur in undifferentiated WT cells (n = 3). Small increases were observed in undifferentiated *PARKIN* overexpressing cells and differentiated WT cells (n = 2). 'n' values refer to independent biological replicates, where cells were seeded, treated, protein extracted, western blot analysis and quantification performed per individual replicate. Statistical significance was assessed using a 2way ANOVA (Dunnett's). Error bars represent SEM.

When comparing the Fra-2 doublets across cell types assessed, relative to the unphosphorylated Fra-2, the phosphorylated form appears to be higher in the WT cells (Figures 4.13 and 4.14). This could suggest that Parkin overexpression represses the phosphorylation of Fra-2. However, data presented here is insufficient to determine a final conclusion.

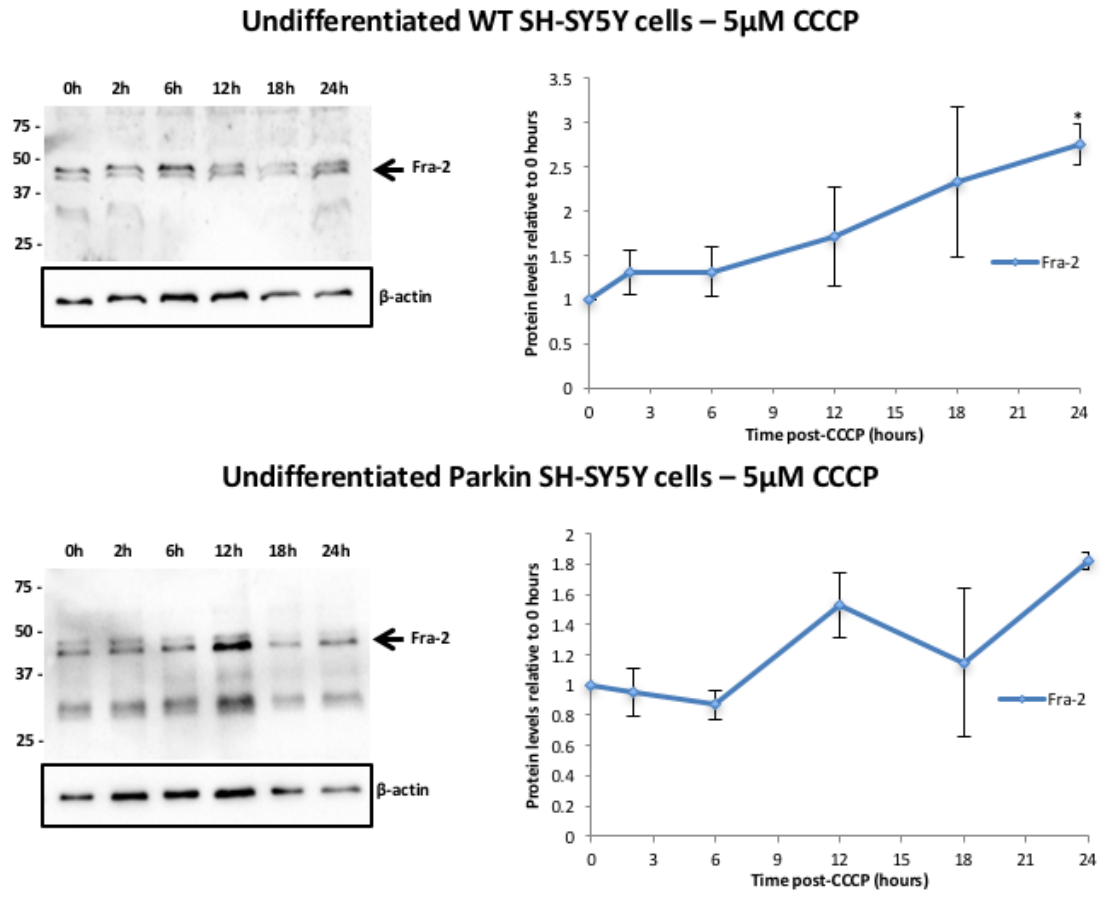

Figure 4.14: Fra-2 protein levels show greater increase 24 hours post-5µM CCCP treatment in WT cells compared to Parkin overexpressing cells. Protein extracts obtained from specific time points were analysed by western blotting. By the end of the assay, greater Fra-2 levels were observed compared to the initial protein levels in both cell lines (n = 2). 'n' values refer to independent biological replicates, where cells were seeded, treated, protein extracted, western blot analysis and quantification performed per individual replicate. Statistical significance was assessed using a 2way ANOVA (Dunnett's). (*$p < 0.05$). Error bars represent SEM.

Over the first 6 hours of CCCP treatment no significant change in Fra-2 levels was observed in all 3 cell lines (Figure 4.13). Over the 24 hour period of CCCP treatment, Fra-2 levels in undifferentiated cell lines showed some escalation by

the final time point (Figure 4.14). The phosphorylated Fra-2 levels appeared lower relative to unphosphorylated levels in the Parkin overexpressing line, with the overall level of the protein being increased to a greater extent in the WT cells. It may be the case that Parkin overexpression perturbs both Fra-2 phosphorylation and expression.

4.3.2 Expression of AP-1 proteins under mitochondrial stress

In order to complement the work performed by western blot analysis in determining how Jun and Fos proteins are modulated in response to CCCP, RT-qPCR analysis was carried out. This was to ascertain how the expression at the transcriptional level of the individual AP-1 genes changed, if at all, after CCCP treatment. By combining this with the data from the western blots, a clearer picture could then be built up. Initially, in order to confirm the validity of any results obtained, the efficiency of the primer/probe sets purchased for each individual AP-1 gene was assessed (Table 4.1 and Figure 4.15).

To determine how the expression of the AP-1 transcription factors are modulated in SH-SY5Y cells upon mitochondrial uncoupling, undifferentiated WT cells were treated with 5μM CCCP. At specific time points, media was removed and RNA extracted using Trizol®. After cDNA synthesis by reverse transcription, mRNA levels for each of the AP-1 proteins was assessed by qPCR to determine their expression relative to basal levels (Figures 4.16 – 4.22).

4.3.2.1 Assessing qPCR primer/probe efficiency

To ensure data detailing changes in the expression levels of the genes monitored, it was critical to firstly evaluate the efficiency of each individual primer/probe set purchased to perform qPCR. The Taqman® Gene Expression Assay primer probe sets purchased are sold with the guarantee of 100% efficiency (-/+ 10%). However, this was assessed to determine the validity of this guarantee for each individual primer/probe set to be used in this thesis. The method for these calculations is detailed in section 2.2.6.

The efficiency of amplicon doubling was calculated for all genes to be analysed. These are detailed below (Table 4.1). An example for the concentration curve used to calculate the efficiency can be found in Appendix H. As well as the Jun and Fos transcription factors, the expression of defined other genes connected with the stress response was also of interest. Parkin is known to play a major role in the mitophagic response after mitochondrial depolarisation (Narendra et al., 2008). The role of BIM in the mitochondrial stress response has not really been evaluated to date. However, its expression is regulated by the JNK/c-Jun pathway and presents pro-apoptotic activity under stress conditions (Whitfield et al., 2001, Perier et al., 2007). Mutations in the endosomal protein, *rab8a*, have recently been implicated in the pathogenesis of FTD and present as a driver for oxidative stress in this disease (West et al., 2015). Moreover, mutations in this gene, as well as leading to endosomal dysfunction, resulted in chronic activation of the JNK/AP-1 signalling pathway. In addition, the *RAB8A* promoter contains many potential TRE binding sites (GeneCards, 2016)

Primer	% Efficiency
B-ACTIN	101.51
c-JUN	83.11
JUNB	92.90
JUND	98.30
c-FOS	79.95
FOSB	78.92
FRA-1	104.31
FRA-2	100.65
PARKIN	94.70
BIM	90.16
RAB8A	109.76

Table 4.1: The amplification efficiency (%) of the individual Taqman Gene Expression Assays purchased. Each dilution of the cDNA template from TPA treated undifferentiated WT SH-SY5Y cells was performed in duplicate. Primers highlighted in red are not within 10% of the desired 100% efficiency.

In this chapter, only the expression of AP-1 transcription factors and Parkin following CCCP-induced mitochondrial insult was evaluated. The other genes of interest were assessed at a later date. These data are presented in the

following chapter of this thesis. Furthermore, multiple attempts to make the initial *JUND* primer/probe supplied (Cat. Number – Hs02330233_u1) work were unsuccessful as no amplification was observed. An alternative was therefore sourced from Applied Biosystems (Cat. Number – Hs04187679_s1) and this was then used for future assays.

Overall, many of the primer/probe sets used are efficient enough for the modulation of gene expression to be calculated using the standard ΔCt method described in section 2.2.6. However, this was not the case for all. The *c-JUN*, *c-FOS* and *FOSB* assay sets were not within 10% of the desired 100% efficiency standard guaranteed by Applied Biosystems. Therefore, to calculate the fold change in expression of these genes, the formula described in section 2.2.6 was applied to the Ct values obtained.

An efficiency of between 90-110% is generally considered acceptable for primers in qPCR. However, normalisation of primer/probe sets with efficiency lower that this produces robust analysis of relative expression (Pfaffl, 2001). Efficiencies of greater than 100% are not possible and are most likely produced by inhibitors still in with the cDNA solution (Svec et al., 2015). Without the normalisation for primers that have <90% efficiency, the relative change in expression of the target gene may not be as apparent as what is actually occurring. Therefore, normalisation is critical. Although primer efficiency marginally above 90% may still not be ideal for measuring relative changes in expression, it is still generally viewed in the literature as an acceptable cut-off value.

4.3.2.2 Jun transcription factors

Initially, how the relative mRNA expression of the Jun family transcription factor genes, *c-JUN*, *JUNB* and *JUND*, changed after undifferentiated WT SH-SY5Y cells were treated with 5μM CCCP was determined. Cells were treated with CCCP (TPA as a positive control to induce AP-1 expression) and RNA obtained at specific time points over a 24 hour period post-treatment. mRNA levels for each gene were assessed for each time point by RT-qPCR and normalised to *β-ACTIN* expression, the housekeeping gene used here.

The expression of all 3 Jun family members was induced by TPA treatment in these cells (Figures 4.16). Upon CCCP treatment, *c-JUN* expression was rapidly upregulated by the 1 hour time point. A decrease was then observed between 1 and 2 hours (**p = 0.0012 and ****p < 0.0001 for experiments 1 and 2, respectively) before mRNA levels increased between 6 and 12 hours (**p = 0.0032 and ***p = 0.0001 for experiments 1 and 2, respectively) and continued to be elevated until the 24 hour mark (Figure 4.15). This response was biphasic, showing 2 separate increases in the expression of the *c-JUN* gene. This could suggest 2 separate roles for this AP-1 transcription factor under these conditions. The most significant increase in expression is seen at the 24 hour time point. A constant and significant rise in the level of *c-JUN* mRNA is observed from 6 hours onwards. It was, however, unclear whether this continued beyond the final time point.

The expression of *JUNB* was very strongly induced by TPA (Figure 4.15). Similarly, CCCP treatment of the SH-SY5Y cells led to a rapid increase in the expression of *JUNB*, which remained elevated, relative to the 0 hours control, all the way up to the 24 hour time point. By the final 2 time points assessed, the mRNA levels of this gene were approximately 12 times greater compared to normal conditions. It would also appear that these cells are capable of upregulating *JUNB* expression to close to this level within the first hour of mitochondrial insult, suggesting JunB may have a function under these conditions.

In contrast, the relative increase in *JUND* expression was not as marked as *c-JUN* or *JUNB* (Figure 4.15). Although some increase is seen in the mRNA levels by 1 hour, this is relatively low compared to the increase observed for the other 2 Jun family members at this time point. Furthermore, the final relative 3-fold increase in *JUND* expression 24 hours after the initial mitochondrial damage is again modest when compared to *c-JUN* and *JUNB*. Nevertheless, this 3-fold increase may have significant functional implications in the response to mitochondrial uncoupling and does not inform us of the relative activity of the JunD protein. Moreover, both isoforms (37kDa and 41kDa) are quantified

together by this technique, thus not indicating if there is any difference between these two in terms of their transcriptional rate.

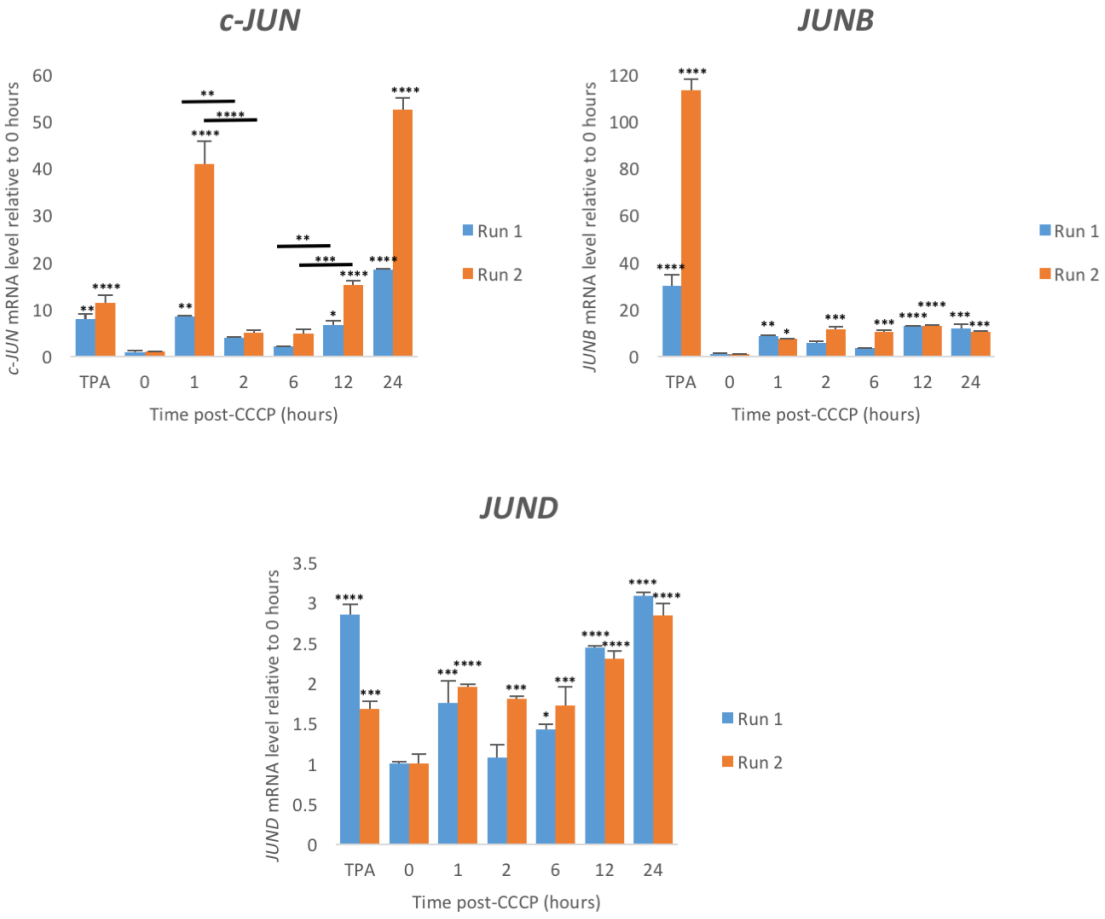

Figure 4.15: Expression of the *JUN* family genes are rapidly modulated in response to mitochondrial uncoupling. Undifferentiated WT SH-SY5Y cells were treated with 5μM CCCP and RNA extracted at specific time points. Values are fold increases relative to a 0 time point of 1 unit of expression. TPA was administered as a positive control. Expression was assessed in duplicate per experiment and results are shown from the two fully independent biological replicates (n=2). For each individual biological replicate, cells were seeded, treated, RNA extracted and the mRNA levels quantified. Statistical significance of relative changes in expression compared to control was assessed using a 2way ANOVA (Dunnett's) (*p < 0.05, **p < 0.01, ***p < 0.005, ****p < 0.001). Error bars represent standard deviation (SD).

4.3.2.3 Fos transcription factors

The expression of the Fos family transcription factors was assessed in an identical manner to the Jun family, described above. The uncoupling of the mitochondrial network in the undifferentiated SH-SY5Ys by 5μM CCCP led to a

significant increase in *c-FOS* mRNA after just 1 hour (Figure 4.16). A higher level of *c-FOS* expression was maintained throughout the 24 hour time period. However, the levels of mRNA declined towards the 6 hour point then increased again by 12 hours. Interestingly, the peak of expression appeared to be early on at the 1 hour time point, suggesting c-Fos activity may be important in the initial response to mitochondrial stress.

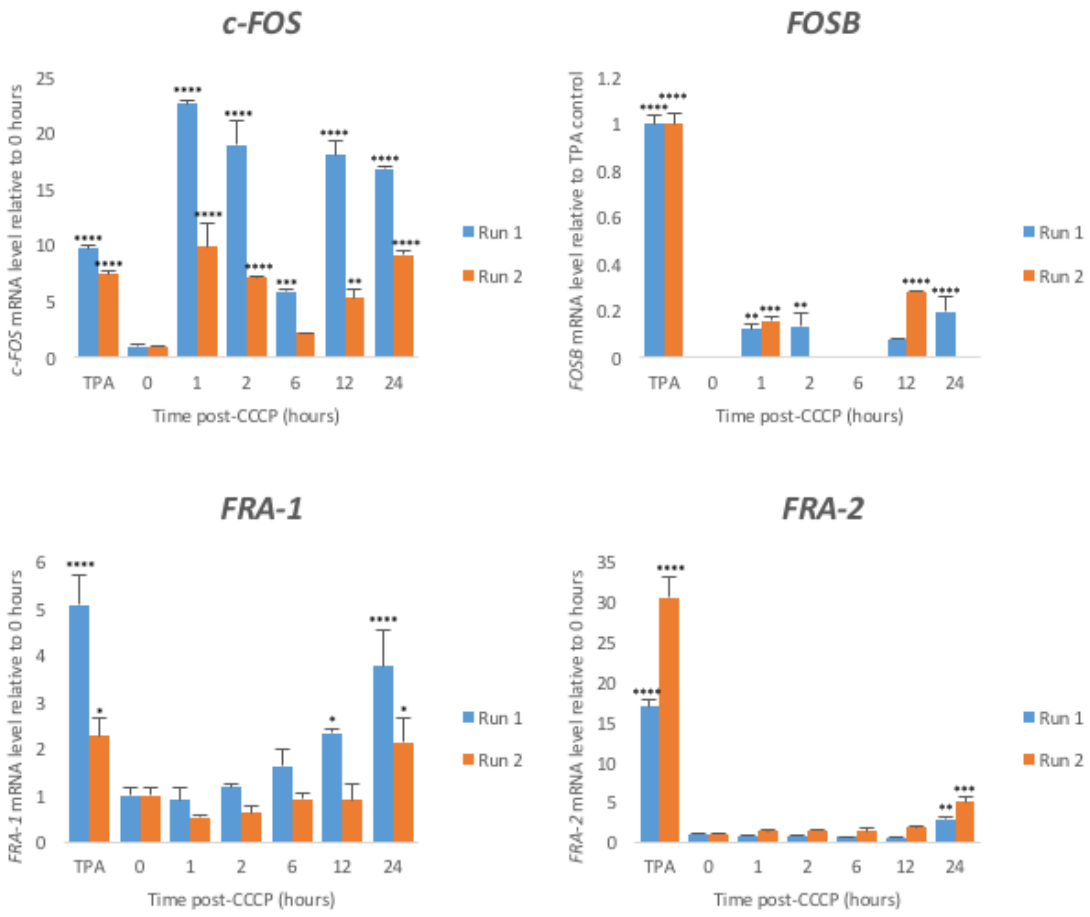

Figure 4.16: Modulation of Fos family genes is variable upon mitochondrial uncoupling in SH-SY5Y cells. Undifferentiated WT SH-SY5Y cells were treated with 5μM CCCP and RNA extracted at specific time points. Values are fold increases relative to a 0 time point of 1 unit of expression, except for *FOSB* where fold changes are are relative to TPA-treated cells. TPA was as a positive control. Expression was assessed in duplicate per experiment and results are from two fully independent experiments (n=2). For each individual biological replicate, cells were seeded, treated, RNA extracted and the mRNA levels quantified. Statistical significance of relative changes in expression was assessed using a 2way ANOVA (Dunnett's) (*p < 0.05, **p < 0.01, ***p < 0.005, ****p < 0.001). Error bars represent SD.

Like JunD, FosB also has 2 different isoforms separately identifiable by western blot analysis, which were not distinguishable by RT-qPCR. Under normal conditons, quantification of *FOSB* mRNA was below the detection limit (Figure 4.16). Due to this, expression levels were calculated relative to the TPA induced positive control rather than mRNA levels at the 0 hour time point. Although mRNA levels were low, 2 'pulses' of expression were identified. Interestingly, the drop in *FOSB* expression at 6 hours mimics the expression pattern shown by *c-FOS* above. Nevertheless, a clear indication that *FOSB* expression is induced following mitochondrial uncoupling was demonstrated here.

In contrast to the other AP-1 transcription factors assessed thus far, rapid modulation of *FRA-1* expression was not observed (Figure 4.16). Although some increase may be seen in *FRA-1* mRNA levels by 6 hours post-CCCP, it was not until the 12 hour time point that this became more apparent. Nevertheless, the approximate 4-fold increase relative to normal conditions observed 24 hours after CCCP treatment was modest compared to *c-FOS*. The expression pattern of the *FRA-1* gene may indicate that its function occurs in the later response to mitochondrial stress.

The induction of *FRA-2* expression by TPA treatment (Figure 4.16) was much greater than that of *FRA-1* (Figure 4.16). The modulation of *FRA-2* expression appeared to occur later under mitochondrial stress when compared to *FRA-1*. No significant change was observed in *FRA-2* expression during the first 12 hours of CCCP treatment in this cell line. However, an increase of around 3-fold, relative to normal conditions, was observable by the 24 hour time point. This data would suggest that, like *FRA-1*, the *FRA-2* gene may play a functional role in the late response to mitochondrial depolarisation in neuronal cells. Furthermore, the role of *FRA-1* may come earlier than that of *FRA-2* under these conditions.

4.3.2.4 Summary of AP-1 modulation in response to CCCP

Graphs combining the data for the modulation of AP-1 transcription factors at the levels of mRNA and protein in undifferentiated WT SH-SY5Y cells can be found in Appendices I and J. Over the 24 hour period following CCCP

challenge, the biphasic modulation of c-Jun is observed at mRNA level. No significant delay is observed in the initial increase in c-Jun protein levels suggesting that translation of *c-JUN* mRNA occurs rapidly under these conditions. The JunB protein response also suggests that expression is induced in response to mitochondrial uncoupling. *JUNB* mRNA levels show that expression increases significantly under these conditions. The JunD response to mitochondrial damage appears to be different to that of the other Jun genes, as its major upregulation occurs relatively late on after the initial stress. The major increase in expression is mirrored by a progressive increase in protein levels for both isoforms.

c-Fos protein was detected at very low levels by 2-3 hours after CCCP treatment, although when monitoring expression over a 24 hour period c-Fos bands were not observed (other than for the TPA positive control). This may be because detectable protein levels only occurred at 3 hours, which was not one of the time points in the 24 hour assay. Expression of *c-FOS* was markedly induced by mitochondrial uncoupling, with 2 clear pulses of expression occurring. The mRNA levels induced were higher than the TPA control yet protein was not clearly detected in response to mitochondrial damage. *FOSB* expression was also induced by CCCP challenge and both isoforms were detectable by western blotting at around 3-6 hours after uncoupling. This would be in line with the first increase in mRNA observed. A second increase in protein levels was not observed to follow the second upregulation of *FOSB* mRNA. However, this may occur after the 24 hour period observed here. Fra-1 protein levels remained relatively constant throughout the 24 hour time course. In contrast, *FRA-1* expression increased from 12 hours after uncoupling, suggesting either a delay in translation or Fra-1 is being degraded. Fra-2 protein levels show significant increase 24 hours after CCCP addition, which is also seen at the mRNA level. This protein may therefore play a role in the later response to mitochondrial stress.

For several of the Jun and Fos transcription factors, there appears to be 2 phases of AP-1 regulation over the first 24 hours of CCCP-induced mitochondrial uncoupling. This could suggest that 2 different forms of stress are

occurring sequentially, or even that many of the AP-1 transcription factors have 2 separate functions under these conditions.

4.3.2.5 Parkin

Parkin plays a critical role in the mitophagic response to mitochondrial uncoupling (Narendra et al., 2008, Vives-Bauza et al., 2010), with upregulation of *PARKIN* expression being previously demonstrated under similar conditions (Bouman et al., 2011). As data presented here shows how the expression of AP-1 genes can be rapidly modulated in response to mitochondrial stress, the change in expression of *PARKIN* over the same time period was also assessed. *PARKIN* expression was rapidly increased in response to CCCP-induced uncoupling (Figure 4.17). Expression peaked at 6 hours after treatment with 5μM CCCP in the first experiment. However, even after the 6 hour time point, *PARKIN* mRNA was still maintained at a higher level than under normal conditions.

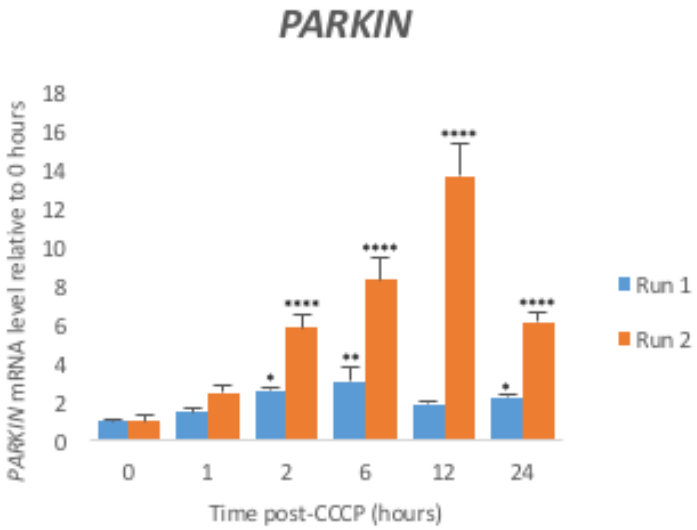

Figure 4.17: *PARKIN* expression is induced by mitochondrial uncoupling in SH-SY5Y cells. Undifferentiated WT SH-SY5Y cells were treated with 5μM CCCP and RNA extracted at specific time points. Expression was assessed in duplicate per experiment and results are from two fully individual experiments. For each individual biological replicate, cells were seeded, treated, RNA extracted and the mRNA levels quantified. Statistical significance of relative changes in expression was assessed using a 2way ANOVA (Dunnett's) (*p < 0.05, **p < 0.01, ****p < 0.001). Error bars represent SD.

In both experiments performed, *PARKIN* mRNA became significantly elevated 2 hours after CCCP treatment. In the second experiment *PARKIN* expression peaked at 12 hours post-CCCP, but was still significantly elevated by the 6 hour time point like in the first experiment.

4.3.3 Functional analysis of AP-1 transcription factors under mitochondrial stress in SH-SY5Y cells

To identify their functional capacity under stress conditions, AP-1 proteins were targeted by specific siRNAs prior to CCCP treatment in order to investigate their role in mitochondrial stress-induced cell death (Figure 4.18).

Several controls were used for this experiment. Non-targeting 1 (NT1) siRNA provided a negative control for the small RNA molecule, not specific to any gene investigated. *Polo-like kinase 1* (*PLK1*) knockdown functions to induce apoptosis in mitotic cells, thus allowing an estimate of transfection efficiency for each individual experiment. Controls were also used in which cells were incubated with siRNA buffer and Lipofectmine transfection reagent but no siRNA (no siRNA) or normal media only lacking any transfection or siRNA reagents (cells only). Furthermore, prior to the assay, all SMARTpools were assessed for predicted off target effects by a BLAST search using their target sequence. A slight reduction in cell number did occur due to the use of NT1 siRNA relative to the ‘no siRNA’ and ‘cells only’ control. All percentages were therefore calculated relative to the NT1 control. The use of *PLK1*-specific siRNA, reducing the cell population by around 60%, indicate successful uptake of the siRNA by the SH-SY5Y cells.

Despite being expressed at very low levels under basal conditions, c-Fos siRNA lead to dramatic cell loss without CCCP (**p = 0.0012) (Figure 4.18a). This may suggest that the low level of c-Fos maintained under normal conditions serves an important function in these mitotic cells. Although c-Fos siRNA increased cell death induced by CCCP (*p = 0.0209), it is likely this is because of the death induced by the siRNA treatment alone. Interestingly, Parkin siRNA did not affect the level of CCCP-induced cell death.

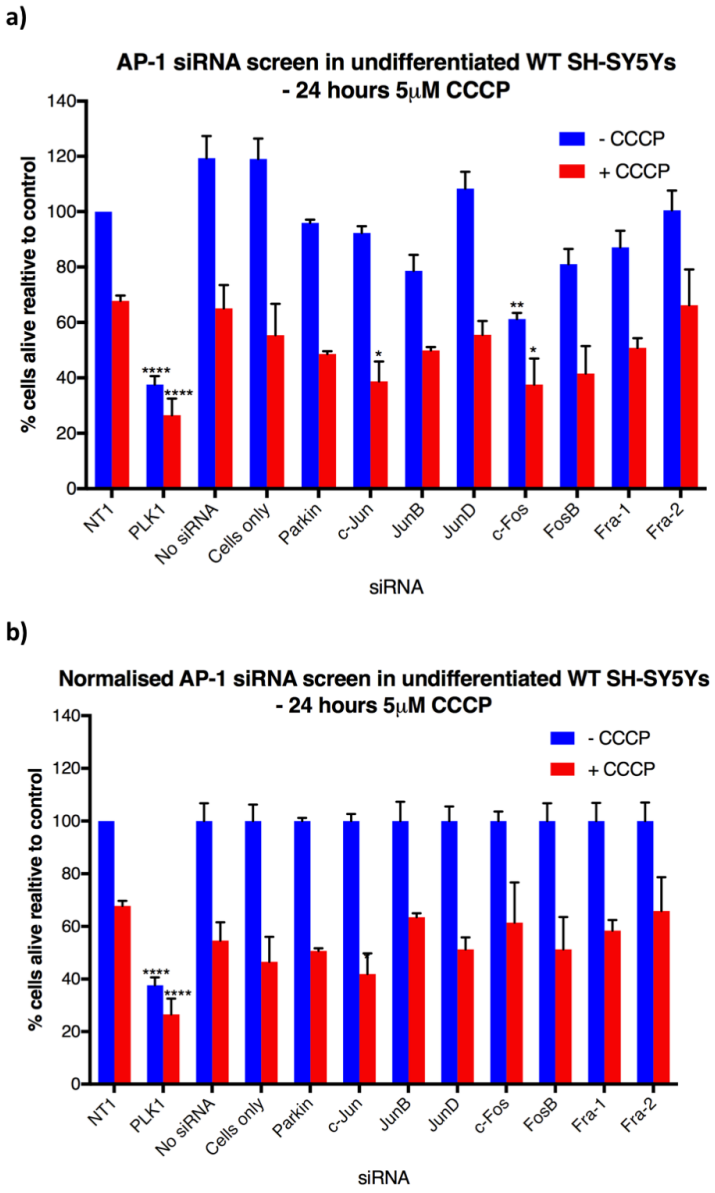

Figure 4.18: siRNA screen of individual AP-1 transcription factors can alter cell survival after mitochondrial uncoupling by CCCP for 24 hours in undifferentiated WT SH-SY5Y cells. Cell were treated with individual siRNA SMARTpools for 48 hours prior to 5μM CCCP and cell counts performed on the Operetta high-throughput immunofluorescence microscope from nuclei stained with DAPI. (a) Data is shown relative to NT-1 siRNA treated cells –CCCP. (b) Each individual siRNA group was normalised relative to cells not treated with CCCP. Each condition was performed in duplicate per experiment. Three biological replicates, in which cells were seeded and reverse transfection with siRNA performed, cells treated, fixed, stained and DAPI counts performed (n=3). Cell counts were relative to DMSO treated NT-1 cells. Significance was assessed using a 2way ANOVA (Bonferroni's) comparing -/+ CCCP to the NT1 control (*$p < 0.05$, **$p < 0.01$, ****$p < 0.001$). Error bars represent SEM calculated from the mean of each individual experiment.

Treatment with c-Jun siRNA caused a significant increase in CCCP-induced cell death in the SH-SY5Y cells (*p = 0.0296) (Figure 4.18a). No significant cell death was observed from c-Jun siRNA treatment alone, however, when this data was normalised and CCCP-induced apoptosis assessed relative to untreated cells in this c-Jun siRNA group no significant increase was observed (Figure 4.18b).

A limitation of the screen conducted here was that successful knockdown of each gene was not assessed at either mRNA or protein level by qPCR or western blot, respectively. Given more time, the knockdown efficiency of each gene assessed here would have been determined by western blot analysis.

4.4 CONCLUSIONS

The combined use of western blot and RT-qPCR analysis allowed the determination of the changes of each of AP-1 transcription factors at mRNA and protein levels. It is clear from the data presented here that many of the AP-1 genes undergo modulation in response to mitochondrial uncoupling in SH-SY5Y cells. Moreover, clear distinctions in their modulation between undifferentiated and differentiated cells were found. Along with this, *PARKIN* overexpression appears to result in changes to certain AP-1 response signatures.

Overall, c-Jun presented the most intriguing candidate for further study. Several previous studies have suggested c-Jun may play a role in neurodegenerative conditions such as PD. However, c-Jun is generally considered an apoptotic AP-1 transcription factor under neurodegenerative-associated stress conditions. Conversely, data from the siRNA experiment shown here suggests that c-Jun siRNA is anti-apoptotic in SH-SY5Y cells treated with 5μM CCCP. Furthermore, the biphasic modulation of *c-JUN* expression observed by qPCR in undifferentiated WT cells may suggest multiple roles for c-Jun under these conditions. The overexpression of Parkin, a protein previously shown to be regulated by c-Jun activity, appeared to amplify c-Jun accumulation 24 hours-post CCCP.

To investigate the role of c-Jun in mitochondrial dysfunction and oxidative stress associated with PD, the next chapter looked to extend these observations into differentiated cells. Moreover, the biphasic modulation of *c-JUN* may in fact represent an ability to differentiate between levels of stress, something that was investigated further. The initial upregulation of c-Jun may be part of the initial adaptive response to the stress, whereas the final increase in c-Jun levels after the 6 hour point could be an apoptotic mechanism associated with the PD state.

Understanding the regulation of c-Jun by upstream kinases such as JNK, a MAPK strongly associated with several neurodegenerative conditions, could prove critical in gaining further insight into this protective system. Finally, dissecting how c-Jun and Parkin may act in order to function together under mitochondrial stress could prove critical. Previous data shows c-Jun represses the expression of *PARKIN*. Data presented here suggests that Parkin overexpression leads to a greater increase in c-Jun protein levels upon mitochondrial depolarisation. This may suggest a feedback loop between the Parkin and c-Jun pathways.

CHAPTER 5
THE ROLE AND REGULATION OF c-JUN IN THE MITOCHONDRIAL STRESS RESPONSE

5.1 INTRODUCTION

The role of c-Jun in cellular stress responses has been the subject of many studies over the past few decades. However, much of this work has focused on the pro-apoptotic role of c-Jun and in non-neuronal models. Furthermore, c-Jun is surprisingly often overlooked as significantly more work has been directed towards examining JNK, the major MAPK responsible for the regulation of c-Jun. The role and regulation of c-Jun is therefore still far from understood. In particular, determining how upstream cascades regulate c-Jun and identifying the adaptive responses mediated by it could be critical in understanding the neuronal response to stress.

To date, there is much evidence suggesting that c-Jun promotes neuronal apoptosis under stress conditions (Ham et al., 1995, Watson et al., 1998, Ham et al., 2000, Whitfield et al., 2001, Gearan et al., 2001, Wilhelm et al., 2007). The c-Jun-dependent induction of BCL-2-interacting mediator of cell death (BIM), a member of the pro-apoptotic BH3-only family, appears to be a critical step in this neuronal death mechanism (Putcha et al., 2001, Whitfield et al., 2001). The activity of JNK cascades, the primary regulator of c-Jun, have been extensively linked with neurodegenerative conditions (Yang et al., 1997, Hunot et al., 2004, Borsello and Forloni, 2007, Centeno et al., 2007, Colombo et al., 2007, Johnson and Nakamura, 2007, Pan et al., 2009, Pan et al., 2012).

The JNK/c-Jun pathway has been implicated in several studies examining PD-related models of intracellular stress. Firstly, the repression of *PARKIN* expression by c-Jun, which binds to the *PARKIN* promoter in order to block ATF4-mediated upregulation of this gene, can be decreased by the inhibition of the JNK signalling pathway in SH-SY5Y cells (Bouman et al., 2011). JNK has also been shown to localise to mitochondria and initiate apoptotic signalling after 6-OHDA treatment (Chambers et al., 2013). Here, the inhibition of JNK signalling or its mitochondrial translocation proved to be neuroprotective, both *in vitro* and *in vivo*. Interestingly, exposure to 6-OHDA also induced ERK2 translocation to mitochondria, which in turn initiated mitophagy and autophagic cell death (Dagda et al., 2008). Furthermore, the localisation of phosphorylated ERK to early endosomes and mitochondria is also observed in Lewy body

disease models (Zhu et al., 2003). These data could suggest that MAPK signalling as a whole plays a combined role in regulating neuronal fate under stress conditions. A similar hypothesis for AD, referred to as the 'two-hit hypothesis', has previously been suggested (Zhu et al., 2001, Zhu et al., 2007). This proposes that ERK signalling alone is not sufficient to drive AD pathology, whereas the activation of both JNK and ERK pathways is sufficient.

Data presented in Chapter 4 suggests that the expression of *c-JUN* was modulated in a biphasic manner in response to mitochondrial uncoupling in undifferentiated SH-SY5Y cells. This required further investigation in differentiated cells and at the level of phosphorylation. In addition, c-Jun siRNA reduced cell survival after mitochondrial uncoupling (Figure 4.18). This data could be contradictory to several other studies and therefore warranted further investigation. Importantly, it should be noted that the AP-1 siRNA knockdown experiments previously described gave a simple read out of cell survival under a single level of mitochondrial and oxidative stress (Figure 4.18). It therefore did not uncover the regulatory role played by MAPKs upstream of c-Jun or how downstream genes were modulated. Moreover, how the cellular response of mitophagy was linked into MAPK/AP-1 pathways was also not determined.

5.2 AIMS

Many previous studies have found c-Jun to be pro-apoptotic in neurons under stress. The aim of this chapter was to investigate the role of c-Jun in the cellular response to mitochondrial uncoupling and how this was regulated upstream of the transcription factor.

5.3 RESULTS

5.3.1 Unphosphorylated c-Jun is turned over in a proteasome-dependent manner

Both undifferentiated and differentiated SH-SY5Y cells provide a neuronal-like model system. Mitochondrial depolarisation results in the initial rapid degradation of c-Jun (Figure 4.1) in both undifferentiated and differentiated SH-SY5Y cells. To investigate whether this degradation was mediated by the proteasome, UPS-deficient undifferentiated WT cells were subjected to mitochondrial uncoupling. Proteasomal inhibition was achieved using a concentration of epoxomicin (100nM) previously shown to effectively perturb 26S proteasome activity (Bouman et al., 2011).

Western blotting showed that inhibition of the proteasome prevented the degradation of c-Jun post-mitochondrial uncoupling (Figure 5.1a and 5.1c). Moreover, c-Jun did not return to basal levels by 6 hours post-CCCP. Importantly, c-Jun levels were comparable with and without proteasomal inhibition (Figure 5.1b).

c-Jun can exist in either an unphosphorylated or phosphorylated state, with several phospho-acceptor sites available within its amino acid sequence. To investigate how phosphorylation altered the stability of c-Jun under mitochondrial stress, an antibody specific to the phospho S63 form of c-Jun was used. There are 4 phosphorylation sites within the protein and all would have been assessed, given more time and appropriate reagents. No immediate decline in the levels of c-Jun phosphorylated at Ser63 was observed upon mitochondrial damage in WT (undifferentiated and differentiated) or Parkin (undifferentiated) SH-SY5Y cells (Figure 5.2), suggesting S63 phosphorylation stabilises c-Jun here.

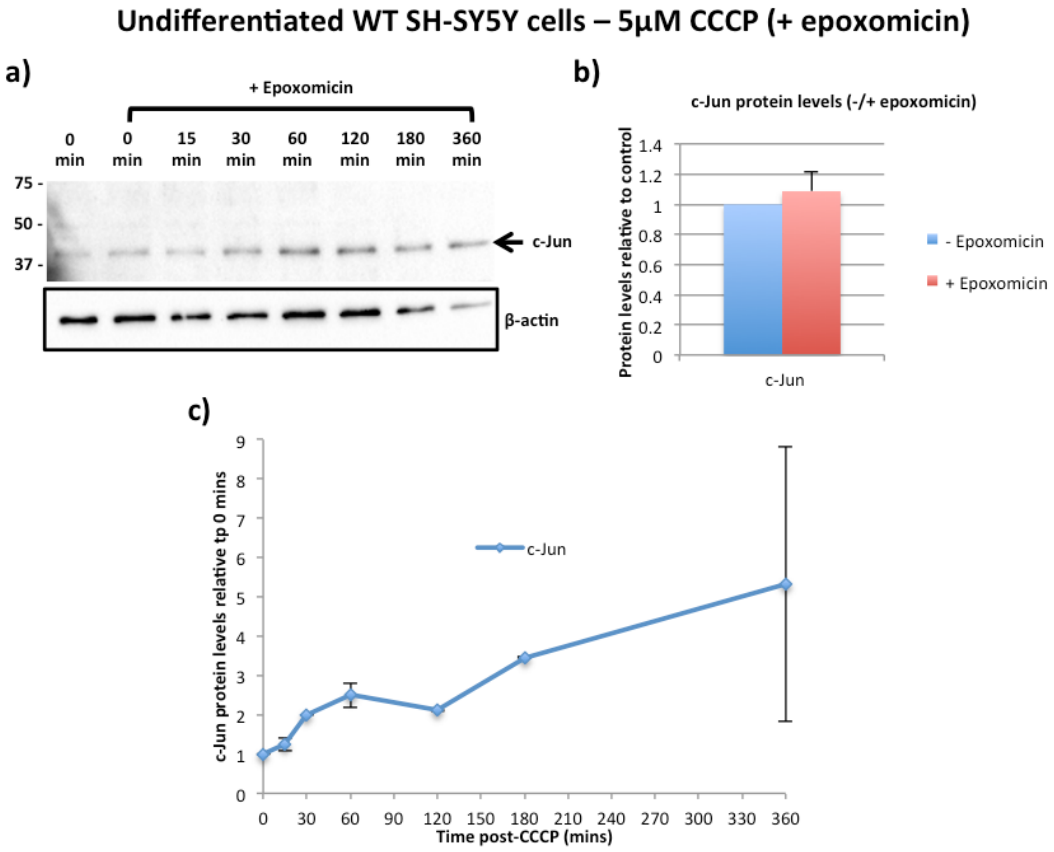

Figure 5.1: Proteasomal inhibition in SH-SY5Y cells prior to mitochondrial uncoupling prevents c-Jun degradation. Undifferentiated WT SH-SY5Y cells were incubated with 100nM epoxomicin 1 hour prior to treatment with 5μM CCCP. Protein extracts from time points were then analysed by western blotting. (a) Western blotting for c-Jun at specific time points throughout assay. (b) Densitometry showed no change in c-Jun protein levels after 1 hour post-epoxomicin (n = 2). (c) c-Jun densitometry was calculated relative to β–actin (n = 2). 'n' values refer to independent biological replicates, where cells were seeded, treated, protein extracted, western blot analysis and quantification performed per individual replicate. Statistical significance was assessed using a 2way ANOVA (Dunnett's). (*$p < 0.05$). Error bars represent SEM.

These data suggest that phosphorylation of c-Jun occurs to a greater extent in differentiated cells in response to mitochondrial uncoupling. It should, however, be noted that this data does not indicate what occurs at the other phospho acceptor sites (Ser73, Thr91 and Thr93). These may have opposing or synergistic effects on the stability and activity of the protein. What must also be noted is that no statistically significant increase in phosphorylated c-Jun levels is observed in the first 6 hours of uncoupling in undifferentiated WT and Parkin

cells. Again, this may be a reflection of the low number of replicates. A higher number of replicates would be needed for a greater degree of statistical certainty.

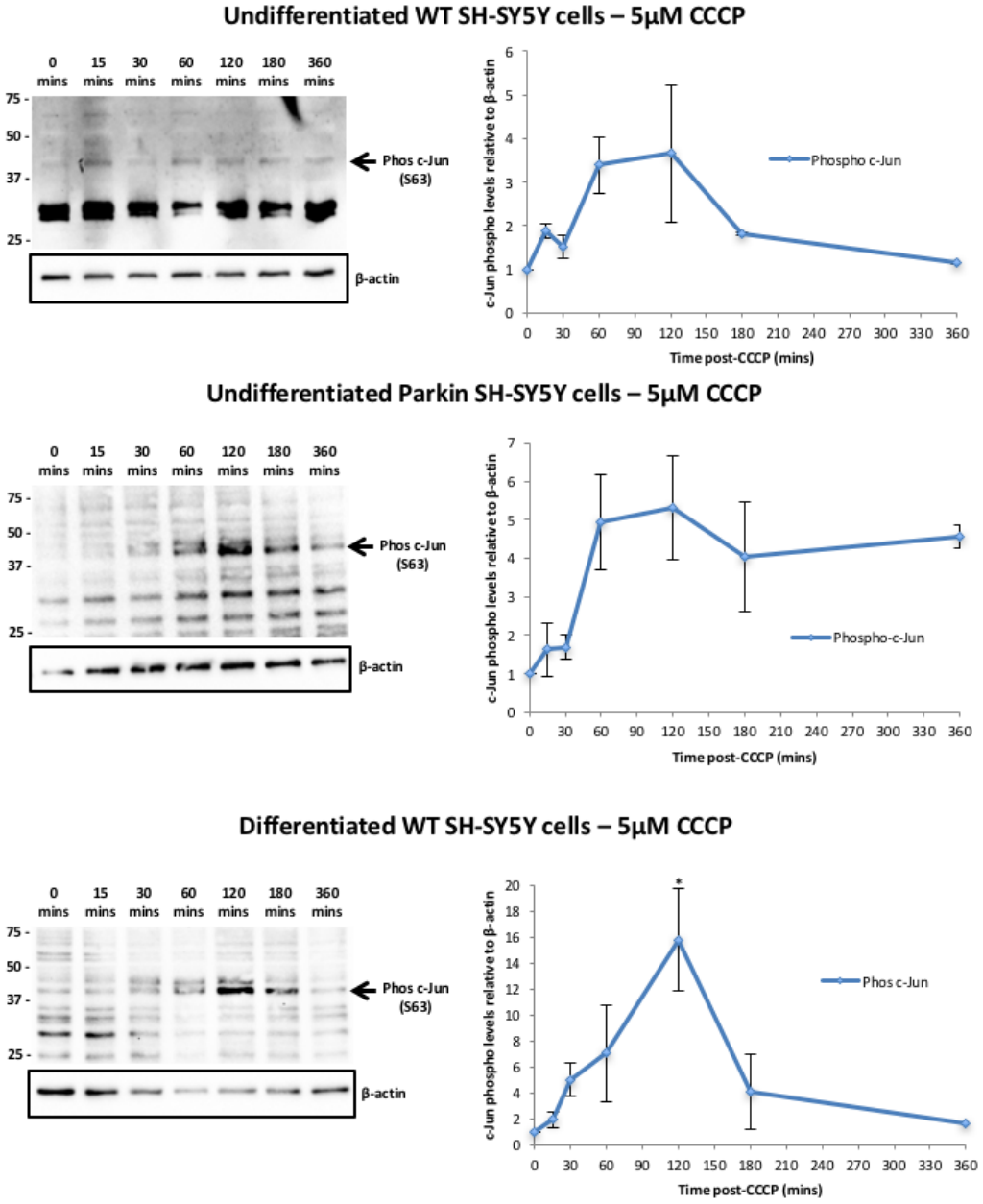

Figure 5.2: c-Jun is rapidly phosphorylated in response to mitochondrial damage in all 3 cell lines analysed. Parkin overexpression maintains phosphorylated c-Jun levels 2 hours post-CCCP. The SH-SY5Y cell lines were treated with 5µM CCCP and protein extracts obtained at specific time points then analysed by western blotting (n = 2). 'n' values refer to independent biological replicates, where cells were seeded, treated, protein extracted, western blot analysis and quantification performed per individual replicate. Statistical significance was assessed using a 2way ANOVA (Dunnett's). (*$p < 0.05$). Error bars represent SEM.

To investigate c-Jun after the initial 6 hours of mitochondrial damage under proteasomal inhibition, UPS inhibited cells underwent mitochondrial uncoupling. Inhibition of the proteasome prior to uncoupling led to a drastic increase in c-Jun protein levels compared to cells with a functional UPS (Figure 5.3).

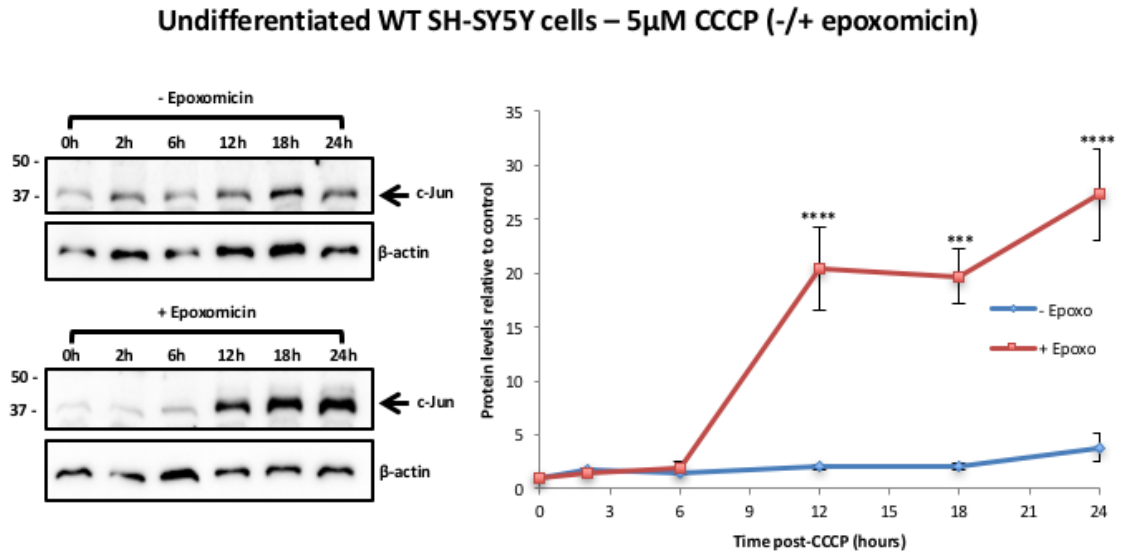

Figure 5.3: Proteasomal inhibition with epoxomicin results in an increased c-Jun response to mitochondrial damage. Undifferentiated WT SH-SY5Y cells were treated with 100nM epoxomicin (red line) or DMSO (blue line) 1 hour prior to treatment with 5µM CCCP. Protein extracts obtained at specific time points for the two conditions were analysed by western blotting (n = 2). 'n' values refer to independent biological replicates, where cells were seeded, treated, protein extracted, western blot analysis and quantification performed per individual replicate. Statistical significance was assessed using a 2way ANOVA (Bonferonni's). (***p < 0.005, ****p < 0.001). Error bars represent SEM.

Although a rise in c-Jun protein levels was observed 24 hours post-mitochondrial uncoupling (see also Figure 4.2), inhibition of the 26S proteasome lead to approximately a 5-fold greater increase, an effect initiated between 6 and 12 hours after uncoupling under UPS dysfunction. Such a significant increase has 2 potential explanations. First, that c-Jun is normally degraded by the proteasome after playing a role in the initial response to mitochondrial stress, perhaps as part of a regulatory process that limits the level and extent of its activity. Second, additional stress caused by UPS block leads

to a greater increase in c-Jun expression than is seen after uncoupling alone, which could mean c-Jun levels represent the overall degree of stress.

5.3.2 Phosphorylation of c-Jun 24 hours-post CCCP

Figure 5.2 assessed how the S63 residue of c-Jun is immediately phosphorylated in response to mitochondrial stress. To investigate how this phosphorylation was modulated over a longer period, the levels of S63 phosphorylated c-Jun undifferentiated SH-SY5Y cells after uncoupling were determined. In response to uncoupling, c-Jun was phosphorylated in both WT and *PARKIN* overexpressing cells (Figure 5.4). In WT cells 6 hours after the initiation of mitochondrial stress, c-Jun phosphorylation returned to basal levels and does not change after this. However, *PARKIN* overexpression resulted in c-Jun Ser63 phosphorylation being maintained for at least 12 hours after uncoupling. Nevertheless, this level of overexpression was not maintained and normal phosphorylation levels returned by the 18 hour time point.

These data suggest that Parkin activity in undifferentiated SH-SY5Y cells prolongs the phosphorylation of c-Jun in response to mitochondrial stress. This may occur by the exacerbation of upstream signalling cascades or even a direct result of excessive mitophagy, since previous work in this laboratory has suggested that Parkin levels are a rate-limiting step in CCCP-induced mitophagy (Morrison et al., 2011).

The fact that a significant increase in Ser63 phosphorylated c-Jun in undifferentiated WT cells is observed at 2 hours post-CCCP in the 24 hour assay (Figure 5.4) but not the 6 hour assay (Figure 5.2) may be a reflection of the lower number of replicates for the latter. It is therefore difficult to properly conclude how c-Jun is phosphorylated during this early period.

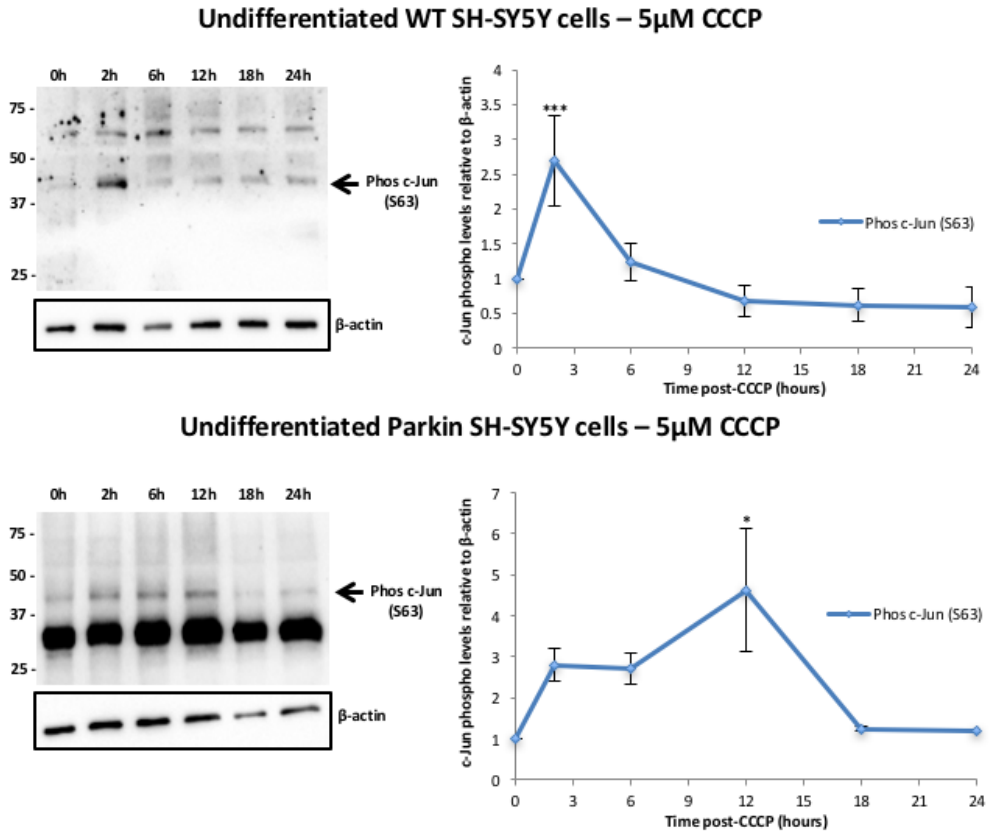

Figure 5.4: c-Jun phosphorylation in response to CCCP treatment is altered by Parkin overexpression. Protein extracts were obtained from both cell line at specific time points after CCCP treatment in undifferentiated WT (n = 3) and *PARKIN* overexpressing (n = 2) SH-SY5Ys and analysed by western blotting and densitometry. 'n' values refer to independent biological replicates, where cells were seeded, treated, protein extracted, western blot analysis and quantification performed per individual replicate. Statistical significance was assessed using a 2way ANOVA (Dunnett's). (*p < 0.05, ***p < 0.005). Error bars represent SEM.

5.3.3 c-Jun in differentiated SH-SY5Y cells

Although modulation in protein levels and phosphorylation of c-Jun in differentiated SH-SY5Y cells during the first 6 hours of uncoupling was assessed in Chapter 4, observations were not made past this time. This was due to the sensitivity of cells to both differentiation and CCCP treatment. The differentiation process resulted in a reduced number of cells prior to the experiment. Furthermore, the subsequent exposure of differentiated WT cells to CCCP resulted in much greater cell death compared to the undifferentiated

cells. Together, these factors made it impractical to obtain enough protein extract to assess all 7 AP-1 proteins by western blotting.

Data from Chapter 4 turned attention towards c-Jun as the main AP-1 protein of interest in this paradigm, making further analysis of c-Jun protein levels at longer times post CCCP-challenge a priority. To investigate the modulation of both total c-Jun protein levels and Ser63 phosphorylation, WT SH-SY5Y cells were differentiated, mitochondrial uncoupling induced and Ser63 phosphorylated c-Jun levels assessed (Figure 5.5).

Due to the sensitivity of differentiated cells to CCCP, protein levels were only assessed from extracts up to 12 hours post-uncoupling (Figure 5.5). Although extracts from the 18 and 24 hour time points were obtained, they were too dilute to be of use here. This in itself shows how differentiated cell cultures undergo rapid apoptosis after significant mitochondrial damage and are much more sensitive to this form of stress compared to undifferentiated cultures. c-Jun protein levels consistently increased upon mitochondrial uncoupling all the way up to the 12 hour mark. Interestingly, the phosphorylation levels of c-Jun did not follow this pattern and may occur in 2 phases of modulation. This indicates c-Jun expression continues to increase independent of Ser63 phosphorylation levels in differentiated SH-SY5Y cultures.

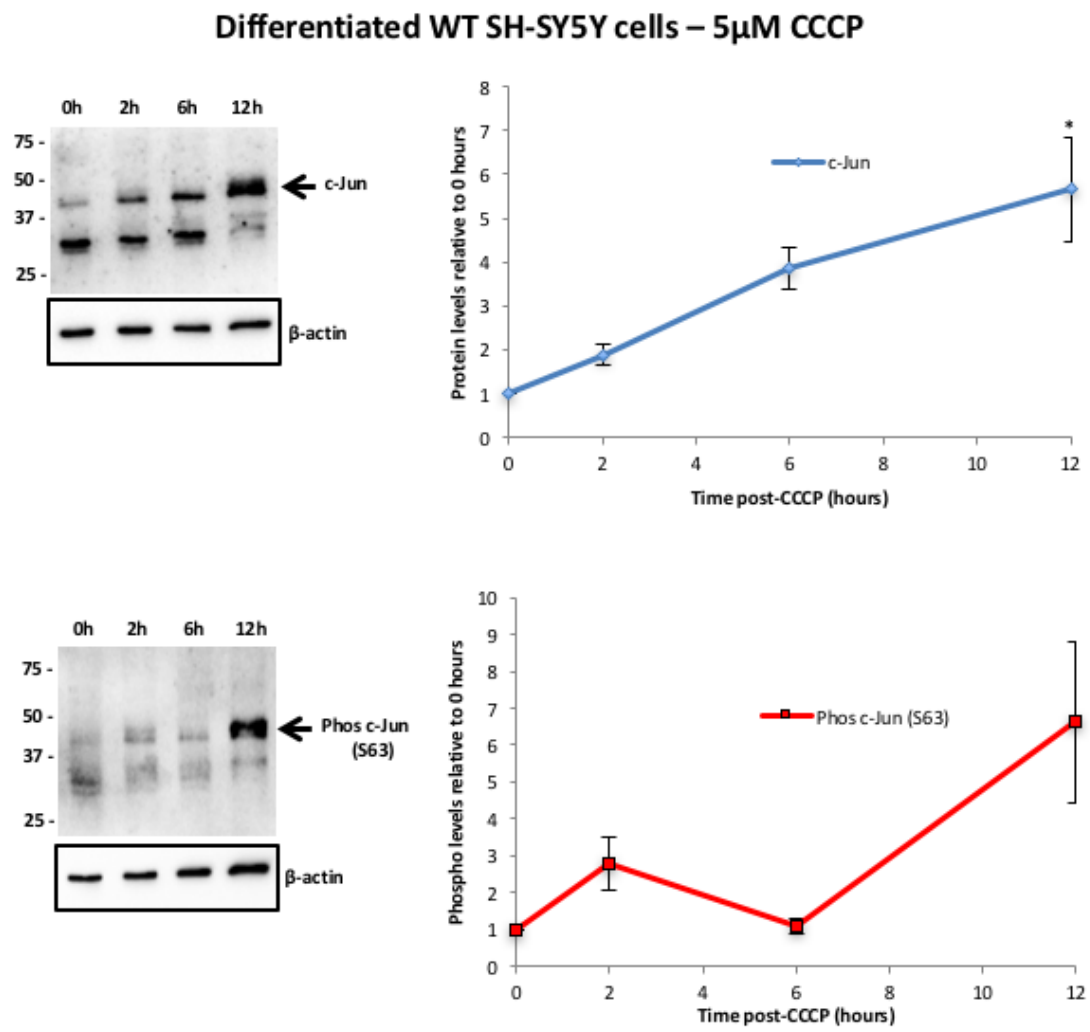

Figure 5.5: c-Jun is phosphorylated and expression increased in response to 5µM CCCP in differentiated WT SH-SY5Y cells. RA/BDNF differentiated cells were treated with 5µM CCCP and protein extracts obtained for western blot analysis. c-Jun protein levels steadily increased up to the 12 hour time point, whereas S63 phosphorylation occurred in two phases (n = 2). 'n' values refer to independent biological replicates, where cells were seeded, treated, protein extracted, western blot analysis and quantification performed per individual replicate. Statistical significance was assessed using a 2way ANOVA (Dunnett's). (*p < 0.05). Error bars represent SEM.

5.3.4 c-Jun and the regulation of *PARKIN* expression

c-Jun plays a role in the regulation of *PARKIN* expression by binding to the CREB site within the *PARKIN* promoter, blocking ATF4-mediated upregulation of *PARKIN* expression (Bouman et al., 2011). This was observed in SH-SY5Y cells suggesting this regulation can occur in this model system. As c-Jun is

rapidly degraded in a proteasome-dependent manner following mitochondrial uncoupling (Figure 5.1), one could hypothesise that this degradation may be part of an adaptive response that relieves c-Jun-dependent repression of *PARKIN* transcription, thus allowing for an increase in levels of the E3 ligase.

To test this hypothesis, c-Jun degradation after uncoupling (Figure 4.1) was blocked to investigate the rapid upregulation of *PARKIN* expression previously observed (Figure 4.17). Proteasomal inhibition prevented c-Jun degradation (Figure 5.1). If proteasomal degradation was required for a rapid increase in *PARKIN* mRNA in response to mitochondrial stress, then blocking it should perturb this upregulation. c-Jun siRNA may rescue this effect if successful knockdown occurred (although this was not validated here), as protein levels of c-Jun would be reduced despite proteasomal inhibition. Undifferentiated WT SH-SY5Y cells were transfected with siRNA specific to c-Jun prior to UPS inhibition, then mitochondria uncoupled. As an increase in *PARKIN* mRNA levels occurred just 1 hour after uncoupling (Figure 4.17) mRNA levels were assessed at this time point (Figure 5.6).

Under all conditions assessed, c-Jun siRNA resulted in higher *PARKIN* expression (Figure 5.6), consistent with the previous observation that c-Jun represses the transcription of Parkin (Bouman et al., 2011). However, as epoxomicin alone induced a marked increase in *PARKIN* mRNA levels it was unclear what role the proteasome-dependent turnover of c-Jun after CCCP treatment played in regulating Parkin expression in response to mitochondrial uncoupling.

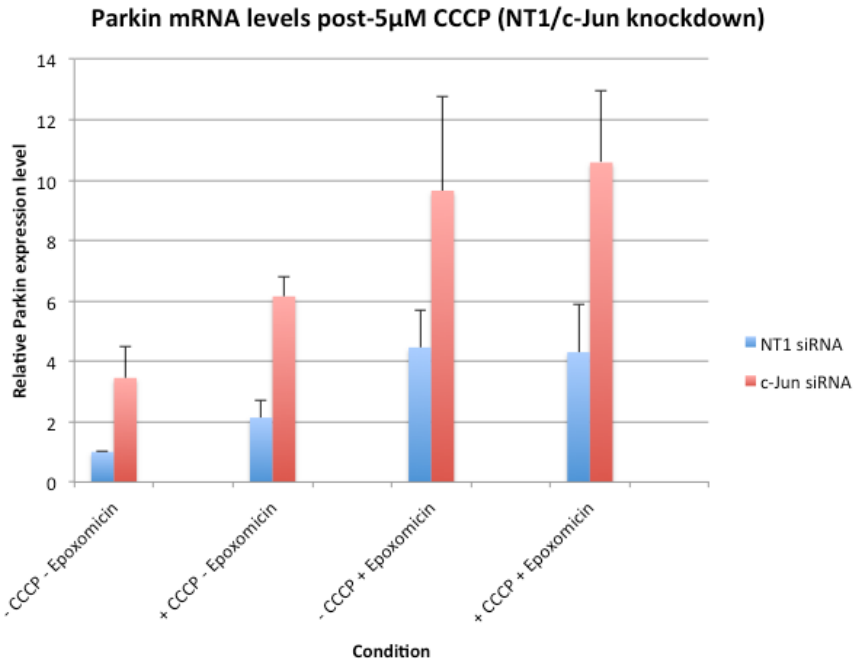

Figure 5.6: *PARKIN* expression is consistently increased by CCCP treatment. Relative *PARKIN* mRNA levels in undifferentiated WT SH-SY5Y cells treated with CCCP or vehicle (DMSO) were assessed by qPCR. Treatment using siRNA specific to *c-JUN* (NT1 as control) was carried out 48 hours prior to CCCP challenge and/or proteasomal inhibition. mRNA quantification was carried out in duplicate wells per experiment. Two independent biological replicates were performed, for each of which cells were seeded, treated, RNA extracted and mRNA levels quantified (n=2). *PARKIN* mRNA levels (relative to *β–ACTIN*) were assessed from extracts obtained 1 hour after CCCP treatment and compared to '–CCCP –epoxomicin' levels from ΔCt values. Statistical significance was determined using a 2way ANOVA (Bonferroni's) (95% confidence interval). Error bars represent SEM calculated from the mean of each individual experiment.

5.3.5 c-Jun siRNA can be either anti- or pro-apoptotic, depending on the level of stress

Previous results unexpectedly indicated that c-Jun was an anti-apoptotic factor in response to mitochondrial uncoupling in undifferentiated SH-SY5Y cells. The concentration of CCCP had been chosen after careful titration to cause a level of stress that cells could tolerate for 24 hours without causing death of the entire population. To test whether c-Jun siRNA was anti-apoptotic under higher levels of stress cells were treated with 30µM CCCP. An identical siRNA transfection protocol was used as described in Chapter 4 (Figure 5.7).

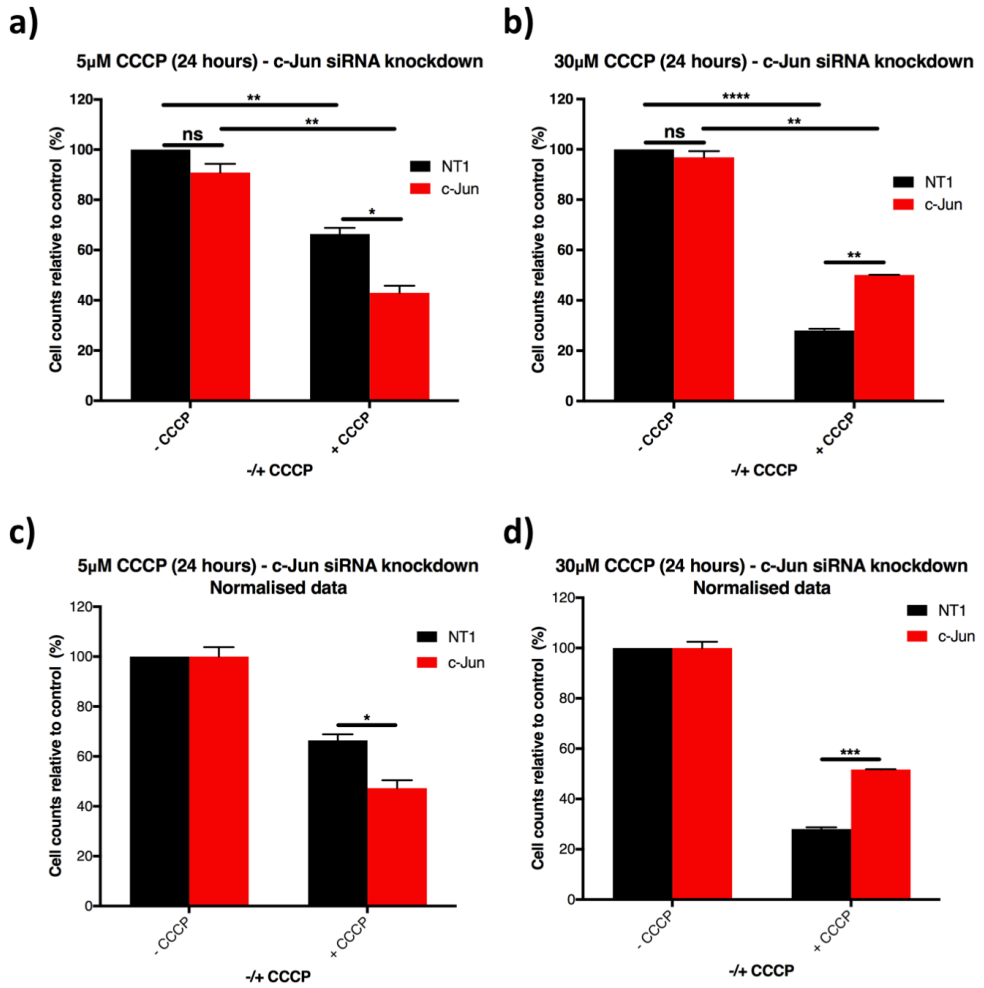

Figure 5.7: c-Jun siRNA is anti-apoptotic under higher levels of mitochondrial stress. (a) Data taken from Figure 4.18 for c-Jun and NT1 siRNA treatment prior to 24 hour treatment with 5μM CCCP. (b) c-Jun siRNA was performed prior to 24 hour 30μM CCCP treatment. (c) Data from c-Jun siRNA-treated cells was normalised so that cells not treated with 5μM CCCP represented 100%. (d) Data from c-Jun siRNA-treated cells was normalised so that cells not treated with 30μM CCCP represented 100%. Cell counts were performed in duplicate per experiment. Two individual biological replicates were performed in which cells were seeded and reverse transfected with siRNA 48 hours prior to CCCP treatment, fixation and analysis (n=2). Statistical analysis was carried out using an unpaired Student's t-test (*p<0.05, **p<0.01). Error bars represent SEM calculated from the mean of each individual experiment.

Despite data showing that c-Jun siRNA acts to increase cell death in SH-SY5Y cells treated with 5μM CCCP (Figures 4.24 and 5.7a c-Jun siRNA prior to 30μM CCCP treatment (Figure 5.7b) led to a significant rescue of apoptosis (**p = 0.0011), although significant cell death still occurred. Again, no significant cell

death was observed from c-Jun siRNA compared to controls (p = 0.3221). When c-Jun siRNA-treated data was normalised, opposing effects on stress-induced death was still observed at 5μM (*p = 0.0408) and 30μM CCCP (***p = 0.0009). If successful knockdown has been demonstrated here, this would be consistent with a model where c-Jun has the capacity to act as a molecular switch able to dictate cell fate decisions in response to differing levels of stress

5.3.6 CCCP-induced apoptosis is independent of JNK signalling in undifferentiated cells

As c-Jun siRNA had differing effects on cell survival depending on the level of mitochondrial stress applied to cells, it seemed possible that this might be due to c-Jun activity being differentially regulated by upstream kinases. The MAPK JNK pathway is generally considered the primary regulator of c-Jun phosphorylation and thus activity. Furthermore, much evidence has previously been presented showing JNK-dependent cell death under stressful conditions in a range of model systems. The next aim was therefore to determine whether JNK-regulated apoptosis occurred following mitochondrial damage in undifferentiated SH-SY5Y cells using a pharmacological JNK inhibitor.

Pre-treatment of cells with 10μM SP600125, a concentration previously shown to effectively inhibit JNK activity in SH-SY5Y cells (Bouman et al., 2011), prior to mitochondrial uncoupling had no significant effect on cell death at any CCCP concentration tested (Figure 5.8). Although significant death did not occur at 5μM CCCP when comparing JNK inhibitor-treated cells, no rescue is observed between inhibitor-treated and untreated groups. It should also be noted that SP600125, although developed as a specific JNK inhibitor, has been shown to inhibit at least 13 other kinases (Bain et al., 2003), thus limiting the certainty with which any effects can be attributed to JNK activity.

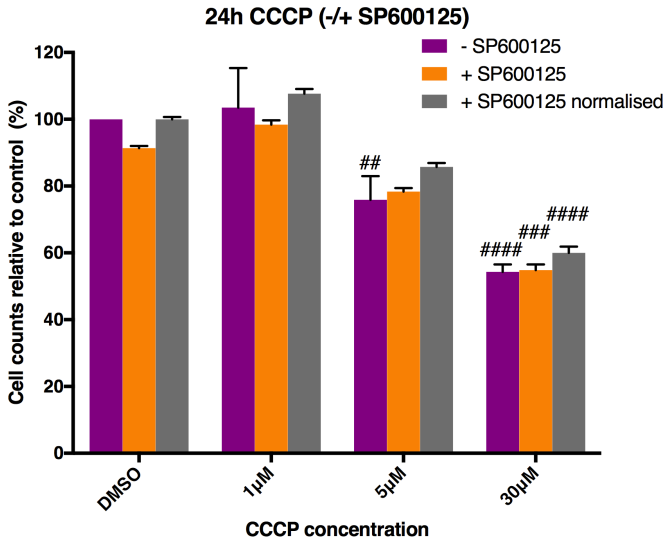

Figure 5.8: JNK inhibition has no significant effect on apoptosis induced by 24 hours exposure to a range of CCCP concentrations in undifferentiated WT SH-SY5Y cells. Cells seeded in a 96-well plate were pre-treated with 10μM SP600125 prior CCCP exposure. After 24 hours in a range of CCCP concentrations, cells were fixed, stained with DAPI and surviving cells counted using the Operetta microscope and Columbus software (n = 2). Each condition was performed in duplicate per experiment and the means of individual experiments used to calculate values presented here. Cell counts relative to the DMSO control. Additionally, data obtained from the SP600125-treated cells were normalised to the DMSO control group (grey bar) to allow for comparison of CCCP-induced cell death within this group. The grey bar therefore represents the % of cells relative to SP600125-treated cells not exposed to CCCP. Statistical significance determined using a 2way ANOVA (Bonferroni's) (95% confidence interval) comparing each CCCP concentration -/+ SP600125 (*) or CCCP concentrations to respective DMSO control -/+ SP600125 (#). (* or #p<0.05, ** or ##p<0.01, *** or ###p<0.005). Error bars represent SEM.

To ensure JNK-dependent apoptosis did not occur later than 24 hours post-mitochondrial uncoupling, 48 hours post-CCCP was also assessed (Figure 5.9). Again, no alteration in apoptosis was observed with JNK inhibition. JNK inhibition over 48 hours does appear to be cytotoxic under normal and low-level mitochondrial stress conditions, suggesting that JNK may act cytoprotectively to maintain homeostasis under normal, or near normal conditions. Alternatively, off target effects of the inhibitor could also be detrimental under these conditions.

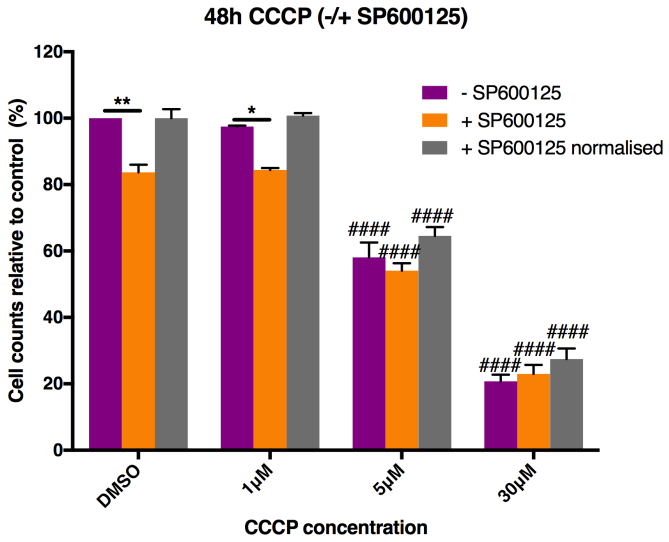

Figure 5.9: JNK inhibition does not rescue apoptosis induced by 48 hours exposure to a range of CCCP concentrations in undifferentiated WT SH-SY5Y cells. Cells were pre-treated with 10μM SP600125 prior CCCP exposure. After 48 hours in a range of CCCP concentrations, cells were fixed and stained with DAPI and surviving cells counted using the Operetta microscope and Columbus software (n=2). Each condition was performed in duplicate per experiment and the means of individual experiments used to calculate values presented here. Cell counts were relative to the DMSO control wells. Additionally, data obtained from the SP600125-treated cells were normalised to the DMSO control group (grey bar) to allow for comparison of CCCP-induced cell death within this group. The grey bar therefore represents the % of cells relative to SP600125-treated cells not exposed to CCCP. Statistical significance was determined using a 2way ANOVA (Bonferroni's) (95% confidence interval) comparing each CCCP concentration -/+ SP600125 (*) or CCCP concentrations to respective DMSO control -/+ SP600125 (#). (* or #p<0.05, ** or ##p<0.01, **** or ####p<0.001). Error bars represent SEM.

5.3.7 JNK signalling does not regulate ER or cellular oxidative stress-induced apoptosis

CCCP induces stress by uncoupling the mitochondrial proton gradient leading leads to secondary stress such as ROS accumulation and energy depletion. To see if JNK signalling played a role in apoptosis induced by other forms of stress, cell JNK function was blocked prior to hydrogen peroxide (to induce cellular oxidative stress) or tunicamycin (an ER stressor) exposure. Cell death induced by a range of H_2O_2 concentrations for 24 or 48 hours was not perturbed by JNK

inhibition in the undifferentiated SH-SY5Y cells (Figure 5.10). As hydrogen peroxide induces widespread cellular damage, the ER-specific stress was used to induce apoptosis via a different pathway. Similarly, JNK inhibition did not significantly alter ER-induced apoptosis in these cells over a 24 or 48 hours period (Figure 5.11).

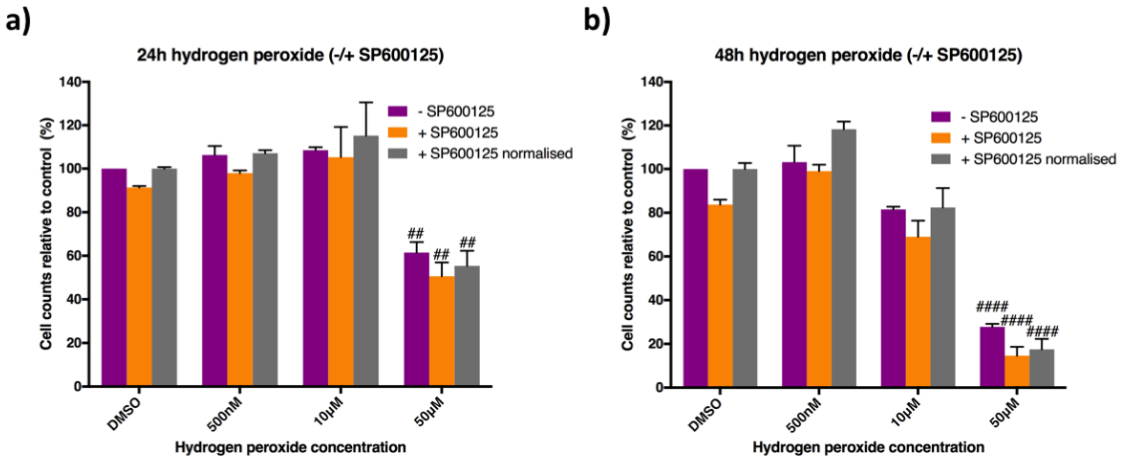

Figure 5.10: JNK inhibition does not rescue H_2O_2-induced cell death in undifferentiated WT SH-SY5Y cells. Cells were pre-treated with 10μM SP600125 prior to H_2O_2 exposure. After 24 hours (a) or 48 hours (b) cells were fixed and stained with DAPI and surviving cells counted using the Operetta microscope and Columbus analysis software (n = 2). Each condition was performed in duplicate and the means of individual experiments used to calculate values presented here. Cell counts were relative to the DMSO control wells. Additionally, data obtained from the SP600125-treated cells were normalised to the DMSO control group (grey bar) to allow for comparison of hydrogen peroxide-induced cell death within this group. The grey bar therefore represents the % of cells relative to SP600125-treated cells not exposed to hydrogen peroxide. Statistical significance was determined using a 2way ANOVA (Bonferroni's) (95% confidence interval) comparing each hydrogen peroxide concentration -/+ SP600125 (*) or CCCP concentrations to respective DMSO control -/+ SP600125 (#). (* or #p<0.05, ** or ##p<0.01, **** or ####p<0.001). Error bars represent SEM.

As no significant decrease or increase in cell death induced by either stressor was observed when comparing inhibitor-treated and untreated groups at either 24 and 48 hours post-treatment (Figures 5.10 and 5.11) this would suggest JNK

signalling does not play a major role in either ER or oxidative stress-induced apoptosis in undifferentiated WT SH-SY5Y cells.

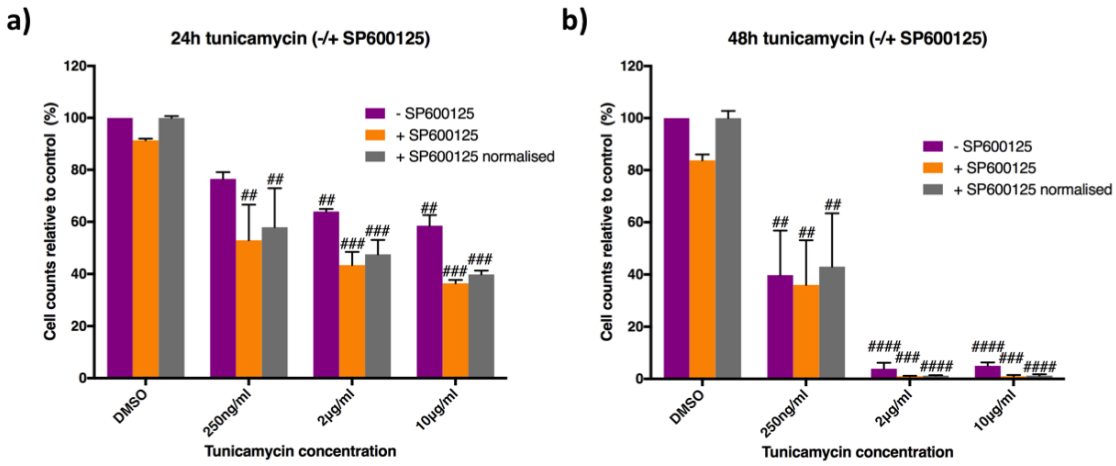

Figure 5.11: JNK inhibition does not rescue tunicamycin-induced cell death in undifferentiated WT SH-SY5Y cells. Cells were pre-treated with 10μM SP600125 prior to tunicamycin exposure. After 24 hours (a) or 48 hours (b) cells were fixed and stained with DAPI and surviving cells counted using the Operetta microscope and Columbus analysis software (n = 2). Each condition was performed in duplicate and the means of individual experiments used to calculate values presented here. Cell counts were relative to the DMSO control wells. Additionally, data obtained from the SP600125-treated cells were normalised to the DMSO control group (grey bar) to allow for comparison of tunicamycin-induced cell death within this group. The grey bar therefore represents the % of cells relative to SP600125-treated cells not exposed to tunicamycin. Statistical significance was determined using a 2way ANOVA (Bonferroni's) (95% confidence interval) comparing each tunicamycin concentration -/+ SP600125 (*) or CCCP concentrations to respective DMSO control -/+ SP600125 (#). (* or #p<0.05, ** or ##p<0.01, *** or ###p<0.005). Error bars represent SEM.

5.3.8 ERK signalling regulates apoptosis under mitochondrial stress conditions in undifferentiated SH-SY5Y cells

As JNK did not appear to regulate cell death at low or high levels of mitochondrial uncoupling, the next aim was to investigate whether another MAPK pathway could be involved in the regulation of apoptosis in response to mitochondrial depolarisation. ERKs are a separate class of MAPKs to JNK that have been previously implicated in several stress response pathways. To

determine they promoted apoptosis under mitochondrial stress, a specific ERK inhibitor was used (Figure 5.12).

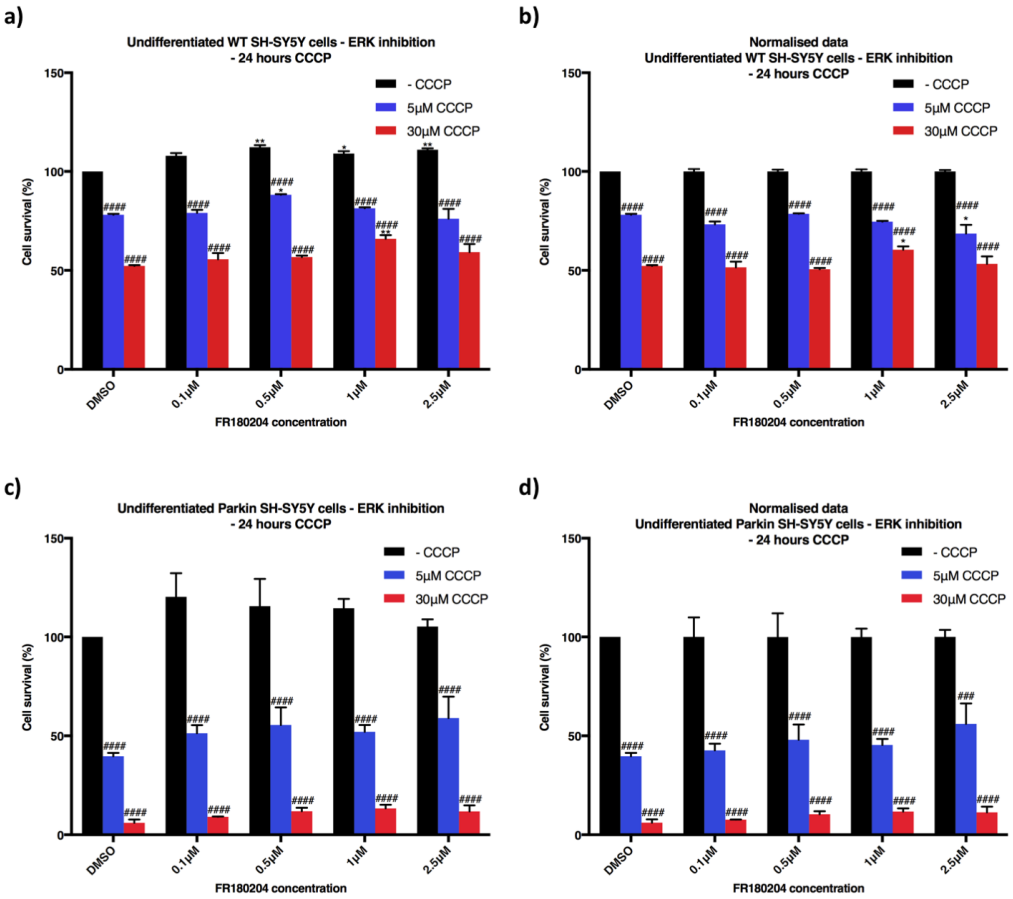

Figure 5.12: ERK inhibition in undifferentiated WT and Parkin SH-SY5Y cells. Cell survival was calculated by cell counts by DAPI staining on the Operetta. Each condition was performed in duplicate and the means of individual experiments used to calculate values presented here. Two independent biological replicates were performed in which cells were seeded, treated, fixed and analysed (n=2). Cell counts were relative to the DMSO control wells. (a) Undifferentiated WT cells treated with ERK inhibitor prior to CCCP challenge. (b) Each of the FR180204 controls (-CCCP) for undifferentiated WT cells was normalised to 100% and CCCP-treated wells for each concentration of FR180204 normalised relative to this. (c) Undifferentiated WT cells treated with ERK inhibitor prior to CCCP challenge. (d) Each of the FR180204 controls (-CCCP) for undifferentiated WT cells was normalised to 100% and CCCP-treated wells for each concentration of FR180204 normalised relative to this. Statistical significance was determined using a 2way ANOVA (Bonferroni's) (95% confidence interval) comparing each CCCP concentration -/+ FR180204 (*) or CCCP concentrations to respective DMSO control -/+ FR180204 (#). (* or #p<0.05, ** or ##p<0.01, **** or ####p<0.001). Error bars represent SEM.

FR180204 is a highly selective ERK1/2 inhibitor (Ohori et al., 2007), although has been shown to exhibit some inhibition of unphosphorylated and monophosphorylated insulin receptor (Anastassiadis et al., 2013). To date, no publications have shown the effectiveness of this inhibitor on ERK signalling in SH-SY5Y cells. Treatment of WT cells with increasing ERK inhibitor concentrations led to increased cell numbers without uncoupling ($p = 0.0063$, 0.0482 and 0.0144, respectively). Mitochondrial uncoupling-induced apoptosis was partially rescued by 0.5μM FR180204 in cells treated with 5μM CCCP (*$p = 0.026$) and by 1μM FR180204 in cells treated with 30μM CCCP (*$p = 0.0025$) (Figure 5.12a). In non-uncoupled cells, an increased cell number was observed suggesting that ERK inhibition marginally increases proliferation rate. This may account for the small rescue in CCCP-induced apoptosis seen here. Comparing cell death observed with FR180204 concentration groups, CCCP consistently results in a significant reduction in cell number (####$p<0.001$). When inhibitor-treated groups were normalised, a small rescue in 30μM CCCP-induced death was observed in cells treated with 1μM FR180204 (*$p = 0.0306$). An increase in 5μM CCCP-induced death occurred, according to normalised data, in cells treated with 2.5μM FR180204 (*$p = 0.0102$).

Parkin overexpressing cells FR180204 treatment did not have any significant effect on mitochondrial damage-induced cell death (Figure 5.12c and 12d), although this may be due to larger standard errors. This highlights the limitation of a low number of biological replicates used here.

5.3.9 JNK and ERK differentially regulate c-Jun

As JNK and ERK inhibition led to different outcomes when mitochondria are uncoupled, it would be important to determine if they both played a role in regulating c-Jun activity and phosphorylation under mitochondrial stress. Furthermore, it could prove critical to elucidate this if the roles of JNK and ERK in the regulation of c-Jun were dependent on the level of stress.

To investigate the role of JNK and ERK in c-Jun regulation, the selective inhibitors (above) were again utilised. Undifferentiated WT SH-SY5Y cells were treated with either inhibitor 2 hours prior to low or high uncoupling treatment

and c-Jun or phospho c-Jun (S63) assessed. Initially, total c-Jun levels were analysed for low uncoupling after MAPK inhibition (Figure 5.13).

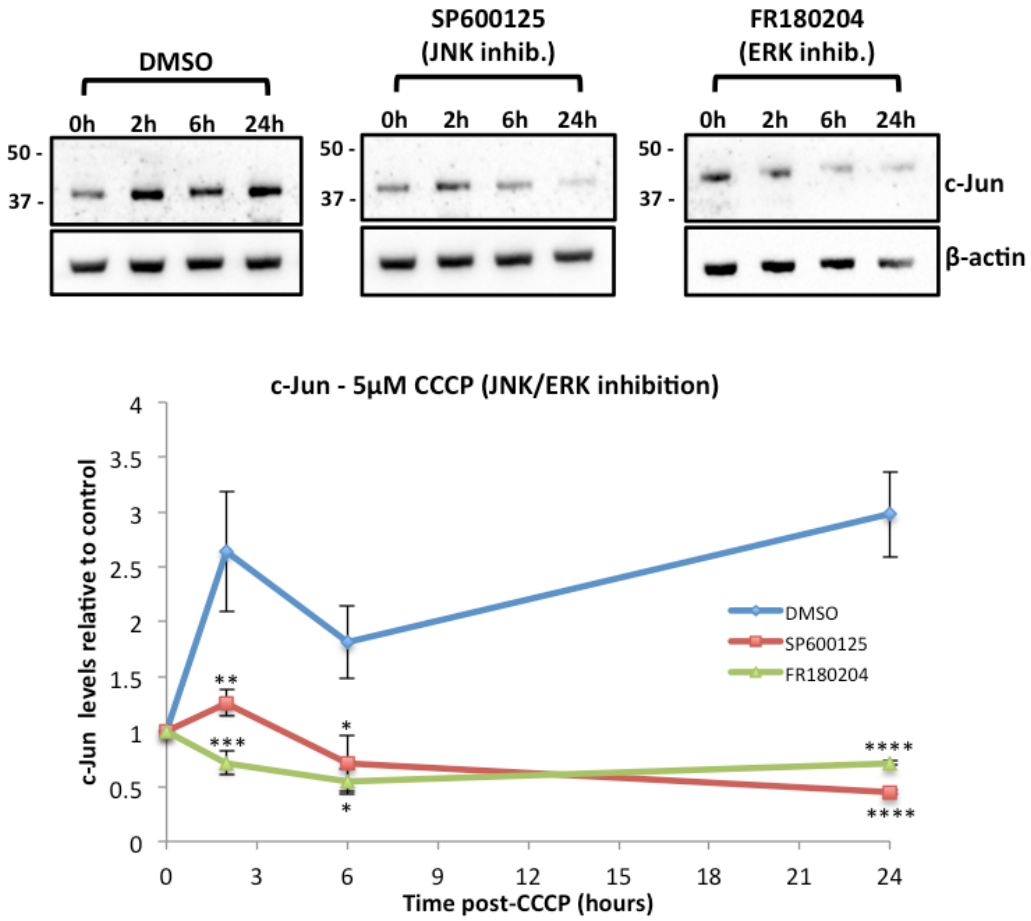

Figure 5.13: MAPK inhibition prevents c-Jun upregulation after 5µM CCCP treatment in undifferentiated WT cells. Cells were treated with SP600125 (JNK inhibitor), FR180204 (ERK inhibitor) or DMSO 2 hours prior to CCCP treatment. Protein extracts were obtained at specific times post-CCCP and relative c-Jun levels analysed by western blotting (n = 2). 'n' values refer to independent biological replicates, where cells were seeded, treated, protein extracted, western blot analysis and quantification performed per individual replicate. Statistical significance within each time point relative to DMSO (vehicle control for inhibitors) was determined using a 2way ANOVA (Tukey's) (95% confidence interval) (*p < 0.05, **p < 0.01, ***p < 0.005, ****p < 0.001). Error bars represent SEM.

Inhibition of both JNK and ERK significantly reduced the peak in c-Jun protein levels 2 hours-post uncoupling (**p = 0.0035 and ***p = 0.0004, respectively) relative to controls. JNK and ERK inhibitors continued to down regulate c-Jun

levels at both 6 hours (*p = 0.0154 and 0.012, respectively) and 24 hours (****p < 0.0001) after uncoupling. This suggests both JNK and ERK are critical in regulating c-Jun upregulation in response to mitochondrial stress, either increasing its stability or decreasing its degradation.

It was next investigated how c-Jun were regulated under greater levels of mitochondrial stress (Figure 5.14). Under higher stress JNK and ERK inhibition had strikingly different effects. Inhibition of ERK significantly prevented c-Jun upregulation at 2-hours (**p = 0.0091), 6 hours (****p < 0.0001) and 24 hours (**p = 0.0079) post-uncoupling. In marked contrast JNK inhibition increased c-Jun levels at 6 hours after higher levels of uncoupling (**p= 0.0028) relative to control, suggesting that ERK is solely responsible for upregulating c-Jun levels in response to higher levels of mitochondrial stress in this system. Furthermore, JNK may act to inhibit this effect to a degree, explaining why the use of JNK inhibition led to increased c-Jun levels at 6 hours post-CCCP relative to the control.

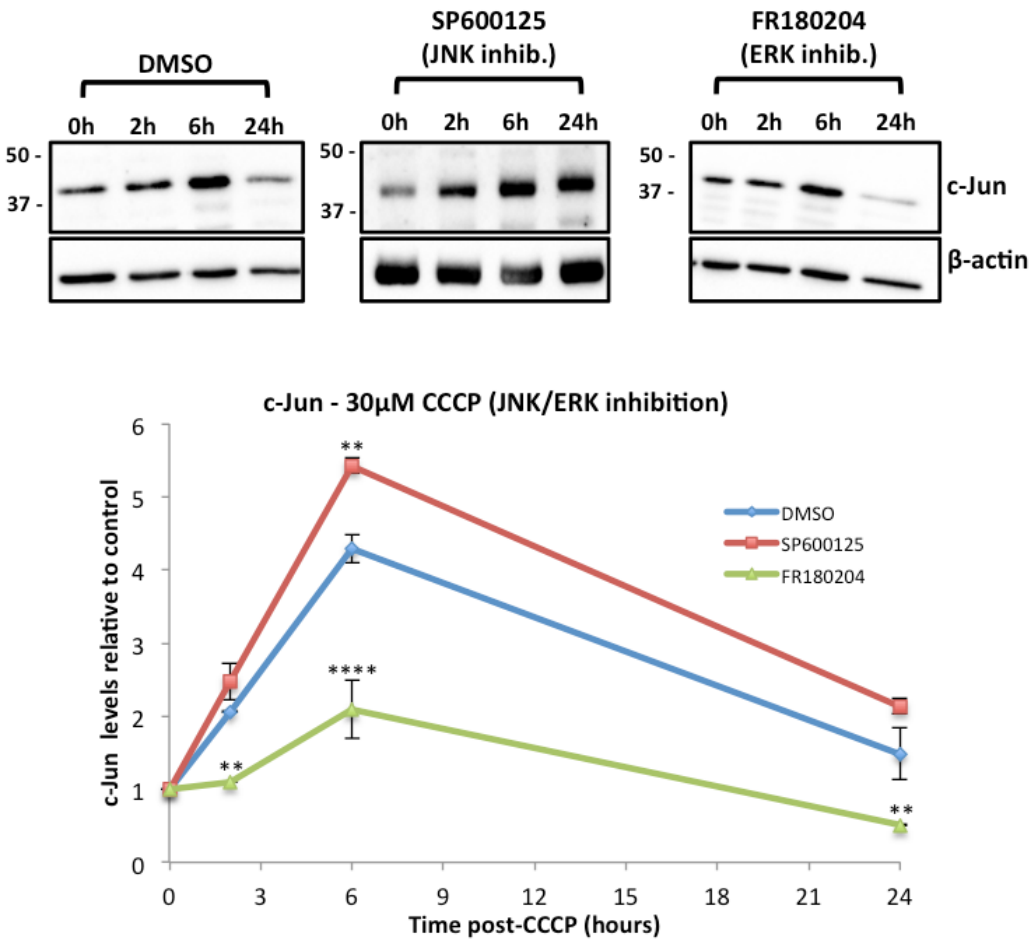

Figure 5.14: ERK inhibition down regulates the c-Jun response to 30µM CCCP in undifferentiated WT cells. Furthermore, JNK activity appears to oppose ERK activity. Cells were treated with SP600125 (JNK inhibitor), FR180204 (ERK inhibitor) or DMSO 2 hours prior to CCCP treatment. Protein extracts were obtained at specific times post-CCCP and relative c-Jun levels analysed by western blotting (n = 2). 'n' values refer to independent biological replicates, where cells were seeded, treated, protein extracted, western blot analysis and quantification performed per individual replicate. Statistical significance within each time point relative to DMSO (vehicle control for inhibitors) was determined using a 2way ANOVA (Tukey's) (95% confidence interval) (**p < 0.01, ****p < 0.001). Error bars represent SEM.

To gain an insight into how the phosphorylation and transactivation potential of c-Jun is regulated by these 2 MAPKs, an antibody specific to the Ser63 phosphorylated form of c-Jun was used (Figures 5.15 and 5.16, respectively). It must, however, be noted that the polyclonal antibody utilised here is specific

only to the Ser63 phosphorylated form of c-Jun, thus is not indicative of the phosphorylation status of other residues within the protein.

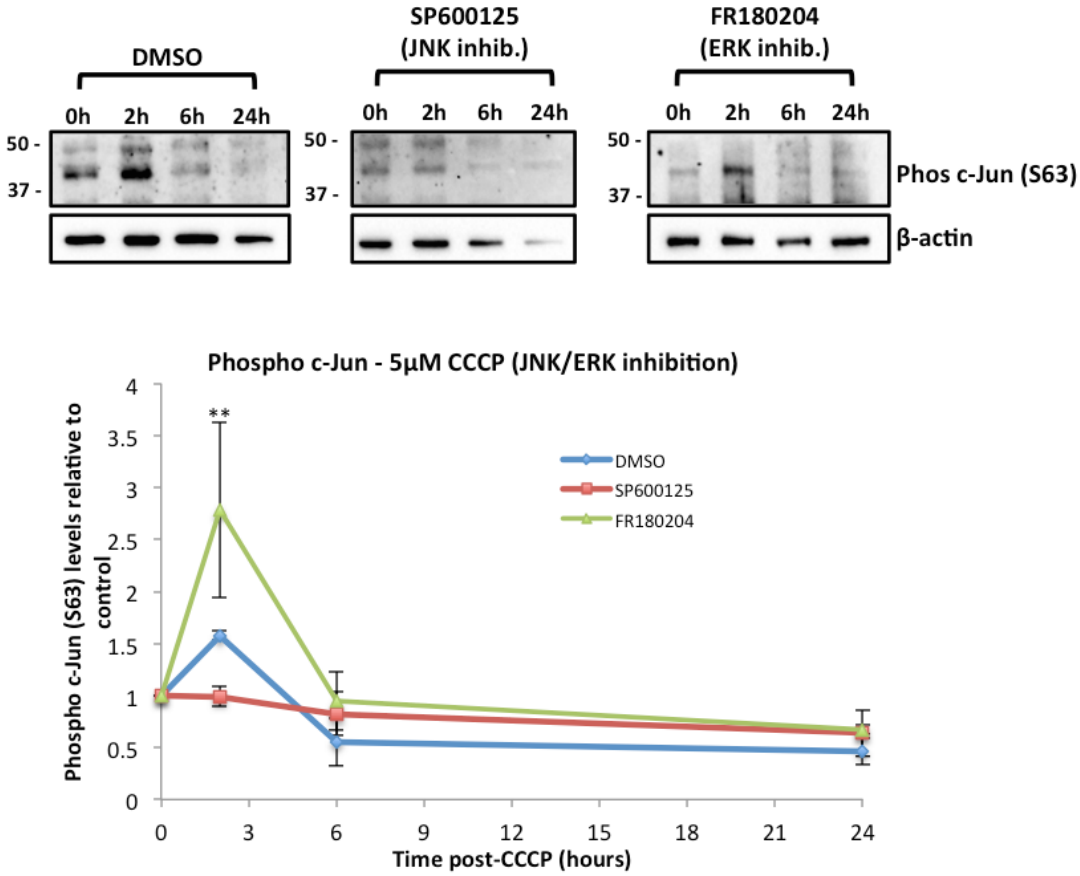

Figure 5.15: JNK rapidly phosphorylates c-Jun in response to 5μM CCCP in undifferentiated WT cells, whereas ERK activity perturbs the phosphorylation of the S63 residue. Cells were treated with SP600125 (JNK inhibitor), FR180204 (ERK inhibitor) (n = 2) or DMSO (n = 3) 2 hours prior to CCCP treatment. Protein extracts were obtained at specific times post-CCCP and relative c-Jun levels analysed by western blotting. 'n' values refer to independent biological replicates, where cells were seeded, treated, protein extracted, western blot analysis and quantification performed per individual replicate. Statistical significance within each time point relative to DMSO (vehicle control for inhibitors) was determined using a 2way ANOVA (Tukey's) (95% confidence interval) (**p < 0.01). Error bars represent SEM.

Although not deemed statistically significant, the inhibition of JNK prior to 5μM CCCP does appear to completely abolish the phosphorylation of c-Jun observed in the control 2 hours post-treatment. Conversely, the phosphorylation of c-Jun was increased by ERK inhibition 2 hours post-CCCP (**p = 0.0072) relative to the control. Despite both JNK and ERK inhibition having different

effects on c-Jun phosphorylation, levels comparable to the control are observed in both cases from 6 hours onwards.

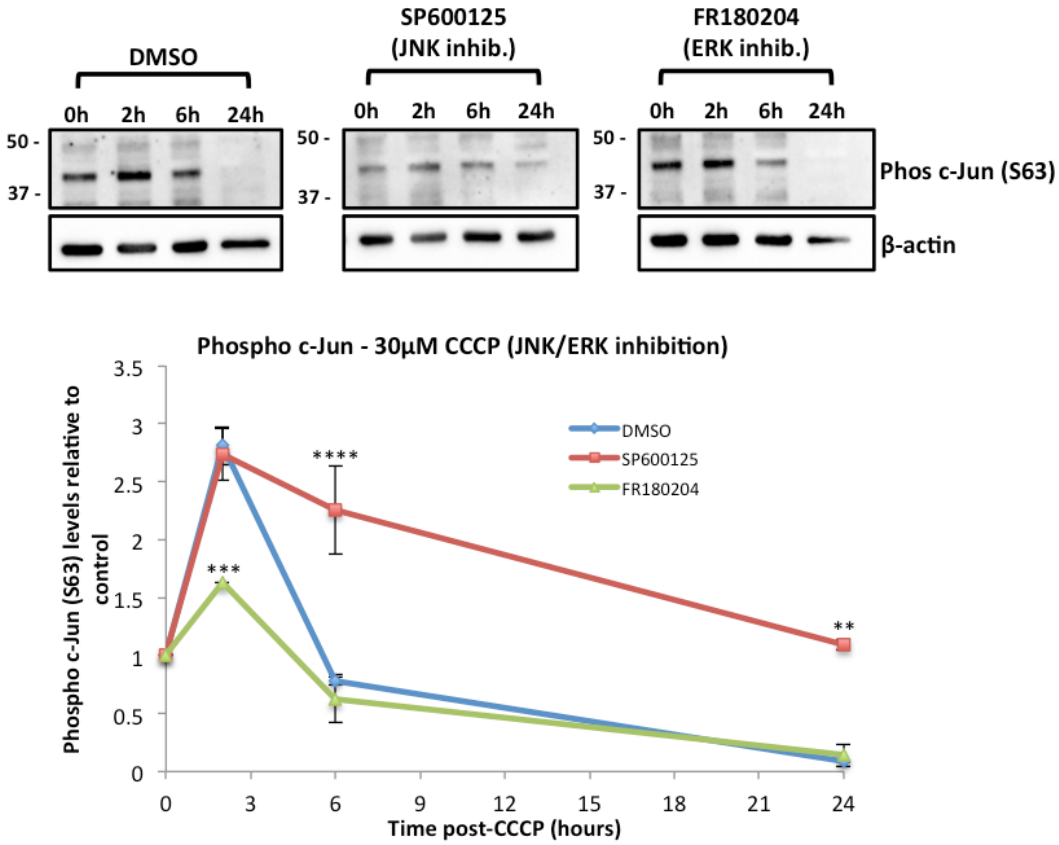

Figure 5.16: ERK immediately phosphorylates c-Jun in response to 30μM CCCP in undifferentiated WT cells. However, inhibition of JNK activity suggests that the later response is repressed by JNK. Cells were treated with SP600125 (JNK inhibitor), FR180204 (ERK inhibitor) or DMSO 2 hours prior to CCCP treatment. Protein extracts were obtained at specific times post-CCCP and relative c-Jun levels analysed by western blotting (n = 2). 'n' values refer to independent biological replicates, where cells were seeded, treated, protein extracted, western blot analysis and quantification performed per individual replicate. Statistical significance within each time point relative to DMSO (vehicle control for inhibitors) was determined using a 2way ANOVA (Tukey's) (95% confidence interval) (**p < 0.01, ***p < 0.005, ****p < 0.001). Error bars represent SEM.

Again, phospho c-Jun (S63) levels from cells treated with high uncoupling conditions after MAPK inhibition were assessed to determine if they were regulated differently by either JNK or ERK under varying levels of stress. Remarkably, as seen with total c-Jun levels (Figures 5.13 and 5.14), ERK and

JNK again appear to act differently in terms of their regulation of c-Jun phosphorylation depending on the level of uncoupling (Figures 5.15 and 5.16). JNK inhibition prior to high uncoupling did not alter c-Jun phosphorylation 2 hours post-treatment (Figure 5.16). However, the rapid decline in the levels of phosphorylated c-Jun observed in the control after the 2-hour time point was significantly perturbed by JNK inhibition, leading to higher levels at 6 hours (****$p < 0.0001$) and 24 hours (**$p = 0.0014$) post-uncoupling. ERK inhibition led to a marked decrease in c-Jun phosphorylation (***$p = 0.0004$) compared to the control, although levels were similar at the 6 and 24 hour time points.

Overall these data show that, at least in undifferentiated SH-SY5Y cells, both ERK and JNK have the capacity to regulate c-Jun. Moreover, both regulate c-Jun in different manners. It is notable that ERK may in fact inhibit JNK-dependent phosphorylation of c-Jun after lower levels of uncoupling (Figure 5.15). JNK and ERK appear to be able to regulate c-Jun expression independent of S63 phosphorylation.

5.3.10 Apoptosis is only regulated by JNK in differentiated neuronal cells under extreme stress

As JNK inhibition in undifferentiated cells did not have any effect on apoptosis induced by mitochondrial uncoupling, whereas ERK showed minor rescue, the next objective was to determine whether this would be replicated in differentiated cells. The role of MAPKs in directing the cellular response to the uncoupling of the mitochondrial network is yet to be determined in these cells.

In differentiated WT cells (Figure 5.17), MAPK inhibition did not have a significant effect on cell death induced by low uncoupling conditions. A small rise in survival in JNK inhibited cells prior to low uncoupling was not deemed statistically significant ($p = 0.4280$). However, JNK inhibition did have a severe effect on cells undergoing higher uncoupling, increasing survival by around 6-fold (***$p = 0.0004$). The lower concentration of JNK inhibitor failed to increase cell survival, as did both concentrations of the ERK inhibitor. This is consistent with a model in which JNK-regulated apoptosis is only initiated once a critical threshold of mitochondrial damage is passed.

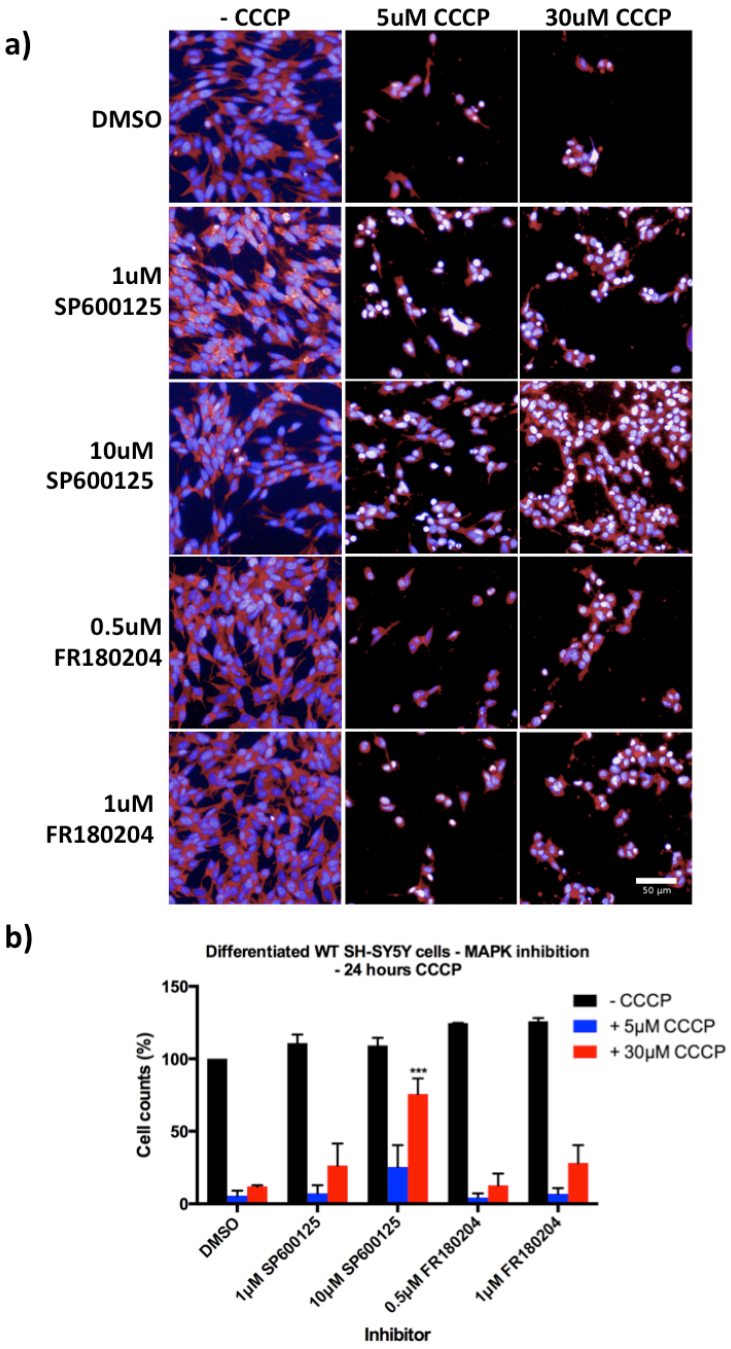

Figure 5.17: JNK inhibition under high level mitochondrial stress in differentiated WT SH-SY5Y cells is protective. Cells were seeded in a 96-well plate and differentiated prior to JNK (SP600125) and ERK (FR180204) inhibition and mitochondrial uncoupling. (a) Images captured on Operetta at 20X magnification. (b) Statistical significance was determined using a 2way ANOVA (95% confidence interval) (***p<0.005). Two fully independent biological replicates were performed on separate occasions in which cells were seeded, differentiated, treated and analysed for each experiment (n=2). Comparisons were made between inhibitor-treatment and vehicle control of same CCCP concentration. Scale bar is 50µM. Error bars represent SEM calculated from the mean of each individual experiment.

Undifferentiated *PARKIN* overexpressing cells are significantly more sensitive to CCCP than WT cells (Figure 3.4). However, using a 2way ANOVA, statistically relevant rescue was not achieved using either MAPK inhibitor in the differentiated Parkin overexpression model (Figure 5.18b). This was despite over a 25-fold increase in cell survival in cells treated with 10μM SP600125 (JNK inhibitor) and 5μM CCCP when compared to the control for that CCCP concentration. However, by comparing this result to the control directly using an unpaired 2-tailed student *t*-test the result is deemed as significant (p*** = 0.0006). The variation observed between replicates may skew data toward a non-statistical significance under more stringent conditions. Nevertheless, JNK inhibition was certainly less proficient at inhibiting CCCP-induced apoptosis in *PARKIN* overexpressing cells compared to the WT line. It may be that in the overexpressing line, excessive mitophagy initiates alternative cell death pathways or the complete obliteration of the mitochondrial network results in necrotic death instead.

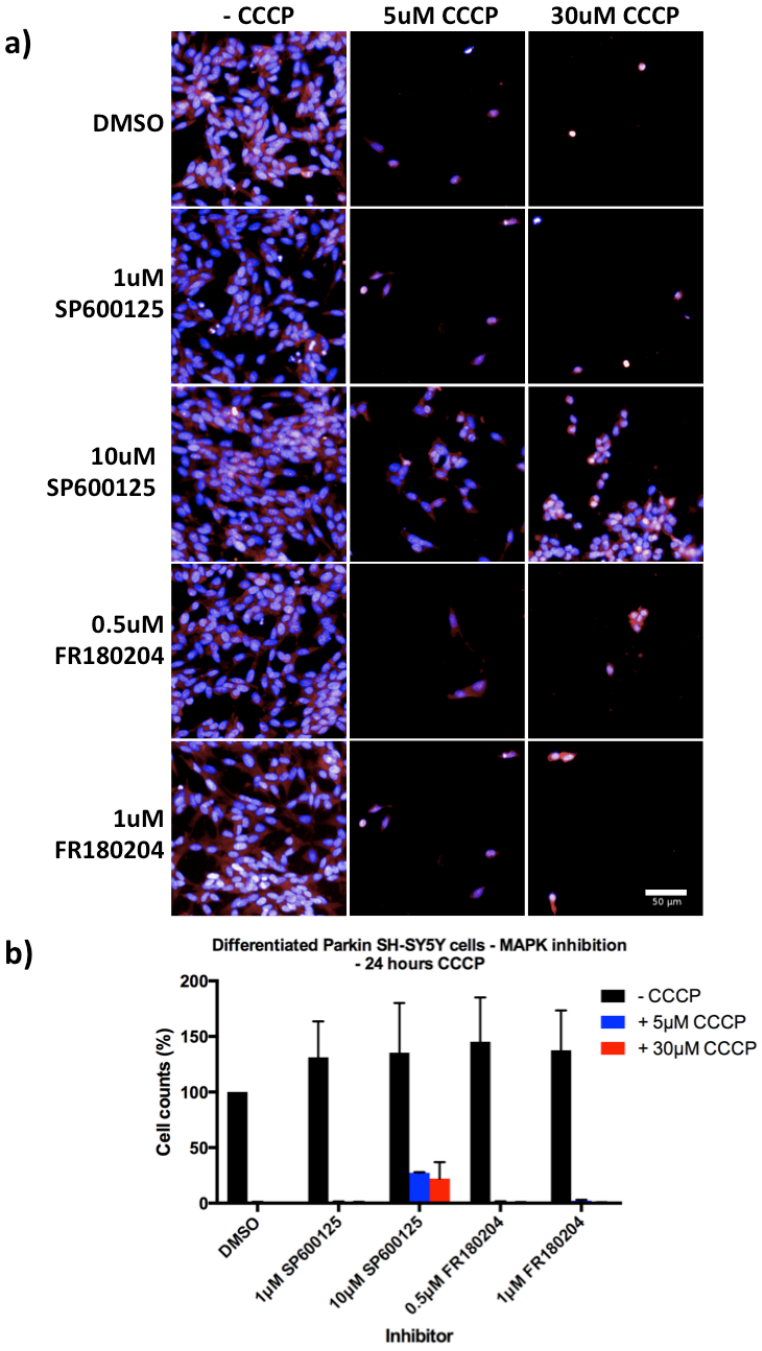

Figure 5.18: MAPK inhibition under mitochondrial stress in differentiated *PARKIN* overexpressing cells has no significant effect on cell death. Cells were seeded in a 96-well plate and differentiated prior to JNK (SP600125) and ERK (FR180204) inhibition and mitochondrial uncoupling (a) Images captured on Operetta at 20X magnification. (b) Statistical significance was determined using a 2way ANOVA (95% confidence interval). Two fully independent biological replicates were performed on separate occasions in which cells were seeded, differentiated, treated and analysed for each experiment (n=2). Comparisons were made between inhibitor-treatment and vehicle control of same CCCP concentration. Scale bar is 50µM. Error bars represent SEM calculated from the mean of each individual experiment.

5.3.11 Proteasomal inhibition

To investigate if proteasomal inhibition exacerbated cell death in response to mitochondrial stress and whether this was regulated by MAPK signalling, proteasomal inhibition in differentiated cells was induced prior to uncoupling and cells imaged for counting.

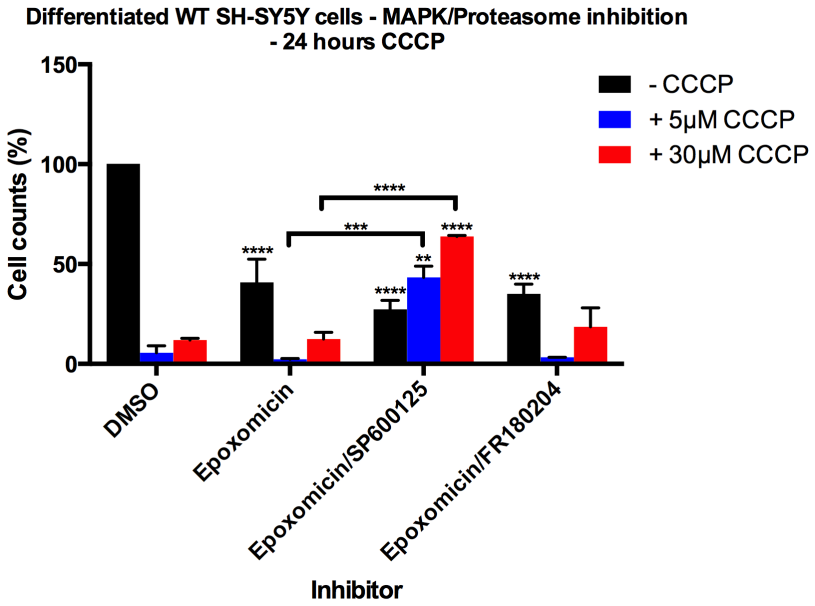

Figure 5.19: JNK inhibition is cytoprotective against CCCP-induced apoptosis in UPS-deficient differentiated WT SH-SY5Y cells. Cells were differentiated in 96-well plates the treated with inhibitors prior to 24 hour CCCP exposure. Cells fixed and stained for DAPI and images captured using the high-throughput Operetta IF microscope then analysed using Columbus software to obtain cell counts (n = 2). Statistical significance was determined using a 2way ANOVA (95% confidence interval) (**p<0.01, ***p<0.005, ****p<0.001). Two fully independent biological replicates were performed on separate occasions in which cells were seeded, differentiated, treated and analysed for each experiment (n=2). Comparisons were made between inhibitor-treatment and vehicle control of same CCCP concentration. Error bars represent SEM calculated from the mean of each individual experiment.

UPS block induced significant cell death (****p < 0.0001) in differentiated WT SH-SY5Y cells (Figure 5.19). The inhibition of either JNK or ERK pathways failed to rescue UPS dysfunction-induced cell death in non-uncoupled cells, suggesting apoptosis induced by proteasomal inhibition occurs independently of these MAPK pathways in differentiated cells. However, JNK inhibition did

significantly increase cell survival in UPS deficient cells undergoing low or high uncoupling relative to UPS blocked cells (***p = 0.006 or ****p < 0.0001, respectively) or cells only uncoupled (**p = 00012 or ****p < 0.0001, respectively). These data show that JNK-dependent apoptosis in SH-SY5Y cells is not initiated upon proteasomal dysfunction but if mitochondrial depolarisation occurs under UPS-deficiency, this pathway is dominant in inducing neuronal cell death. On the other hand, inhibition of ERK signalling did not alter the rate of cell death under any condition investigated.

This experiment was also carried out in differentiated *PARKIN* overexpressing cells. In an identical manner to differentiated WT cells, 100nM epoxomicin treatment over a 24 hours period induced significant apoptosis in differentiated *PARKIN* overexpressing SH-SY5Y cells (****p < 0.0001). Neither JNK nor ERK inhibition rescued this (p = 0.9758 and p = 0.9036, respectively). The JNK inhibitor in UPS deficient cells was able to partially rescue apoptosis in cells undergoing lower levels of mitochondrial uncoupling (**p = 0.0028). JNK inhibition in cells undergoing proteasomal dysfunction also rescued cell death induced by low levels of uncoupling in cells not undergoing UPS disruption (**p = 0.0027). Unlike in WT cells (Figure 5.19), JNK inhibition did not rescue apoptosis induced by higher levels of uncoupling in the *PARKIN* overexpressing cells (Figure 5.20).

These data suggest that the JNK pathway in differentiated *PARKIN* overexpressing SH-SY5Y cells, as in the WT cells, acts as the dominant apoptotic pathway if mitochondrial dysfunction occurs (with or without proteasomal inhibition), but is not initiated by proteasomal dysfunction alone. However, in Parkin overexpressing cells, apoptosis induced by high levels of mitochondrial uncoupling is independent of JNK signalling. This may be due to levels of mitophagy above the threshold for apoptotic induction occurring under this level of CCCP treatment due to high Parkin activity. Equally, this may be due to elevated Parkin activity inducing alternative cell death pathways under this level of mitochondrial stress. Again, as in the WT cell line, ERK activity does not appear to play a regulatory role in apoptosis here.

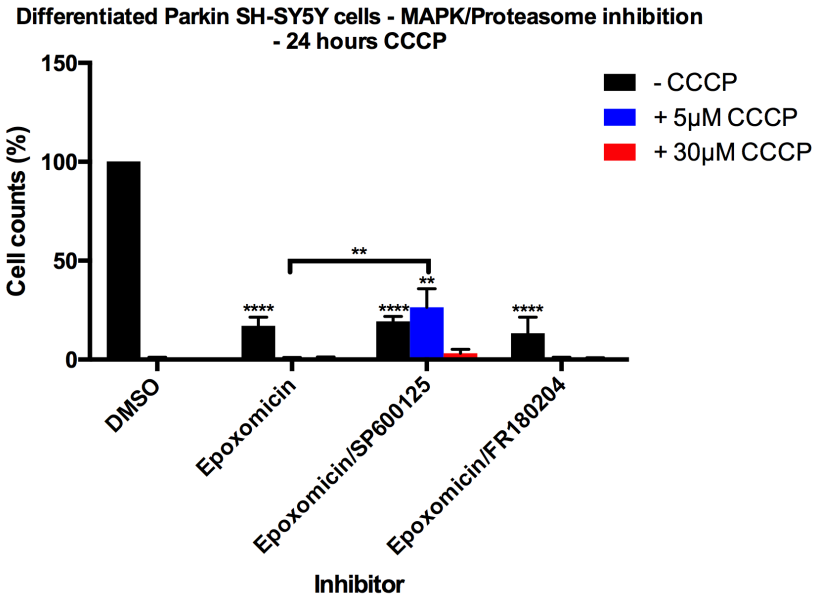

Figure 5.20: JNK inhibition has limited cytoprotectivity against CCCP-induced apoptosis in UPS-deficient differentiated *PARKIN* overexpressing SH-SY5Y cells. Cells were differentiated in 96-well plates the treated with inhibitors prior to 24 hour CCCP exposure. Cells fixed and stained for DAPI and images captured using the high-throughput Operetta IF microscope then analysed using Columbus software to obtain cell counts (n = 2). Statistical significance was determined using a 2way ANOVA (95% confidence interval) (**p<0.01, ****p<0.001). Two fully independent biological replicates were performed on separate occasions in which cells were seeded, differentiated, treated and analysed for each experiment (n=2). Comparisons were made between inhibitor-treatment and vehicle control of same CCCP concentration. Error bars represent SEM calculated from the mean of each individual experiment.

Together these data suggest that apoptotic JNK signalling is only initiated under specific stress conditions, which appears to occur after a threshold is surpassed. In the conditions assessed here, JNK activity was only pro-apoptotic when mitochondrial stress occurred, indicating that JNK does not regulate apoptosis induced by proteasomal dysfunction. Furthermore, data from the *PARKIN* overexpressing cells suggests that Parkin activity can limit the apoptotic activity of JNK under higher levels of stress.

5.3.12 Mitochondrial clustering in differentiated cells

Mitochondria inherently produce ROS and upon uncoupling excessive oxidative stress occurs (Figure 3.3). Thus, to ensure cellular homeostasis, damaged or

ageing mitochondria must be removed via quality control pathways. The PINK1-Parkin mitophagic pathway is critical in clearing damaged and senescent mitochondria by a specific, regulated form of autophagic degradation (Narendra et al., 2008, Narendra et al., 2010b). Extensive data generated in cell lines or non-neuronal primary cells has previously demonstrated that upon depolarisation, mitochondria undergo fragmentation and perinuclear clustering as part of the initial stages of mitophagy (Narendra et al., 2010a, Okatsu et al., 2010, Vives-Bauza et al., 2010, Shi et al., 2015).

The occurrence of clustering around the perinuclear region in neurons has been extensively debated, as a large proportion of neuronal mitochondria reside within axons, dendrites and at synapses, far from the soma. When considered in this context, it would appear counterintuitive to transport a damaged mitochondrion, or group of mitochondria, exuding high levels of ROS along an axon in order to be degraded in the soma. The suggestion that axonal lysosomes and autophagosomes are present in neurons (Lee et al., 2011b, Lee et al., 2011a, Maday et al., 2012) would therefore represent a logical observation. A recent study demonstrated that inducing damage in a small subset of hippocampal axonal mitochondria led to the rapid and local recruitment of Parkin and other mitophagic machinery (Ashrafi et al., 2014). Furthermore, inducing damage in a handful of mitochondria is likely to be more representative of physiological levels of mitochondrial dysfunction experienced in PD compared to the global uncoupling induced by compounds such as CCCP. Ashrafi et al., show that upon induction of damage, multiple axonal mitochondria colocalise within autophagosomes, suggesting that localised clustering had occurred. These data suggest that mitochondrial clustering after damage to these organelles is an early and representative occurrence of the neuronal stress response.

From this, the question can be asked: which pathways can prevent or promote mitochondrial clustering upon CCCP treatment in differentiated SH-SY5Y cells? The implication of determining pathways or processes that modulate mitochondrial clustering is that this could elucidate new therapeutic targets to rectify a faulty or overrun mitophagic response in PD neurons. In order to

investigate this, differentiated WT SH-SY5Y cells were treated with JNK, ERK or proteasomal inhibitors (or a combination) prior to mitochondrial uncoupling (Figure 5.21 and Appendix K). To calculate the rate of mitochondrial clustering, an algorithm on Columbus software was designed to count mitochondrial 'spots' in relation to nuclei (Appendix G). This allowed mitochondrial clusters per cell to be quantified. Results obtained from this were similar to counts by eye (Appendix L).

Importantly, mitochondrial uncoupling induced a significant increase in the number of mitochondrial clusters (Figure 5.21) for both 5μM and 30μM CCCP after just 3 hours (****$p < 0.001$ and **$p = 00023$, respectively). Proteasomal function is critical for mitophagy (Chan et al., 2011). It was therefore reasoned that proteasomal inhibition, which is known to inhibit mitophagy, would significantly perturb mitochondrial clustering and thus provide a valid control. UPS inhibition significantly reduced cellular capacity to form mitochondrial aggregates post-uncoupling (***$p = 0.0008$), although an increase in mitochondrial clustering relative to non-CCCP exposed cells was still observed (**$p = 0.0031$). These data indicate that this assay has the capacity to provide a functional readout of the initial stages of mitophagy.

Interestingly, JNK inhibition significantly reduced mitochondrial clustering in epoxomicin-treated cells at the highest level of mitochondrial uncoupling (**$p = 0.0072$). This could suggest that the JNK pathway is involved in regulating mitophagy in UPS-deficient cells. However, as this did not occur after 5μM CCCP exposure with UPS and JNK inhibition, this pathway may only be activated under higher levels of mitochondrial damage.

Although proteasomal inhibition antagonised mitochondrial clustering, no significant effect was found from the inhibition of either JNK or ERK signalling alone (Figure 5.21). Furthermore, both MAPK inhibitors failed to restore clustering in cells that were UPS deficient, although inhibition of JNK in these cells did reduce 30μM CCCP-induced clustering. These data would suggest that neither JNK nor ERK signalling functions to regulate this early step in the

mitophagic pathway in healthy neurons. However, the JNK pathway may play a role upon proteasomal inhibition.

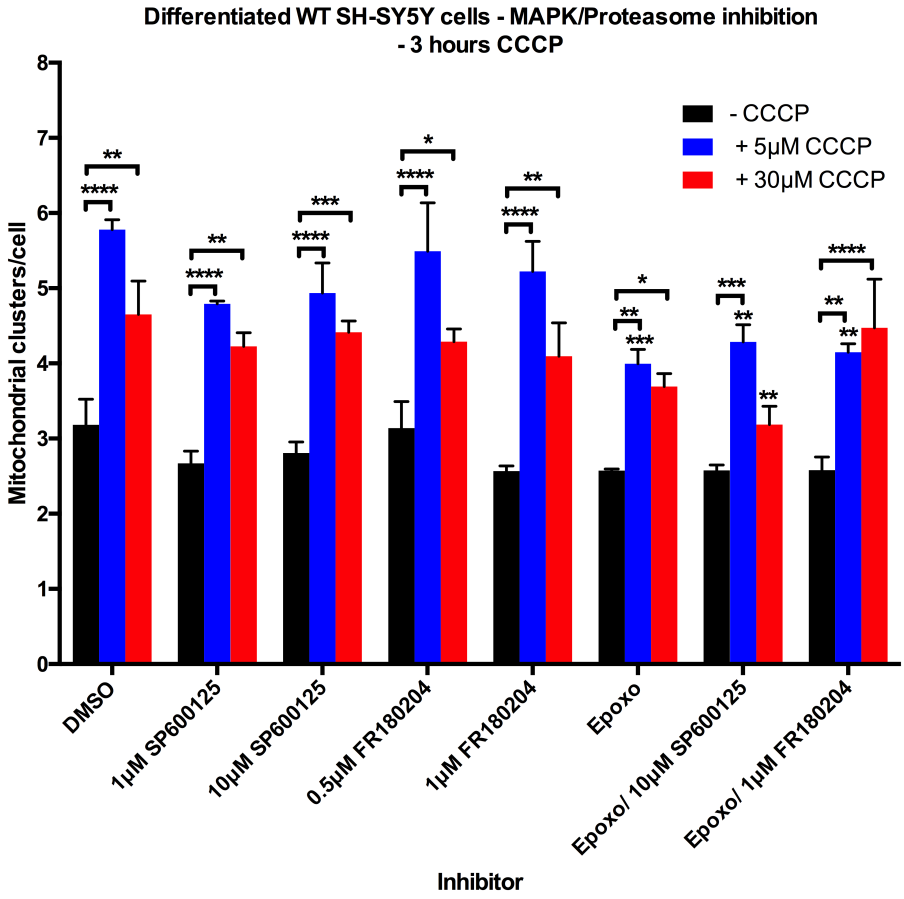

Figure 5.21: Mitochondrial clustering 3 hours post-CCCP in differentiated WT SH-SY5Y cells is perturbed by proteasomal inhibition but not MAPK inhibition. Cells were differentiated in 96-well Operetta plates, then treated with SP600125 (JNK inhibitor), FR180204 (ERK inhibitor) and/or 100nM epoxomicin (proteasomal inhibitor) prior to CCCP exposure. Images were then captured using the Operetta and analysed using Columbus software to calculate the mitochondrial clusters/cell in individual wells. Three fully independent biological replicates were performed on separate occasions in which cells were seeded, differentiated, treated and analysed for each experiment (n=3). Statistically significance compared to the DMSO control was ascertained by 2way ANOVA (*$p < 0.05$, **$p < 0.01$, ***$p < 0.005$, ****$p < 0.001$). Error bars represent SEM calculated from the mean of each individual experiment.

5.3.13 Parkin activity and the regulation of c-Jun

By comparing c-Jun protein levels post-uncoupling in the WT and *PARKIN* overexpressing SH-SY5Y cell lines (Figures 4.1. and 4.2) it appeared that higher Parkin levels induced a greater increase in c-Jun levels. c-Jun has been

previously shown to bind to the *PARKIN* promoter in order to repress expression (Bouman et al., 2011). To investigate this link further and to determine whether increased c-Jun levels during mitochondrial uncoupling was unique to SH-SY5Y cells, previously characterised HEK293 cell lines inducibly over-expressing different Parkin mutants (Morrison et al., 2011) were utilised. By using cells expressing different mutants, some of which were non-functional PD-associated mutations, it was possible to assess if c-Jun modulation was dependent on Parkin E3 ligase activity. Details of each individual Parkin mutant are extensively summarised and evaluated in the Discussion section of this thesis (Section 6.1.4 and Table 6.1) along with the results presented here.

HEK293 cell lines expressing the different Parkin mutants were set up, with 4 different conditions per line to be assessed (Figure 5.23). Compared to untransfected TREx HEK293 cells, induction of WT Parkin and subsequent uncoupling resulted in a significant increase in c-Jun levels (*p = 0.0205). This concurs with data from the SH-SY5Y cell lines (Figures 4.1 and 4.2) in which *PARKIN* overexpression upregulated the c-Jun response to uncoupling.

Induction of any Parkin construct without uncoupling did not result in any significant difference in c-Jun levels (Figure 5.22). R42C was the only cell line to show a significant difference in c-Jun levels relative to WT cells after CCCP treatment (**p = 0.0091), but this was without the induction of the Parkin construct. This mutation, previously identified in cancer (Veeriah et al., 2010), has more recently been identified in EOPD patients (Hussain et al., 2014). It is currently unknown if this Parkin mutant retains E3 ligase activity, although its overexpression in HEK293 cells does not increase mitochondrial degradation after uncoupling (Roper, 2015), suggesting it has no mitophagic activity. Induction of the R42C construct prior to uncoupling significantly decreased c-Jun protein levels relative to WT Parkin (****p < 0.0001). The fact uncoupling resulted in a reduction in c-Jun levels both with and without induction of the Parkin^{R42P} construct suggests that expression was ‘leaky’ and occurred to some degree prior to induction. Nevertheless, it is clear this mutation in Parkin either represses c-Jun expression or promotes its degradation upon mitochondrial depolarisation.

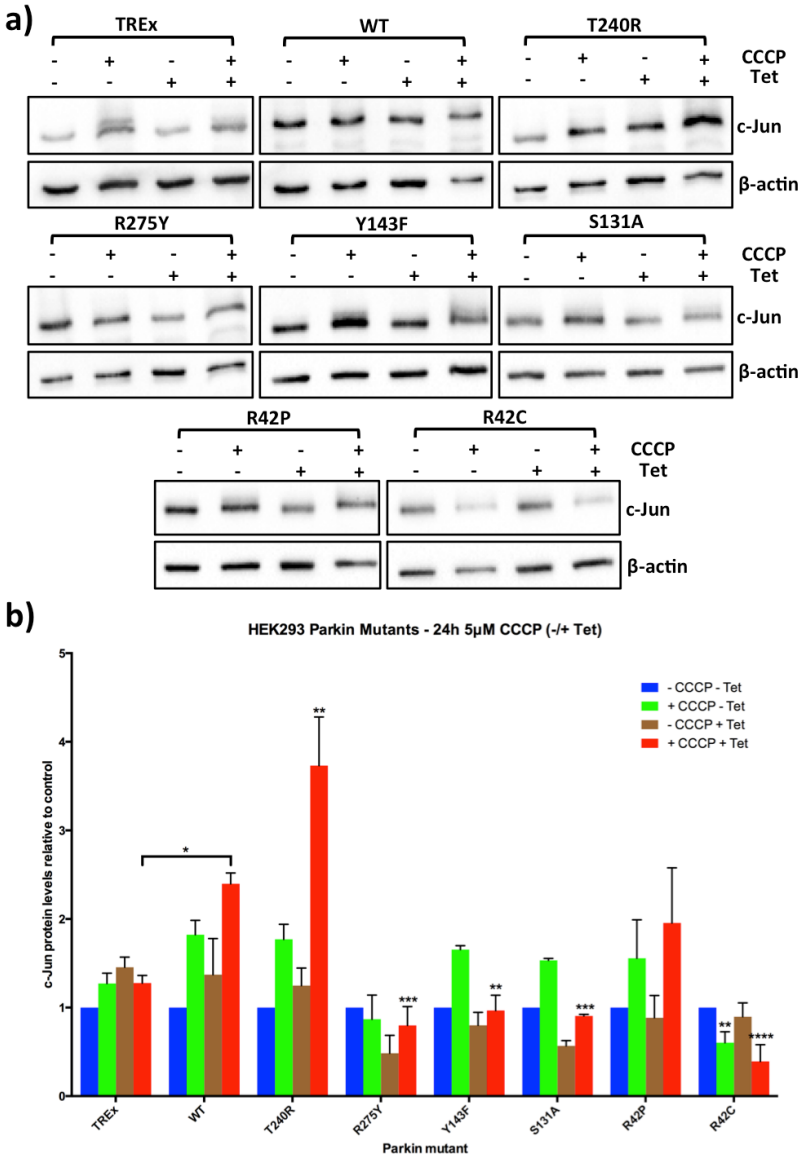

Figure 5.22: Parkin activity modulates the c-Jun response to mitochondrial stress. HEK293 cells inducibly overexpressing different Parkin mutants were treated with 5μM CCCP (or DMSO) for 24 hours and c-Jun levels measured by western blotting. Expression of constructs was induced using tetracycline 24 hours prior to uncoupling. Two independent biological replicates were performed where cells were seeded, construct expression induced then cells were treated, protein extracted and western blot analysis and quantification performed per individual replicate (n=2). (a) Representative western blots for each Parkin mutant. (b) Quantitative analysis from blots derived from densitometry of c-Jun and β–actin bands to obtain a ratio of protein levels. c-Jun levels for different Parkin mutants, as well as the parental HEK 293 TREx cell line not transfected with any Parkin construct, were compared to the WT cell line for each separate condition unless otherwise stated (horizontal bar comparing WT to TREx cell lines after combined tetracycline and CCCP treatment). Statistically

significance was ascertained by 2way ANOVA comparing WT values with mutants (*p < 0.05, **p < 0.01, ***p < 0.005, ****p < 0.001). Error bars represent SEM.

Upon mitochondrial uncoupling, the expression of the E3 ligase-deficient T240R Parkin mutant resulted in significantly increased c-Jun levels compared to the WT control (**p = 0.0034) (Figure 5.23). Interestingly, overexpression of R275Y and R42C, both of which are also E3 ligase-deficient, resulted in the repression of c-Jun levels after mitochondrial damage (***p = 0.0003 and ****p < 0.0001), respectively). Furthermore, the S131A and Y143F mutants also caused a decrease in c-Jun levels 24 hours post-uncoupling compared to the cells expressing WT Parkin (***p = 0.0008 and **p = 0.0014, respectively), despite both possessing a fully functional E3 ligase activity. Interestingly, the expression of the R42P Parkin mutant, which maintains functional activity, albeit at a lower level, did not significantly alter c-Jun levels after uncoupling compared to cells expressing WT Parkin. This would therefore indicate that the T240R mutant functions to somehow exacerbate c-Jun expression, or at least increase its stability, under mitochondrial stress.

5.3.14 BIM and Rab8a in the c-Jun-regulated response to mitochondrial depolarisation

The data presented thus far has focused on c-Jun and its regulation, demonstrating how c-Jun is modulated in response to mitochondrial damage in SH-SY5Y and HEK293 cells. However, very little is known about the genes regulated by c-Jun in response to mitochondrial and oxidative stress in neurons. One aspect that has been explored here was to assess the repressive nature of c-Jun on *PARKIN* expression (Figure 5.6). Although intended to determine if blocking c-Jun degradation prevents *PARKIN* upregulation, this data did confirm that c-Jun siRNA results in an increase in *PARKIN* expression. This supports the data previously put forward that c-Jun blocks ATF4-mediated expression of the *PARKIN* gene (Bouman et al., 2011).

In order to begin to investigate the direct downstream consequences of c-Jun activity, the relative expression of *BIM* and *RAB8A* in undifferentiated WT SH-SY5Y cells in response to 5μM CCCP was determined at mRNA level. BIM is

upregulated in response to oxidative stress in neurons by the JNK/c-Jun pathway (Jin et al., 2006) and is critical for neuronal apoptosis (Putcha et al., 2001). ER-stressors that initiate the UPR, such as tunicamycin, induce a BIM-dependent response in MEFs (Renault et al., 2015). Here BIM isoforms accumulated on the MOM of ER-stressed MEFs, which was critical for cytochrome *c* release mediated by BAX, an apoptotic protein activated by BIM. Together, data from these studies suggest that *BIM* could provide a useful readout of apoptotic activity induced by the function of c-Jun.

Analysis of mRNA levels revealed that mitochondrial uncoupling led to a rapid increase in *BIM* expression (Figure 5.23). These levels remained generally elevated compared to basal levels, although expression did return to these levels 12 hours after uncoupling in the first experiment before becoming elvevated again by the 24 hour time point.

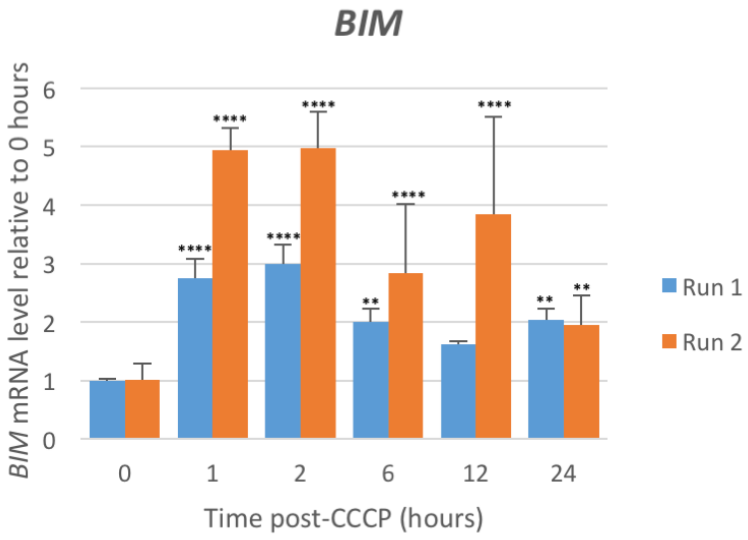

Figure 5.23: *BIM* mRNA expression is modulated in response to mitochondrial stress in undifferentiated WT SH-SY5Y cells. *BIM* mRNA levels were assessed relative to *β–ACTIN* expression (housekeeping gene) by qPCR from cDNA obtained from SH-SY5Y cells treated with 5μM CCCP. Expression was assessed in duplicate per experiment and results are from two fully independent experiments (n=2). For each individual biological replicate, cells were seeded, treated, RNA extracted and the mRNA levels quantified. Statistical significance of relative changes in expression was assessed using a 2way ANOVA (Dunnett's) (*p < 0.05, **p < 0.01, ****p < 0.001). Error bars represent SD.

As the expression of *BIM* has been shown to be regulated by c-Jun activity under stress conditions in neurons, the modulation of both was compared (Figure 5.24). The expression of *BIM* does show similar modulation to the phosphorylation of c-Jun at Ser63, which may suggest that this transient phosphorylation is enough to boost *BIM* mRNA after uncoupling.

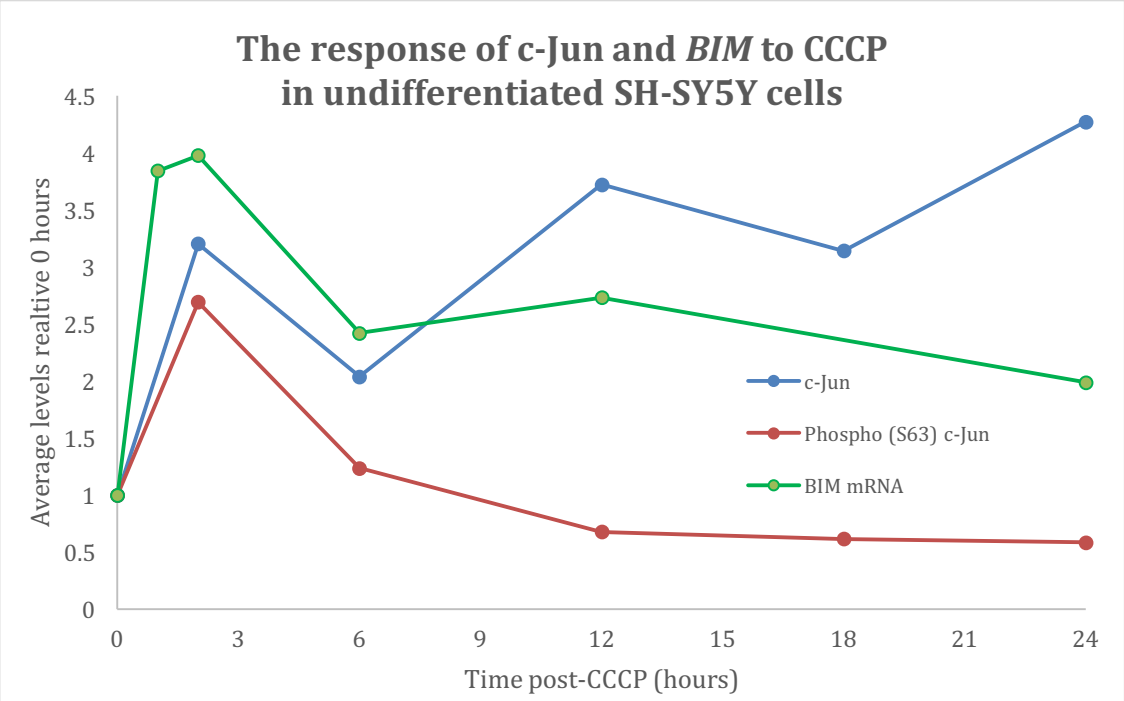

Figure 5.24: The modulation of *BIM* expression mimics that of c-Jun S63 phosphorylation in response to 5μM CCCP in undifferentiated SH-SY5Y cells. This graph combines data shown for total c-Jun protein levels (blue; Figure 4.2), S63 phosphorylation of c-Jun (red; Figure 5.4) and BIM mRNA levels (mean of both replicates) (green; Figure 5.23). For simplicity, only average values are shown to highlight the trend.

To observe the response of another potential c-Jun target gene, *RAB8A* was assessed in the same manner as *BIM* above. Rab GTPases are critical regulators in a number of membrane trafficking pathways (Seabra and Wasmeier, 2004). Specifically, Rab8a has been shown to localise to endosomes (Ang et al., 2003, Rowe et al., 2008, Kanerva et al., 2013), where it is a key component of endosomal recycling of lipids to the plasma membrane (Kanerva et al., 2013). A recent study in *Drosophila* identified *rab8* mutations as pathogenic in an FTD screen, with mutants showing endosomal dysfunction

and synaptic overgrowth associated with aberrant JNK/AP-1 signalling (West et al., 2015). As ROS-driven overgrowth at the neuromuscular junction also occurs via JNK/AP-1 signalling (Milton et al., 2011), the functional role of Rab8a may be regulated in neurons under the mitochondrial and oxidative stress induced upon mitochondrial uncoupling by c-Jun activity. Furthermore, the *RAB8A* promoter contains 16 TRE, or AP-1 binding sites, or 6 c-Jun binding sites whereas *RAB8B* does not (GeneCards, 2016) making it possible for AP-1 signalling to regulate its expression. However, to date no data has been presented to conclusively demonstrate this.

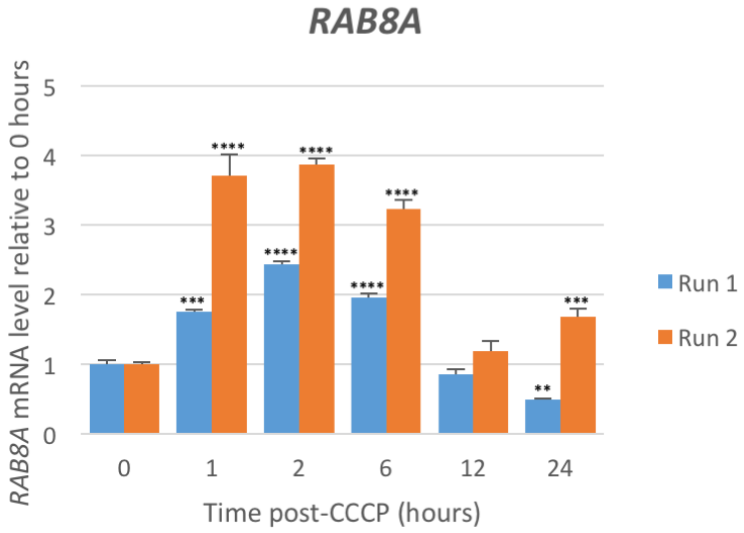

Figure 5.25: *RAB8A* mRNA expression is initially upregulated in response to 5μM CCCP in SH-SY5Y cells. Levels peak 2 hours after CCCP challenge and progressively diminish up until the 24 hour time point. *RAB8A* mRNA levels were assessed relative to *β–ACTIN* expression (housekeeping gene) by qPCR from cDNA obtained from SH-SY5Y cells treated with 5μM CCCP. Expression was assessed in duplicate per experiment and results are from two fully independent experiments (n=2). For each individual biological replicate, cells were seeded, treated, RNA extracted and the mRNA levels quantified. Statistical significance of relative changes in expression was assessed using a 2way ANOVA (Dunnett's) (**p < 0.01, ***p < 0.005, ****p < 0.001). Error bars represent SD.

The mRNA levels of *RAB8A* peak at around 1-6 hours post-uncoupling treatment in undifferentiated SH-SY5Y cells (Figure 5.25). By 12 hours, mRNA had returned to normal. However, a difference between the 2 biological replicates was observed at the 24 hour time point in which the first and second

experiments show a reduction or elevation, respectively, relative to basal levels. The initial upsurge in expression followed by a decrease could suggest that Rab8a plays a role in the initial response to mitochondrial damage but not the late stage response. What is also apparent is that *RAB8A* mRNA levels follow the levels of Ser63 phosphorylated c-Jun in the cell after CCCP challenge (Figure 5.26). As previously stated, the *RAB8A* promoter region contains AP-1 binding sites, which in turn may allow c-Jun-dependent regulation of this gene under mitochondrial stress.

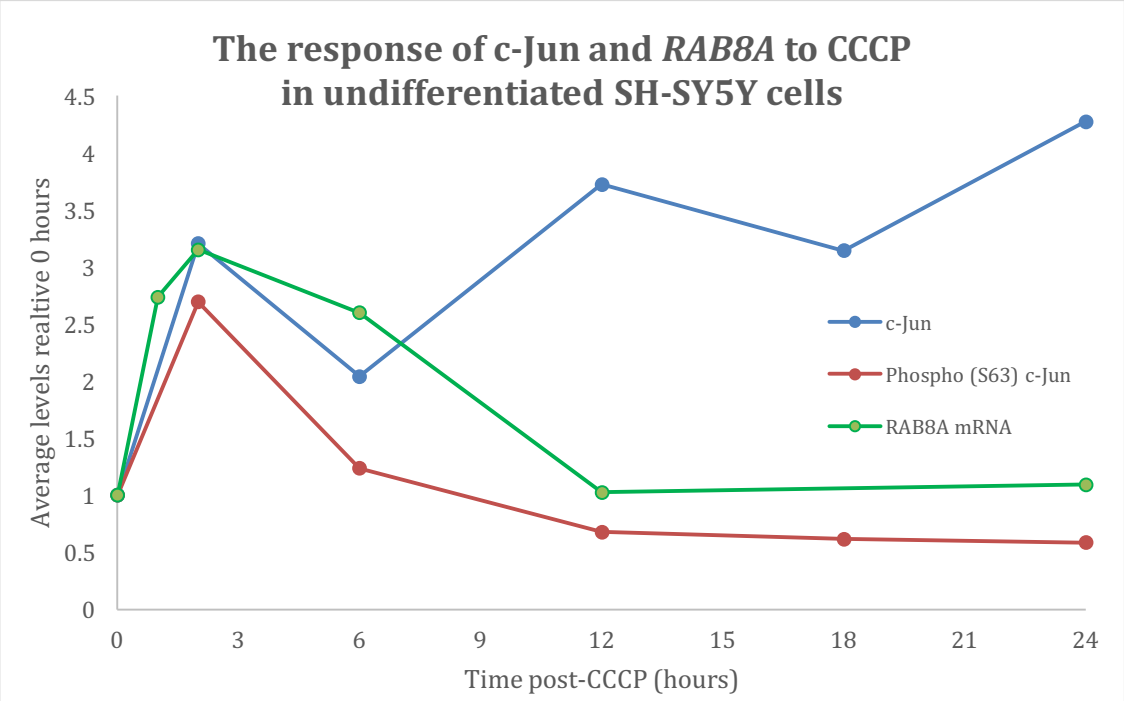

Figure 5.26: Modulation of *RAB8A* expression closely mimics that of c-Jun S63 phosphorylation in response to 5μM CCCP in undifferentiated SH-SY5Y cells. This graph combines data shown for total c-Jun protein levels (blue; Figure 4.2), S63 phosphorylation of c-Jun (red; Figure 5.4) and BIM mRNA levels (mean of both replicates) (green; Figure 5.25). For simplicity, only average values are shown to highlight the trend.

5.4 CONCLUSIONS

Data shown in Chapter 4 of this thesis indicated that c-Jun was a good candidate to study in the neuronal response to mitochondrial damage and oxidative stress. c-Jun siRNA in Chapters 4 and 5 show opposing effects on apoptosis, depending on the level of stress. Normalisation of c-Jun siRNA

treated groups still showed these opposing effects to occur. Despite this, knockdown of c-Jun was not demonstrated and thus it cannot be concluded as to whether these effects were due to loss of c-Jun.

In terms of c-Jun modulation, its phosphorylation may stabilise it against proteasomal turnover, with Parkin activity appearing to prolong this phosphorylation in SH-SY5Y cells. An intricate system linking mitophagy and c-Jun-regulated neuronal fate decisions therefore appears to exist. Unfortunately, efforts to assess if rapid c-Jun degradation was required for the initial upregulation of *PARKIN* in response to mitochondrial challenge were not successful. However, the data did concur with the previous hypothesis that c-Jun represses *PARKIN* expression.

The transactivation potential of c-Jun is largely regulated by its post-translational modification by upstream MAPKs, thus it was important to investigate this. Data obtained from undifferentiated SH-SY5Y cells showed that both ERK and JNK have the capacity to differentially mediate c-Jun phosphorylation (and expression) after mitochondrial uncoupling. How c-Jun is regulated and by which MAPK appears to be highly dependent on the level of mitochondrial stress exhibited. ERK, to some extent, showed pro-apoptotic potential in undifferentiated cells under conditions of high mitochondrial uncoupling, whereas JNK did not. When ERK-inhibitor groups were normalised to account for inhibitor-only effects, a slight rescue in cell death was observed at a higher level of uncoupling. Conversely, in differentiated SH-SY5Ys JNK was the main neuronal death regulator. However, this pro-apoptotic activity was not exhibited until a higher level of mitochondrial damage was induced. Clearly, the use of 30μM CCCP is unlikely to represent the physiological cellular stress occurring in PD patient brains, though it may mimic the Parkinsonisms induced by exposure to toxins. As many model systems in the past relied on similarly exaggerated forms of stress to mimic Parkinson's, this may explain why compounds such as CEP-1347, an inhibitor of the JNK pathway, failed to delay PD progression in patients during clinical trials (even resulting in increased disease progression at certain doses, although this was not deemed statistically

significant) (Parkinson Study Group, 2007), despite so much promise demonstrated in animal and cell models. From the results presented here, one might conclude that although JNK inhibition is not a viable therapeutic target for most forms of PD, it might represent a useful first-line response for individuals exposed to chemicals known to cause Parkinsonism. In the context of the cell system used here, given the differential cellular responses observed it seems reasonable to propose that exposure to 5μM and 30μM CCCP represent useful models of chronic and acute mitochondrial stresses respectively.

JNK inhibition also appeared to rescue mitochondrial uncoupling-induced apoptosis in differentiated SH-SY5Ys also undergoing proteasomal dysfunction. As JNK inhibition partially rescued cell death under mitochondrial stress in UPS-inhibited cells, to a point in which greater cell survival occurred compared to cells with only UPS deficiency, it would appear that JNK-regulated apoptosis is the dominant cell death pathway over that initiated by proteasomal dysfunction. However, *PARKIN* overexpression may limit the role of JNK in response to mitochondrial challenge, most likely due to the induction of excessive mitophagy and thus alternate death pathways. Although JNK plays a role in apoptosis here it, along with ERK, does not appear to play any role in mitochondrial clustering, an early stage in the mitophagic response. Nevertheless, inhibition of the proteasome does perturb the efficiency of mitochondrial clustering under stress, in agreement with the previously presented idea that UPS function is critical to mitophagy (Chan et al., 2011, Morrison et al., 2011).

Another point of interest examined was the link between Parkin activity and that of c-Jun, as data presented in Chapter 4 showed that the overexpression of *PARKIN* in SH-SY5Y cells resulted in an increased c-Jun response to mitochondrial depolarisation. HEK293 cells express very little endogenous Parkin, making them an ideal, albeit non-neuronal, model to dissect Parkin function by the expression of *PARKIN* constructs. Using HEK293 cells inducibly overexpressing different Parkin mutants exposed to CCCP, it was observed that WT Parkin overexpression does increase c-Jun levels in response to mitochondrial stress. However, all mutations decreased the c-Jun response to

this stress, except the PD-associated T240R mutant that significantly increased c-Jun protein levels by 24 hours post-uncoupling treatment. The T240R mutation in the RING1 domain of Parkin renders the E3 ligase unable to translocate to the MOM in response to mitochondrial damage. This could suggest that the translocation of Parkin to damaged mitochondria plays a role in dampening down the c-Jun response to mitochondrial stress.

Although the expression of *BIM* and *RAB8A* closely follow c-Jun phosphorylation, it is unclear from data presented here whether they are actually part of the response mediated by c-Jun. Previous data presented on these genes suggest that they may play a role in the c-Jun response to mitochondrial or oxidative stress in neurons. However, the use of siRNA and chromatin immunoprecipitation with sequencing (ChIP-seq) would be useful tools in determining whether c-Jun regulates expression of these genes under these conditions. If this proved to be the case it would then be critical to dissect the functions of the BIM and particularly the RAB8A proteins in the response to PD-related stress.

Overall, data presented in this chapter suggests that MAPK/c-Jun signalling plays a role in the adaptive and apoptotic responses to both chronic and acute mitochondrial and oxidative stress in neuronal (and non-neuronal in the case of HEK293s) cells. Unfortunately, the lack of statistical power of many experiments, due to a low number of biological replicates performed, means that it is not possible to conclusively state that these findings are real. It is also apparent that undifferentiated and differentiated cells present two distinctly separate model systems. This is perhaps unsurprising since neurons are more metabolically active than other cell types while simultaneously being unable to replenish their numbers if cells are lost to oxidative damage. One might therefore expect them to possess more highly developed and specialized responses to oxidative stress, including a more effective adaptive response, than cycling cells. Whilst differentiated SH-SY5Y cells will more closely represent neuronal cells, the undifferentiated lines may provide a useful tool to compliment data obtained from differentiated SH-SY5Ys due to their greater tolerance to mitochondrial uncoupling, thus allowing some of the subtler

aspects of the cellular stress response to be determined. What does seem to be clear is that the adaptive and apoptotic response share considerable crossover, making the inhibition of apoptotic pathways a difficult therapeutic target that may lack the subtlety required for effective use in PD patients.

CHAPTER 6
DISCUSSION

6.1 DISCUSSION

Parkinson's is a condition characterised by the loss of dopaminergic neurons in the SNpc. Here, the aim was to determine how AP-1 transcription factors are modulated in response to mitochondrial dysfunction, a prominent characteristic of PD, and how this modulation relates to the cellular stress response. The major model system used here was the SH-SY5Y neuroblastoma cell line, a widely used cell line for studying Parkinson's (Xie et al., 2010). A recent systems genomic evaluation of the SH-SY5Y cell line found consistency between DNA, RNA and protein levels and found that at least 1 intact copy of all PD-related genes evaluated was present (Krishna et al., 2014). Interestingly, this approach also ranked SH-SY5Ys as appropriate for ALS, HD and, to a lesser extent, AD.

Neurons differ from many other cell types as they are not mitotically active. Moreover, they are energetically demanding compared to other cells and have extensive mitochondrial networks, which function to supply the unusual energy demands of neuronal activity. Simply put, it is critical that neuronal adaptive responses to stress are highly attuned, as a neuron cannot be replaced. It would therefore seem paradoxical that Nrf2, a critical regulator in the antioxidant responses (Ma, 2013), is epigenetically repressed in neuronal cells (Bell et al., 2015). However, this repression was necessary in order to allow proper ROS-driven neuronal development. It must therefore be appreciated that oxidative stress plays a role in both neuronal development and neurodegeneration, thus the responses to it are likely to be diverse, sensitive and interlinked. The absence of an Nrf2-response in neurons, despite being partially provided by surrounding astrocytes (Shih et al., 2003), must therefore be covered, at least to a certain degree, by other pathways. Some Nrf2 target genes, such as *Srxn1* encoding the antioxidant reductase Sulfiredoxin, can be induced in neurons by AP-1 activity (Papadia et al., 2008), although it is unclear which specific dimeric complex is involved. Neurons experience significant ROS production intermittently as part of their normal function and thus have a higher baseline of stress. They may therefore have unique and powerful antioxidant defences in order to maintain normal function. Yet the fact they cannot be replaced may

make them appear more sensitive to stress. Together, this highlights the inherent difficulty in dissecting the neuronal response to oxidative stress and may go some way to explaining the apparent sensitivity of neurons to ROS accumulation.

6.1.1 SH-SY5Y cells, Parkin and mitochondrial dysfunction

Parkin plays a critical role in maintaining mitochondrial homeostasis through the process of mitophagy (Narendra et al., 2008, Vives-Bauza et al., 2010). It is therefore generally considered a cytoprotective protein. However, data presented here suggests that the overexpression of Parkin increases cellular sensitivity to mitochondrial depolarisation (Figure 3.4). Undifferentiated SH-SY5Y cells overexpressing *PARKIN* were significantly more sensitive to mitochondrial uncoupling. This may be due to increased mitophagic activity leading to increased loss of the mitochondrial network, essentially meaning cell death is due to excessive autophagy.

In conjunction with this, a recent study found that Parkin activation can lead to either mitophagy or apoptosis (Carroll et al., 2014). *PARKIN* overexpression greatly sensitised cells towards apoptosis by mitochondrial depolarisation. Upon mitochondrial uncoupling, Mcl-1, a Bcl-2 family protein, underwent PINK1/Parkin-dependent ubiquitination and degradation. In turn, this pushed the cell into apoptosis via the opening of the Bax/Bak channel. These data suggest that Parkin has the capacity to act cytoprotectively in neurons by maintaining the integrity of the mitochondrial network through mitophagy, but upon excessive damage apoptosis is initiated via Parkin-dependent mechanisms. However, this appears to be specific to mitochondrial depolarisation. Interestingly, Carroll et al. (2014) found that siRNA knockdown of endogenous Parkin in SH-SY5Y cells reduced apoptosis induced by 20μM CCCP. Conversely, this thesis shows that knockdown of Parkin in this cell line did not alter towards 5μM CCCP-induced apoptosis (Figure 4.18), indicating the level of uncoupling is critical in determining what role Parkin plays (Figure 6.1). This concurs with the hypothesis proposed by these authors that Parkin-dependent apoptosis is only initiated upon greater levels of mitochondrial

stress. The fact that greater sensitivity to CCCP in *PARKIN* overexpressing SH-SY5Ys was observed, something previously demonstrated by this lab in HEK293 cells (Morrison et al., 2011), suggests that overexpression lowers the threshold by which Parkin can act as a molecular switch towards apoptosis. Since the amount of Parkin available seems to be the rate-limiting factor in this process, one possibility is that the switch from mitophagy to apoptosis may simply depend on the level of Parkin activity in the stressed cell, consistent with a situation where an increase in the number of defective mitochondria in a cell directly correlates with the likelihood that the cell will commit to apoptosis.

Previous data indicates Parkin sensitises cells specifically to mitochondrial damage as both CCCP and valinomycin (which disrupts mitochondrial membrane potential)-induced apoptosis was increased in undifferentiated SH-SY5Ys and HEK293s overexpressing Parkin, whereas no effect was seen for cisplatin (induces DNA damage) treatment (Carroll et al., 2014). Supporting this, SH-SY5Y cells overexpressing Parkin used here show no increased sensitivity towards either H_2O_2 or rotenone (Figure 3.4). On the other hand, rotenone induces apoptosis by inhibiting complex I and increasing mitochondrial ROS production (Li et al., 2003). As rotenone induces mitochondrial damage, but *PARKIN* overexpression did not increase apoptosis caused by rotenone, this indicates the dysfunction of mitochondria alone is not enough to initiate Parkin-mediated apoptosis and that this pathway is specific to mitochondrial uncoupling.

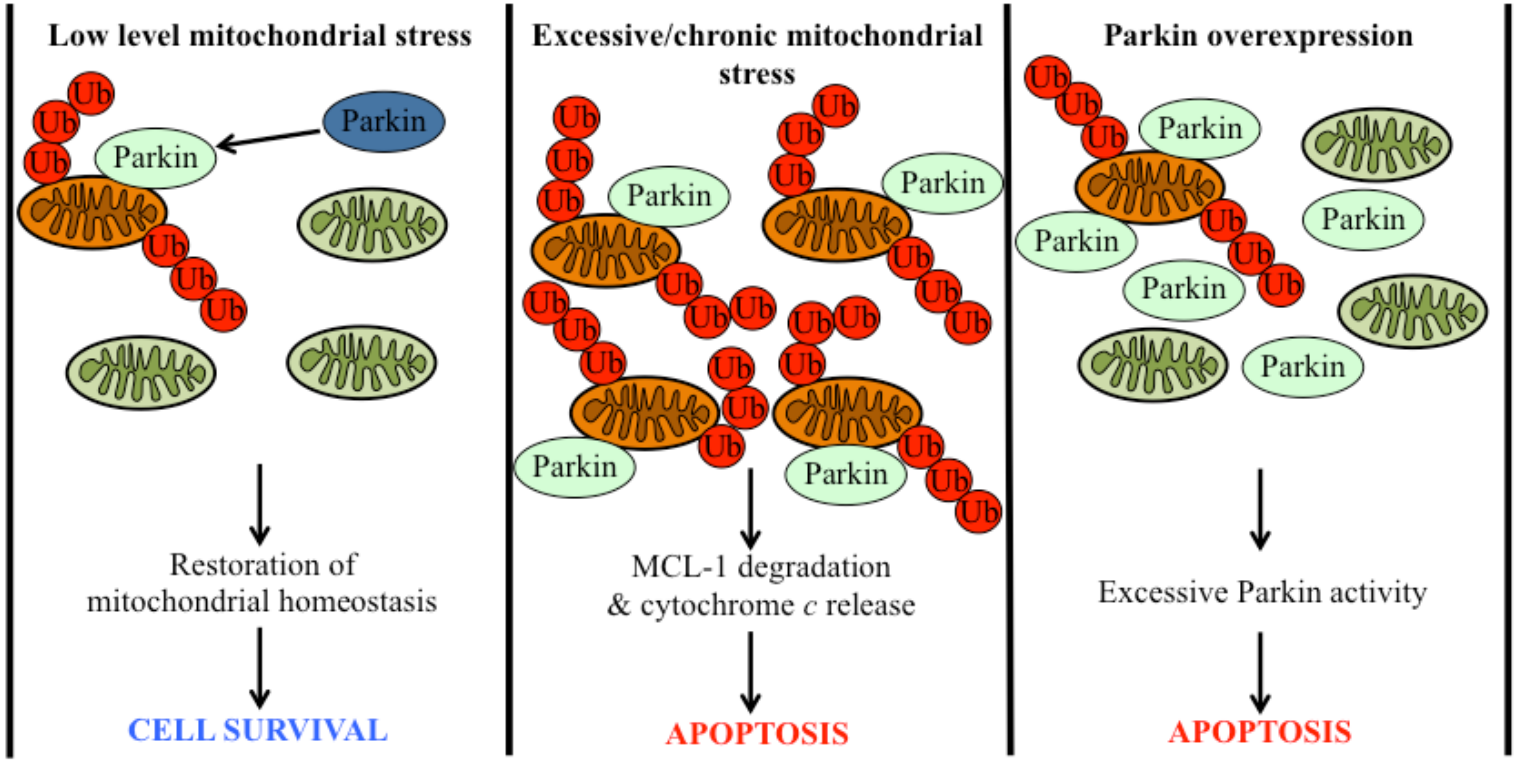

Figure 6.1: Parkin acts as a 'molecular switch' in determining the route taken by the cell in response to mitochondrial depolarisation. Inactive Parkin (blue) is activated (green) and recruited by PINK1 accumulated on the outer membrane of uncoupled mitochondria (orange), which in turn are polyubiquitinated and degraded. Carroll et al., (2014) showed that excessive mitochondrial damage leads to Parkin-dependent degradation of MCL-1, therefore preventing its inhibition of BAX recruitment to mitochondria. Thus, the opening of the BAX/BAK channel and subsequent cytochrome *c* release occurs. Increased sensitivity in *PARKIN* overexpressing SH-SY5Ys may be due to the propensity of excessive levels of activated Parkin pushing the cell down this same apoptotic pathway.

These data suggest Parkin has the capacity to determine cellular fate depending on both the level and the type of stress and Parkin levels. If neurons containing mutated Parkin were more susceptible to stress, would this be due to a decrease in Parkin's cytoprotective abilities or because the initiation of apoptotic pathways was affected? In the latter case, both possibilities are feasible; mutants that abrogate the induction of apoptosis could allow excessive damage to occur in response to uncontrolled ROS, leading to cell death by other pathways and possibly damage to neighbouring neurons. Conversely, mutants that enhanced apoptotic commitment could drive cell loss in response to inappropriately low levels of ROS that would normally be accommodated by the neuron. Defining which of these possibilities is true would be critical in considering therapeutics for PD, since choosing the wrong intervention could accelerate the progression of the disease.

Additionally, *PARKIN* overexpression also led to sensitisation towards differentiation in SH-SY5Y cells (Figure 3.2b). Initially, the aim was to assess 3 different 7-day protocols for the differentiation of WT and *PARKIN* overexpressing SH-SY5Y cell lines based around protocols previously described (Presgraves et al., 2004a, Mastroeni et al., 2009, Pennington et al., 2010, Encinas et al., 2000). The RA/BDNF method resulted in cells with the greatest neuronal outgrowth when assessed by eye (Figure 3.2a) and so was chosen to continue these studies. Moreover, differentiation by sequential treatment with RA and the neurotrophin BDNF has been previously shown to induce dopaminergic characteristics, such as DAT activity, in SH-SY5Y cells (Mastroeni et al., 2009). The use of a neurite outgrowth kit could have been used, given more time, in order to quantify and confirm the differences in outgrowth between differentiation methods. The reason for the increased sensitivity of cells overexpressing Parkin to RA/BDNF differentiation is unclear here. Whilst it may be due to increased levels of intracellular Parkin, it may equally be due to the genomic location of the inserted expression vector. Due to time constraints it was not possible to fully assess this. Utilising the T-REx SH-SY5Y cells created here, which inducibly overexpress *PARKIN*, it may have been possible to confirm if elevated protein levels of Parkin induced susceptibility to RA/BDNF differentiation-associated apoptosis.

By using both undifferentiated and differentiated cells, it was hoped to gain a clear picture of AP-1 function in responses to stress associated with PD in an *in vitro* neuronal-like model. Multiple compounds have been utilised to induce Parkinson's-related stress in cell and animal models. This thesis largely focuses on mitochondrial and oxidative stress in SH-SY5Y cells. Using both undifferentiated and differentiated lines is advantageous as their differing sensitivity can allow for subtler manipulation of pathways, as well as the fact the mitotic activity of the undifferentiated form is required for siRNA knockdowns. Rotenone induces PD-like symptoms in rat via the degeneration of neurons in the SNpc (Betarbet et al., 2000, Sherer et al., 2003) and apoptosis in SH-SY5Y cells mediated by JNK and p38 (Newhouse et al., 2004). The dopaminergic cell neurotoxin 6-OHDA induces cytotoxicity by generating ROS such as H_2O_2 (Galindo et al., 2003), DRP1-dependent mitochondrial fragmentation (Gomez-Lazaro et al., 2008) and autophagosomal formation (Solesio et al., 2012) in SH-SY5Ys. Furthermore, it is the ROS generated by 6-OHDA, and not the neurotoxin directly, that act as autophagic mediators (Solesio et al., 2012). Consequently, these data may suggest that SH-SY5Y cells provide an appropriate PD model to study the molecular basis behind oxidative stress-induced apoptosis, which is inherently linked to mitochondrial dysfunction.

Despite being a highly utilised cell model, many aspects of SH-SY5Ys have yet to be fully elucidated. The uncoupling of the mitochondrial network by the protonophore CCCP has been demonstrated in multiple studies using this cell line, (Matsuda et al., 2010, Tanaka et al., 2010, Vives-Bauza et al., 2010, Van Humbeeck et al., 2011, Gomez-Sanchez et al., 2014) as well as others (Narendra et al., 2008, Geisler et al., 2010, Narendra et al., 2010a, Narendra et al., 2010b, Tanaka et al., 2010, Vives-Bauza et al., 2010, Morrison et al., 2011). However, to date no study has shown the induction of oxidative stress in SH-SY5Ys following CCCP treatment. Using CellROX® Green reagent here, CCCP efficiently induced oxidative stress (Figure 3.3b), peaking at 2 hours post-induction and returning to basal levels by 24 hours. Ser63 phosphorylated c-Jun levels also peak around 2 hours post-CCCP (Figures 5.4), with this being the only point at which a significant increase was observed over a 24 hour period of CCCP-induced stress. As c-Jun transactivation potential is increased by its

phosphorylation (Hess et al., 2004), this may indicate that c-Jun activity is proportional to the level of oxidative stress a cell is experiencing. Nevertheless, c-Jun is only one of a number of AP-1 transcription factors and will be discussed later in this chapter in greater detail.

6.1.2 The AP-1 response in SH-SY5Y cells

Prior to studying the modulation of the AP-1 transcription factors in response to stress, their expression was confirmed by qPCR (Figures 4.15 and 4.16) and the presence of protein in the cell was assessed by immunofluorescence (Figures 3.5 – 3.7) and western blotting (Figure 4.1 - 4.14).

Immunofluorescence showed that both c-Jun and c-Fos were largely localised in the nucleus, although some cytoplasmic staining was observed in all 4 SH-SY5Y lines (Figures 3.5 – 3.7). This is not a novel finding as both c-Fos and c-Jun have been reported to undergo nucleocytoplasmic shuttling (Malnou et al., 2007). Despite this, while c-Jun was clearly detectable by western blot analysis under normal conditions (Figures 4.1 and 4.2), c-Fos was not (Figures 4.7 and 4.8). However, TPA treatment of SH-SY5Y cells induced clearly detectable c-Fos protein levels by western blotting and qPCR analysis indicated that both *c-JUN* (Figure 4.15) and *c-FOS* (Figure 4.16) expression was significantly increased upon TPA addition.

c-Fos siRNA in undifferentiated WT SH-SY5Ys resulted in significant cell death, even without CCCP treatment (Figure 4.18). As basal expression (Figure 4.16) and protein levels (Figures 4.7 and 4.8) of c-Fos are very low (not detectable by western blotting), it is would be hard to say if c-Fos had any role under basal conditions. c-Fos expression is induced upon mitochondrial depolarisation in undifferentiated SH-SY5Y cells (Figures 4.7, 4.8 and 4.16). In extracts obtained from differentiated SH-SY5Y cells, no c-Fos protein was detected other than in TPA treated cells. If c-Fos induction does occur under these conditions in these cells it may occur after the 6-hour time point. This occurred in undifferentiated *PARKIN* overexpressing SH-SY5Y cells and so further investigation would be needed to determine if this is the case for the differentiated line.

Although immunofluorescence analysis of JunD showed this protein to be largely localised to the nucleus (but excluded from nucleoli), it also appeared to be present in the perinuclear region. This occurred in all 4 of the SH-SY5Y cell lines analysed. Therefore, it may be the case that JunD is situated in other organelles such as the Golgi apparatus. A role for JunD in the Golgi has not been shown yet.

JUND expression peaked 24 hours after mitochondrial uncoupling in undifferentiated SH-SY5Y cells, although it was significantly increased from just 1 hour post-uncoupling (Figure 4.15). However, it is unclear whether the progressive accumulation of mRNA shown here continues after this time point. JunD has previously been reported to dimerise with FosB and ΔFosB, forming long-term active neuronal AP-1 complexes in response to electroconvulsive seizures in mice, which may play a role in long-term adaptations and neuronal plasticity (Chen et al., 1995, Hiroi et al., 1998). Therefore, it could be suggested that JunD has a role in the long term response to stress, thus the progressive increase in its expression may continue after 24 hours-post CCCP treatment at which time its functional relevance may then come into play. Alternatively, it has been suggested that signalling pathways downstream of ROS may feed into neuronal plasticity, with ROS acting as a signalling proxy for high levels of neuronal activity (Milton et al., 2011, Bell et al., 2015). In this context, the observation that JunD expression increases in response to mitochondrial stress without contributing to the cellular responses maintaining homeostasis in response to such stress makes sense and is potentially interesting, since JunD may instead contribute to cellular adaptations aimed at modifying other aspects of neuronal function.

Interestingly, *PARKIN* overexpression appears to alter the JunD response in undifferentiated cells. In the Parkin overexpressing line JunD protein levels do not reach the significantly elevated values that is detected in WT cells 24 hours after CCCP challenge (Figure 4.6). Therefore, Parkin may dampen down or inhibit the JunD response to mitochondrial damage and/or oxidative stress. Alternatively, an increased Parkin response could negate the need for a full JunD response to stress to be initiated. If the hypothesis that JunD regulates a

response to mitochondrial stress, perhaps by heterodimerisation with FosB, by modifying neuronal function and activity rather than regulating mitochondrial homeostasis or apoptosis is true, then these data also implicate Parkin in the modulation of such pathways.

FosB also showed strong nuclear staining. This was despite later experiments performed by western blotting showing both FosB isoforms were not detectable unless induced by TPA or CCCP. In both undifferentiated WT and *PARKIN* overexpressing lines, FosB staining was not entirely uniform as some cells showed more intense nuclear fluorescence (Figures 3.4 and 3.6, respectively). Several studies have linked FosB or ΔFosB to neuronal functions, including stress response. Accumulated levels of ΔFosB, a much more stable isoform compared to the full-length protein, has been strongly linked with addiction to drug abuse. Increased levels of this stable protein, occurring in brain regions associated with addiction (e.g. dorsal striatum), are believed to act as a sustained molecular switch that induces the long term neuronal plasticity associated with drug addiction (reviewed by Nestler et al., 2001). As previously mentioned, the activity and upregulation of the FosB isoforms have also been associated with behavioural adaptations induced by electroconvulsive seizures in mice (Chen et al., 1995, Hiroi et al., 1998). Again these associations were with long-term neural plasticity. In terms of association with PD, overexpression of the ΔFosB isoform using a viral vector was shown to induce the involuntary movements that develop in rats due to chronic levodopa treatment (Cao et al., 2010). Despite accumulation of ΔFosB in the striatum of these rats, there was no change in JunD levels, the AP-1 protein partner it usually heterodimerises with. However, the authors did not consider if the basal levels of JunD are sufficient to provide dimerisation partnering to the increased ΔFosB levels. Interestingly, chronic L-DOPA treatment in mice induces ERK phosphorylation alongside elevated expression of FosB/ΔFosB (Pavon et al., 2006), suggesting that FosB activity could be regulated by ERK signalling under these conditions.

Since there are studies linking FosB activity with long-term neuronal responses to stress, it may be the case that the periods of time observed in the experiments in this thesis are not sufficient to investigate the role of the FosB

transcription factors. From qPCR and western blot experiments it was clear that the expression of this gene was very low under normal conditions in undifferentiated WT SH-SY5Y cells (Figures 4.9, 4.10 and 4.16). In the undifferentiated WT line, FosB protein levels were observably upregulated around 3 hours after CCCP treatment and remained elevated for at least another 9 hours. As qPCR analysis showed that *FOSB* upregulation occurred in two 'pulses' during the first 24 hours after mitochondrial uncoupling, western blotting might only be detecting the first upregulation. FosB protein may become detectable again after the 24 hours assessed here. This would support the hypothesis that FosB functions as a regulator of a long-term neuronal response.

Although the 24-hour FosB response in differentiated cells was not assessed, induction was observed by 6 hours post-CCCP treatment (Figure 4.9). Interestingly, FosB proteins were clearly induced in *PARKIN* overexpressing cells over this initial 6-hour period following mitochondrial uncoupling. However, no induction was observed when this cell line was analysed over a 24-hour period after CCCP, suggesting this would require further investigation to fully elucidate the FosB response in the presence of excess Parkin.

Fra-1 was shown to be completely nuclear in all cell lines observed and, like JunD, it appeared to be excluded from nucleoli. Importantly, Fra-1 showed strong staining in all 4 SH-SY5Y lines analysed suggesting constitutive expression in these cells. In the undifferentiated WT SH-SY5Y cell line Fra-1 protein levels remained relatively constant and did not appear to be modulated in response to mitochondrial depolarisation (Figures 4.11 and 4.12). However, *FRA-1* expression began to increase around 12-24 hours after CCCP treatment in these cells (Figure 4.16). Fra-1 has previously been shown to attenuate the Nrf2 response by increasing Nrf2 turnover in MEFs undergoing oxidative stress, thus leading to increased cell death (Vaz et al., 2012). As the H_2O_2 and diquat used by Vaz *et al* (2012) can both result in mitochondrial depolarisation as an indirect part of their cytotoxicity (Ryter et al., 2007), this function of Fra-1 could occur in CCCP-treated SH-SY5Ys. As the Nrf2 transcription factor is a major regulator of the antioxidant response pathway (Ma, 2013), it would make sense that Fra-1 protein levels are not significantly upregulated in SH-SY5Y cells upon

mitochondrial uncoupling (Figures 4.11 and 4.12), which is shown in this thesis to induce oxidative stress. The later upregulation of *FRA-1* expression induced by CCCP may therefore be part of the apoptotic response to this mitochondrial stressor. However, as Nrf2 is epigenetically silenced in at least some neurons (Bell et al., 2015), this may not be the case here and Fra-1 may function differently, perhaps contributing to the neuronal plasticity seen in response to oxidative stress.

Although JunB was not observed by immunofluorescence, both qPCR and western blotting confirmed its expression. If time had allowed, immunofluorescence of TPA treated SH-SY5Y cells would have been performed in order to visualise JunB localisation. Treatment with JunB siRNA did not result in a significant reduction in cell survival post-CCCP (Figure 4.18). Nonetheless, the induction of *JUNB* expression in response to 5μM CCCP does appear to occur (Figure 4.15). The upregulation of this gene appears to occurs after the initial CCCP challenge. Western blot data, although not accurately quantifiable, supports this, suggesting an initial steady increase in JunB protein levels after CCCP treatment (Figures 4.3 and 4.4). To date, no data has been presented implicating a role for JunB in the neuronal mitochondrial stress response. This could therefore represent a viable option for further study. The JunB response appears exaggerated in differentiated cells during the first 6 hours of mitochondrial uncoupling (Figure 4.3). As these cells are more likely to accurately represent neurons, it could be the case that JunB plays a more prominent role in this stress response in neuronal cells.

In contrast to the other AP-1 transcription factors observed by immunofluoresence, Fra-2 was entirely cytoplasmic and showed no nuclear staining at all. It is not clear whether this was a real result for Fra-2 staining as, to date, no subcellular localisation studies for this protein have been conducted in SH-SY5Y cells. In HEK293 cells, p38-mediated phosphorylation of c-Fos in response to UV light-induced stress results in cytoplasmic c-Fos translocating to the nucleus (Tanos et al., 2005). It may be the case that, in SH-SY5Y cells, phosphorylation of Fra-2 is required for its nuclear accumulation. Alternatively,

Fra-2, like c-Fos, may need to dimerise with a Jun protein in order to be retained in the nucleus (Malnou et al., 2007). Given more time, alternative antibodies and/or siRNA knockdown of Fra-2 prior to immunofluorescence analysis would have been utilised to confirm this result.

For Fra-2 western blotting did suggest at least some modulation in response to mitochondrial uncoupling in the undifferentiated WT SH-SY5Y cells. Here, both protein and mRNA levels were elevated by 24 hours after CCCP treatment (Figures 4.14 and 4.16). This would suggest Fra-2 could perhaps play a role in late neuronal responses to stress.

Interestingly, *PARKIN* overexpression in SH-SY5Y cells appeared to attenuate Fra-2 phosphorylation and elevation (Figures 4.13 and 4.14). The doublet observed when blotting for Fra-2 has previously been attributed to its phosphorylation causing a shift in its electrophoretic mobility (Alli et al., 2013). Here, the phosphorylated Fra-2 to non-phosphorylated Fra-2 ratio appears lower in the *PARKIN* overexpressing cells compared to the WT line. ERK can phosphorylate and upregulate Fra-2 (Reich et al., 2010, Alli et al., 2013), with Fra-2 stability substantially increased by ERK-dependent phosphorylation of S320 and T322 residues (Alli et al., 2013). As well as having the capacity to attenuate JNK (Jiang et al., 2004, Cha et al., 2005, Liu et al., 2008, Ren et al., 2009, Hwang et al., 2010), Parkin has also been shown to inhibit ERK activity (Ren et al., 2009). However, Ren et al (2009) did not show a direct interaction between Parkin and ERK. Instead, rotenone- and colchicine-induced ERK activation was suppressed by Parkin-dependent stabilisation of microtubules. Therefore, *PARKIN* overexpression may indirectly reduce Fra-2 phosphorylation by suppressing low levels of subcellular stress, thus ERK activity is attenuated.

In terms of research on PD-related stress, c-Jun has been significantly more studied than other AP-1 transcription factors. Several studies have demonstrated JNK/c-Jun signalling to act as an apoptotic driver in neurons undergoing stress (Ham et al., 1995, Watson et al., 1998, Ham et al., 2000, Gearan et al., 2001, Whitfield et al., 2001, Hunot et al., 2004, Jin et al., 2006, Borsello and Forloni, 2007, Centeno et al., 2007, Colombo et al., 2007, Johnson

and Nakamura, 2007, Wilhelm et al., 2007, Pan et al., 2009, Yang et al., 2010, Pan et al., 2012, Sclip et al., 2014). It therefore presented a possible candidate for further study here. Treatment of cells with c-Jun siRNA prior to 5μM CCCP-induced mitochondrial uncoupling lead to an increase in cell death, but decreased cell death after 30μM CCCP. This alone was not sufficient to warrant further investigation into this pathway as knockdown was not confirmed. However, significant modulation in c-Jun at mRNA and protein levels was observed after CCCP challenge, as well as differential modulation of c-Jun phosphorylation by upstream kinases upon different levels of mitochondrial stress. These data suggest that c-Jun may play a role in the cellular response to mitochondrial uncoupling.

6.1.3 The MAPK/c-Jun-mediated response to mitochondrial uncoupling

A recent study found that neuronal fate after L-DOPA treatment is regulated by c-Jun, which can act either cytoprotectively or pro-apoptotically (Park et al., 2016). Here, the authors investigated the c-Jun response to non-toxic (20μM), toxic (200μM) and multiple non-toxic doses of L-DOPA in PC12 cells, later extending this into an *in vivo* rat model. Interestingly, they found that non-toxic L-DOPA levels induced transient ERK activation leading to Ser73 c-Jun phosphorylation and cell survival. However, toxic or multiple long-term non-toxic concentrations of L-DOPA leads to sustained activation of ERK and JNK mediating S63 phosphorylation of c-Jun and inducing apoptosis. Data presented here would suggest that the c-Jun pathway also has the capacity to dictate cellular fate by acting as a molecular switch in order to detect the level of mitochondrial stress. It was hypothesised that MAPK signalling upstream regulates this.

In response to mitochondrial damage in undifferentiated SH-SY5Y cells, *c-JUN* expression levels undergo a biphasic response. Under these conditions, c-Jun protein levels also saw a rapid rise and significant accumulation by 24 hours post-CCCP. The fact that the biphasic response at expression level was not mirrored exactly by the protein levels of c-Jun may be explained by delays in protein degradation, thus a significant drop does not occur after c-Jun protein

levels initially rise. As c-Jun can act in both a pro- or anti-apoptotic manner (Park et al., 2016), it was hypothesised that the initial phase in upregulation may represent the adaptive response, followed by an apoptotic phase (Figure 6.2). As c-Jun can act as sensor of the level of damage a cell undergoes, this biphasic regulation may be the mechanism by which a cell initially attempts to adapt to the stress, but then the apoptotic phase is initiated if the adaptive phase cannot reverse the damage. Therefore, this may represent the 2 arms of the stress response, adaptive and apoptotic (summarised in Figure 1.3).

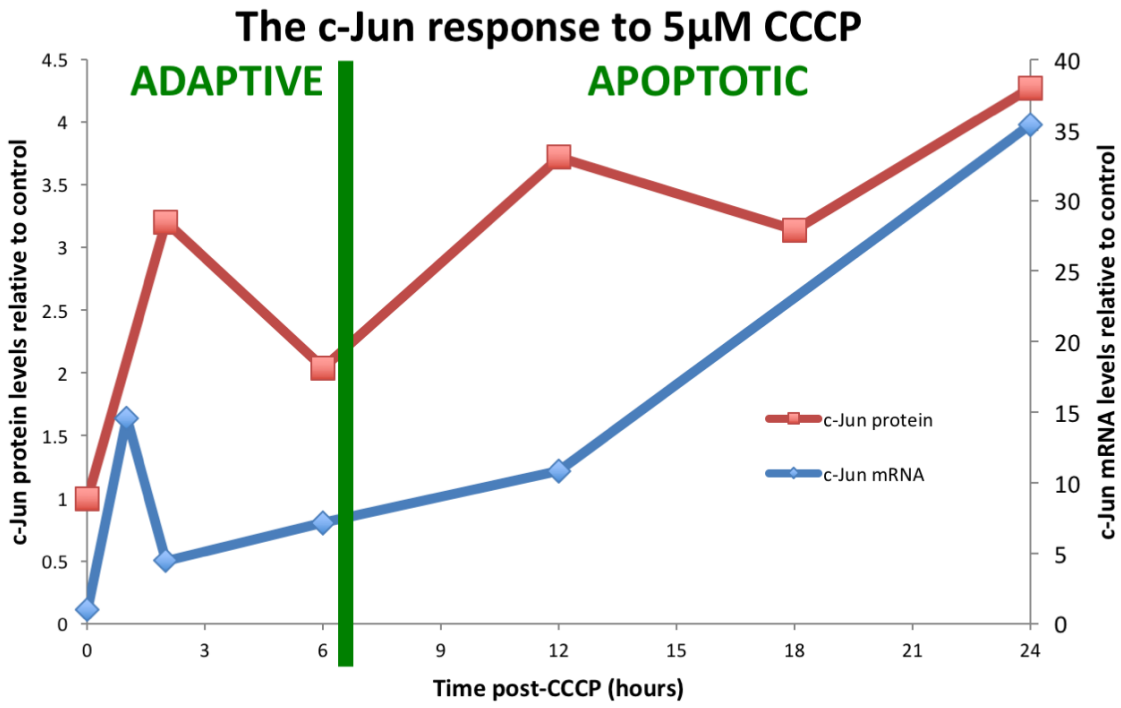

Figure 6.2: The biphasic modulation of *c-JUN* in response to CCCP exposure in undifferentiated WT cells. Data shown represents changes in the average relative protein levels of c-Jun (red line) and mRNA levels (blue line) detailed in chapter 4. Biphasic modulation of *c-JUN* expression suggests it may be involved in two parts of the stress response.

Elucidating how the AP-1 response functions could provide insight into neuronal development and how these cells adapt or die under stress conditions. Parts of the stress response may even serve in adaptive functions during synaptic plasticity driven by redox. Indeed, there may even be overlap between these developmentally important processes and the responses to potentially damaging oxidative stress. c-Jun is differentially regulated by both JNK and

ERK in response to different levels of neuronal stress (Figures 5.13 – 5.16) (Park et al., 2016). A change in the overall phosphorylation status of c-Jun occurs after mitochondrial uncoupling in SH-SY5Y cells. What is also apparent is that *PARKIN* overexpression alters how c-Jun is modulated here (Figures 6.3 and Appendices L and M).

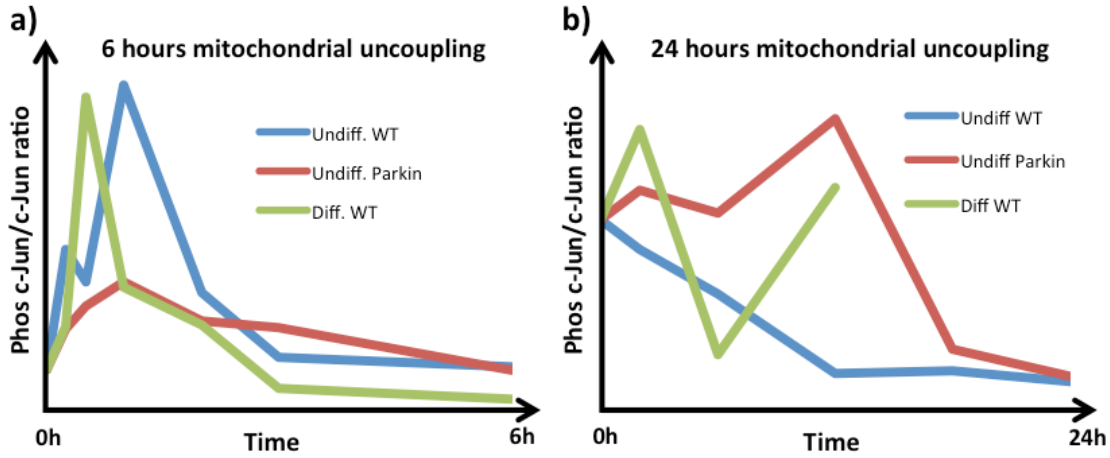

Figure 6.3: The modulation of phosphorylated c-Jun (S63)/c-Jun ratio upon mitochondrial uncoupling in SH-SY5Y cells. Cartoon representation of modulation of ratio extrapolated from data in Chapters 4 and 5. (a) The phosphorylated c-Jun (S63)/c-Jun ratio over the first 6 hours of CCCP exposure. (b) The phosphorylated c-Jun (S63)/c-Jun ratio over the first 24 hours of CCCP exposure. Average values from western blot analysis used.

Differentiation results in a greater c-Jun response, which may be as a result of the increased sensitivity of differentiated cultures compared with undifferentiated ones. Figures 6.3 shows the change in the ratio of phosphorylated c-Jun to c-Jun in response to mitochondrial uncoupling in SH-SY5Y cells. What seems apparent is that the initial response in the 2 WT SH-SY5Y cell lines during the first hour of stress is where the greatest increase in this ratio is observed (Figure 6.3). This may suggest that the most critical part of the c-Jun response is during the initial stage of mitochondrial stress.

Although during the first 6 hours of CCCP challenge differentiated WT SH-SY5Y cells demonstrate a much greater response in terms of the changes in total c-Jun (Figure 4.1) levels compared to the undifferentiated cell line, both WT lines

have similar responses when comparing the phosphorylated c-Jun/total c-Jun ratio (Figure 6.3). However, total levels of c-Jun in differentiated cells show a very different response fingerprint compared to undifferentiated cells (Figure 4.1). Not only was this initial modulation hugely exaggerated in the differentiated line but c-Jun levels remained elevated. Further analysis showed that levels had not decreased by 12 hours post-CCCP challenge (Figure 5.5). As differentiated cells were found to be significantly more sensitive to CCCP treatment than undifferentiated cells, this continual rise in c-Jun protein levels would support the biphasic model in which the adaptive and apoptotic arms of the stress response are separated into 2 separate phases of c-Jun modulation (Figure 6.2).

Differentiated cells rely more heavily on their mitochondrial network than cycling cells (Malkus et al., 2009). Mitochondrial uncoupling is more likely to induce fatal damage in differentiated cells, which may explain the greater and continual increase in c-Jun levels after mitochondrial challenge in differentiated cells. It could be that c-Jun acts as a sensor or molecular switch whereby chronic activation of c-Jun transcription (probably induced by the prolonged or intense activation of one or more MAPK cascades) leads to elevated levels of c-Jun, which can in turn be phosphorylated by the MAPKs activated under these conditions. It may therefore be the case that the level of the c-Jun response is proportional to the level of stress a cell undergoes. However, if the early upregulation in both c-Jun levels and its phosphorylation (at 1 or more of the 4 phospho-acceptor sites) is part of the initial (i.e. adaptive) response to mitochondrial stress, which is then followed by irreversibly damaged cells inducing a second upregulation in order to enter apoptosis, as suggested by the biphasic model (Figure 6.2), then the kinases upstream of c-Jun may prove an invalid therapeutic target since their inhibition may block cytoprotective pathways as well as apoptotic ones.

It has been suggested that c-Jun phosphorylation is only important in regulating the earliest death response in neurons and JNK inhibition merely delays apoptosis (Besirli et al., 2005). Here, c-Jun may only regulate part of the initial response to mitochondrial uncoupling, with the second phase controlling the

first apoptotic pathway available to the cell. It may then be the case that a cell surviving past this second phase of c-Jun regulation, possibly due to a number of reasons (e.g. adaptive responses restore homeostasis, JNK/c-Jun pathway inhibition, stress not great enough to initiate apoptosis etc.), could still be pushed into apoptosis by a late-response regulator induced by chronic stress. Therefore, it could be reasoned that c-Jun regulates both cytoprotective and first pass apoptotic pathway regulation. After this, AP-1 proteins such as JunD and ΔFosB, which can form long-term stable heterodimers and have been linked to long-term neuronal stress outcomes (Chen et al., 1995, Hiroi et al., 1998, Nestler et al., 2001, Pavon et al., 2006, Cao et al., 2010), may take over apoptotic regulation under prolonged stress.

Further to this, greater elevation in c-Jun levels during the initial period of stress in differentiated cells could indicate that differentiated cells have an increased c-Jun-mediated adaptive response. If Nrf2 is epigenetically repressed in neurons (Bell et al., 2015) the c-Jun response could be more sensitive to compensate. As AP-1 has already been shown to regulate Nrf2-mediated antioxidant genes (Papadia et al., 2008) this would seem plausible. As neurons cannot be replaced yet are constantly undergoing oxidative stress due to high energy demands, it would make sense to have a strong adaptive response. Despite this, differentiated SH-SY5Y cells undergo massive apoptosis in response to mitochondrial uncoupling via JNK (Figure 5.17) and possibly c-Jun.

Although, like differentiated cells, *PARKIN* overexpressing cells showed greater sensitivity to CCCP treatment compared to undifferentiated WT cells (Figure 3.4), the c-Jun response to mitochondrial uncoupling was dissimilar to that of the differentiated cell line (Figures 6.3). As well as a greater c-Jun response (Figure 4.1 and 4.2), *PARKIN* overexpression also prolongs c-Jun phosphorylation (Figure 5.4). This was unexpected, as Parkin has previously been shown to downregulate JNK activity in SH-SY5Y cells (Jiang et al., 2004) and *Drosophila* (Cha et al., 2005). One would therefore expect c-Jun phosphorylation to be decreased due to Parkin-mediated repression of JNK signalling. This increase in the c-Jun response may be partly responsible for the

greater CCCP-induced apoptosis observed in the *PARKIN* overexpressing cells (Figure 3.4). Although the c-Jun response was not examined by western blotting in differentiated Parkin cells, JNK inhibition does not significantly perturb cell death induced by CCCP treatment in these cells (Figure 5.18), as was observed in differentiated WT cells (Figure 5.17). Several explanations exist for this as alternate death pathways may be taken. Firstly, *PARKIN* overexpression could induce excessive mitophagy and thus cells die after complete and rapid autophagy of their entire mitochondrial network. Secondly, increased Parkin activity could result in the degradation of the cytoprotective MCL-1 protein (Carroll et al., 2014) thereby preventing its blockade of BAX/BAK-mediated cytochrome *c* release. Thirdly, if Parkin does inhibit JNK activity here, as suggested in other studies, then alternate pathways may be activated to compensate for the loss of a key apoptotic regulator. This may in turn increase c-Jun activity and promote apoptosis.

To identify the role of upstream kinases in the regulation of c-Jun in response to mitochondrial depolarisation, SP600125 (JNK inhibitor) and FR180204 (ERK inhibitor) were used to pre-treat undifferentiated WT SH-SY5Y cells prior to CCCP exposure. What was clear from these experiments was that JNK- and ERK-mediated regulation of c-Jun is dependent on the level of mitochondrial stress in undifferentiated SH-SY5Y cells (Figures 5.13 – 5.16).

After 5μM CCCP-induced mitochondrial depolarisation, the increase in c-Jun protein levels that normally occurs is perturbed by both JNK and ERK inhibition (Figure 5.13), although JNK appears to be the sole mediator of S63 phosphorylation (Figure 5.15). ERK inhibition increased c-Jun phosphorylation, suggesting ERK represses JNK-mediated c-Jun S63 phosphorylation in this situation. As substantial crosstalk between MAPKs occurs, providing a major part of their regulation (Fey et al., 2012), ERK and JNK may function synergistically to regulate one another. ERK has previously been shown to activate the phosphatases DUSP4 and DUSP16, which negatively regulate JNK (Monick et al., 2006, Paumelle et al., 2000). In turn, ERK may increase the threshold of the JNK-mediated apoptotic switch so that greater stress is needed

to induce the JNK feedback loops that are required to lock this pathway into a chronically highly active apoptotic state (Fey et al., 2012). Fey *et al*., suggest this as a possible mechanism by which hyperactivation of ERK in some cancers may suppress apoptotic induction by chemotherapeutics. In contrast, ERK inhibition in undifferentiated SH-SY5Ys decreased CCCP-induced cell death (Figure 5.12a). However, this was a marginal rescue suggesting ERK is likely to only have a small role at most in apoptosis under these conditions, although it has been shown previously to promote apoptosis (Dagda et al., 2008, Shin et al., 2015, Park et al., 2016).

JNK can repress ERK activation via c-Jun-dependent upregulation of *DUSP2* expression, a phosphatase, which leads to increased ERK dephosphorylation (Shen and Liu, 2006, Fey et al., 2012). This may occur in undifferentiated SH-SY5Y cells treated with 30μM CCCP (Figure 5.14). Here, ERK inhibition decreases c-Jun upregulation, whereas JNK inhibition increased it, suggesting that under the higher level of mitochondrial stress the ERK mediated increase in *c-JUN* expression or stability is repressed by JNK. Alternatively, JNK may function to phosphorylate specific c-Jun residues under this level of stress that target c-Jun for degradation; phosphorylation of c-Jun can either promote or reduce its proteasomal-dependent degradation, depending on the conditions (Fuchs et al., 1996, Fuchs et al., 1997, Musti et al., 1997, Nateri et al., 2004, Kyriakis and Avruch, 2012). Moreover, c-Jun and JunB proteasomal turnover is increased by JNK-mediated phosphorylation of ITCH, an E3 ubiquitin ligase (Gao et al., 2004). This may even explain the initial proteasome-dependent turnover of non-S63 phosphorylated c-Jun observed immediately after mitochondrial uncoupling (Figure 4.1), as stress may transiently induce JNK-mediated activation of ITCH (Gallagher et al., 2006), resulting in c-Jun ubiquitination. Interestingly, ERK-mediated phosphorylation of Fra-1 promotes heterodimerisation with c-Jun, increasing c-Jun stability (Talotta et al., 2010). Therefore, it is likely that regulation of c-Jun turnover occurs via both its phosphorylation and dimerisation partner, which will dictate how c-Jun modulates its target genes.

If possible, these inhibitors would have been assessed further. Although different alterations to c-Jun modulation were observed between these 2 inhibitors indicated that they were having on-target effects, this could have been assessed further by quantifying levels of phosphorylated JNK or ERK by western blotting under these conditions. Assessing any changes to other kinase phosphorylation levels in response to these inhibitors could also give insight into any off-target effects exhibited. Additional confirmation that the observations were due to the kinases targeted by each inhibitor could be potentially obtained using siRNA specific to each kinase and taken further by looking at individual isoforms.

How MAPK regulation of c-Jun will compare between undifferentiated and differentiated cells after mitochondrial depolarisation is currently unclear, although one aspect demonstrated by the data presented here (Figures 5.13 – 5.16) is that both JNK and ERK have the capacity to differentially regulate c-Jun expression, stability and activity (Figure 6.4). In differentiated WT cells, JNK inhibition rescued cell death induced by 30μM but not 5μM CCCP (Figure 5.17). This suggests that JNK-mediated apoptosis is only switched on under conditions of very high stress. Whether this occurs via c-Jun is unclear, although c-Jun does have the capacity to act cytoprotectively and apoptotically, depending on the level and type of neuronal stress (Park et al., 2016). However, in the study by Park *et al*, apoptosis was predominantly regulated by ERK. Nevertheless, the JNK/c-Jun pathway does initiate BIM activity under oxidative stress (Jin et al., 2006) and NGF-withdrawal (Whitfield et al., 2001), and therefore represents a viable hypothetical pathway for apoptotic regulation under the CCCP-induced stress studied in this thesis. If the JNK/c-Jun pathway does affect *BIM* expression in order to regulate mitochondrial damage-associated cell death then this may represent a viable therapeutic target in neurodegeneration. As excessively high levels of stress can essentially “lock” JNK signalling into an apoptotic mode via JNK feedback loops and ERK/p38 repression (Fey et al., 2012), modulating particular points in these pathways could prove therapeutically useful. This may reduce apoptotic promotion via c-Jun by suppressing cell death pathways or increasing the threshold at which they are induced.

Despite JNK inhibition often being the subject of study in the development of possible treatments for neurodegeneration, a successful compound is yet to make it through clinical trials. Therefore, understanding how this pathway works (i.e. under what conditions JNK-mediated apoptotic signalling is induced) is critical. Although JNK inhibition rescues 30μM CCCP-induced apoptosis in differentiated WT SH-SY5Y cells (Figure 5.17), this was not observed in the *PARKIN* overexpressing cells (Figure 5.18). Further investigation revealed that apoptosis by proteasomal inhibition was not altered by JNK inhibition in differentiated cells (Figures 5.19 and 5.20), suggesting that although apoptosis induced by mitochondrial uncoupling is promoted by JNK, this pathway does not regulate UPS inhibition-induced apoptosis, thus JNK-mediated apoptotic response is signal dependent (Figure 6.4).

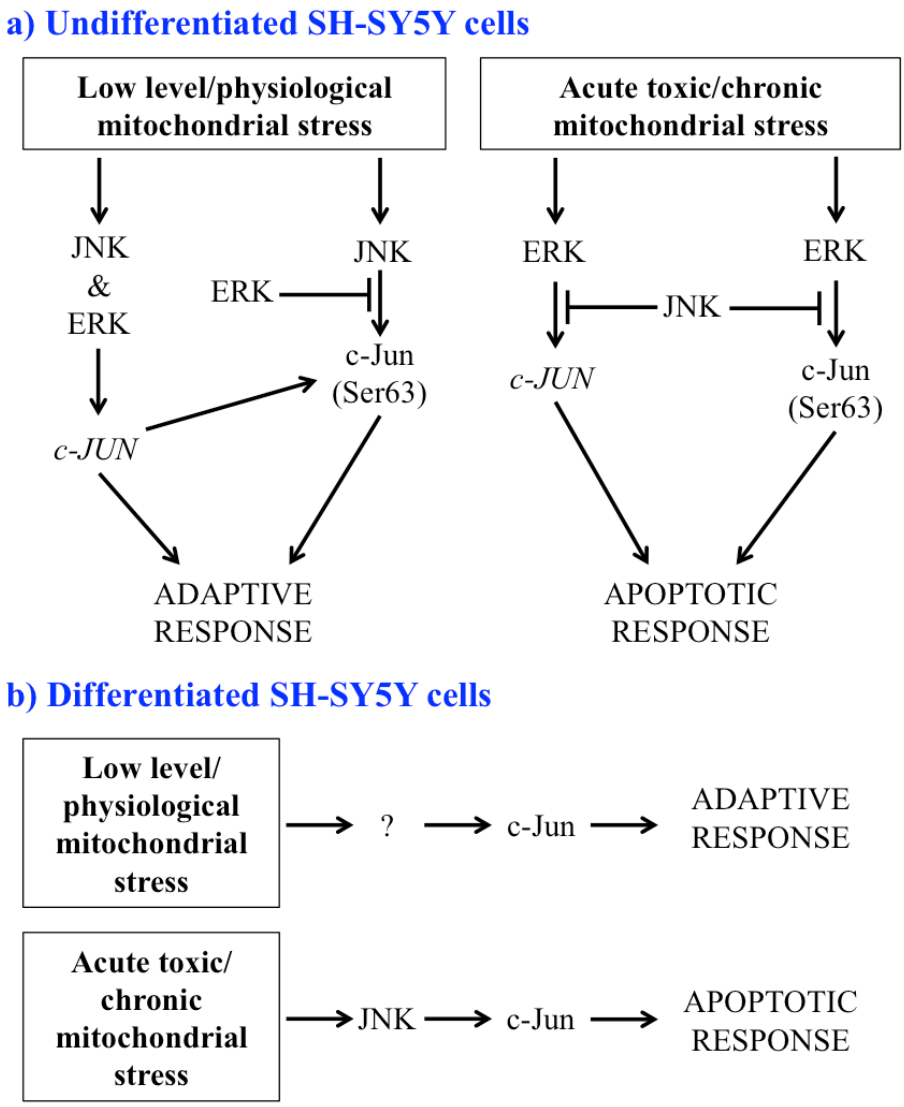

Figure 6.4: The hypothetical regulation and activity of c-Jun in response to CCCP-induced stress in SH-SY5Y cells. (a) Data presented in this thesis demonstrates the cross-talk between MAPK pathways in their mediation of the phosphorylation, transcriptional modulation and regulation of stability of c-Jun in response to mitochondrial uncoupling. ERK acts to perturb the JNK-mediated phosphorylation of c-Jun in the adaptive response but promotes c-Jun-dependent apoptosis under high levels of stress. (b) The MAPK-dependent regulation of c-Jun was not investigated in as greater detail in differentiated cells. A significant and rapid increase in c-Jun phosphorylation after CCCP challenge suggests it functions in the adaptive response. JNK mediated apoptosis under high levels of stress (30μM CCCP) probably occurs via c-Jun, as well as other JNK targets.

Interestingly, although SP600125-mediated JNK inhibition did not rescue apoptosis from proteasomal inhibition, mitochondrial uncoupling-induced

apoptosis in UPS-deficient differentiated WT and *PARKIN* overexpressing cells was promoted by JNK activity (Figures 5.19 and 5.20). Therefore, JNK-mediated apoptosis only occurs under mitochondrial stress in differentiated SH-SY5Y cells. Furthermore, the inhibition of JNK in UPS-deficient cells not only reduced mitochondrial stress-induced apoptosis, but also resulted in greater cell survival compared to cells treated with epoxomicin alone. This suggests that mitochondrial stress JNK-dependent neuronal death is the dominant apoptotic pathway even under proteasomal inhibition. Proteasomal inhibition prevented c-Jun protein levels from dropping after the initial increase (Figure 5.1), thus c-Jun activity may continually increase, preventing the early adaptive response from shutting down and driving the activation of apoptosis due to continually rising c-Jun levels. Furthermore, the c-Jun response to mitochondrial stress continues to be exacerbated in UPS-deficient cells (Figure 5.3). A functional UPS is required for Parkin-mediated mitophagy to occur (Chan et al., 2011, Morrison et al., 2011) and it may be required for a normal c-Jun response. Alternatively, blocking mitophagy could mean ROS-induced stress from dysfunctional mitochondria cannot be resolved and thus chronic activation of the c-Jun stress response is induced.

Parkin plays a key role in the response to mitochondrial stress in neurons. Data presented in this thesis suggests that the MAPK/c-Jun pathway is also involved in this response. c-Jun represses the ATF4-mediated transcription of *PARKIN* (Bouman et al., 2011) (Figure 5.6). Here, it was also observed that *PARKIN* overexpression may alter the c-Jun response by amplifying c-Jun protein level increases 24 hours after incubation with CCCP (Figure 4.2). This was unexpected and required further investigation as it could suggest a feedback loop between Parkin and MAPK/c-Jun signalling that regulates the balance between adaptive and apoptotic responses to mitochondrial uncoupling.

6.1.4 A Parkin-MAPK/c-Jun feedback loop may dictate neuronal cell fate decisions under mitochondrial stress

In *PARKIN* overexpressing cells, c-Jun protein levels were higher compared to WT cells 24 hours post-CCCP (Figure 4.2). Current data detailing the link between c-Jun and Parkin is ambiguous. Parkin is implicated in down regulating

JNK/c-Jun-mediated expression of Eg5, a kinesin motor (Liu et al., 2008). This occurs through Parkin-mediated inactivation of JNK via ubiquitination that reduces c-Jun phosphorylation, as well as separately blocking c-Jun binding to the *Eg5* promoter. Conversely, c-Jun acts as a transcriptional repressor of *PARKIN* by blocking ATF4 binding to its promoter (Bouman et al., 2011). Furthermore, there has been some indication that Parkin may act to supress JNK expression and activity in *Drosophila* (Cha et al., 2005, Hwang et al., 2010). Taken together, these data suggest a feedback loop exists between Parkin and MAPK/c-Jun signalling.

To investigate if the overexpression of WT Parkin in a different model system still led to an increase in c-Jun levels 24 hours post-CCCP, an inducible HEK293 cell line (non-neuronal) was utilised. Further to this, a range of HEK293 cells inducibly expressing a number of different Parkin mutants (Morrison et al., 2011) were also used to determine whether this increase in c-Jun was dependent on Parkin E3 activity (summarised in Table 6.1).

	Parkin mutant													
	WT	**R275Y**	**T240R**	**S131A**	**Y143F**	**R42P**	**R42C**	**R275W**	**T415N**	**C289G**	**G430D**	**C352G**	**K161N**	**K211N**
Region of mutation	n/a	RING1	RING1	Linker region	Linker region	UBL domain	UBL domain	RING1	RING2	RING1	RING2	IBR domain	SH2-like domain	SH2-like domain
E3 ubiquitin ligase activity	✓	✗	✗	✓	✓	✓	?	✗	✗	?	✗	✗	✗	✗
Mitophagy blocked by proteasomal inhibition	✓	n/a	n/a	✓	✗	✓	n/a	n/a	n/a	n/a	n/a	n/a	n/a	n/a
Recruited to depolarised mitochondria	✓	?	✗	✓	✓	✓	?	✓	✓	✗	✗✓	✓	✓	✗
Induces mitochondrial clustering	✓	✗	✗	✓	✓	✓	✓	Delayed	✓✗	✗	✗	✗	✓	✗
Induces mitochondrial degradation	✓	✗	✗	✓	✓	✓	✗	✗	✗	✗	✗	✗	✗	✗
Change in c-Jun levels 24h post-CCCP (relative to WT)	n/a	Decrease	Increase	Decrease	Decrease	No change	Decrease	?	?	?	?	?	?	?

Table 6.1: Parkin mutations perturb mitophagy at different stages. Previous data demonstrates dysfunction occur at different stages of mitophagy, depending on the Parkin mutant. To date, all the steps at which disruption takes place for each mutant has not been elucidated for all Parkin mutants shown here. Data showing the changes in c-Jun level induced by CCCP treatment in HEK293 cells expressing different Parkin mutants relative to the WT form are shown in Chapter 5 (Figure 5.22). Note: some studies demonstrate contradictory data.

Overexpression of WT *PARKIN* resulted in a significant increase in c-Jun after CCCP treatment compared to host cells (Figure 5.22), concurring with data from SH-SY5Y cells (Figure 4.2) suggesting Parkin activity may increase c-Jun expression or stability under mitochondrial stress. As c-Jun represses *PARKIN* expression (Bouman et al., 2011), one could hypothesise that this may serve as a regulatory feedback in which high Parkin activity results in increased c-Jun levels, thus in turn decreasing Parkin mRNA levels in order to regulate mitophagy. Dysregulation of this functional feedback could lead to unregulated apoptosis induced by c-Jun. This was not investigated further, although c-Jun siRNA does not alter CCCP-induced apoptosis in *PARKIN* overexpressing SH-SY5Y cells (Appendix O). In terms of a greater c-Jun response in the SH-SY5Y or HEK293 cells overexpressing *PARKIN,* in response to excessive Parkin activity the cell may increase c-Jun protein levels to prevent a further increase in Parkin, which is essentially degrading the entire mitochondrial network. As the *PARKIN* overexpressed in this system is under the control of a different promoter than endogenous Parkin (one that does not contain the AP-1 binding site), c-Jun is unable to gain any traction in the regulation of this feedback loop. Therefore, ever-increasing c-Jun levels/activity add to the apoptosis already induced by excessive mitophagy.

If c-Jun levels were directly increased by Parkin activity as part of the regulation of mitophagy then Parkin mutants that still maintain their mitophagic function should have comparable effects to WT Parkin. However, overexpression of the functional mutants S131A and Y143F instead resulted in a decrease in c-Jun protein levels after mitochondrial uncoupling (Figure 5.22). Cdk5 phosphorylates Parkin at Ser131 to reduce its autoubiquitination activity (Avraham et al., 2007). The S131A mutant used here cannot be phosphorylated by Cdk5, thus its activity is not repressed by this regulation. The Y143F mutant lacks the phosphorylation site for the tyrosine kinase c-Abl, which mediates inhibition of Parkin ubiquitin ligase activity (Ko et al., 2010). Furthermore, we have recently found that the proteasome is able to regulate Parkin activity via the c-Abl-mediated phosphorylation of Tyr143 (Roper, 2015). Despite both the Y143F and S131A Parkin mutants being functional in mitophagy, this lack of

regulation results in a significantly different effect on c-Jun protein levels under mitochondrial stress relative to the WT protein (Figure 5.22).

Parkin^{R42P}, a PD-associated missense mutant (Terreni et al., 2001), is also considered a functional mutant, although its translocation to (Geisler et al., 2010) and mitophagy of damaged mitochondria, is reduced compared to WT Parkin (Narendra et al., 2010b). Conversely, another study found that R42P Parkin protein was not recruited to damaged mitochondria (Lee et al., 2010). However this was rat Parkin transfected into MEFs and protein concentrations were significantly lower than other mutants and controls used. The R42P mutation is in the UBL domain and results in the unfolding of this region, reducing protein stability (Safadi and Shaw, 2007). As R42P is a functional mutant, albeit with reduced activity compared to WT, it is unsurprising its effects on c-Jun are similar to WT Parkin (Figure 5.22). This is however, different to S131A and Y143F, which appear to either repress c-Jun expression or lower its stability. It is possible that mutations in the linker region disrupt any function that Parkin has in order to increase c-Jun protein levels, which may explain the differences between overexpressing WT and R42P Parkin compared to Y143F and S131A observed here.

The R42C mutation plays a causative role in glioblastoma development (Veeriah et al., 2010) and has recently been identified in patients suffering with an early onset form of PD (Hussain et al., 2014), although the muatation it is not confirmed as a pathogenic alteration. Parkin^{R42C} is capable of mediating mitochondrial perinuclear clustering following CCCP-induced uncoupling (Roper, 2015). Although no data currently exists to demonstrate that this mutation is recruited to depolarised mitochondria, it is reasonable to assume it does due to its ability to induce mitochondrial clustering (Table 6.1). Upon mitochondrial uncoupling, Parkin^{R42C} overexpression reduces c-Jun levels compared to WT (Figure 5.22).

Both the R275Y and T240R mutations occur in the RING1 domain of Parkin and abrogate the protein's mitophagic activity (Morrison et al., 2011, Roper, 2015). However, they have significantly different effects on c-Jun protein levels

following mitochondrial uncoupling (Figure 5.22), which could be due to the different stages at which mitophagy halts for these two mutants. The Parkin^{T240R} mutant perturbs the earliest stage of mitophagy by preventing recruitment to dysfunctional mitochondria (Geisler et al., 2010), as well as rendering it E3 ligase-deficient (Okatsu et al., 2010). To date, no data has been published to demonstrate R275Y translocating to mitochondria upon depolarisation but we have recently found its overexpression cannot induce mitophagy (Roper, 2015). In comparison, the PD-causing R275W mutation is recruited to mitochondria under these conditions and has been shown to either promote clustering at a reduced rate to the WT protein (Geisler et al., 2010, Narendra et al., 2010a) or not at all (Okatsu et al., 2010). As both tryptophan and tyrosine are both aromatic residues, the mutations leading to the replacement of the positively charged arginine may have the same effect.

The T240R mutation in Parkin renders the protein completely non-functional (Matsuda et al., 2010, Narendra et al., 2010a, Narendra et al., 2010b, Okatsu et al., 2010, Geisler et al., 2010) and induces a significant increase in c-Jun levels following mitochondrial uncoupling (Figure 5.22). This is interesting as it is significantly different to every other mutant studied here, indicating that its failure to be recruited to the mitochondria may result in an increase in c-Jun expression or stability. As it is not known if R275Y is recruited, it is difficult to ascertain whether the failure of this stage of mitophagy for T240R does in fact cause this increase in c-Jun levels. It would therefore be critical to either show R275Y Parkin colocalisation, or lack of, with depolarised mitochondria in order to draw a conclusion, as well as examining other mutants. Parkin^{C289G} is not recruited to mitochondria and does not induce aggregation (Rose et al., 2011), although the neuronal molecular chaperones HSJ1a and DNAJB6 were able to partially restore mitophagy. As this mutant, like T240R, is not recruited to depolarised mitochondria, it would be interesting to determine if this also induced an increase in c-Jun when overexpressed. As both the T240R and C289G mutations occur in the same domain of Parkin, the K211N mutant (RING0 (SH2) domain) would also make an ideal candidate, as it does not localise with damaged mitochondria (Geisler et al., 2010). It could therefore indicate whether over-induction of c-Jun requires both the complete cytoplasmic

localisation of Parkin as well as a non-functional RING1 domain under mitochondrial stress conditions.

If the dysfunctional translocation of Parkin^{T240R} alone is responsible for the increase in c-Jun levels, several explanations may exist. As demonstrated in Chapter 5, both JNK and ERK have the capacity to phosphorylate c-Jun, as well as induce its expression. Both JNK and ERK have previously been shown to localise to mitochondria under stress conditions in PD models (Dagda et al., 2008, Chambers et al., 2013). Therefore, Parkin may localise to a damaged mitochondrion and reduce or inhibit the phosphotransferase activity of JNK or ERK associated with it.

Inhibition of JNK following its 6-OHDA-induced localisation to mitochondria is neuroprotective (Chambers et al., 2013). Furthermore, JNK phosphorylates the MOM protein MFN2 in response to doxorubicin treatment, leading to its degradation (Leboucher et al., 2012). The stress-induced localisation of ERK2 to mitochondria is sufficient for the activation of mitophagy (Dagda et al., 2008) and can promote mitochondrial fragmentation via phosphorylation of DRP1 (Kashatus et al., 2015). In addition, stress-induced ERK-mediated phosphorylation of MFN1 decreases mitochondrial fusion but potentiates its binding to BAK, a pro-apoptotic BCL-2 protein (Pyakurel et al., 2015). This lead to cytochrome *c* release and neuronal apoptosis. As several studies have linked Parkin to the regulation of JNK/c-Jun signalling (Jiang et al., 2004, Cha et al., 2005, Liu et al., 2008, Hwang et al., 2010), it may be that the failure of Parkin to localise to mitochondria upon uncoupling results in the dysregulation of MAPK activity, thus c-Jun levels are increased.

Time point western blot analysis, as performed in Chapter 4, could also prove insightful in determining how soon c-Jun levels begin to rise in cells expressing the different Parkin constructs. It could be interesting to characterise the c-Jun response in HEK293 cells expressing WT and T240R Parkin and whether disparities in the level of c-Jun upregulation occurs, as this may lead to dysregulation of the stress response. By also observing phosphorylated levels

of c-Jun, JNK and ERK for these cell lines it may be possible to dissect the cascade of signalling events under these conditions.

The increased or decreased levels of c-Jun observed in the different mutant lines could be explained by a change in either protein stability/reduced degradation or transcriptional modulation. Analysing c-Jun mRNA levels by qRT-PCR would elucidate whether defective/altered Parkin activity leads to the modulation of c-Jun expression. As c-Jun regulates its own transcription, it may be the case that modulation of upstream effectors of c-Jun activity by Parkin is the key regulator of c-Jun expression. If this was the case, the fact that c-Jun not only regulates *PARKIN* expression (Bouman et al., 2011), but is also in turn regulated by Parkin activity would suggest a critical feedback loop that regulates the cytoprotective or apoptotic activities of c-Jun.

If the mitochondrial translocation of Parkin was required for this feedback loop, then PINK1 would also play a role. PINK1 is critical in the recruitment of Parkin to the MOM upon mitochondrial uncoupling to initiate mitophagy (Narendra et al., 2008, Narendra et al., 2010b). As PINK1 mutations occur in some familial forms of PD and perturb the recruitment of Parkin to damaged mitochondria it may in turn lead to elevated c-Jun levels, as observed with the T240R mutant. siRNA knockdown of PINK1 would give some indication as to whether the failure of Parkin to colocalise with depolarised mitochondria due to the loss of PINK1 function led to increased c-Jun levels. Further to this, observing phosphorylated levels of JNK and ERK by western blotting of mitochondrial fractions with and without the knockdown of PINK1 would determine whether the failure of Parkin recruitment elevates MAPK activity at mitochondria.

To date no full investigation has been carried out studying JNK activity and mitochondrial uncoupling, although some data that has been published. As previously stated, stress induced by 6-OHDA in SH-SY5Y cells and rat neurons *in vivo* results in the translocation of JNK to mitochondria (Chambers et al., 2013). Mitochondrial JNK (mitoJNK) transduced apoptotic signalling, which was inhibited by a number of methods including JNK-specific siRNA and SR-3306, a potent JNK inhibitor proposed as a potential PD therapeutic. Moreover, SR-

3306 inhibited c-Jun phosphorylation under these conditions, suggesting that this mitochondrial JNK translocation results in signalling via c-Jun modulation. Stress-induced mitochondrial localisation of JNK occurs via its interaction with Sab (SH3BP5), a MOM protein containing a MAPK interaction motif (Wiltshire et al., 2004), Interestingly, mitochondrial JNK acts to amplify superoxide generation by Complex I (Chambers and LoGrasso, 2011), as well as induce mitochondrial respiration inhibition and apoptosis (Win et al., 2014, Win et al., 2015). Disruption of the JNK-Sab interaction perturbed JNK mitochondrial translocation, Bcl-2 phosphorylation and apoptosis but c-Jun phosphorylation was not affected (Chambers et al., 2011a). However, this study only observed Ser73 phosphorylation and utilised HeLa cells, which do not express the neuron-specific JNK3 isoform that may play a critical role here. Nevertheless, this study does suggest that mitoJNK may initiate apoptotic signalling independently of c-Jun activity, whereas nuclear JNK functions via c-Jun phosphorylation. This paints a complex picture in which JNK localisation may be critical and multiple signalling cascades are activated.

A potentially promising result in the search for PD treatment was that use of SR-3306, a small molecule JNK inhibitor, was effective in protecting dopaminergic neurons in MPTP-treated mice (Chambers et al., 2011b). JNK inhibition reduced c-Jun phosphorylation in a dose-dependent manner, leading to neuronal rescue. Despite being highly studied, the role of c-Jun phosphorylation in neuronal death is still far from understood, as whilst evidence points to it being critical (Watson et al., 1998, Whitfield et al., 2001, Reddy et al., 2013) some data has shown that the loss of c-Jun phosphorylation merely delays apoptosis in neurons (Besirli et al., 2005). In the latter study, induction of pro-apoptotic genes such as *bim* was delayed in mice carrying a mutant *c-jun* gene lacking S63 and S73 phosphoacceptor sites. However, it was not considered whether lower level c-Jun activity might be achieved via alternative phosphorylation sites or by dimerisation with other AP-1 proteins, thus inducing genes such as *bim* at a later time-point. Further to this, unphosphorylated c-Jun may still have the capacity to repress cytoprotective genes such as *PARKIN* (although apoptotic upon extensive mitochondrial uncoupling).

Data presented in this thesis suggest c-Jun plays a role in regulating cell fate after mitochondrial and/or oxidative stress. JNK inhibition also rescues apoptosis under higher levels of mitochondrial uncoupling. Considered with recently published data showing c-Jun can be both pro- and anti-apoptotic in dopaminergic neurons (depending on the level L-DOPA-induced stress) (Park et al., 2016), this would imply that the functional outcome of JNK/c-Jun pathway is specified by thresholds. It may therefore be the case that this pathway promotes activation of apoptosis upon excessive or sustained damage in a neuron that would be deemed irreversible.

In AD, the “2-hit hypothesis” in which both JNK and ERK must be activated to induce neuronal cell death under pathophysiological levels of stress (Zhu et al., 2007) could apply to PD progression as both JNK and ERK localise to damaged mitochondria (Zhu et al., 2003, Dagda et al., 2008, Chambers et al., 2011a, Chambers and LoGrasso, 2011, Chambers et al., 2013, Win et al., 2014, Kashatus et al., 2015). This could provide a “gated threshold regulation” by which crosstalk between MAPKs determines the type of pathway activated, depending on the strength, duration and form of input from stress. The apparent elevation in c-Jun in response to CCCP-induced stress in HEK293 cells expressing the T240R Parkin mutant would also suggest that Parkin or the mitophagic process plays a role in regulating c-Jun. Therefore, when mitophagy fails or is overrun, apoptosis induces the destruction of an irreversibly damaged cell. Mitochondrial stress-induced apoptosis mediated by JNK is dominant over apoptosis caused by proteasomal inhibition in differentiated SH-SY5Y cells demonstrating the capacity of this pathway. As multiple forms of stress are associated with PD, MAPK/AP-1-regulated apoptosis may be stress-specific.

The chronic long-term progressive nature of most forms of PD will make this signalling pathway difficult to dissect. However, PD symptoms resulting from acute exposure to certain compounds (e.g. pesticides) may be induced via the apoptotic JNK pathway, which data presented here suggests occurs under the highest levels of stress, at least in the short term. Nevertheless, the c-Jun response in dopaminergic neurons has the capacity to differentiate between the duration (acute/chronic) and intensity (low/cytotoxic) of stress (Park et al.,

2016). This capacity would be critical due to the inherent nature of their bio-energetic needs of these neurons (Pacelli et al., 2015), which experience repeated peaks in mitochondrial ROS production.

The overall hypothesis arising from this thesis, involving feedback loops and regulatory pathways between Parkin, JNK, ERK and c-Jun, is unavoidably a highly complex one (Figure 6.5). Upon mitochondrial damage, Parkin-mediated mitophagy can occur rapidly and locally along axonal outgrowths far from the soma, and thus the nucleus (Ashrafi et al., 2014), with Parkin probably targeting Miro for degradation in order to arrest mitochondrial transport (Wang et al., 2011). Therefore, mitochondrial-localised JNK and/or ERK are unlikely to exhibit regulation over their nuclear targets. However, as mitoJNK amplifies ROS production by dysfunctional mitochondria (Chambers and LoGrasso, 2011), it may be that prolonged mitoJNK activity induces prolonged cytoplasmic/nuclear JNK activity via increased ROS, which in turn regulates c-Jun phosphorylation. The overall level or duration of mitochondrial damage is critical in dictating neuronal fate via these pathways.

Parkin can act in both a cytoprotective and apoptotic manner, depending on the level of stress (Carroll et al., 2014). BIM, is induced by c-Jun to initiate apoptosis in neurons (Whitfield et al., 2001) and may regulate crosstalk between autophagy and apoptosis (Luo et al., 2012, Luo and Rubinsztein, 2013), promoting Parkin recruitment to depolarised mitochondria that is normally perturbed by pro-survival Bcl-2 proteins (Hollville et al., 2014). Indeed, BIM accumulates on the MOM under stress conditions in order to initiate BAX-dependent cytochrome *c* release (Renault et al., 2015). Therefore, chronic activation of the JNK/c-Jun pathway may lead to increased BIM-mediated recruitment of Parkin to damaged mitochondria, promoting cell death once a threshold of damage is surpassed. This may be one process by which the sporadic late-onset form of PD progresses. Here we see that *BIM* expression is upregulated in response to CCCP-induced stress (Figure 5.23). It could be the case that c-Jun activity indirectly regulates Parkin recruitment to mitochondria, and that sustained or excessive MAPK/c-Jun activity increases Parkin mitochondrial localisation in order to induce Parkin-dependent apoptosis.

Further experiments under different stress levels, as well as determining the subcellular localisation of BIM and Parkin after CCCP challenge would be required to draw any conclusions. *RAB8A* expression was also modulated in a similar manner to c-Jun phosphorylation after CCCP addition (Figures 5.25 and 5.26). Despite its association with autophagosomal dysfunction, oxidative stress and chronic JNK/AP-1 signalling in FTD (West et al., 2015), its link to the processes described here remains tenuous and requires further elucidation.

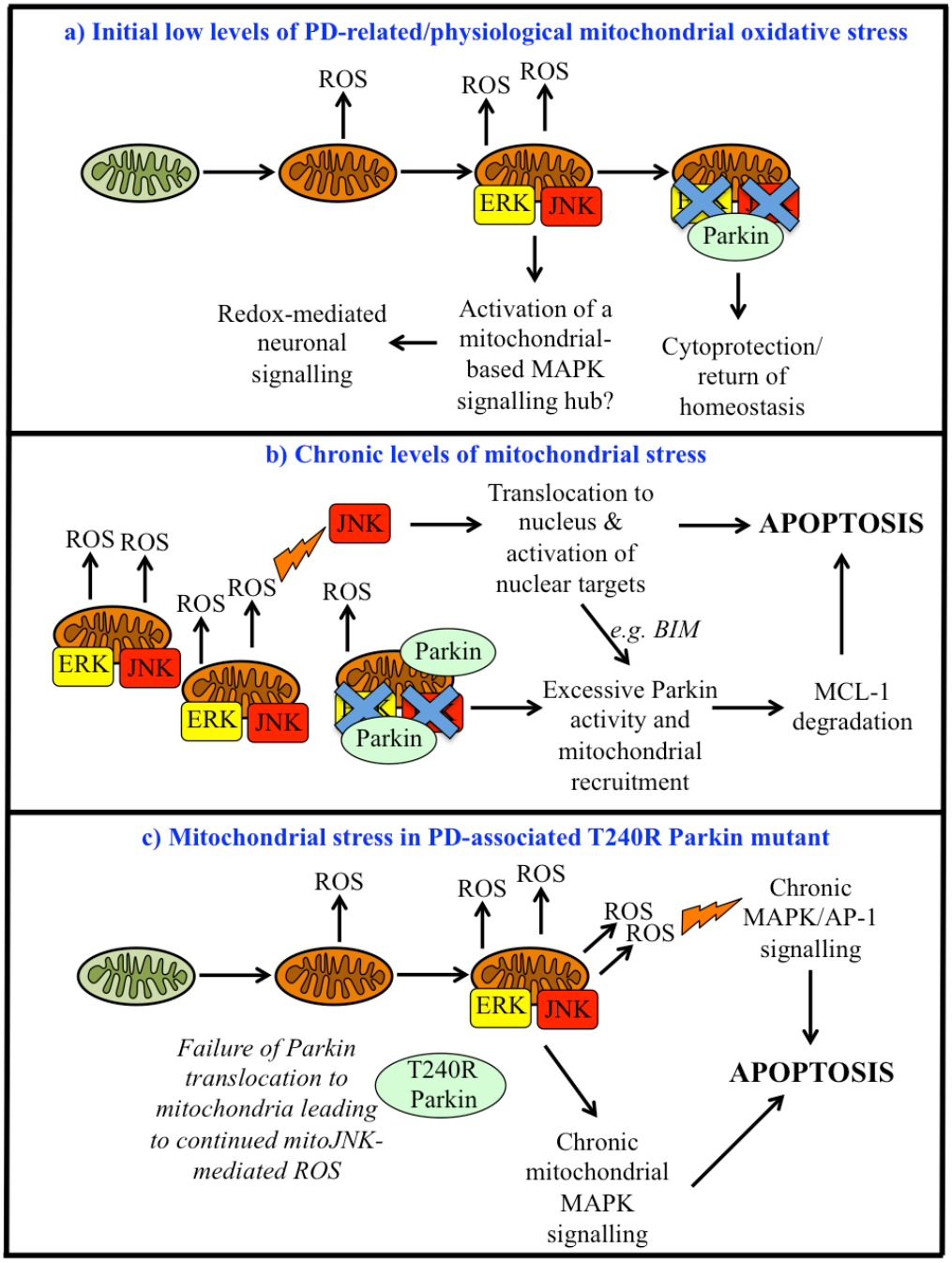

Figure 6.5: Hypothetical responses to mitochondrial stress in normal neuronal function and neurodegeneration. (a) Increased ROS production occurs in damaged mitochondria (orange) relative to healthy mitochondria (green). Acute bursts of mitochondrial ROS initiate redox-sensitive signalling as part of normal neuronal function, with Parkin suppressing mitochondrial MAPK activity. (b) Chronic stress is exacerbated by mitochondrial and nuclear MAPK signalling, ROS accumulation and Parkin-dependent degradation of MCL-1. (c) Certain Parkin mutations result in less efficient or complete lack of mitochondrial translocation and resulting MAPK suppression. Mitochondrial ROS production increased by mitoJNK promotes neuronal death pathways.

As ER stress leads to the induction of mitochondrial stress in neuronal cells (Bouman et al., 2011), multiple forms of cellular stress could lead to the initiation of these pathways. JNK-mediated apoptosis only occurred in UPS-deficient differentiated SH-SY5Y cells upon the induction of mitochondrial stress as a secondary insult (Figures 5.19 and 5.20). As previously noted, these data suggest that JNK-dependent apoptosis is the dominant cell death pathway under these conditions. Interestingly, JNK inhibition rescues cell death in 5μM CCCP-treated cells that had been pre-treated with epoxomicin (Figure 5.19) but not in cells challenged solely with CCCP (Figure 5.17). This can be accommodated by the hypothesis proposed here (Figure 6.5), as JNK and/or ERK will accumulate on damaged mitochondria following CCCP challenge. Normally, Parkin-mediated mitophagy, along with the hypothetical activity of Parkin that has been suggested here where it supresses mitochondrial MAPK transduction, will act to degrade damaged mitochondria and prevent thresholds for apoptotic initiation being surpassed. However, UPS inhibition prevents the activation of Parkin and subsequent mitophagy (Tanaka et al., 2010, Chan et al., 2011), even perturbing the early phase of mitochondrial clustering (Figure 5.22), potentially via regulatory feedback signalling pathways. Therefore, epoxomicin-induced 26S proteasomal inhibition would block Parkin-mediated mitophagy and mitochondrial MAPK suppression and thus the apoptotic JNK pathway would be initiated at a lower threshold of mitochondrial damage. As UPS dysfunction is associated with PD (as well as other neurodegenerative conditions), the hypothesis that proteasome malfunction renders neurons more sensitive to stress by lowering the threshold at which apoptosis is induced would seem plausible. A recent study showed that apoptosis in Aβ-treated cultured neurons and an AD transgenic mouse model was induced by the JNK/c-Jun-mediated upregulation of the pro-apoptotic genes *bim* and *puma* (Akhter et al., 2015). This would suggest that the JNK/c-Jun pathway may actually be an endpoint in the initiation of neuronal cell death and this has implications across the spectra of neurodegenerative conditions.

Potentially, neurons in patients with inherited or sporadic forms of PD experience years or even perhaps decades of cellular stress before apoptotic

pathways are initiated, whereas acute exposure to certain stressors or neurotoxins could induce these rapidly. Either way, a stress response will be mounted to determine neuronal fate and the manipulation of these pathways may provide opportunities for the development of therapeutic interventions. However, increased understanding of these processes is required first.

6.2 CONCLUSIONS

The neuronal cellular stress response is a complex and multi-faceted process involving a number of signalling pathways, allowing the cell to opt for the most appropriate outcome. From the data presented here, it may be that aberrant regulation of a single one of the many pathways involved in the adaptive response can increase the likelihood of, or prematurely initiate an apoptotic response. Prolonging or boosting the capacity of the cellular adaptive response may therefore represent a valid therapeutic strategy. However, more data is needed on the downstream targets of c-Jun, as well as a greater understanding of the interplay between upstream kinases and Parkin. Many of the experiments conducted in this thesis have a low number of biological replicates. The lack of full assessment of the reproducibility of this data, as well as the chance of false positives or false negatives being found due to low statistical power, means that much of this data requires further investigation in order to correctly and confidently interpret. It must also be taken into account that the role of c-Jun and other proteins within the stress response are likely to differ depending on the type of stress a neuron is experiencing. Furthermore, the apoptotic response plays an important role in the protection of surrounding cells and tissue from damage therefore merely inhibiting stress-induced cellular death seems likely cause greater complications over a prolonged period. Thus, a combinatorial treatment that works to alleviate the stress alongside strategies aimed at prolonging the adaptive response to it (or inhibiting/delaying the apoptotic response) is likely to be the most viable solution to prevent disease progression. Nevertheless, it must be remembered that neuronal cells do not regenerate. Neuronal cells within a network that have already died cannot be readily replaced so early diagnosis of Parkinson's will always play a key role in the successful development of an effective treatment.

6.3 FUTURE WORK

Data presented in this thesis centres largely around c-Jun as part of the response to mitochondrial uncoupling in SH-SY5Y cells. Here, the SH-SY5Y cell line, both undifferentiated and differentiated, was used a neuronal cell model. The overexpression of *PARKIN* was also utilised to exaggerate the mitophagic response. Experiments with siRNA are often used to elucidate a functional role for specific genes and proteins. As effective knockdown of target genes was not confirmed in this thesis, conclusions cannot be drawn from these experiments. Confirmation of this would therefore be a critical next step. Even with this confirmation however, the use of siRNA to knock down c-Jun has several limitations. Firstly, the efficiency of the knock down will not be 100% in every cell within the experiment. Secondly, despite controlling for off-target effects these do present other variables to take into account. Thirdly, siRNA knock down can only be easily utilised in undifferentiated SH-SY5Y cells since the lack of mitotic activity once these cells have undergone differentiation reduces transfection efficiency. Whilst stably transfected lines overexpressing different mutants of a protein can be useful and do allow for differentiation, it is arguable how representative these systems are. The use of CRISPR/Cas9 genome editing has greatly increased in recent years as this technique has been honed and improved to allow the accurate and efficient modification of genes in eukaryotic systems (Ran et al., 2013, Doudna and Charpentier, 2014, Hsu et al., 2014). By inducing changes in genes of interest in SH-SY5Y cells it could be possible to generate lines expressing phospho-deficient c-Jun mutants, mutants mimicking constitutively phosphorylated c-Jun, mutations in MAPKs (that would allow for the individual JNK and ERK isoforms to be studied) as well as alterations to Parkin. These lines could then be subjected to PD-linked stressors such as CCCP exposure. Importantly though, these cell lines would stably express these alterations and could therefore be differentiated.

As nigral dopaminergic neurons have exceptionally high levels of axonal arborisation, which in turn leads to higher oxidative phosphorylation occurring to meet the increased bioenergetics demands, they are more vulnerable to certain PD-associated neurotoxic agents (Pacelli et al, 2015). Therefore, dysfunction in

the pathways investigated in this thesis may render these specific neurons more susceptible to cellular damage above the threshold at which apoptosis occurs. It was for this reason that the RA/BDNF differentiation method for SH-SY5Ys was chosen in this thesis as it induced the greatest neurite outgrowth of the protocols tested. However, greater arborisation probably occurs *in vivo* and thus utilization of other model systems would be advantageous. The use of *in vivo* model systems such as mice and *Drosophila* would provide further insight, with the latter allowing for the simpler manipulation of specific genes to test the ideas presented here. Furthermore, cultured primary neurons would likely provide a useful tool. Simple experiments such as exposure to CCCP and MAPK inhibition, along with IF staining for tyrosine hydroxylase-positive cells would indicate relative sensitivities of dopaminergic and other neurons and the possible signalling pathways specifically involved in neuronal subtypes.

Nevertheless, data from cell lines will provide a more realistic approach to gaining large amounts of preliminary data before moving on to the more precious model systems just mentioned. Recently, the Lund human mesencephalic (LUHMES) cell line has begun to receive attention in PD research. From the Lund University in Sweden, these immortalised cells are a sub-clone of the mesencephalic MESC2.10 line that was derived from a human foetal ventral mesencephalon (Lotharius et al., 2002). Several studies have already utilised the highly dopaminergic-like differentiated form of these cells to study PD-related stress (Lotharius et al., 2005, Schmidt et al., 2009, Zhang et al., 2014b). Moreover, apoptosis resulting from oxidative stress induced by dopamine was mediated by JNK in these cells (Lotharius et al., 2005). Essentially these cells represent an immortalised dopaminergic stem cell and are therefore are likely to provide a powerful *in vitro* model for future PD research. Therefore, this cell line would be a useful cell system to extend data obtained from SH-SY5Y cells into. The mitochondrial clustering data presented here could prove useful in developing a high-throughput screen for compounds that restore defective mitophagy in neurons. If this data was transferable to differentiated LUHMES cells then these may provide a more accurate representation of *in vivo* dopaminergic neurons in a screen set up. As well as this, induced pluripotent stem cells (iPSCs) have begun to be more readily

utilised in PD research. Despite labour-intensive set up, iPSCs provide one of the most representative *in vitro* models available and would certainly allow the generation of data more transferable to *in vivo* systems. Therefore, the use of iPSCs as a tool to extend data presented in this thesis would be highly desirable.

Utilising resources such as the Parkinson's UK Brain Bank could also prove insightful. If samples were obtained from a range of stages of the disease then perhaps changes in parameters such as c-Jun phosphorylation or MAPK activity/localisation could be observed and correlated with PD progression. Other proteins studied here, such as Parkin, RAB8A and BIM, as well as the structure, function and dynamic behaviour of the mitochondrial network could also be investigated in order to further elucidate how the neuronal response to stress switches from adaptive to apoptotic in long-term dopaminergic degeneration.

Data from HEK293 cells indicated a possible role for Parkin activity regulating the c-Jun pathway under mitochondrial stress. As this was only the preliminary step in this area of investigation, much more data could be obtained. Firstly, how these different Parkin mutants affect the MAPK signalling pathways activated in response to CCCP-induced stress and how this in turn affects c-Jun phosphorylation. To further extend this, other phosphorylation sites on c-Jun could also be investigated. One thing that would be critical in understanding this overall process and determining if a feedback loop exists between Parkin and MAPK/AP-1 signalling would be to show whether Parkin regulates MAPK signalling at the mitochondria following uncoupling. Inhibitors could then be used to see if they could prevent excessive c-Jun upregulation in cells expressing the T240R Parkin mutant. Assessing this through the quantification of mitochondrial clustering (Figure 5.21) could also be used to determine if certain compounds restore effective mitophagy.

Finally, one key area not assessed directly in this thesis was long-term neuronal function and how these cells adapt to physiological stress. Dopaminergic neurons inherently undergo high levels of oxidative stress due to their

bioenergetic demands and extensive arborisation (Pacelli et al., 2015). However, ROS-induced stress is clearly also required for proper neuronal development (Bell et al., 2015). This paradox means that the division between adaptive and apoptotic responses is fine. However, these cell fate decisions are likely to be determined over years or decades in respect to PD progression. Therefore, the long-term effects of low-level chronic or repeated mitochondrial stress on MAPK/AP-1 signalling and related pathways in neurons would be an important area to investigate. This thesis largely focused on the initial 24 hours post-challenge. Some evidence has been presented previously showing that a change in c-Jun phosphorylation can dictate neuronal fate in response to L-DOPA-induced acute and chronic oxidative stress (Park et al., 2016). As well as this, JNK/c-Jun signalling has the ability to regulate *PARKIN* expression under stress conditions (Bouman et al., 2011) and eventually induce pro-apoptotic induction of *BIM* (Putcha et al., 2001, Whitfield et al., 2001, Besirli et al., 2005, Jin et al., 2006). Further elucidation of how these pathways are modulated in the long-term under physiologically relevant stress levels of different forms of stress could prove critical in increasing our understanding of the mechanisms underlying PD progression.

REFERENCES

ADISESHAIAH, P., LI, J., VAZ, M., KALVAKOLANU, D. V. & REDDY, S. P. 2008. ERK signaling regulates tumor promoter induced c-Jun recruitment at the Fra-1 promoter. *Biochemical and biophysical research communications,* 371**,** 304-8.

ADISESHAIAH, P., PAPAIAHGARI, S. R., VUONG, H., KALVAKOLANU, D. V. & REDDY, S. P. 2003. Multiple cis-elements mediate the transcriptional activation of human fra-1 by 12-O-tetradecanoylphorbol-13-acetate in bronchial epithelial cells. *The Journal of biological chemistry,* 278**,** 47423-33.

ADISESHAIAH, P., PEDDAKAMA, S., ZHANG, Q., KALVAKOLANU, D. V. & REDDY, S. P. 2005. Mitogen regulated induction of FRA-1 proto-oncogene is controlled by the transcription factors binding to both serum and TPA response elements. *Oncogene,* 24**,** 4193-205.

AHN, T. B., KIM, S. Y., KIM, J. Y., PARK, S. S., LEE, D. S., MIN, H. J., KIM, Y. K., KIM, S. E., KIM, J. M., KIM, H. J., CHO, J. & JEON, B. S. 2008. alpha-Synuclein gene duplication is present in sporadic Parkinson disease. *Neurology,* 70**,** 43-9.

AKHTER, R., SANPHUI, P., DAS, H., SAHA, P. & BISWAS, S. C. 2015. The regulation of p53 up-regulated modulator of apoptosis by JNK/c-Jun pathway in beta-amyloid-induced neuron death. *J Neurochem,* 134**,** 1091-103.

ALBERTS, B., WILSON, J. & HUNT, T. 2008. *Molecular biology of the cell,* New York, Garland Science.

ALLI, N. S., YANG, E. C., MIYAKE, T., AZIZ, A., COLLINS-HOOPER, H., PATEL, K. & MCDERMOTT, J. C. 2013. Signal-dependent fra-2 regulation in skeletal muscle reserve and satellite cells. *Cell Death Dis,* 4**,** e692.

ANASTASSIADIS, T., DUONG-LY, K. C., DEACON, S. W., LAFONTANT, A., MA, H., DEVARAJAN, K., DUNBRACK, R. L., JR., WU, J. & PETERSON, J. R. 2013. A highly selective dual insulin receptor (IR)/insulin-like growth factor 1 receptor (IGF-1R) inhibitor derived from an extracellular signal-regulated kinase (ERK) inhibitor. *J Biol Chem,* 288**,** 28068-77.

ANDERSSON, F. I., WERRELL, E. F., MCMORRAN, L., CRONE, W. J., DAS, C., HSU, S. T. & JACKSON, S. E. 2011. The effect of Parkinson's-disease-associated mutations on the deubiquitinating enzyme UCH-L1. *J Mol Biol,* 407**,** 261-72.

ANG, A. L., FOLSCH, H., KOIVISTO, U. M., PYPAERT, M. & MELLMAN, I. 2003. The Rab8 GTPase selectively regulates AP-1B-dependent basolateral transport in polarized Madin-Darby canine kidney cells. *J Cell Biol,* 163**,** 339-50.

ARDLEY, H. C., SCOTT, G. B., ROSE, S. A., TAN, N. G., MARKHAM, A. F. & ROBINSON, P. A. 2003. Inhibition of proteasomal activity causes inclusion formation in neuronal and non-neuronal cells overexpressing Parkin. *Mol Biol Cell,* 14**,** 4541-56.

ASHRAFI, G., SCHLEHE, J. S., LAVOIE, M. J. & SCHWARZ, T. L. 2014. Mitophagy of damaged mitochondria occurs locally in distal neuronal axons and requires PINK1 and Parkin. *The Journal of cell biology,* 206**,** 655-70.

AVRAHAM, E., ROTT, R., LIANI, E., SZARGEL, R. & ENGELENDER, S. 2007. Phosphorylation of Parkin by the cyclin-dependent kinase 5 at the linker region modulates its ubiquitin-ligase activity and aggregation. *J Biol Chem,* 282**,** 12842-50.

BAIK, J. H., PICETTI, R., SAIARDI, A., THIRIET, G., DIERICH, A., DEPAULIS, A., LE MEUR, M. & BORRELLI, E. 1995. Parkinsonian-like locomotor impairment in mice lacking dopamine D2 receptors. *Nature,* 377**,** 424-8.

BAIN, J., MCLAUCHLAN, H., ELLIOTT, M. & COHEN, P. 2003. The specificities of protein kinase inhibitors: an update. *Biochem J,* 371**,** 199-204.

BARILA, D., MANGANO, R., GONFLONI, S., KRETZSCHMAR, J., MORO, M., BOHMANN, D. & SUPERTI-FURGA, G. 2000. A nuclear tyrosine phosphorylation circuit: c-Jun as an activator and substrate of c-Abl and JNK. *EMBO J,* 19**,** 273-81.

BARTELS, T., CHOI, J. G. & SELKOE, D. J. 2011. alpha-Synuclein occurs physiologically as a helically folded tetramer that resists aggregation. *Nature,* 477**,** 107-10.

BARTELS, T. & SELKOE, D. 2013. Bartels & Selkoe reply. *Nature* 498**,** E6-E7.

BASBOUS, J., JARIEL-ENCONTRE, I., GOMARD, T., BOSSIS, G. & PIECHACZYK, M. 2008. Ubiquitin-independent- versus ubiquitin-dependent proteasomal degradation of the c-Fos and Fra-1 transcription factors: is there a unique answer? *Biochimie,* 90**,** 296-305.

BEAL, M. F., MATTHEWS, R. T., TIELEMAN, A. & SHULTS, C. W. 1998. Coenzyme Q10 attenuates the 1-methyl-4-phenyl-1,2,3,tetrahydropyridine (MPTP) induced loss of striatal dopamine and dopaminergic axons in aged mice. *Brain Res,* 783**,** 109-14.

BEAULIEU, J. M. & GAINETDINOV, R. R. 2011. The physiology, signaling, and pharmacology of dopamine receptors. *Pharmacol Rev,* 63**,** 182-217.

BELL, K. F., AL-MUBARAK, B., MARTEL, M. A., MCKAY, S., WHEELAN, N., HASEL, P., MARKUS, N. M., BAXTER, P., DEIGHTON, R. F., SERIO, A., BILICAN, B., CHOWDHRY, S., MEAKIN, P. J., ASHFORD, M. L., WYLLIE, D. J., SCANNEVIN, R. H., CHANDRAN, S., HAYES, J. D. & HARDINGHAM, G. E. 2015. Neuronal development is promoted by weakened intrinsic antioxidant defences due to epigenetic repression of Nrf2. *Nat Commun,* 6**,** 7066.

BENCE, N. F., SAMPAT, R. M. & KOPITO, R. R. 2001. Impairment of the ubiquitin-proteasome system by protein aggregation. *Science,* 292**,** 1552-5.

BENEDETTI, M. D., BOWER, J. H., MARAGANORE, D. M., MCDONNELL, S. K., PETERSON, B. J., AHLSKOG, J. E., SCHAID, D. J. & ROCCA, W. A. 2000. Smoking, alcohol, and coffee consumption preceding Parkinson's disease: a case-control study. *Neurology,* 55**,** 1350-8.

BERG, J. M., TYMOCZKO, J. L. & STRYER, L. 2007. *Biochemistry,* New York, N.Y., W. H. Freeman.

BERGER, A. K., CORTESE, G. P., AMODEO, K. D., WEIHOFEN, A., LETAI, A. & LAVOIE, M. J. 2009. Parkin selectively alters the intrinsic threshold for mitochondrial cytochrome c release. *Hum Mol Genet,* 18**,** 4317-28.

BERHOW, M. T., HIROI, N. & NESTLER, E. J. 1996. Regulation of ERK (extracellular signal regulated kinase), part of the neurotrophin signal transduction cascade, in the rat mesolimbic dopamine system by chronic exposure to morphine or cocaine. *J Neurosci,* 16**,** 4707-15.

BERTRAM, L. & TANZI, R. E. 2008. Thirty years of Alzheimer's disease genetics: the implications of systematic meta-analyses. *Nat Rev Neurosci,* 9**,** 768-78.

BESIRLI, C. G., WAGNER, E. F. & JOHNSON, E. M., JR. 2005. The limited role of NH2-terminal c-Jun phosphorylation in neuronal apoptosis: identification of the nuclear pore complex as a potential target of the JNK pathway. *The Journal of cell biology,* 170**,** 401-11.

BETARBET, R., SHERER, T. B., MACKENZIE, G., GARCIA-OSUNA, M., PANOV, A. V. & GREENAMYRE, J. T. 2000. Chronic systemic pesticide exposure reproduces features of Parkinson's disease. *Nature neuroscience,* 3**,** 1301-6.

BIEDLER, J. L., HELSON, L. & SPENGLER, B. A. 1973. Morphology and growth, tumorigenicity, and cytogenetics of human neuroblastoma cells in continuous culture. *Cancer research,* 33**,** 2643-52.

BIEDLER, J. L., ROFFLER-TARLOV, S., SCHACHNER, M. & FREEDMAN, L. S. 1978. Multiple neurotransmitter synthesis by human neuroblastoma cell lines and clones. *Cancer research,* 38**,** 3751-7.

BIRSA, N., NORKETT, R., WAUER, T., MEVISSEN, T. E., WU, H. C., FOLTYNIE, T., BHATIA, K., HIRST, W. D., KOMANDER, D., PLUN-FAVREAU, H. & KITTLER, J. T. 2014. Lysine 27 ubiquitination of the mitochondrial transport protein Miro is dependent on serine 65 of the Parkin ubiquitin ligase. *J Biol Chem,* 289**,** 14569-82.

BOGERTS, B., HANTSCH, J. & HERZER, M. 1983. A morphometric study of the dopamine-containing cell groups in the mesencephalon of normals, Parkinson patients, and schizophrenics. *Biol Psychiatry,* 18**,** 951-69.

BOILEAU, I., GUTTMAN, M., RUSJAN, P., ADAMS, J. R., HOULE, S., TONG, J., HORNYKIEWICZ, O., FURUKAWA, Y., WILSON, A. A., KAPUR, S. & KISH, S. J. 2009. Decreased binding of the D3 dopamine receptor-preferring ligand [11C]-(+)-PHNO in drug-naive Parkinson's disease. *Brain,* 132**,** 1366-75.

BONIFATI, V. 2009. Is GIGYF2 the defective gene at the PARK11 locus? *Curr Neurol Neurosci Rep,* 9**,** 185-7.

BONIFATI, V., RIZZU, P., SQUITIERI, F., KRIEGER, E., VANACORE, N., VAN SWIETEN, J. C., BRICE, A., VAN DUIJN, C. M., OOSTRA, B., MECO, G. & HEUTINK, P. 2003. DJ-1(PARK7), a novel gene for autosomal recessive, early onset parkinsonism. *Neurol Sci,* 24**,** 159-60.

BORSELLO, T. & FORLONI, G. 2007. JNK signalling: a possible target to prevent neurodegeneration. *Curr Pharm Des,* 13**,** 1875-86.

BOSSIS, G., FERRARA, P., ACQUAVIVA, C., JARIEL-ENCONTRE, I. & PIECHACZYK, M. 2003. c-Fos proto-oncoprotein is degraded by the proteasome independently of its own ubiquitinylation in vivo. *Mol Cell Biol,* 23**,** 7425-36.

BOSSIS, G., MALNOU, C. E., FARRAS, R., ANDERMARCHER, E., HIPSKIND, R., RODRIGUEZ, M., SCHMIDT, D., MULLER, S., JARIEL-ENCONTRE, I. & PIECHACZYK, M. 2005. Down-regulation of c-Fos/c-Jun AP-1 dimer activity by sumoylation. *Mol Cell Biol,* 25**,** 6964-79.

BOUMAN, L., SCHLIERF, A., LUTZ, A. K., SHAN, J., DEINLEIN, A., KAST, J., GALEHDAR, Z., PALMISANO, V., PATENGE, N., BERG, D., GASSER, T., AUGUSTIN, R., TRUMBACH, D., IRRCHER, I., PARK, D. S., WURST, W., KILBERG, M. S., TATZELT, J. & WINKLHOFER, K. F. 2011. Parkin is transcriptionally regulated by ATF4: evidence for an interconnection between mitochondrial stress and ER stress. *Cell death and differentiation,* 18**,** 769-82.

BURCHELL, V. S., NELSON, D. E., SANCHEZ-MARTINEZ, A., DELGADO-CAMPRUBI, M., IVATT, R. M., POGSON, J. H., RANDLE, S. J., WRAY, S., LEWIS, P. A., HOULDEN, H., ABRAMOV, A. Y., HARDY, J., WOOD, N. W., WHITWORTH, A. J., LAMAN, H. & PLUN-FAVREAU, H. 2013. The Parkinson's disease-linked proteins Fbxo7 and Parkin interact to mediate mitophagy. *Nature neuroscience,* 16**,** 1257-65.

BURRE, J., VIVONA, S., DIAO, J., SHARMA, M., BRUNGER, A. T. & SUDHOF, T. C. 2013. Properties of native brain alpha-synuclein. *Nature,* 498**,** E4-6; discussion E6-7.

BUSSOLINO, D. F., GUIDO, M. E., GIL, G. A., BORIOLI, G. A., RENNER, M. L., GRABOIS, V. R., CONDE, C. B. & CAPUTTO, B. L. 2001. c-Fos associates with the endoplasmic reticulum and activates phospholipid metabolism. *FASEB J,* 15**,** 556-8.

BUTTIGLIONE, M., VITIELLO, F., SARDELLA, E., PETRONE, L., NARDULLI, M., FAVIA, P., D'AGOSTINO, R. & GRISTINA, R. 2007. Behaviour of SH-SY5Y neuroblastoma cell line grown in different media and on different chemically modified substrates. *Biomaterials,* 28**,** 2932-45.

CAI, Q., ZAKARIA, H. M., SIMONE, A. & SHENG, Z. H. 2012. Spatial parkin translocation and degradation of damaged mitochondria via mitophagy in live cortical neurons. *Curr Biol,* 22**,** 545-52.

CAO, X., YASUDA, T., UTHAYATHAS, S., WATTS, R. L., MOURADIAN, M. M., MOCHIZUKI, H. & PAPA, S. M. 2010. Striatal overexpression of DeltaFosB reproduces chronic levodopa-induced involuntary movements. *J Neurosci,* 30**,** 7335-43.

CARGNELLO, M. & ROUX, P. P. 2011. Activation and function of the MAPKs and their substrates, the MAPK-activated protein kinases. *Microbiol Mol Biol Rev,* 75**,** 50-83.

CARROLL, R. G., HOLLVILLE, E. & MARTIN, S. J. 2014. Parkin sensitizes toward apoptosis induced by mitochondrial depolarization through promoting degradation of Mcl-1. *Cell Rep,* 9**,** 1538-53.

CENTENO, C., REPICI, M., CHATTON, J. Y., RIEDERER, B. M., BONNY, C., NICOD, P., PRICE, M., CLARKE, P. G., PAPA, S., FRANZOSO, G. & BORSELLO, T. 2007. Role of the JNK pathway in NMDA-mediated excitotoxicity of cortical neurons. *Cell Death Differ,* 14**,** 240-53.

CERNAIANU, G., BRANDMAIER, P., SCHOLZ, G., ACKERMANN, O. P., ALT, R., ROTHE, K., CROSS, M., WITZIGMANN, H. & TROBS, R. B. 2008. All-trans retinoic acid arrests neuroblastoma cells in a dormant state. Subsequent nerve growth factor/brain-derived neurotrophic factor treatment adds modest benefit. *J Pediatr Surg,* 43**,** 1284-94.

CHA, G. H., KIM, S., PARK, J., LEE, E., KIM, M., LEE, S. B., KIM, J. M., CHUNG, J. & CHO, K. S. 2005. Parkin negatively regulates JNK pathway in the dopaminergic neurons of Drosophila. *Proceedings of the National Academy of Sciences of the United States of America,* 102**,** 10345-50.

CHAMBERS, J. W., CHERRY, L., LAUGHLIN, J. D., FIGUERA-LOSADA, M. & LOGRASSO, P. V. 2011a. Selective inhibition of mitochondrial JNK signaling achieved using peptide mimicry of the Sab kinase interacting motif-1 (KIM1). *ACS Chem Biol,* 6**,** 808-18.

CHAMBERS, J. W., HOWARD, S. & LOGRASSO, P. V. 2013. Blocking c-Jun N-terminal kinase (JNK) translocation to the mitochondria prevents 6-hydroxydopamine-induced toxicity in vitro and in vivo. *J Biol Chem,* 288**,** 1079-87.

CHAMBERS, J. W. & LOGRASSO, P. V. 2011. Mitochondrial c-Jun N-terminal kinase (JNK) signaling initiates physiological changes resulting in amplification of reactive oxygen species generation. *J Biol Chem,* 286**,** 16052-62.

CHAMBERS, J. W., PACHORI, A., HOWARD, S., GANNO, M., HANSEN, D., JR., KAMENECKA, T., SONG, X., DUCKETT, D., CHEN, W., LING, Y. Y., CHERRY, L., CAMERON, M. D., LIN, L., RUIZ, C. H. & LOGRASSO, P. 2011b. Small Molecule c-jun-N-terminal Kinase (JNK) Inhibitors Protect Dopaminergic Neurons in a Model of Parkinson's Disease. *ACS Chem Neurosci,* 2**,** 198-206.

CHAN, N. C., SALAZAR, A. M., PHAM, A. H., SWEREDOSKI, M. J., KOLAWA, N. J., GRAHAM, R. L., HESS, S. & CHAN, D. C. 2011. Broad activation of the ubiquitin-proteasome system by Parkin is critical for mitophagy. *Human molecular genetics,* 20**,** 1726-37.

CHANG, D. T., HONICK, A. S. & REYNOLDS, I. J. 2006. Mitochondrial trafficking to synapses in cultured primary cortical neurons. *J Neurosci,* 26**,** 7035-45.

CHANG, K. H., CHEN, C. M., CHEN, Y. C., LYU, R. K., CHANG, H. S., RO, L. S., LEE-CHEN, G. J. & WU, Y. R. 2013. Association between PARK16 and Parkinson's disease in the Han Chinese population: a meta-analysis. *Neurobiol Aging,* 34**,** 2442 e5-9.

CHARAN, R. A., JOHNSON, B. N., ZAGANELLI, S., NARDOZZI, J. D. & LAVOIE, M. J. 2014. Inhibition of apoptotic Bax translocation to the mitochondria is a central function of parkin. *Cell Death Dis,* 5**,** e1313.

CHARTIER-HARLIN, M. C., DACHSEL, J. C., VILARINO-GUELL, C., LINCOLN, S. J., LEPRETRE, F., HULIHAN, M. M., KACHERGUS, J., MILNERWOOD, A. J., TAPIA, L., SONG, M. S., LE RHUN, E., MUTEZ, E., LARVOR, L., DUFLOT, A., VANBESIEN-MAILLIOT, C., KREISLER, A., ROSS, O. A., NISHIOKA, K., SOTO-ORTOLAZA, A. I., COBB, S. A., MELROSE, H. L., BEHROUZ, B., KEELING, B. H., BACON, J. A., HENTATI, E., WILLIAMS, L., YANAGIYA, A., SONENBERG, N., LOCKHART, P. J., ZUBAIR, A. C., UITTI, R. J., AASLY, J. O., KRYGOWSKA-WAJS, A., OPALA, G., WSZOLEK, Z. K., FRIGERIO, R., MARAGANORE, D. M., GOSAL, D., LYNCH, T., HUTCHINSON, M., BENTIVOGLIO, A. R., VALENTE, E. M., NICHOLS, W. C., PANKRATZ, N., FOROUD, T., GIBSON, R. A., HENTATI, F., DICKSON, D. W., DESTEE, A. & FARRER, M. J. 2011. Translation initiator EIF4G1 mutations in familial Parkinson disease. *Am J Hum Genet,* 89**,** 398-406.

CHARTIER-HARLIN, M. C., KACHERGUS, J., ROUMIER, C., MOUROUX, V., DOUAY, X., LINCOLN, S., LEVECQUE, C., LARVOR, L., ANDRIEUX, J., HULIHAN, M., WAUCQUIER, N., DEFEBVRE, L., AMOUYEL, P., FARRER, M. & DESTEE, A. 2004. Alpha-synuclein locus duplication as a cause of familial Parkinson's disease. *Lancet,* 364**,** 1167-9.

CHAUGULE, V. K., BURCHELL, L., BARBER, K. R., SIDHU, A., LESLIE, S. J., SHAW, G. S. & WALDEN, H. 2011. Autoregulation of Parkin activity through its ubiquitin-like domain. *The EMBO journal,* 30**,** 2853-67.

CHEN, C., SETH, A. K. & APLIN, A. E. 2006. Genetic and expression aberrations of E3 ubiquitin ligases in human breast cancer. *Mol Cancer Res,* 4**,** 695-707.

CHEN, J., NYE, H. E., KELZ, M. B., HIROI, N., NAKABEPPU, Y., HOPE, B. T. & NESTLER, E. J. 1995. Regulation of delta FosB and FosB-like proteins by electroconvulsive seizure and cocaine treatments. *Mol Pharmacol,* 48**,** 880-9.

CHEN, Y. & DORN, G. W., 2ND 2013. PINK1-phosphorylated mitofusin 2 is a Parkin receptor for culling damaged mitochondria. *Science,* 340**,** 471-5.

CHEUNG, Y. T., LAU, W. K., YU, M. S., LAI, C. S., YEUNG, S. C., SO, K. F. & CHANG, R. C. 2009. Effects of all-trans-retinoic acid on human SH-SY5Y neuroblastoma as in vitro model in neurotoxicity research. *Neurotoxicology,* 30**,** 127-35.

CHINTA, S. J. & ANDERSEN, J. K. 2005. Dopaminergic neurons. *Int J Biochem Cell Biol,* 37**,** 942-6.

CIECHANOVER, A. & BRUNDIN, P. 2003. The ubiquitin proteasome system in neurodegenerative diseases: sometimes the chicken, sometimes the egg. *Neuron,* 40**,** 427-46.

CLARK, I. E., DODSON, M. W., JIANG, C., CAO, J. H., HUH, J. R., SEOL, J. H., YOO, S. J., HAY, B. A. & GUO, M. 2006. Drosophila pink1 is required for mitochondrial function and interacts genetically with parkin. *Nature,* 441**,** 1162-6.

COCHRAN, B. H., REFFEL, A. C. & STILES, C. D. 1983. Molecular cloning of gene sequences regulated by platelet-derived growth factor. *Cell,* 33**,** 939-47.

COLLINS, C. A., WAIRKAR, Y. P., JOHNSON, S. L. & DIANTONIO, A. 2006. Highwire restrains synaptic growth by attenuating a MAP kinase signal. *Neuron,* 51**,** 57-69.

COLOMBO, A., REPICI, M., PESARESI, M., SANTAMBROGIO, S., FORLONI, G. & BORSELLO, T. 2007. The TAT-JNK inhibitor peptide interferes with beta amyloid protein stability. *Cell Death Differ,* 14**,** 1845-8.

COOK, J. C. & CHOCK, P. B. 1992. Isoforms of mammalian ubiquitin-activating enzyme. *J Biol Chem,* 267**,** 24315-21.

CROCKER, S. J., LAMBA, W. R., SMITH, P. D., CALLAGHAN, S. M., SLACK, R. S., ANISMAN, H. & PARK, D. S. 2001. c-Jun mediates axotomy-induced dopamine neuron death in vivo. *Proceedings of the National Academy of Sciences of the United States of America,* 98**,** 13385-90.

CURRAN, T. 1992. Fos and Jun: oncogenic transcription factors. *Tohoku J Exp Med,* 168**,** 169-74.

CURRAN, T., MILLER, A. D., ZOKAS, L. & VERMA, I. M. 1984. Viral and cellular fos proteins: a comparative analysis. *Cell,* 36**,** 259-68.

CURRAN, T. & MORGAN, J. I. 1995. Fos: an immediate-early transcription factor in neurons. *Journal of neurobiology,* 26**,** 403-12.

DAGDA, R. K., ZHU, J., KULICH, S. M. & CHU, C. T. 2008. Mitochondrially localized ERK2 regulates mitophagy and autophagic cell stress: implications for Parkinson's disease. *Autophagy,* 4**,** 770-82.

DAL-CIM, T., MOLZ, S., EGEA, J., PARADA, E., ROMERO, A., BUDNI, J., MARTIN DE SAAVEDRA, M. D., DEL BARRIO, L., TASCA, C. I. & LOPEZ, M. G. 2012. Guanosine protects human neuroblastoma SH-SY5Y cells against mitochondrial oxidative stress by inducing heme oxigenase-1 via PI3K/Akt/GSK-3beta pathway. *Neurochem Int,* 61**,** 397-404.

DAVIS, R. J. 2000. Signal transduction by the JNK group of MAP kinases. *Cell,* 103**,** 239-52.

DE PALMA, G., MOZZONI, P., MUTTI, A., CALZETTI, S. & NEGROTTI, A. 1998. Case-control study of interactions between genetic and environmental factors in Parkinson's disease. *Lancet,* 352**,** 1986-7.

DEAS, E., WOOD, N. W. & PLUN-FAVREAU, H. 2011. Mitophagy and Parkinson's disease: the PINK1-parkin link. *Biochimica et biophysica acta,* 1813**,** 623-33.

DENG, H., WU, Y. & JANKOVIC, J. 2015. The EIF4G1 gene and Parkinson's disease. *Acta Neurol Scand,* 132**,** 73-8.

DESTEFANO, A. L., LEW, M. F., GOLBE, L. I., MARK, M. H., LAZZARINI, A. M., GUTTMAN, M., MONTGOMERY, E., WATERS, C. H., SINGER, C., WATTS, R. L., CURRIE, L. J., WOOTEN, G. F., MAHER, N. E., WILK, J. B., SULLIVAN, K. M., SLATER, K. M., SAINT-HILAIRE, M. H., FELDMAN, R. G., SUCHOWERSKY, O., LAFONTAINE, A. L., LABELLE, N., GROWDON, J. H., VIEREGGE, P., PRAMSTALLER, P. P., KLEIN, C., HUBBLE, J. P., REIDER, C. R., STACY, M., MACDONALD, M. E., GUSELLA, J. F. & MYERS, R. H. 2002. PARK3 influences age at onset in Parkinson disease: a genome scan in the GenePD study. *Am J Hum Genet,* 70**,** 1089-95.

DI FONZO, A., DEKKER, M. C., MONTAGNA, P., BARUZZI, A., YONOVA, E. H., CORREIA GUEDES, L., SZCZERBINSKA, A., ZHAO, T., DUBBEL-HULSMAN, L. O., WOUTERS, C. H., DE GRAAFF, E., OYEN, W. J., SIMONS, E. J., BREEDVELD, G. J., OOSTRA, B. A., HORSTINK, M. W. & BONIFATI, V. 2009. FBXO7 mutations cause autosomal recessive, early-onset parkinsonian-pyramidal syndrome. *Neurology,* 72**,** 240-5.

DICK, F. D., DE PALMA, G., AHMADI, A., SCOTT, N. W., PRESCOTT, G. J., BENNETT, J., SEMPLE, S., DICK, S., COUNSELL, C., MOZZONI, P., HAITES, N., WETTINGER, S. B., MUTTI, A., OTELEA, M., SEATON, A., SODERKVIST, P. & FELICE, A. 2007. Environmental risk factors for Parkinson's disease and parkinsonism: the Geoparkinson study. *Occup Environ Med,* 64**,** 666-72.

DOUDNA, J. A. & CHARPENTIER, E. 2014. Genome editing. The new frontier of genome engineering with CRISPR-Cas9. *Science,* 346**,** 1258096.

DRAGO, J., GERFEN, C. R., LACHOWICZ, J. E., STEINER, H., HOLLON, T. R., LOVE, P. E., OOI, G. T., GRINBERG, A., LEE, E. J., HUANG, S. P. & ET AL. 1994. Altered striatal function in a mutant mouse lacking D1A dopamine receptors. *Proc Natl Acad Sci U S A,* 91**,** 12564-8.

ENCINAS, M., IGLESIAS, M., LIU, Y., WANG, H., MUHAISEN, A., CENA, V., GALLEGO, C. & COMELLA, J. X. 2000. Sequential treatment of SH-SY5Y cells with retinoic acid and brain-derived neurotrophic factor gives rise to fully differentiated, neurotrophic factor-dependent, human neuron-like cells. *Journal of neurochemistry,* 75**,** 991-1003.

ESPOSITO, C. L., D'ALESSIO, A., DE FRANCISCIS, V. & CERCHIA, L. 2008. A cross-talk between TrkB and Ret tyrosine kinases receptors mediates neuroblastoma cells differentiation. *PloS one,* 3**,** e1643.

FARRER, M., WAVRANT-DE VRIEZE, F., CROOK, R., BOLES, L., PEREZ-TUR, J., HARDY, J., JOHNSON, W. G., STEELE, J., MARAGANORE, D., GWINN, K. & LYNCH, T. 1998. Low frequency of alpha-synuclein mutations in familial Parkinson's disease. *Annals of neurology,* 43**,** 394-7.

FARRER, M. J., HAUGARVOLL, K., ROSS, O. A., STONE, J. T., MILKOVIC, N. M., COBB, S. A., WHITTLE, A. J., LINCOLN, S. J., HULIHAN, M. M., HECKMAN, M. G., WHITE, L. R., AASLY, J. O., GIBSON, J. M., GOSAL, D., LYNCH, T., WSZOLEK, Z. K., UITTI, R. J. & TOFT, M. 2006. Genomewide association, Parkinson disease, and PARK10. *Am J Hum Genet,* 78**,** 1084-8; author reply 1092-4.

FENG, Z., LI, L., NG, P. Y. & PORTER, A. G. 2002. Neuronal differentiation and protection from nitric oxide-induced apoptosis require c-Jun-dependent expression of NCAM140. *Mol Cell Biol,* 22**,** 5357-66.

FERRARA, P., ANDERMARCHER, E., BOSSIS, G., ACQUAVIVA, C., BROCKLY, F., JARIEL-ENCONTRE, I. & PIECHACZYK, M. 2003. The structural

determinants responsible for c-Fos protein proteasomal degradation differ according to the conditions of expression. *Oncogene,* 22**,** 1461-74.

FEY, D., CROUCHER, D. R., KOLCH, W. & KHOLODENKO, B. N. 2012. Crosstalk and signaling switches in mitogen-activated protein kinase cascades. *Front Physiol,* 3**,** 355.

FINEBERG, N. A., HADDAD, P. M., CARPENTER, L., GANNON, B., SHARPE, R., YOUNG, A. H., JOYCE, E., ROWE, J., WELLSTED, D., NUTT, D. J. & SAHAKIAN, B. J. 2013. The size, burden and cost of disorders of the brain in the UK. *J Psychopharmacol,* 27**,** 761-70.

FLINN, L., MORTIBOYS, H., VOLKMANN, K., KOSTER, R. W., INGHAM, P. W. & BANDMANN, O. 2009. Complex I deficiency and dopaminergic neuronal cell loss in parkin-deficient zebrafish (Danio rerio). *Brain,* 132**,** 1613-23.

FUCHS, S. Y., DOLAN, L., DAVIS, R. J. & RONAI, Z. 1996. Phosphorylation-dependent targeting of c-Jun ubiquitination by Jun N-kinase. *Oncogene,* 13**,** 1531-5.

FUCHS, S. Y., XIE, B., ADLER, V., FRIED, V. A., DAVIS, R. J. & RONAI, Z. 1997. c-Jun NH2-terminal kinases target the ubiquitination of their associated transcription factors. *J Biol Chem,* 272**,** 32163-8.

FUJIWARA, H., HASEGAWA, M., DOHMAE, N., KAWASHIMA, A., MASLIAH, E., GOLDBERG, M. S., SHEN, J., TAKIO, K. & IWATSUBO, T. 2002. alpha-Synuclein is phosphorylated in synucleinopathy lesions. *Nat Cell Biol,* 4**,** 160-4.

FULDA, S., GORMAN, A. M., HORI, O. & SAMALI, A. 2010. Cellular stress responses: cell survival and cell death. *Int J Cell Biol,* 2010**,** 214074.

FUNAYAMA, M., HASEGAWA, K., KOWA, H., SAITO, M., TSUJI, S. & OBATA, F. 2002. A new locus for Parkinson's disease (PARK8) maps to chromosome 12p11.2-q13.1. *Ann Neurol,* 51**,** 296-301.

FURUHATA, M., TAKADA, E., NOGUCHI, T., ICHIJO, H. & MIZUGUCHI, J. 2009. Apoptosis signal-regulating kinase (ASK)-1 mediates apoptosis through activation of JNK1 following engagement of membrane immunoglobulin. *Exp Cell Res,* 315**,** 3467-76.

GALINDO, M. F., JORDAN, J., GONZALEZ-GARCIA, C. & CENA, V. 2003. Chromaffin cell death induced by 6-hydroxydopamine is independent of mitochondrial swelling and caspase activation. *Journal of neurochemistry,* 84**,** 1066-73.

GALLAGHER, E., GAO, M., LIU, Y. C. & KARIN, M. 2006. Activation of the E3 ubiquitin ligase Itch through a phosphorylation-induced conformational change. *Proc Natl Acad Sci U S A,* 103**,** 1717-22.

GALVIN, J. E., LEE, V. M. & TROJANOWSKI, J. Q. 2001. Synucleinopathies: clinical and pathological implications. *Arch Neurol,* 58**,** 186-90.

GANGULY, A., OO, T. F., RZHETSKAYA, M., PRATT, R., YARYGINA, O., MOMOI, T., KHOLODILOV, N. & BURKE, R. E. 2004. CEP11004, a novel inhibitor of the mixed lineage kinases, suppresses apoptotic death in dopamine neurons of the substantia nigra induced by 6-hydroxydopamine. *Journal of neurochemistry,* 88**,** 469-80.

GANTOIS, I., FANG, K., JIANG, L., BABOVIC, D., LAWRENCE, A. J., FERRERI, V., TEPER, Y., JUPP, B., ZIEBELL, J., MORGANTI-KOSSMANN, C. M., O'BRIEN, T. J., NALLY, R., SCHUTZ, G., WADDINGTON, J., EGAN, G. F. & DRAGO, J. 2007. Ablation of D1 dopamine receptor-expressing cells generates mice with seizures, dystonia, hyperactivity, and impaired oral behavior. *Proc Natl Acad Sci U S A,* 104**,** 4182-7.

GAO, M., LABUDA, T., XIA, Y., GALLAGHER, E., FANG, D., LIU, Y. C. & KARIN, M. 2004. Jun turnover is controlled through JNK-dependent phosphorylation of the E3 ligase Itch. *Science,* 306**,** 271-5.

GASSER, T., MULLER-MYHSOK, B., WSZOLEK, Z. K., OEHLMANN, R., CALNE, D. B., BONIFATI, V., BEREZNAI, B., FABRIZIO, E., VIEREGGE, P. & HORSTMANN, R. D. 1998. A susceptibility locus for Parkinson's disease maps to chromosome 2p13. *Nat Genet,* 18**,** 262-5.

GAUTIER, C. A., KITADA, T. & SHEN, J. 2008. Loss of PINK1 causes mitochondrial functional defects and increased sensitivity to oxidative stress. *Proc Natl Acad Sci U S A,* 105**,** 11364-9.

GEARAN, T., CASTILLO, O. A. & SCHWARZSCHILD, M. A. 2001. The parkinsonian neurotoxin, MPP+ induces phosphorylated c-Jun in dopaminergric neurons of mesencephalic cultures. *Parkinsonism Relat Disord,* 8**,** 19-22.

GEGG, M. E., COOPER, J. M., CHAU, K. Y., ROJO, M., SCHAPIRA, A. H. & TAANMAN, J. W. 2010. Mitofusin 1 and mitofusin 2 are ubiquitinated in a PINK1/parkin-dependent manner upon induction of mitophagy. *Hum Mol Genet,* 19**,** 4861-70.

GEISLER, S., HOLMSTROM, K. M., SKUJAT, D., FIESEL, F. C., ROTHFUSS, O. C., KAHLE, P. J. & SPRINGER, W. 2010. PINK1/Parkin-mediated mitophagy is dependent on VDAC1 and p62/SQSTM1. *Nature cell biology,* 12**,** 119-31.

GENECARDS. 2016. Available: http://www.genecards.org/ [Accessed 2016].

GERMAN, D. C. & MANAYE, K. F. 1993. Midbrain dopaminergic neurons (nuclei A8, A9, and A10): three-dimensional reconstruction in the rat. *J Comp Neurol,* 331**,** 297-309.

GIL, G. A., BUSSOLINO, D. F., PORTAL, M. M., ALFONSO PECCHIO, A., RENNER, M. L., BORIOLI, G. A., GUIDO, M. E. & CAPUTTO, B. L. 2004. c-Fos activated phospholipid synthesis is required for neurite elongation in differentiating PC12 cells. *Molecular biology of the cell,* 15**,** 1881-94.

GILLE, H., KORTENJANN, M., THOMAE, O., MOOMAW, C., SLAUGHTER, C., COBB, M. H. & SHAW, P. E. 1995. ERK phosphorylation potentiates Elk-1-mediated ternary complex formation and transactivation. *The EMBO journal,* 14**,** 951-62.

GIRAULT, J. A. & GREENGARD, P. 2004. The neurobiology of dopamine signaling. *Arch Neurol,* 61**,** 641-4.

GLATER, E. E., MEGEATH, L. J., STOWERS, R. S. & SCHWARZ, T. L. 2006. Axonal transport of mitochondria requires milton to recruit kinesin heavy chain and is light chain independent. *J Cell Biol,* 173**,** 545-57.

GLOVER, J. N. & HARRISON, S. C. 1995. Crystal structure of the heterodimeric bZIP transcription factor c-Fos-c-Jun bound to DNA. *Nature,* 373**,** 257-61.

GOMEZ-LAZARO, M., BONEKAMP, N. A., GALINDO, M. F., JORDAN, J. & SCHRADER, M. 2008. 6-Hydroxydopamine (6-OHDA) induces Drp1-dependent mitochondrial fragmentation in SH-SY5Y cells. *Free radical biology & medicine,* 44**,** 1960-9.

GOMEZ-SANCHEZ, R., GEGG, M. E., BRAVO-SAN PEDRO, J. M., NISO-SANTANO, M., ALVAREZ-ERVITI, L., PIZARRO-ESTRELLA, E., GUTIERREZ-MARTIN, Y., ALVAREZ-BARRIENTOS, A., FUENTES, J. M., GONZALEZ-POLO, R. A. & SCHAPIRA, A. H. 2014. Mitochondrial impairment increases FL-PINK1 levels by calcium-dependent gene expression. *Neurobiol Dis,* 62**,** 426-40.

GREENE, J. C., WHITWORTH, A. J., KUO, I., ANDREWS, L. A., FEANY, M. B. & PALLANCK, L. J. 2003. Mitochondrial pathology and apoptotic muscle degeneration in Drosophila parkin mutants. *Proc Natl Acad Sci U S A,* 100**,** 4078-83.

GROSS, A., JOCKEL, J., WEI, M. C. & KORSMEYER, S. J. 1998. Enforced dimerization of BAX results in its translocation, mitochondrial dysfunction and apoptosis. *EMBO J,* 17**,** 3878-85.

GROUP, H. C. 1993. A novel gene containing a trinucleotide repeat that is expanded and unstable on Huntington's disease chromosomes. The Huntington's Disease Collaborative Research Group. *Cell,* 72**,** 971-83.

GRUNEWALD, A., VOGES, L., RAKOVIC, A., KASTEN, M., VANDEBONA, H., HEMMELMANN, C., LOHMANN, K., OROLICKI, S., RAMIREZ, A., SCHAPIRA, A. H., PRAMSTALLER, P. P., SUE, C. M. & KLEIN, C. 2010. Mutant Parkin impairs mitochondrial function and morphology in human fibroblasts. *PLoS One,* 5**,** e12962.

GUPTA, S., BARRETT, T., WHITMARSH, A. J., CAVANAGH, J., SLUSS, H. K., DERIJARD, B. & DAVIS, R. J. 1996. Selective interaction of JNK protein kinase isoforms with transcription factors. *The EMBO journal,* 15**,** 2760-70.

GUSTAVSSON, A., SVENSSON, M., JACOBI, F., ALLGULANDER, C., ALONSO, J., BEGHI, E., DODEL, R., EKMAN, M., FARAVELLI, C., FRATIGLIONI, L., GANNON, B., JONES, D. H., JENNUM, P., JORDANOVA, A., JONSSON, L., KARAMPAMPA, K., KNAPP, M., KOBELT, G., KURTH, T., LIEB, R., LINDE, M., LJUNGCRANTZ, C., MAERCKER, A., MELIN, B., MOSCARELLI, M., MUSAYEV, A., NORWOOD, F., PREISIG, M., PUGLIATTI, M., REHM, J., SALVADOR-CARULLA, L., SCHLEHOFER, B., SIMON, R., STEINHAUSEN, H. C., STOVNER, L. J., VALLAT, J. M., VAN DEN BERGH, P., VAN OS, J., VOS, P., XU, W., WITTCHEN, H. U., JONSSON, B. & OLESEN, J. 2011. Cost of disorders of the brain in Europe 2010. *Eur Neuropsychopharmacol,* 21**,** 718-79.

HAAS, A. L., WARMS, J. V., HERSHKO, A. & ROSE, I. A. 1982. Ubiquitin-activating enzyme. Mechanism and role in protein-ubiquitin conjugation. *J Biol Chem,* 257**,** 2543-8.

HAILEY, D. W., RAMBOLD, A. S., SATPUTE-KRISHNAN, P., MITRA, K., SOUGRAT, R., KIM, P. K. & LIPPINCOTT-SCHWARTZ, J. 2010. Mitochondria supply membranes for autophagosome biogenesis during starvation. *Cell,* 141**,** 656-67.

HALAZONETIS, T. D., GEORGOPOULOS, K., GREENBERG, M. E. & LEDER, P. 1988. c-Jun dimerizes with itself and with c-Fos, forming complexes of different DNA binding affinities. *Cell,* 55**,** 917-24.

HAM, J., BABIJ, C., WHITFIELD, J., PFARR, C. M., LALLEMAND, D., YANIV, M. & RUBIN, L. L. 1995. A c-Jun dominant negative mutant protects sympathetic neurons against programmed cell death. *Neuron,* 14**,** 927-39.

HAM, J., EILERS, A., WHITFIELD, J., NEAME, S. J. & SHAH, B. 2000. c-Jun and the transcriptional control of neuronal apoptosis. *Biochem Pharmacol,* 60**,** 1015-21.

HAMDANE, M., SAMBO, A. V., DELOBEL, P., BEGARD, S., VIOLLEAU, A., DELACOURTE, A., BERTRAND, P., BENAVIDES, J. & BUEE, L. 2003. Mitotic-like tau phosphorylation by p25-Cdk5 kinase complex. *J Biol Chem,* 278**,** 34026-34.

HARA, T., NAKAMURA, K., MATSUI, M., YAMAMOTO, A., NAKAHARA, Y., SUZUKI-MIGISHIMA, R., YOKOYAMA, M., MISHIMA, K., SAITO, I., OKANO, H. & MIZUSHIMA, N. 2006. Suppression of basal autophagy in neural cells causes neurodegenerative disease in mice. *Nature,* 441**,** 885-9.

HARDY, J. 2009. The amyloid hypothesis for Alzheimer's disease: a critical reappraisal. *Journal of neurochemistry,* 110**,** 1129-34.

HARDY, J. & ALLSOP, D. 1991. Amyloid deposition as the central event in the aetiology of Alzheimer's disease. *Trends Pharmacol Sci,* 12**,** 383-8.

HARDY, J. A. & HIGGINS, G. A. 1992. Alzheimer's disease: the amyloid cascade hypothesis. *Science,* 256**,** 184-5.

HASEGAWA, M., FUJIWARA, H., NONAKA, T., WAKABAYASHI, K., TAKAHASHI, H., LEE, V. M., TROJANOWSKI, J. Q., MANN, D. & IWATSUBO, T. 2002. Phosphorylated alpha-synuclein is ubiquitinated in alpha-synucleinopathy lesions. *J Biol Chem,* 277**,** 49071-6.

HEALY, D. G., ABOU-SLEIMAN, P. M., CASAS, J. P., AHMADI, K. R., LYNCH, T., GANDHI, S., MUQIT, M. M., FOLTYNIE, T., BARKER, R., BHATIA, K. P., QUINN, N. P., LEES, A. J., GIBSON, J. M., HOLTON, J. L., REVESZ, T., GOLDSTEIN, D. B. & WOOD, N. W. 2006. UCHL-1 is not a Parkinson's disease susceptibility gene. *Ann Neurol,* 59**,** 627-33.

HESS, J., ANGEL, P. & SCHORPP-KISTNER, M. 2004. AP-1 subunits: quarrel and harmony among siblings. *Journal of cell science,* 117**,** 5965-73.

HICKS, A. A., PETURSSON, H., JONSSON, T., STEFANSSON, H., JOHANNSDOTTIR, H. S., SAINZ, J., FRIGGE, M. L., KONG, A., GULCHER, J. R., STEFANSSON, K. & SVEINBJORNSDOTTIR, S. 2002. A susceptibility gene for late-onset idiopathic Parkinson's disease. *Ann Neurol,* 52**,** 549-55.

HIROI, N., MAREK, G. J., BROWN, J. R., YE, H., SAUDOU, F., VAIDYA, V. A., DUMAN, R. S., GREENBERG, M. E. & NESTLER, E. J. 1998. Essential role of the fosB gene in molecular, cellular, and behavioral actions of chronic electroconvulsive seizures. *J Neurosci,* 18**,** 6952-62.

HISAHARA, S. & SHIMOHAMA, S. 2011. Dopamine receptors and Parkinson's disease. *Int J Med Chem,* 2011**,** 403039.

HOLLENBECK, P. J. & SAXTON, W. M. 2005. The axonal transport of mitochondria. *J Cell Sci,* 118**,** 5411-9.

HOLLVILLE, E., CARROLL, R. G., CULLEN, S. P. & MARTIN, S. J. 2014. Bcl-2 family proteins participate in mitochondrial quality control by regulating Parkin/PINK1-dependent mitophagy. *Molecular cell,* 55**,** 451-66.

HRISTOVA, V. A., BEASLEY, S. A., RYLETT, R. J. & SHAW, G. S. 2009. Identification of a novel Zn2+-binding domain in the autosomal recessive juvenile Parkinson-related E3 ligase parkin. *J Biol Chem,* 284**,** 14978-86.

HSU, P. D., LANDER, E. S. & ZHANG, F. 2014. Development and applications of CRISPR-Cas9 for genome engineering. *Cell,* 157**,** 1262-78.

HUNG, C. C. 2007. *In Vitro Model Systems of Alpha-Synuclein Over-expression.* PhD Thesis, The University of Leeds.

HUNOT, S., VILA, M., TEISMANN, P., DAVIS, R. J., HIRSCH, E. C., PRZEDBORSKI, S., RAKIC, P. & FLAVELL, R. A. 2004. JNK-mediated induction of cyclooxygenase 2 is required for neurodegeneration in a mouse model of Parkinson's disease. *Proceedings of the National Academy of Sciences of the United States of America,* 101**,** 665-70.

HUSSAIN, M., BABAR, M. E., HUSSAIN, T., NADEEM, A., NIAZ, S. & MEHBOOB, R. 2014. Novel R42C mutation identified in Early Onset of Parkinson's disease in Pakistani Patients. *HealthMED,* 8**,** 1073-1078.

HWANG, S., KIM, D., CHOI, G., AN, S. W., HONG, Y. K., SUH, Y. S., LEE, M. J. & CHO, K. S. 2010. Parkin suppresses c-Jun N-terminal kinase-induced cell death via transcriptional regulation in Drosophila. *Mol Cells,* 29**,** 575-80.

IBANEZ, P., LESAGE, S., JANIN, S., LOHMANN, E., DURIF, F., DESTEE, A., BONNET, A. M., BREFEL-COURBON, C., HEATH, S., ZELENIKA, D., AGID, Y., DURR, A. & BRICE, A. 2009. Alpha-synuclein gene rearrangements in dominantly inherited parkinsonism: frequency, phenotype, and mechanisms. *Arch Neurol,* 66**,** 102-8.

IKEDA, F. & DIKIC, I. 2008. Atypical ubiquitin chains: new molecular signals. 'Protein Modifications: Beyond the Usual Suspects' review series. *EMBO Rep,* 9**,** 536-42.

IMAM, S. Z., ZHOU, Q., YAMAMOTO, A., VALENTE, A. J., ALI, S. F., BAINS, M., ROBERTS, J. L., KAHLE, P. J., CLARK, R. A. & LI, S. 2011. Novel regulation of parkin function through c-Abl-mediated tyrosine phosphorylation: implications for Parkinson's disease. *The Journal of neuroscience : the official journal of the Society for Neuroscience,* 31**,** 157-63.

INVESTIGATORS, N. N.-P. 2007. A randomized clinical trial of coenzyme Q10 and GPI-1485 in early Parkinson disease. *Neurology,* 68**,** 20-8.

ISOYAMA, T., MURAYAMA, A., NOMOTO, A. & KUGE, S. 2001. Nuclear import of the yeast AP-1-like transcription factor Yap1p is mediated by transport receptor Pse1p, and this import step is not affected by oxidative stress. *The Journal of biological chemistry,* 276**,** 21863-9.

ITOH, K., NAKAMURA, K., IIJIMA, M. & SESAKI, H. 2013. Mitochondrial dynamics in neurodegeneration. *Trends Cell Biol,* 23**,** 64-71.

JANKOVIC, J. & AGUILAR, L. G. 2008. Current approaches to the treatment of Parkinson's disease. *Neuropsychiatr Dis Treat,* 4**,** 743-57.

JIANG, H., REN, Y., ZHAO, J. & FENG, J. 2004. Parkin protects human dopaminergic neuroblastoma cells against dopamine-induced apoptosis. *Human molecular genetics,* 13**,** 1745-54.

JIN, H. O., PARK, I. C., AN, S., LEE, H. C., WOO, S. H., HONG, Y. J., LEE, S. J., PARK, M. J., YOO, D. H., RHEE, C. H. & HONG, S. I. 2006. Up-regulation of Bak and Bim via JNK downstream pathway in the response to nitric oxide in human glioblastoma cells. *J Cell Physiol,* 206**,** 477-86.

JOHNSON, G. L. & NAKAMURA, K. 2007. The c-jun kinase/stress-activated pathway: regulation, function and role in human disease. *Biochimica et biophysica acta,* 1773**,** 1341-8.

KALLUNKI, T., DENG, T., HIBI, M. & KARIN, M. 1996. c-Jun can recruit JNK to phosphorylate dimerization partners via specific docking interactions. *Cell,* 87**,** 929-39.

KANE, L. A., LAZAROU, M., FOGEL, A. I., LI, Y., YAMANO, K., SARRAF, S. A., BANERJEE, S. & YOULE, R. J. 2014. PINK1 phosphorylates ubiquitin to activate Parkin E3 ubiquitin ligase activity. *J Cell Biol,* 205**,** 143-53.

KANERVA, K., URONEN, R. L., BLOM, T., LI, S., BITTMAN, R., LAPPALAINEN, P., PERANEN, J., RAPOSO, G. & IKONEN, E. 2013. LDL cholesterol recycles to the plasma membrane via a Rab8a-Myosin5b-actin-dependent membrane transport route. *Dev Cell,* 27**,** 249-62.

KAPLAN, D. R. & MILLER, F. D. 2000. Neurotrophin signal transduction in the nervous system. *Curr Opin Neurobiol,* 10**,** 381-91.

KARRAN, E. & HARDY, J. 2014. A critique of the drug discovery and phase 3 clinical programs targeting the amyloid hypothesis for Alzheimer disease. *Annals of neurology,* 76**,** 185-205.

KASHATUS, J. A., NASCIMENTO, A., MYERS, L. J., SHER, A., BYRNE, F. L., HOEHN, K. L., COUNTER, C. M. & KASHATUS, D. F. 2015. Erk2 phosphorylation of Drp1 promotes mitochondrial fission and MAPK-driven tumor growth. *Mol Cell,* 57**,** 537-51.

KERPPOLA, T. K. & CURRAN, T. 1991a. DNA bending by Fos and Jun: the flexible hinge model. *Science,* 254**,** 1210-4.

KERPPOLA, T. K. & CURRAN, T. 1991b. Fos-Jun heterodimers and Jun homodimers bend DNA in opposite orientations: implications for transcription factor cooperativity. *Cell,* 66**,** 317-26.

KERPPOLA, T. K. & CURRAN, T. 1993. Selective DNA bending by a variety of bZIP proteins. *Mol Cell Biol,* 13**,** 5479-89.

KERR, J. F., WYLLIE, A. H. & CURRIE, A. R. 1972. Apoptosis: a basic biological phenomenon with wide-ranging implications in tissue kinetics. *Br J Cancer,* 26**,** 239-57.

KIRKIN, V., MCEWAN, D. G., NOVAK, I. & DIKIC, I. 2009. A role for ubiquitin in selective autophagy. *Mol Cell,* 34**,** 259-69.

KITADA, T., ASAKAWA, S., HATTORI, N., MATSUMINE, H., YAMAMURA, Y., MINOSHIMA, S., YOKOCHI, M., MIZUNO, Y. & SHIMIZU, N. 1998. Mutations in the parkin gene cause autosomal recessive juvenile parkinsonism. *Nature,* 392**,** 605-8.

KLEIN, C. & SCHLOSSMACHER, M. G. 2006. The genetics of Parkinson disease: Implications for neurological care. *Nat Clin Pract Neurol,* 2**,** 136-46.

KLEIN, C. & WESTENBERGER, A. 2012. Genetics of Parkinson's disease. *Cold Spring Harb Perspect Med,* 2**,** a008888.

KLEIN, R., NANDURI, V., JING, S. A., LAMBALLE, F., TAPLEY, P., BRYANT, S., CORDON-CARDO, C., JONES, K. R., REICHARDT, L. F. & BARBACID, M. 1991. The trkB tyrosine protein kinase is a receptor for brain-derived neurotrophic factor and neurotrophin-3. *Cell,* 66**,** 395-403.

KO, H. S., LEE, Y., SHIN, J. H., KARUPPAGOUNDER, S. S., GADAD, B. S., KOLESKE, A. J., PLETNIKOVA, O., TRONCOSO, J. C., DAWSON, V. L. & DAWSON, T. M. 2010. Phosphorylation by the c-Abl protein tyrosine kinase inhibits parkin's ubiquitination and protective function. *Proceedings of the National Academy of Sciences of the United States of America,* 107**,** 16691-6.

KOEGL, M., HOPPE, T., SCHLENKER, S., ULRICH, H. D., MAYER, T. U. & JENTSCH, S. 1999. A novel ubiquitination factor, E4, is involved in multiubiquitin chain assembly. *Cell,* 96**,** 635-44.

KOMATSU, M., WAGURI, S., CHIBA, T., MURATA, S., IWATA, J., TANIDA, I., UENO, T., KOIKE, M., UCHIYAMA, Y., KOMINAMI, E. & TANAKA, K. 2006. Loss of autophagy in the central nervous system causes neurodegeneration in mice. *Nature,* 441**,** 880-4.

KONDAPALLI, C., KAZLAUSKAITE, A., ZHANG, N., WOODROOF, H. I., CAMPBELL, D. G., GOURLAY, R., BURCHELL, L., WALDEN, H., MACARTNEY, T. J., DEAK, M., KNEBEL, A., ALESSI, D. R. & MUQIT, M. M. 2012. PINK1 is activated by

mitochondrial membrane potential depolarization and stimulates Parkin E3 ligase activity by phosphorylating Serine 65. *Open Biol,* 2**,** 120080.

KOVARY, K. & BRAVO, R. 1991. Expression of different Jun and Fos proteins during the G0-to-G1 transition in mouse fibroblasts: in vitro and in vivo associations. *Mol Cell Biol,* 11**,** 2451-9.

KOYANO, F., OKATSU, K., KOSAKO, H., TAMURA, Y., GO, E., KIMURA, M., KIMURA, Y., TSUCHIYA, H., YOSHIHARA, H., HIROKAWA, T., ENDO, T., FON, E. A., TREMPE, J. F., SAEKI, Y., TANAKA, K. & MATSUDA, N. 2014. Ubiquitin is phosphorylated by PINK1 to activate parkin. *Nature,* 510**,** 162-6.

KRISHNA, A., BIRYUKOV, M., TREFOIS, C., ANTONY, P. M., HUSSONG, R., LIN, J., HEINANIEMI, M., GLUSMAN, G., KOGLSBERGER, S., BOYD, O., VAN DEN BERG, B. H., LINKE, D., HUANG, D., WANG, K., HOOD, L., THOLEY, A., SCHNEIDER, R., GALAS, D. J., BALLING, R. & MAY, P. 2014. Systems genomics evaluation of the SH-SY5Y neuroblastoma cell line as a model for Parkinson's disease. *BMC Genomics,* 15**,** 1154.

KRUGER, R., SHARMA, M., RIESS, O., GASSER, T., VAN BROECKHOVEN, C., THEUNS, J., AASLY, J., ANNESI, G., BENTIVOGLIO, A. R., BRICE, A., DJARMATI, A., ELBAZ, A., FARRER, M., FERRARESE, C., GIBSON, J. M., HADJIGEORGIOU, G. M., HATTORI, N., IOANNIDIS, J. P., JASINSKA-MYGA, B., KLEIN, C., LAMBERT, J. C., LESAGE, S., LIN, J. J., LYNCH, T., MELLICK, G. D., DE NIGRIS, F., OPALA, G., PRIGIONE, A., QUATTRONE, A., ROSS, O. A., SATAKE, W., SILBURN, P. A., TAN, E. K., TODA, T., TOMIYAMA, H., WIRDEFELDT, K., WSZOLEK, Z., XIROMERISIOU, G., MARAGANORE, D. M. & GENETIC EPIDEMIOLOGY OF PARKINSON'S DISEASE, C. 2011. A large-scale genetic association study to evaluate the contribution of Omi/HtrA2 (PARK13) to Parkinson's disease. *Neurobiol Aging,* 32**,** 548 e9-18.

KUGE, S., ARITA, M., MURAYAMA, A., MAETA, K., IZAWA, S., INOUE, Y. & NOMOTO, A. 2001. Regulation of the yeast Yap1p nuclear export signal is mediated by redox signal-induced reversible disulfide bond formation. *Mol Cell Biol,* 21**,** 6139-50.

KUGE, S., JONES, N. & NOMOTO, A. 1997. Regulation of yAP-1 nuclear localization in response to oxidative stress. *The EMBO journal,* 16**,** 1710-20.

KUGE, S., TODA, T., IIZUKA, N. & NOMOTO, A. 1998. Crm1 (XpoI) dependent nuclear export of the budding yeast transcription factor yAP-1 is sensitive to oxidative stress. *Genes Cells,* 3**,** 521-32.

KULTZ, D. 2005. Molecular and evolutionary basis of the cellular stress response. *Annu Rev Physiol,* 67**,** 225-57.

KUMARI, U. & TAN, E. K. 2009. LRRK2 in Parkinson's disease: genetic and clinical studies from patients. *FEBS J,* 276**,** 6455-63.

KUZUHARA, S., MORI, H., IZUMIYAMA, N., YOSHIMURA, M. & IHARA, Y. 1988. Lewy bodies are ubiquitinated. A light and electron microscopic immunocytochemical study. *Acta Neuropathol,* 75**,** 345-53.

KYRIAKIS, J. M. & AVRUCH, J. 2012. Mammalian MAPK signal transduction pathways activated by stress and inflammation: a 10-year update. *Physiol Rev,* 92**,** 689-737.

LANGSTON, J. W., BALLARD, P., TETRUD, J. W. & IRWIN, I. 1983. Chronic Parkinsonism in humans due to a product of meperidine-analog synthesis. *Science,* 219**,** 979-80.

LAZARO, D. F., RODRIGUES, E. F., LANGOHR, R., SHAHPASANDZADEH, H., RIBEIRO, T., GUERREIRO, P., GERHARDT, E., KROHNERT, K., KLUCKEN, J., PEREIRA, M. D., POPOVA, B., KRUSE, N., MOLLENHAUER, B., RIZZOLI, S. O., BRAUS, G. H., DANZER, K. M. & OUTEIRO, T. F. 2014. Systematic comparison of the effects of alpha-synuclein mutations on its oligomerization and aggregation. *PLoS Genet,* 10**,** e1004741.

LEBOUCHER, G. P., TSAI, Y. C., YANG, M., SHAW, K. C., ZHOU, M., VEENSTRA, T. D., GLICKMAN, M. H. & WEISSMAN, A. M. 2012. Stress-induced phosphorylation and proteasomal degradation of mitofusin 2 facilitates mitochondrial fragmentation and apoptosis. *Mol Cell,* 47**,** 547-57.

LEE, D., HUANG, W. & LIM, A. T. 2000. Dopamine induces a biphasic modulation of hypothalamic ANF neurons: a ligand concentration-dependent effect involving D5 and D2 receptor interaction. *Mol Psychiatry,* 5**,** 39-48.

LEE, J. Y., NAGANO, Y., TAYLOR, J. P., LIM, K. L. & YAO, T. P. 2010. Disease-causing mutations in parkin impair mitochondrial ubiquitination, aggregation, and HDAC6-dependent mitophagy. *J Cell Biol,* 189**,** 671-9.

LEE, S., SATO, Y. & NIXON, R. A. 2011a. Lysosomal proteolysis inhibition selectively disrupts axonal transport of degradative organelles and causes an Alzheimer's-like axonal dystrophy. *J Neurosci,* 31**,** 7817-30.

LEE, S., SATO, Y. & NIXON, R. A. 2011b. Primary lysosomal dysfunction causes cargo-specific deficits of axonal transport leading to Alzheimer-like neuritic dystrophy. *Autophagy,* 7**,** 1562-3.

LEHMAN, N. L. 2009. The ubiquitin proteasome system in neuropathology. *Acta Neuropathol,* 118**,** 329-47.

LEPPA, S., ERIKSSON, M., SAFFRICH, R., ANSORGE, W. & BOHMANN, D. 2001. Complex functions of AP-1 transcription factors in differentiation and survival of PC12 cells. *Mol Cell Biol,* 21**,** 4369-78.

LEPPA, S., SAFFRICH, R., ANSORGE, W. & BOHMANN, D. 1998. Differential regulation of c-Jun by ERK and JNK during PC12 cell differentiation. *The EMBO journal,* 17**,** 4404-13.

LEROY, E., BOYER, R., AUBURGER, G., LEUBE, B., ULM, G., MEZEY, E., HARTA, G., BROWNSTEIN, M. J., JONNALAGADA, S., CHERNOVA, T., DEHEJIA, A., LAVEDAN, C., GASSER, T., STEINBACH, P. J., WILKINSON, K. D. & POLYMEROPOULOS, M. H. 1998. The ubiquitin pathway in Parkinson's disease. *Nature,* 395**,** 451-2.

LEVINE, B. & KROEMER, G. 2008. Autophagy in the pathogenesis of disease. *Cell,* 132**,** 27-42.

LEVY, E., CARMAN, M. D., FERNANDEZ-MADRID, I. J., POWER, M. D., LIEBERBURG, I., VAN DUINEN, S. G., BOTS, G. T., LUYENDIJK, W. & FRANGIONE, B. 1990. Mutation of the Alzheimer's disease amyloid gene in hereditary cerebral hemorrhage, Dutch type. *Science,* 248**,** 1124-6.

LI, N., RAGHEB, K., LAWLER, G., STURGIS, J., RAJWA, B., MELENDEZ, J. A. & ROBINSON, J. P. 2003. Mitochondrial complex I inhibitor rotenone induces apoptosis through enhancing mitochondrial reactive oxygen species production. *J Biol Chem,* 278**,** 8516-25.

LI, Y. J., DENG, J., MAYHEW, G. M., GRIMSLEY, J. W., HUO, X. & VANCE, J. M. 2007. Investigation of the PARK10 gene in Parkinson disease. *Ann Hum Genet,* 71**,** 639-47.

LIESA, M., PALACIN, M. & ZORZANO, A. 2009. Mitochondrial dynamics in mammalian health and disease. *Physiol Rev,* 89**,** 799-845.

LIN, M. T. & BEAL, M. F. 2006. Mitochondrial dysfunction and oxidative stress in neurodegenerative diseases. *Nature,* 443**,** 787-95.

LISNOCK, J., GRIFFIN, P., CALAYCAY, J., FRANTZ, B., PARSONS, J., O'KEEFE, S. J. & LOGRASSO, P. 2000. Activation of JNK3 alpha 1 requires both MKK4 and MKK7: kinetic characterization of in vitro phosphorylated JNK3 alpha 1. *Biochemistry,* 39**,** 3141-8.

LIU, G., SGOBIO, C., GU, X., SUN, L., LIN, X., YU, J., PARISIADOU, L., XIE, C., SASTRY, N., DING, J., LOHR, K. M., MILLER, G. W., MATEO, Y., LOVINGER, D. M. & CAI, H. 2015. Selective expression of Parkinson's disease-related Leucine-rich repeat kinase 2 G2019S missense mutation in midbrain dopaminergic neurons impairs dopamine release and dopaminergic gene expression. *Hum Mol Genet,* 24**,** 5299-312.

LIU, H., DENG, X., SHYU, Y. J., LI, J. J., TAPAROWSKY, E. J. & HU, C. D. 2006. Mutual regulation of c-Jun and ATF2 by transcriptional activation and subcellular localization. *The EMBO journal,* 25**,** 1058-69.

LIU, M., ANEJA, R., SUN, X., XIE, S., WANG, H., WU, X., DONG, J. T., LI, M., JOSHI, H. C. & ZHOU, J. 2008. Parkin regulates Eg5 expression by Hsp70 ubiquitination-dependent inactivation of c-Jun NH2-terminal kinase. *The Journal of biological chemistry,* 283**,** 35783-8.

LOCKSHIN, R. A. & WILLIAMS, C. M. 1965. Programmed Cell Death--I. Cytology of Degeneration in the Intersegmental Muscles of the Pernyi Silkmoth. *J Insect Physiol,* 11**,** 123-33.

LOPEZ-BERGAMI, P., HUANG, C., GOYDOS, J. S., YIP, D., BAR-ELI, M., HERLYN, M., SMALLEY, K. S., MAHALE, A., EROSHKIN, A., AARONSON, S. & RONAI, Z. 2007. Rewired ERK-JNK signaling pathways in melanoma. *Cancer Cell,* 11**,** 447-60.

LOTHARIUS, J., BARG, S., WIEKOP, P., LUNDBERG, C., RAYMON, H. K. & BRUNDIN, P. 2002. Effect of mutant alpha-synuclein on dopamine homeostasis in a new human mesencephalic cell line. *J Biol Chem,* 277**,** 38884-94.

LOTHARIUS, J., FALSIG, J., VAN BEEK, J., PAYNE, S., DRINGEN, R., BRUNDIN, P. & LEIST, M. 2005. Progressive degeneration of human mesencephalic neuron-derived cells triggered by dopamine-dependent oxidative stress is dependent on the mixed-lineage kinase pathway. *J Neurosci,* 25**,** 6329-42.

LU, B. 2011. *Mitochondrial Dynamics and Neurodegeneration*, Springer Science & Business Media.

LUO, S., GARCIA-ARENCIBIA, M., ZHAO, R., PURI, C., TOH, P. P., SADIQ, O. & RUBINSZTEIN, D. C. 2012. Bim inhibits autophagy by recruiting Beclin 1 to microtubules. *Mol Cell,* 47**,** 359-70.

LUO, S. & RUBINSZTEIN, D. C. 2013. BCL2L11/BIM: a novel molecular link between autophagy and apoptosis. *Autophagy,* 9**,** 104-5.

LUO, Y., KOKKONEN, G. C., HATTORI, A., CHREST, F. J. & ROTH, G. S. 1999. Dopamine stimulates redox-tyrosine kinase signaling and p38 MAPK in activation of astrocytic C6-D2L cells. *Brain Res,* 850**,** 21-38.

MA, Q. 2013. Role of nrf2 in oxidative stress and toxicity. *Annu Rev Pharmacol Toxicol,* 53**,** 401-26.

MACLEOD, D. A., RHINN, H., KUWAHARA, T., ZOLIN, A., DI PAOLO, G., MCCABE, B. D., MARDER, K. S., HONIG, L. S., CLARK, L. N., SMALL, S. A. & ABELIOVICH, A.

2013. RAB7L1 interacts with LRRK2 to modify intraneuronal protein sorting and Parkinson's disease risk. *Neuron,* 77**,** 425-39.

MADAY, S., WALLACE, K. E. & HOLZBAUR, E. L. 2012. Autophagosomes initiate distally and mature during transport toward the cell soma in primary neurons. *J Cell Biol,* 196**,** 407-17.

MAIURI, M. C., ZALCKVAR, E., KIMCHI, A. & KROEMER, G. 2007. Self-eating and self-killing: crosstalk between autophagy and apoptosis. *Nat Rev Mol Cell Biol,* 8**,** 741-52.

MALKUS, K. A., TSIKA, E. & ISCHIROPOULOS, H. 2009. Oxidative modifications, mitochondrial dysfunction, and impaired protein degradation in Parkinson's disease: how neurons are lost in the Bermuda triangle. *Molecular neurodegeneration,* 4**,** 24.

MALNOU, C. E., SALEM, T., BROCKLY, F., WODRICH, H., PIECHACZYK, M. & JARIEL-ENCONTRE, I. 2007. Heterodimerization with Jun family members regulates c-Fos nucleocytoplasmic traffic. *The Journal of biological chemistry,* 282**,** 31046-59.

MANABE, T., KITAYAMA, T., OGITA, K. & YONEDA, Y. 2000. Differential expression and phosphorylation of particular fos family members by kainate in nuclear and cytosolic fractions of murine hippocampus. *Neuroscience,* 100**,** 453-63.

MANABE, T., OGITA, K., NAKAMICHI, N. & YONEDA, Y. 2001. Differential in vitro degradation of particular Fos family members expressed by kainic acid in nuclear and cytosolic fractions of murine hippocampus. *Journal of neuroscience research,* 64**,** 34-42.

MARSH, H. N., SCHOLZ, W. K., LAMBALLE, F., KLEIN, R., NANDURI, V., BARBACID, M. & PALFREY, H. C. 1993. Signal transduction events mediated by the BDNF receptor gp 145trkB in primary hippocampal pyramidal cell culture. *The Journal of neuroscience : the official journal of the Society for Neuroscience,* 13**,** 4281-92.

MASTROENI, D., GROVER, A., LEONARD, B., JOYCE, J. N., COLEMAN, P. D., KOZIK, B., BELLINGER, D. L. & ROGERS, J. 2009. Microglial responses to dopamine in a cell culture model of Parkinson's disease. *Neurobiology of aging,* 30**,** 1805-17.

MATSUDA, N., SATO, S., SHIBA, K., OKATSU, K., SAISHO, K., GAUTIER, C. A., SOU, Y. S., SAIKI, S., KAWAJIRI, S., SATO, F., KIMURA, M., KOMATSU, M., HATTORI, N. & TANAKA, K. 2010. PINK1 stabilized by mitochondrial depolarization recruits Parkin to damaged mitochondria and activates latent Parkin for mitophagy. *The Journal of cell biology,* 189**,** 211-21.

MATSUDA, W., FURUTA, T., NAKAMURA, K. C., HIOKI, H., FUJIYAMA, F., ARAI, R. & KANEKO, T. 2009. Single nigrostriatal dopaminergic neurons form widely spread and highly dense axonal arborizations in the neostriatum. *J Neurosci,* 29**,** 444-53.

MATSUMINE, H., SAITO, M., SHIMODA-MATSUBAYASHI, S., TANAKA, H., ISHIKAWA, A., NAKAGAWA-HATTORI, Y., YOKOCHI, M., KOBAYASHI, T., IGARASHI, S., TAKANO, H., SANPEI, K., KOIKE, R., MORI, H., KONDO, T., MIZUTANI, Y., SCHAFFER, A. A., YAMAMURA, Y., NAKAMURA, S., KUZUHARA, S., TSUJI, S. & MIZUNO, Y. 1997. Localization of a gene for an autosomal recessive form of juvenile Parkinsonism to chromosome 6q25.2-27. *Am J Hum Genet,* 60**,** 588-96.

MCNAUGHT, K. S., OLANOW, C. W., HALLIWELL, B., ISACSON, O. & JENNER, P. 2001. Failure of the ubiquitin-proteasome system in Parkinson's disease. *Nat Rev Neurosci,* 2**,** 589-94.

MEIJER, A. J. & CODOGNO, P. 2006. Signalling and autophagy regulation in health, aging and disease. *Mol Aspects Med,* 27**,** 411-25.

MILBRANDT, J. 1986. Nerve growth factor rapidly induces c-fos mRNA in PC12 rat pheochromocytoma cells. *Proceedings of the National Academy of Sciences of the United States of America,* 83**,** 4789-93.

MILLER, K. E. & SHEETZ, M. P. 2004. Axonal mitochondrial transport and potential are correlated. *J Cell Sci,* 117**,** 2791-804.

MILTON, V. J., JARRETT, H. E., GOWERS, K., CHALAK, S., BRIGGS, L., ROBINSON, I. M. & SWEENEY, S. T. 2011. Oxidative stress induces overgrowth of the Drosophila neuromuscular junction. *Proceedings of the National Academy of Sciences of the United States of America,* 108**,** 17521-6.

MISSALE, C., NASH, S. R., ROBINSON, S. W., JABER, M. & CARON, M. G. 1998. Dopamine receptors: from structure to function. *Physiol Rev,* 78**,** 189-225.

MONICK, M. M., POWERS, L. S., GROSS, T. J., FLAHERTY, D. M., BARRETT, C. W. & HUNNINGHAKE, G. W. 2006. Active ERK contributes to protein translation by preventing JNK-dependent inhibition of protein phosphatase 1. *J Immunol,* 177**,** 1636-45.

MORGAN, J. I., COHEN, D. R., HEMPSTEAD, J. L. & CURRAN, T. 1987. Mapping patterns of c-fos expression in the central nervous system after seizure. *Science,* 237**,** 192-7.

MORRISON, D. K. & DAVIS, R. J. 2003. Regulation of MAP kinase signaling modules by scaffold proteins in mammals. *Annu Rev Cell Dev Biol,* 19**,** 91-118.

MORRISON, E., THOMPSON, J., WILLIAMSON, S. J., CHEETHAM, M. E. & ROBINSON, P. A. 2011. A simple cell based assay to measure Parkin activity. *Journal of neurochemistry,* 116**,** 342-9.

MORTIBOYS, H., THOMAS, K. J., KOOPMAN, W. J., KLAFFKE, S., ABOU-SLEIMAN, P., OLPIN, S., WOOD, N. W., WILLEMS, P. H., SMEITINK, J. A., COOKSON, M. R. & BANDMANN, O. 2008. Mitochondrial function and morphology are impaired in parkin-mutant fibroblasts. *Ann Neurol,* 64**,** 555-65.

MULLER, S., BERGER, M., LEHEMBRE, F., SEELER, J. S., HAUPT, Y. & DEJEAN, A. 2000. c-Jun and p53 activity is modulated by SUMO-1 modification. *The Journal of biological chemistry,* 275**,** 13321-9.

MURPHY, L. O. & BLENIS, J. 2006. MAPK signal specificity: the right place at the right time. *Trends Biochem Sci,* 31**,** 268-75.

MURPHY, L. O., MACKEIGAN, J. P. & BLENIS, J. 2004. A network of immediate early gene products propagates subtle differences in mitogen-activated protein kinase signal amplitude and duration. *Mol Cell Biol,* 24**,** 144-53.

MURPHY, L. O., SMITH, S., CHEN, R. H., FINGAR, D. C. & BLENIS, J. 2002. Molecular interpretation of ERK signal duration by immediate early gene products. *Nature cell biology,* 4**,** 556-64.

MUSTI, A. M., TREIER, M. & BOHMANN, D. 1997. Reduced ubiquitin-dependent degradation of c-Jun after phosphorylation by MAP kinases. *Science,* 275**,** 400-2.

NARENDRA, D., KANE, L. A., HAUSER, D. N., FEARNLEY, I. M. & YOULE, R. J. 2010a. p62/SQSTM1 is required for Parkin-induced mitochondrial clustering but not mitophagy; VDAC1 is dispensable for both. *Autophagy,* 6**,** 1090-106.

NARENDRA, D., TANAKA, A., SUEN, D. F. & YOULE, R. J. 2008. Parkin is recruited selectively to impaired mitochondria and promotes their autophagy. *The Journal of cell biology,* 183**,** 795-803.

NARENDRA, D. P., JIN, S. M., TANAKA, A., SUEN, D. F., GAUTIER, C. A., SHEN, J., COOKSON, M. R. & YOULE, R. J. 2010b. PINK1 is selectively stabilized on impaired mitochondria to activate Parkin. *PLoS biology,* 8**,** e1000298.

NARHI, L., WOOD, S. J., STEAVENSON, S., JIANG, Y., WU, G. M., ANAFI, D., KAUFMAN, S. A., MARTIN, F., SITNEY, K., DENIS, P., LOUIS, J. C., WYPYCH, J., BIERE, A. L. & CITRON, M. 1999. Both familial Parkinson's disease mutations accelerate alpha-synuclein aggregation. *J Biol Chem,* 274**,** 9843-6.

NATERI, A. S., RIERA-SANS, L., DA COSTA, C. & BEHRENS, A. 2004. The ubiquitin ligase SCFFbw7 antagonizes apoptotic JNK signaling. *Science,* 303**,** 1374-8.

NEDELSKY, N. B., TODD, P. K. & TAYLOR, J. P. 2008. Autophagy and the ubiquitin-proteasome system: collaborators in neuroprotection. *Biochimica et biophysica acta,* 1782**,** 691-9.

NESTLER, E. J., BARROT, M. & SELF, D. W. 2001. DeltaFosB: a sustained molecular switch for addiction. *Proc Natl Acad Sci U S A,* 98**,** 11042-6.

NEVE, K. A., SEAMANS, J. K. & TRANTHAM-DAVIDSON, H. 2004. Dopamine receptor signaling. *J Recept Signal Transduct Res,* 24**,** 165-205.

NEWHOUSE, K., HSUAN, S. L., CHANG, S. H., CAI, B., WANG, Y. & XIA, Z. 2004. Rotenone-induced apoptosis is mediated by p38 and JNK MAP kinases in human dopaminergic SH-SY5Y cells. *Toxicological sciences : an official journal of the Society of Toxicology,* 79**,** 137-46.

O'SHEA, E. K., RUTKOWSKI, R. & KIM, P. S. 1992. Mechanism of specificity in the Fos-Jun oncoprotein heterodimer. *Cell,* 68**,** 699-708.

OHORI, M., TAKEUCHI, M., MARUKI, R., NAKAJIMA, H. & MIYAKE, H. 2007. FR180204, a novel and selective inhibitor of extracellular signal-regulated kinase, ameliorates collagen-induced arthritis in mice. *Naunyn Schmiedebergs Arch Pharmacol,* 374**,** 311-6.

OKATSU, K., OKA, T., IGUCHI, M., IMAMURA, K., KOSAKO, H., TANI, N., KIMURA, M., GO, E., KOYANO, F., FUNAYAMA, M., SHIBA-FUKUSHIMA, K., SATO, S., SHIMIZU, H., FUKUNAGA, Y., TANIGUCHI, H., KOMATSU, M., HATTORI, N., MIHARA, K., TANAKA, K. & MATSUDA, N. 2012. PINK1 autophosphorylation upon membrane potential dissipation is essential for Parkin recruitment to damaged mitochondria. *Nat Commun,* 3**,** 1016.

OKATSU, K., SAISHO, K., SHIMANUKI, M., NAKADA, K., SHITARA, H., SOU, Y. S., KIMURA, M., SATO, S., HATTORI, N., KOMATSU, M., TANAKA, K. & MATSUDA, N. 2010. p62/SQSTM1 cooperates with Parkin for perinuclear clustering of depolarized mitochondria. *Genes Cells,* 15**,** 887-900.

OKUNO, H. 2011. Regulation and function of immediate-early genes in the brain: beyond neuronal activity markers. *Neuroscience research,* 69**,** 175-86.

OLANOW, C. W. & SCHAPIRA, A. H. 2013. Therapeutic prospects for Parkinson disease. *Ann Neurol,* 74**,** 337-47.

OLZMANN, J. A., LI, L., CHUDAEV, M. V., CHEN, J., PEREZ, F. A., PALMITER, R. D. & CHIN, L. S. 2007. Parkin-mediated K63-linked polyubiquitination targets misfolded DJ-1 to aggresomes via binding to HDAC6. *J Cell Biol,* 178**,** 1025-38.

OTT, A., BRETELER, M. M., VAN HARSKAMP, F., CLAUS, J. J., VAN DER CAMMEN, T. J., GROBBEE, D. E. & HOFMAN, A. 1995. Prevalence of Alzheimer's disease

and vascular dementia: association with education. The Rotterdam study. *BMJ,* 310**,** 970-3.

OVERLY, C. C., RIEFF, H. I. & HOLLENBECK, P. J. 1996. Organelle motility and metabolism in axons vs dendrites of cultured hippocampal neurons. *J Cell Sci,* 109 (Pt 5)**,** 971-80.

OYARCE, A. M. & FLEMING, P. J. 1991. Multiple forms of human dopamine beta-hydroxylase in SH-SY5Y neuroblastoma cells. *Archives of biochemistry and biophysics,* 290**,** 503-10.

PACELLI, C., GIGUERE, N., BOURQUE, M. J., LEVESQUE, M., SLACK, R. S. & TRUDEAU, L. E. 2015. Elevated Mitochondrial Bioenergetics and Axonal Arborization Size Are Key Contributors to the Vulnerability of Dopamine Neurons. *Curr Biol*.

PAHLMAN, S., RUUSALA, A. I., ABRAHAMSSON, L., MATTSSON, M. E. & ESSCHER, T. 1984. Retinoic acid-induced differentiation of cultured human neuroblastoma cells: a comparison with phorbolester-induced differentiation. *Cell differentiation,* 14**,** 135-44.

PAISAN-RUIZ, C., BHATIA, K. P., LI, A., HERNANDEZ, D., DAVIS, M., WOOD, N. W., HARDY, J., HOULDEN, H., SINGLETON, A. & SCHNEIDER, S. A. 2009. Characterization of PLA2G6 as a locus for dystonia-parkinsonism. *Ann Neurol,* 65**,** 19-23.

PAISAN-RUIZ, C., JAIN, S., EVANS, E. W., GILKS, W. P., SIMON, J., VAN DER BRUG, M., LOPEZ DE MUNAIN, A., APARICIO, S., GIL, A. M., KHAN, N., JOHNSON, J., MARTINEZ, J. R., NICHOLL, D., CARRERA, I. M., PENA, A. S., DE SILVA, R., LEES, A., MARTI-MASSO, J. F., PEREZ-TUR, J., WOOD, N. W. & SINGLETON, A. B. 2004. Cloning of the gene containing mutations that cause PARK8-linked Parkinson's disease. *Neuron,* 44**,** 595-600.

PAN, J., LI, H., MA, J. F., TAN, Y. Y., XIAO, Q., DING, J. Q. & CHEN, S. D. 2012. Curcumin inhibition of JNKs prevents dopaminergic neuronal loss in a mouse model of Parkinson's disease through suppressing mitochondria dysfunction. *Transl Neurodegener,* 1**,** 16.

PAN, J., XIAO, Q., SHENG, C. Y., HONG, Z., YANG, H. Q., WANG, G., DING, J. Q. & CHEN, S. D. 2009. Blockade of the translocation and activation of c-Jun N-terminal kinase 3 (JNK3) attenuates dopaminergic neuronal damage in mouse model of Parkinson's disease. *Neurochemistry international,* 54**,** 418-25.

PANKIV, S., CLAUSEN, T. H., LAMARK, T., BRECH, A., BRUUN, J. A., OUTZEN, H., OVERVATN, A., BJORKOY, G. & JOHANSEN, T. 2007. p62/SQSTM1 binds directly to Atg8/LC3 to facilitate degradation of ubiquitinated protein aggregates by autophagy. *J Biol Chem,* 282**,** 24131-45.

PANKRATZ, N., NICHOLS, W. C., UNIACKE, S. K., HALTER, C., RUDOLPH, A., SHULTS, C., CONNEALLY, P. M., FOROUD, T. & PARKINSON STUDY, G. 2002. Genome screen to identify susceptibility genes for Parkinson disease in a sample without parkin mutations. *Am J Hum Genet,* 71**,** 124-35.

PANKRATZ, N., NICHOLS, W. C., UNIACKE, S. K., HALTER, C., RUDOLPH, A., SHULTS, C., CONNEALLY, P. M., FOROUD, T. & PARKINSON STUDY, G. 2003. Significant linkage of Parkinson disease to chromosome 2q36-37. *Am J Hum Genet,* 72**,** 1053-7.

PAPADIA, S., SORIANO, F. X., LEVEILLE, F., MARTEL, M. A., DAKIN, K. A., HANSEN, H. H., KAINDL, A., SIFRINGER, M., FOWLER, J., STEFOVSKA, V., MCKENZIE, G., CRAIGON, M., CORRIVEAU, R., GHAZAL, P., HORSBURGH, K., YANKNER, B.

A., WYLLIE, D. J., IKONOMIDOU, C. & HARDINGHAM, G. E. 2008. Synaptic NMDA receptor activity boosts intrinsic antioxidant defenses. *Nat Neurosci,* 11**,** 476-87.

PARK, J., LEE, S. B., LEE, S., KIM, Y., SONG, S., KIM, S., BAE, E., KIM, J., SHONG, M., KIM, J. M. & CHUNG, J. 2006. Mitochondrial dysfunction in Drosophila PINK1 mutants is complemented by parkin. *Nature,* 441**,** 1157-61.

PARK, K. H., SHIN, K. S., ZHAO, T. T., PARK, H. J., LEE, K. E. & LEE, M. K. 2016. L-DOPA modulates cell viability through the ERK-c-Jun system in PC12 and dopaminergic neuronal cells. *Neuropharmacology,* 101**,** 87-97.

PARKINSON, J. 1817. *An Essay on the Shaking Palsy*, Whittingham and Rowland.

PARKINSON STUDY GROUP, P. I. 2007. Mixed lineage kinase inhibitor CEP-1347 fails to delay disability in early Parkinson disease. *Neurology,* 69**,** 1480-90.

PAUMELLE, R., TULASNE, D., LEROY, C., COLL, J., VANDENBUNDER, B. & FAFEUR, V. 2000. Sequential activation of ERK and repression of JNK by scatter factor/hepatocyte growth factor in madin-darby canine kidney epithelial cells. *Mol Biol Cell,* 11**,** 3751-63.

PAVON, N., MARTIN, A. B., MENDIALDUA, A. & MORATALLA, R. 2006. ERK phosphorylation and FosB expression are associated with L-DOPA-induced dyskinesia in hemiparkinsonian mice. *Biol Psychiatry,* 59**,** 64-74.

PENG, J. & ANDERSEN, J. K. 2003. The role of c-Jun N-terminal kinase (JNK) in Parkinson's disease. *IUBMB life,* 55**,** 267-71.

PENNINGTON, K., PENG, J., HUNG, C. C., BANKS, R. E. & ROBINSON, P. A. 2010. Differential effects of wild-type and A53T mutant isoform of alpha-synuclein on the mitochondrial proteome of differentiated SH-SY5Y cells. *Journal of proteome research,* 9**,** 2390-401.

PERIER, C., BOVE, J., WU, D. C., DEHAY, B., CHOI, D. K., JACKSON-LEWIS, V., RATHKE-HARTLIEB, S., BOUILLET, P., STRASSER, A., SCHULZ, J. B., PRZEDBORSKI, S. & VILA, M. 2007. Two molecular pathways initiate mitochondria-dependent dopaminergic neurodegeneration in experimental Parkinson's disease. *Proc Natl Acad Sci U S A,* 104**,** 8161-6.

PFAFFL, M. W. 2001. A new mathematical model for relative quantification in real-time RT-PCR. *Nucleic Acids Res,* 29**,** e45.

POLYMEROPOULOS, M. H., HIGGINS, J. J., GOLBE, L. I., JOHNSON, W. G., IDE, S. E., DI IORIO, G., SANGES, G., STENROOS, E. S., PHO, L. T., SCHAFFER, A. A., LAZZARINI, A. M., NUSSBAUM, R. L. & DUVOISIN, R. C. 1996. Mapping of a gene for Parkinson's disease to chromosome 4q21-q23. *Science,* 274**,** 1197-9.

POLYMEROPOULOS, M. H., LAVEDAN, C., LEROY, E., IDE, S. E., DEHEJIA, A., DUTRA, A., PIKE, B., ROOT, H., RUBENSTEIN, J., BOYER, R., STENROOS, E. S., CHANDRASEKHARAPPA, S., ATHANASSIADOU, A., PAPAPETROPOULOS, T., JOHNSON, W. G., LAZZARINI, A. M., DUVOISIN, R. C., DI IORIO, G., GOLBE, L. I. & NUSSBAUM, R. L. 1997. Mutation in the alpha-synuclein gene identified in families with Parkinson's disease. *Science,* 276**,** 2045-7.

PRESGRAVES, S. P., AHMED, T., BORWEGE, S. & JOYCE, J. N. 2004a. Terminally differentiated SH-SY5Y cells provide a model system for studying neuroprotective effects of dopamine agonists. *Neurotoxicity research,* 5**,** 579-98.

PRESGRAVES, S. P., BORWEGE, S., MILLAN, M. J. & JOYCE, J. N. 2004b. Involvement of dopamine D(2)/D(3) receptors and BDNF in the neuroprotective effects

of S32504 and pramipexole against 1-methyl-4-phenylpyridinium in terminally differentiated SH-SY5Y cells. *Experimental neurology,* 190**,** 157-70.

PUTCHA, G. V., MOULDER, K. L., GOLDEN, J. P., BOUILLET, P., ADAMS, J. A., STRASSER, A. & JOHNSON, E. M. 2001. Induction of BIM, a proapoptotic BH3-only BCL-2 family member, is critical for neuronal apoptosis. *Neuron,* 29**,** 615-28.

PYAKUREL, A., SAVOIA, C., HESS, D. & SCORRANO, L. 2015. Extracellular regulated kinase phosphorylates mitofusin 1 to control mitochondrial morphology and apoptosis. *Mol Cell,* 58**,** 244-54.

RAFFAELLO, A., MILAN, G., MASIERO, E., CARNIO, S., LEE, D., LANFRANCHI, G., GOLDBERG, A. L. & SANDRI, M. 2010. JunB transcription factor maintains skeletal muscle mass and promotes hypertrophy. *The Journal of cell biology,* 191**,** 101-13.

RAMANAN, V. K. & SAYKIN, A. J. 2013. Pathways to neurodegeneration: mechanistic insights from GWAS in Alzheimer's disease, Parkinson's disease, and related disorders. *Am J Neurodegener Dis,* 2**,** 145-75.

RAMIREZ, A., HEIMBACH, A., GRUNDEMANN, J., STILLER, B., HAMPSHIRE, D., CID, L. P., GOEBEL, I., MUBAIDIN, A. F., WRIEKAT, A. L., ROEPER, J., AL-DIN, A., HILLMER, A. M., KARSAK, M., LISS, B., WOODS, C. G., BEHRENS, M. I. & KUBISCH, C. 2006. Hereditary parkinsonism with dementia is caused by mutations in ATP13A2, encoding a lysosomal type 5 P-type ATPase. *Nat Genet,* 38**,** 1184-91.

RAN, F. A., HSU, P. D., WRIGHT, J., AGARWALA, V., SCOTT, D. A. & ZHANG, F. 2013. Genome engineering using the CRISPR-Cas9 system. *Nat Protoc,* 8**,** 2281-308.

RAVID, T. & HOCHSTRASSER, M. 2008. Diversity of degradation signals in the ubiquitin-proteasome system. *Nat Rev Mol Cell Biol,* 9**,** 679-90.

RCSB. *Two human c-Fos:c-Jun:DNA complexes* [Online]. http://www.rcsb.org/. Available: http://www.rcsb.org/pdb/explore.do?structureId=1fos [Accessed 2015].

REDDY, C. E., ALBANITO, L., DE MARCO, P., AIELLO, D., MAGGIOLINI, M., NAPOLI, A. & MUSTI, A. M. 2013. Multisite phosphorylation of c-Jun at threonine 91/93/95 triggers the onset of c-Jun pro-apoptotic activity in cerebellar granule neurons. *Cell Death Dis,* 4**,** e852.

REICH, N., MAURER, B., AKHMETSHINA, A., VENALIS, P., DEES, C., ZERR, P., PALUMBO, K., ZWERINA, J., NEVSKAYA, T., GAY, S., DISTLER, O., SCHETT, G. & DISTLER, J. H. 2010. The transcription factor Fra-2 regulates the production of extracellular matrix in systemic sclerosis. *Arthritis Rheum,* 62**,** 280-90.

REN, Y., JIANG, H., YANG, F., NAKASO, K. & FENG, J. 2009. Parkin protects dopaminergic neurons against microtubule-depolymerizing toxins by attenuating microtubule-associated protein kinase activation. *J Biol Chem,* 284**,** 4009-17.

RENAULT, T. T., FLOROS, K. V., ELKHOLI, R., CORRIGAN, K. A., KUSHNAREVA, Y., WIEDER, S. Y., LINDTNER, C., SERASINGHE, M. N., ASCIOLLA, J. J., BUETTNER, C., NEWMEYER, D. D. & CHIPUK, J. E. 2015. Mitochondrial shape governs BAX-induced membrane permeabilization and apoptosis. *Mol Cell,* 57**,** 69-82.

RESNICK, L. & FENNELL, M. 2004. Targeting JNK3 for the treatment of neurodegenerative disorders. *Drug discovery today,* 9**,** 932-9.

REYNAUD, E. 2010. Protein Misfolding and Degenrative Diseases. *Nature Education,* 3**,** 28.

ROGAEVA, E., JOHNSON, J., LANG, A. E., GULICK, C., GWINN-HARDY, K., KAWARAI, T., SATO, C., MORGAN, A., WERNER, J., NUSSBAUM, R., PETIT, A., OKUN, M. S., MCINERNEY, A., MANDEL, R., GROEN, J. L., FERNANDEZ, H. H., POSTUMA, R., FOOTE, K. D., SALEHI-RAD, S., LIANG, Y., REIMSNIDER, S., TANDON, A., HARDY, J., ST GEORGE-HYSLOP, P. & SINGLETON, A. B. 2004. Analysis of the PINK1 gene in a large cohort of cases with Parkinson disease. *Arch Neurol,* 61**,** 1898-904.

ROPER, K. 2012.

ROPER, K. 2015. *RE: Discussion of HEK293 Parkin expressing cell lines.*

ROSE, J. M., NOVOSELOV, S. S., ROBINSON, P. A. & CHEETHAM, M. E. 2011. Molecular chaperone-mediated rescue of mitophagy by a Parkin RING1 domain mutant. *Hum Mol Genet,* 20**,** 16-27.

ROSS, C. A. & TABRIZI, S. J. 2011. Huntington's disease: from molecular pathogenesis to clinical treatment. *Lancet Neurol,* 10**,** 83-98.

ROUX, P., BLANCHARD, J. M., FERNANDEZ, A., LAMB, N., JEANTEUR, P. & PIECHACZYK, M. 1990. Nuclear localization of c-Fos, but not v-Fos proteins, is controlled by extracellular signals. *Cell,* 63**,** 341-51.

ROWE, R. K., SUSZKO, J. W. & PEKOSZ, A. 2008. Roles for the recycling endosome, Rab8, and Rab11 in hantavirus release from epithelial cells. *Virology,* 382**,** 239-49.

RUBINSZTEIN, D. C. 2006. The roles of intracellular protein-degradation pathways in neurodegeneration. *Nature,* 443**,** 780-6.

RYSECK, R. P. & BRAVO, R. 1991. c-JUN, JUN B, and JUN D differ in their binding affinities to AP-1 and CRE consensus sequences: effect of FOS proteins. *Oncogene,* 6**,** 533-42.

RYTER, S. W., KIM, H. P., HOETZEL, A., PARK, J. W., NAKAHIRA, K., WANG, X. & CHOI, A. M. 2007. Mechanisms of cell death in oxidative stress. *Antioxid Redox Signal,* 9**,** 49-89.

SAEKI, Y., KUDO, T., SONE, T., KIKUCHI, Y., YOKOSAWA, H., TOH-E, A. & TANAKA, K. 2009. Lysine 63-linked polyubiquitin chain may serve as a targeting signal for the 26S proteasome. *EMBO J,* 28**,** 359-71.

SAFADI, S. S. & SHAW, G. S. 2007. A disease state mutation unfolds the parkin ubiquitin-like domain. *Biochemistry,* 46**,** 14162-9.

SASAKI, T., KOJIMA, H., KISHIMOTO, R., IKEDA, A., KUNIMOTO, H. & NAKAJIMA, K. 2006. Spatiotemporal regulation of c-Fos by ERK5 and the E3 ubiquitin ligase UBR1, and its biological role. *Molecular cell,* 24**,** 63-75.

SCARFFE, L. A., STEVENS, D. A., DAWSON, V. L. & DAWSON, T. M. 2014. Parkin and PINK1: much more than mitophagy. *Trends Neurosci,* 37**,** 315-24.

SCHMIDT, F., CHAMPY, P., SEON-MENIEL, B., FRANCK, X., RAISMAN-VOZARI, R. & FIGADERE, B. 2009. Chemicals possessing a neurotrophin-like activity on dopaminergic neurons in primary culture. *PLoS One,* 4**,** e6215.

SCHNEIDER, L., GIORDANO, S., ZELICKSON, B. R., M, S. J., G, A. B., OUYANG, X., FINEBERG, N., DARLEY-USMAR, V. M. & ZHANG, J. 2011. Differentiation of SH-SY5Y cells to a neuronal phenotype changes cellular bioenergetics and

the response to oxidative stress. *Free radical biology & medicine,* 51**,** 2007-17.

SCHRECK, I., AL-RAWI, M., MINGOT, J. M., SCHOLL, C., DIEFENBACHER, M. E., O'DONNELL, P., BOHMANN, D. & WEISS, C. 2011. c-Jun localizes to the nucleus independent of its phosphorylation by and interaction with JNK and vice versa promotes nuclear accumulation of JNK. *Biochemical and biophysical research communications,* 407**,** 735-40.

SCHWARZ, C. S., SEYFRIED, J., EVERT, B. O., KLOCKGETHER, T. & WULLNER, U. 2002. Bcl-2 up-regulates ha-ras mRNA expression and induces c-Jun phosphorylation at Ser73 via an ERK-dependent pathway in PC 12 cells. *Neuroreport,* 13**,** 2439-42.

SCLIP, A., TOZZI, A., ABAZA, A., CARDINETTI, D., COLOMBO, I., CALABRESI, P., SALMONA, M., WELKER, E. & BORSELLO, T. 2014. c-Jun N-terminal kinase has a key role in Alzheimer disease synaptic dysfunction in vivo. *Cell Death Dis,* 5**,** e1019.

SCOTT, R. C., JUHASZ, G. & NEUFELD, T. P. 2007. Direct induction of autophagy by Atg1 inhibits cell growth and induces apoptotic cell death. *Curr Biol,* 17**,** 1-11.

SEABRA, M. C. & WASMEIER, C. 2004. Controlling the location and activation of Rab GTPases. *Curr Opin Cell Biol,* 16**,** 451-7.

SELKOE, D., DETTMER, U., LUTH, E., KIM, N., NEWMAN, A. & BARTELS, T. 2014. Defining the native state of alpha-synuclein. *Neurodegener Dis,* 13**,** 114-7.

SELKOE, D. J. 2004. Cell biology of protein misfolding: the examples of Alzheimer's and Parkinson's diseases. *Nature cell biology,* 6**,** 1054-61.

SENBA, E. & UEYAMA, T. 1997. Stress-induced expression of immediate early genes in the brain and peripheral organs of the rat. *Neuroscience research,* 29**,** 183-207.

SHAID, S., BRANDTS, C. H., SERVE, H. & DIKIC, I. 2013. Ubiquitination and selective autophagy. *Cell Death Differ,* 20**,** 21-30.

SHANG, H., LIU, G., JIANG, Y., FU, J., ZHANG, B., SONG, R. & WANG, W. 2015. Pathway analysis of two amyotrophic lateral sclerosis GWAS highlights shared genetic signals with Alzheimer's disease and Parkinson's disease. *Mol Neurobiol,* 51**,** 361-9.

SHAULIAN, E. & KARIN, M. 2001. AP-1 in cell proliferation and survival. *Oncogene,* 20**,** 2390-400.

SHEN, H. M. & LIU, Z. G. 2006. JNK signaling pathway is a key modulator in cell death mediated by reactive oxygen and nitrogen species. *Free Radic Biol Med,* 40**,** 928-39.

SHENG, M. & GREENBERG, M. E. 1990. The regulation and function of c-fos and other immediate early genes in the nervous system. *Neuron,* 4**,** 477-85.

SHERER, T. B., BETARBET, R., TESTA, C. M., SEO, B. B., RICHARDSON, J. R., KIM, J. H., MILLER, G. W., YAGI, T., MATSUNO-YAGI, A. & GREENAMYRE, J. T. 2003. Mechanism of toxicity in rotenone models of Parkinson's disease. *The Journal of neuroscience : the official journal of the Society for Neuroscience,* 23**,** 10756-64.

SHI, J., FUNG, G., DENG, H., ZHANG, J., FIESEL, F. C., SPRINGER, W., LI, X. & LUO, H. 2015. NBR1 is dispensable for PARK2-mediated mitophagy regardless of the presence or absence of SQSTM1. *Cell Death Dis,* 6**,** e1943.

SHIBA-FUKUSHIMA, K., IMAI, Y., YOSHIDA, S., ISHIHAMA, Y., KANAO, T., SATO, S. & HATTORI, N. 2012. PINK1-mediated phosphorylation of the Parkin ubiquitin-like domain primes mitochondrial translocation of Parkin and regulates mitophagy. *Sci Rep,* 2**,** 1002.

SHIH, A. Y., JOHNSON, D. A., WONG, G., KRAFT, A. D., JIANG, L., ERB, H., JOHNSON, J. A. & MURPHY, T. H. 2003. Coordinate regulation of glutathione biosynthesis and release by Nrf2-expressing glia potently protects neurons from oxidative stress. *J Neurosci,* 23**,** 3394-406.

SHIN, S., BUEL, G. R., WOLGAMOTT, L., PLAS, D. R., ASARA, J. M., BLENIS, J. & YOON, S. O. 2015. ERK2 Mediates Metabolic Stress Response to Regulate Cell Fate. *Mol Cell,* 59**,** 382-98.

SHOJAEE, S., SINA, F., BANIHOSSEINI, S. S., KAZEMI, M. H., KALHOR, R., SHAHIDI, G. A., FAKHRAI-RAD, H., RONAGHI, M. & ELAHI, E. 2008. Genome-wide linkage analysis of a Parkinsonian-pyramidal syndrome pedigree by 500 K SNP arrays. *Am J Hum Genet,* 82**,** 1375-84.

SHULTS, C. W., OAKES, D., KIEBURTZ, K., BEAL, M. F., HAAS, R., PLUMB, S., JUNCOS, J. L., NUTT, J., SHOULSON, I., CARTER, J., KOMPOLITI, K., PERLMUTTER, J. S., REICH, S., STERN, M., WATTS, R. L., KURLAN, R., MOLHO, E., HARRISON, M., LEW, M. & PARKINSON STUDY, G. 2002. Effects of coenzyme Q10 in early Parkinson disease: evidence of slowing of the functional decline. *Arch Neurol,* 59**,** 1541-50.

SIMON-SANCHEZ, J. & SINGLETON, A. B. 2008. Sequencing analysis of OMI/HTRA2 shows previously reported pathogenic mutations in neurologically normal controls. *Hum Mol Genet,* 17**,** 1988-93.

SINA, F., SHOJAEE, S., ELAHI, E. & PAISAN-RUIZ, C. 2009. R632W mutation in PLA2G6 segregates with dystonia-parkinsonism in a consanguineous Iranian family. *Eur J Neurol,* 16**,** 101-4.

SINGLETON, A. B., FARRER, M., JOHNSON, J., SINGLETON, A., HAGUE, S., KACHERGUS, J., HULIHAN, M., PEURALINNA, T., DUTRA, A., NUSSBAUM, R., LINCOLN, S., CRAWLEY, A., HANSON, M., MARAGANORE, D., ADLER, C., COOKSON, M. R., MUENTER, M., BAPTISTA, M., MILLER, D., BLANCATO, J., HARDY, J. & GWINN-HARDY, K. 2003. alpha-Synuclein locus triplication causes Parkinson's disease. *Science,* 302**,** 841.

SOLESIO, M. E., SAEZ-ATIENZAR, S., JORDAN, J. & GALINDO, M. F. 2012. Characterization of mitophagy in the 6-hydoxydopamine Parkinson's disease model. *Toxicological sciences : an official journal of the Society of Toxicology,* 129**,** 411-20.

SPILLANTINI, M. G. 1999. Parkinson's disease, dementia with Lewy bodies and multiple system atrophy are alpha-synucleinopathies. *Parkinsonism Relat Disord,* 5**,** 157-62.

STEFANI, A., LOZANO, A. M., PEPPE, A., STANZIONE, P., GALATI, S., TROPEPI, D., PIERANTOZZI, M., BRUSA, L., SCARNATI, E. & MAZZONE, P. 2007. Bilateral deep brain stimulation of the pedunculopontine and subthalamic nuclei in severe Parkinson's disease. *Brain,* 130**,** 1596-607.

STRAPPAZZON, F., NAZIO, F., CORRADO, M., CIANFANELLI, V., ROMAGNOLI, A., FIMIA, G. M., CAMPELLO, S., NARDACCI, R., PIACENTINI, M., CAMPANELLA, M. & CECCONI, F. 2015. AMBRA1 is able to induce mitophagy via LC3 binding, regardless of PARKIN and p62/SQSTM1. *Cell death and differentiation,* 22**,** 517.

STRAUSS, K. M., MARTINS, L. M., PLUN-FAVREAU, H., MARX, F. P., KAUTZMANN, S., BERG, D., GASSER, T., WSZOLEK, Z., MULLER, T., BORNEMANN, A., WOLBURG, H., DOWNWARD, J., RIESS, O., SCHULZ, J. B. & KRUGER, R. 2005. Loss of function mutations in the gene encoding Omi/HtrA2 in Parkinson's disease. *Hum Mol Genet,* 14**,** 2099-111.

STRECK, E. L., CZAPSKI, G. A. & GONCALVES DA SILVA, C. 2013. Neurodegeneration, mitochondrial dysfunction, and oxidative stress. *Oxidative medicine and cellular longevity,* 2013**,** 826046.

SULZER, D. 2007. Multiple hit hypotheses for dopamine neuron loss in Parkinson's disease. *Trends Neurosci,* 30**,** 244-50.

SUN, X., LIU, J., CRARY, J. F., MALAGELADA, C., SULZER, D., GREENE, L. A. & LEVY, O. A. 2013. ATF4 protects against neuronal death in cellular Parkinson's disease models by maintaining levels of parkin. *The Journal of neuroscience : the official journal of the Society for Neuroscience,* 33**,** 2398-407.

SVEC, D., TICHOPAD, A., NOVOSADOVA, V., PFAFFL, M. W. & KUBISTA, M. 2015. How good is a PCR efficiency estimate: Recommendations for precise and robust qPCR efficiency assessments. *Biomol Detect Quantif,* 3**,** 9-16.

TAKAHASHI, T., DENG, Y., MARUYAMA, W., DOSTERT, P., KAWAI, M. & NAOI, M. 1994. Uptake of a neurotoxin-candidate, (R)-1,2-dimethyl-6,7-dihydroxy-1,2,3,4-tetrahydroisoquinoline into human dopaminergic neuroblastoma SH-SY5Y cells by dopamine transport system. *Journal of neural transmission. General section,* 98**,** 107-18.

TALOTTA, F., MEGA, T., BOSSIS, G., CASALINO, L., BASBOUS, J., JARIEL-ENCONTRE, I., PIECHACZYK, M. & VERDE, P. 2010. Heterodimerization with Fra-1 cooperates with the ERK pathway to stabilize c-Jun in response to the RAS oncoprotein. *Oncogene,* 29**,** 4732-40.

TAN, J. M., WONG, E. S., KIRKPATRICK, D. S., PLETNIKOVA, O., KO, H. S., TAY, S. P., HO, M. W., TRONCOSO, J., GYGI, S. P., LEE, M. K., DAWSON, V. L., DAWSON, T. M. & LIM, K. L. 2008. Lysine 63-linked ubiquitination promotes the formation and autophagic clearance of protein inclusions associated with neurodegenerative diseases. *Hum Mol Genet,* 17**,** 431-9.

TANAKA, A., CLELAND, M. M., XU, S., NARENDRA, D. P., SUEN, D. F., KARBOWSKI, M. & YOULE, R. J. 2010. Proteasome and p97 mediate mitophagy and degradation of mitofusins induced by Parkin. *The Journal of cell biology,* 191**,** 1367-80.

TANIK, S. A., SCHULTHEISS, C. E., VOLPICELLI-DALEY, L. A., BRUNDEN, K. R. & LEE, V. M. 2013. Lewy body-like alpha-synuclein aggregates resist degradation and impair macroautophagy. *J Biol Chem,* 288**,** 15194-210.

TANOS, T., MARINISSEN, M. J., LESKOW, F. C., HOCHBAUM, D., MARTINETTO, H., GUTKIND, J. S. & COSO, O. A. 2005. Phosphorylation of c-Fos by members of the p38 MAPK family. Role in the AP-1 response to UV light. *The Journal of biological chemistry,* 280**,** 18842-52.

TERASAWA, K., OKAZAKI, K. & NISHIDA, E. 2003. Regulation of c-Fos and Fra-1 by the MEK5-ERK5 pathway. *Genes Cells,* 8**,** 263-73.

TERRENI, L., CALABRESE, E., CALELLA, A. M., FORLONI, G. & MARIANI, C. 2001. New mutation (R42P) of the parkin gene in the ubiquitinlike domain associated with parkinsonism. *Neurology,* 56**,** 463-6.

THOMAS, B. & BEAL, M. F. 2007. Parkinson's disease. *Human molecular genetics,* 16 Spec No. 2**,** R183-94.

TOONE, W. M. & JONES, N. 1999. AP-1 transcription factors in yeast. *Current opinion in genetics & development,* 9**,** 55-61.

TUCCI, A., NALLS, M. A., HOULDEN, H., REVESZ, T., SINGLETON, A. B., WOOD, N. W., HARDY, J. & PAISAN-RUIZ, C. 2010. Genetic variability at the PARK16 locus. *Eur J Hum Genet,* 18**,** 1356-9.

TWIG, G. & SHIRIHAI, O. S. 2011. The interplay between mitochondrial dynamics and mitophagy. *Antioxid Redox Signal,* 14**,** 1939-51.

UM, J. W., IM, E., LEE, H. J., MIN, B., YOO, L., YOO, J., LUBBERT, H., STICHEL-GUNKEL, C., CHO, H. S., YOON, J. B. & CHUNG, K. C. 2010. Parkin directly modulates 26S proteasome activity. *The Journal of neuroscience : the official journal of the Society for Neuroscience,* 30**,** 11805-14.

VALENTE, E. M., ABOU-SLEIMAN, P. M., CAPUTO, V., MUQIT, M. M., HARVEY, K., GISPERT, S., ALI, Z., DEL TURCO, D., BENTIVOGLIO, A. R., HEALY, D. G., ALBANESE, A., NUSSBAUM, R., GONZALEZ-MALDONADO, R., DELLER, T., SALVI, S., CORTELLI, P., GILKS, W. P., LATCHMAN, D. S., HARVEY, R. J., DALLAPICCOLA, B., AUBURGER, G. & WOOD, N. W. 2004. Hereditary early-onset Parkinson's disease caused by mutations in PINK1. *Science,* 304**,** 1158-60.

VALENTE, E. M., BRANCATI, F., FERRARIS, A., GRAHAM, E. A., DAVIS, M. B., BRETELER, M. M., GASSER, T., BONIFATI, V., BENTIVOGLIO, A. R., DE MICHELE, G., DURR, A., CORTELLI, P., WASSILOWSKY, D., HARHANGI, B. S., RAWAL, N., CAPUTO, V., FILLA, A., MECO, G., OOSTRA, B. A., BRICE, A., ALBANESE, A., DALLAPICCOLA, B., WOOD, N. W. & EUROPEAN CONSORTIUM ON GENETIC SUSCEPTIBILITY IN PARKINSON'S, D. 2002. PARK6-linked parkinsonism occurs in several European families. *Ann Neurol,* 51**,** 14-8.

VALLONE, D., PICETTI, R. & BORRELLI, E. 2000. Structure and function of dopamine receptors. *Neurosci Biobehav Rev,* 24**,** 125-32.

VAN BROECKHOVEN, C., HAAN, J., BAKKER, E., HARDY, J. A., VAN HUL, W., WEHNERT, A., VEGTER-VAN DER VLIS, M. & ROOS, R. A. 1990. Amyloid beta protein precursor gene and hereditary cerebral hemorrhage with amyloidosis (Dutch). *Science,* 248**,** 1120-2.

VAN DUIJN, C. M., DEKKER, M. C., BONIFATI, V., GALJAARD, R. J., HOUWING-DUISTERMAAT, J. J., SNIJDERS, P. J., TESTERS, L., BREEDVELD, G. J., HORSTINK, M., SANDKUIJL, L. A., VAN SWIETEN, J. C., OOSTRA, B. A. & HEUTINK, P. 2001. Park7, a novel locus for autosomal recessive early-onset parkinsonism, on chromosome 1p36. *Am J Hum Genet,* 69**,** 629-34.

VAN HUMBEECK, C., CORNELISSEN, T., HOFKENS, H., MANDEMAKERS, W., GEVAERT, K., DE STROOPER, B. & VANDENBERGHE, W. 2011. Parkin interacts with Ambra1 to induce mitophagy. *J Neurosci,* 31**,** 10249-61.

VAUX, D. L. 2002. Apoptosis timeline. *Cell Death Differ,* 9**,** 349-54.

VAZ, M., MACHIREDDY, N., IRVING, A., POTTETI, H. R., CHEVALIER, K., KALVAKOLANU, D. & REDDY, S. P. 2012. Oxidant-induced cell death and Nrf2-dependent antioxidative response are controlled by Fra-1/AP-1. *Mol Cell Biol,* 32**,** 1694-709.

VEERIAH, S., TAYLOR, B. S., MENG, S., FANG, F., YILMAZ, E., VIVANCO, I., JANAKIRAMAN, M., SCHULTZ, N., HANRAHAN, A. J., PAO, W., LADANYI, M., SANDER, C., HEGUY, A., HOLLAND, E. C., PATY, P. B., MISCHEL, P. S., LIAU, L., CLOUGHESY, T. F., MELLINGHOFF, I. K., SOLIT, D. B. & CHAN, T. A. 2010.

Somatic mutations of the Parkinson's disease-associated gene PARK2 in glioblastoma and other human malignancies. *Nat Genet,* 42**,** 77-82.

VENTURA, J. J., COGSWELL, P., FLAVELL, R. A., BALDWIN, A. S., JR. & DAVIS, R. J. 2004. JNK potentiates TNF-stimulated necrosis by increasing the production of cytotoxic reactive oxygen species. *Genes Dev,* 18**,** 2905-15.

VIVES-BAUZA, C., ZHOU, C., HUANG, Y., CUI, M., DE VRIES, R. L., KIM, J., MAY, J., TOCILESCU, M. A., LIU, W., KO, H. S., MAGRANE, J., MOORE, D. J., DAWSON, V. L., GRAILHE, R., DAWSON, T. M., LI, C., TIEU, K. & PRZEDBORSKI, S. 2010. PINK1-dependent recruitment of Parkin to mitochondria in mitophagy. *Proceedings of the National Academy of Sciences of the United States of America,* 107**,** 378-83.

VOGT, C. 1842. *Untersuchungen uber die Entwicklungsgeschichte der Gerburtshelerkroete*, Jent und Gassman.

VRIZ, S., LEMAITRE, J. M., LEIBOVICI, M., THIERRY, N. & MECHALI, M. 1992. Comparative analysis of the intracellular localization of c-Myc, c-Fos, and replicative proteins during cell cycle progression. *Mol Cell Biol,* 12**,** 3548-55.

WAKABAYASHI, K., TANJI, K., MORI, F. & TAKAHASHI, H. 2007. The Lewy body in Parkinson's disease: molecules implicated in the formation and degradation of alpha-synuclein aggregates. *Neuropathology,* 27**,** 494-506.

WALLACE, D. C. 2005. A mitochondrial paradigm of metabolic and degenerative diseases, aging, and cancer: a dawn for evolutionary medicine. *Annu Rev Genet,* 39**,** 359-407.

WANG, M. C., BOHMANN, D. & JASPER, H. 2003. JNK signaling confers tolerance to oxidative stress and extends lifespan in Drosophila. *Dev Cell,* 5**,** 811-6.

WANG, X. & SCHWARZ, T. L. 2009. The mechanism of Ca2+ -dependent regulation of kinesin-mediated mitochondrial motility. *Cell,* 136**,** 163-74.

WANG, X., WINTER, D., ASHRAFI, G., SCHLEHE, J., WONG, Y. L., SELKOE, D., RICE, S., STEEN, J., LAVOIE, M. J. & SCHWARZ, T. L. 2011. PINK1 and Parkin target Miro for phosphorylation and degradation to arrest mitochondrial motility. *Cell,* 147**,** 893-906.

WATSON, A., EILERS, A., LALLEMAND, D., KYRIAKIS, J., RUBIN, L. L. & HAM, J. 1998. Phosphorylation of c-Jun is necessary for apoptosis induced by survival signal withdrawal in cerebellar granule neurons. *The Journal of neuroscience : the official journal of the Society for Neuroscience,* 18**,** 751-62.

WAUER, T. & KOMANDER, D. 2013. Structure of the human Parkin ligase domain in an autoinhibited state. *EMBO J,* 32**,** 2099-112.

WEI, Y., PATTINGRE, S., SINHA, S., BASSIK, M. & LEVINE, B. 2008. JNK1-mediated phosphorylation of Bcl-2 regulates starvation-induced autophagy. *Molecular cell,* 30**,** 678-88.

WEINREB, P. H., ZHEN, W., POON, A. W., CONWAY, K. A. & LANSBURY, P. T., JR. 1996. NACP, a protein implicated in Alzheimer's disease and learning, is natively unfolded. *Biochemistry,* 35**,** 13709-15.

WELCHMAN, R. L., GORDON, C. & MAYER, R. J. 2005. Ubiquitin and ubiquitin-like proteins as multifunctional signals. *Nat Rev Mol Cell Biol,* 6**,** 599-609.

WEST, R. J., LU, Y., MARIE, B., GAO, F. B. & SWEENEY, S. T. 2015. Rab8, POSH, and TAK1 regulate synaptic growth in a Drosophila model of frontotemporal dementia. *J Cell Biol,* 208**,** 931-47.

WHITFIELD, J., NEAME, S. J., PAQUET, L., BERNARD, O. & HAM, J. 2001. Dominant-negative c-Jun promotes neuronal survival by reducing BIM expression and inhibiting mitochondrial cytochrome c release. *Neuron,* 29**,** 629-43.

WHITMARSH, A. J., CAVANAGH, J., TOURNIER, C., YASUDA, J. & DAVIS, R. J. 1998. A mammalian scaffold complex that selectively mediates MAP kinase activation. *Science,* 281**,** 1671-4.

WHITWORTH, A. J., THEODORE, D. A., GREENE, J. C., BENES, H., WES, P. D. & PALLANCK, L. J. 2005. Increased glutathione S-transferase activity rescues dopaminergic neuron loss in a Drosophila model of Parkinson's disease. *Proc Natl Acad Sci U S A,* 102**,** 8024-9.

WIDER, C., SKIPPER, L., SOLIDA, A., BROWN, L., FARRER, M., DICKSON, D., WSZOLEK, Z. K. & VINGERHOETS, F. J. 2008. Autosomal dominant dopa-responsive parkinsonism in a multigenerational Swiss family. *Parkinsonism Relat Disord,* 14**,** 465-70.

WILHELM, M., XU, Z., KUKEKOV, N. V., GIRE, S. & GREENE, L. A. 2007. Proapoptotic Nix activates the JNK pathway by interacting with POSH and mediates death in a Parkinson disease model. *J Biol Chem,* 282**,** 1288-95.

WILTSHIRE, C., GILLESPIE, D. A. & MAY, G. H. 2004. Sab (SH3BP5), a novel mitochondria-localized JNK-interacting protein. *Biochem Soc Trans,* 32**,** 1075-7.

WIN, S., THAN, T. A., FERNANDEZ-CHECA, J. C. & KAPLOWITZ, N. 2014. JNK interaction with Sab mediates ER stress induced inhibition of mitochondrial respiration and cell death. *Cell Death Dis,* 5**,** e989.

WIN, S., THAN, T. A., LE, B. H., GARCIA-RUIZ, C., FERNANDEZ-CHECA, J. C. & KAPLOWITZ, N. 2015. Sab (Sh3bp5) dependence of JNK mediated inhibition of mitochondrial respiration in palmitic acid induced hepatocyte lipotoxicity. *J Hepatol,* 62**,** 1367-74.

WOOD-KACZMAR, A., GANDHI, S., YAO, Z., ABRAMOV, A. Y., MILJAN, E. A., KEEN, G., STANYER, L., HARGREAVES, I., KLUPSCH, K., DEAS, E., DOWNWARD, J., MANSFIELD, L., JAT, P., TAYLOR, J., HEALES, S., DUCHEN, M. R., LATCHMAN, D., TABRIZI, S. J. & WOOD, N. W. 2008. PINK1 is necessary for long term survival and mitochondrial function in human dopaminergic neurons. *PloS one,* 3**,** e2455.

WU, H., WANG, M. C. & BOHMANN, D. 2009. JNK protects Drosophila from oxidative stress by trancriptionally activating autophagy. *Mech Dev,* 126**,** 624-37.

http://www.parkinsons.org.uk/. *Parkinson's Symptoms* [Online]. Available: http://www.parkinsons.org.uk/ [Accessed].

XIE, H. R., HU, L. S. & LI, G. Y. 2010. SH-SY5Y human neuroblastoma cell line: in vitro cell model of dopaminergic neurons in Parkinson's disease. *Chinese medical journal,* 123**,** 1086-92.

XIE, X., GU, Y., FOX, T., COLL, J. T., FLEMING, M. A., MARKLAND, W., CARON, P. R., WILSON, K. P. & SU, M. S. 1998. Crystal structure of JNK3: a kinase implicated in neuronal apoptosis. *Structure,* 6**,** 983-91.

XIONG, H., WANG, D., CHEN, L., CHOO, Y. S., MA, H., TANG, C., XIA, K., JIANG, W., RONAI, Z., ZHUANG, X. & ZHANG, Z. 2009. Parkin, PINK1, and DJ-1 form a ubiquitin E3 ligase complex promoting unfolded protein degradation. *J Clin Invest,* 119**,** 650-60.

XU, M., MORATALLA, R., GOLD, L. H., HIROI, N., KOOB, G. F., GRAYBIEL, A. M. & TONEGAWA, S. 1994. Dopamine D1 receptor mutant mice are deficient in striatal expression of dynorphin and in dopamine-mediated behavioral responses. *Cell,* 79**,** 729-42.

XU, P., DAS, M., REILLY, J. & DAVIS, R. J. 2011. JNK regulates FoxO-dependent autophagy in neurons. *Genes & development,* 25**,** 310-22.

YAN, C., LEE, L. H. & DAVIS, L. I. 1998. Crm1p mediates regulated nuclear export of a yeast AP-1-like transcription factor. *The EMBO journal,* 17**,** 7416-29.

YANG, D. D., KUAN, C. Y., WHITMARSH, A. J., RINCON, M., ZHENG, T. S., DAVIS, R. J., RAKIC, P. & FLAVELL, R. A. 1997. Absence of excitotoxicity-induced apoptosis in the hippocampus of mice lacking the Jnk3 gene. *Nature,* 389**,** 865-70.

YANG, F., JIANG, Q., ZHAO, J., REN, Y., SUTTON, M. D. & FENG, J. 2005. Parkin stabilizes microtubules through strong binding mediated by three independent domains. *J Biol Chem,* 280**,** 17154-62.

YANG, H. J., WANG, L., XIA, Y. Y., CHANG, P. N. & FENG, Z. W. 2010. NF-kappaB mediates MPP+-induced apoptotic cell death in neuroblastoma cells SH-EP1 through JNK and c-Jun/AP-1. *Neurochem Int,* 56**,** 128-34.

YANG, S. H., SHARROCKS, A. D. & WHITMARSH, A. J. 2013. MAP kinase signalling cascades and transcriptional regulation. *Gene,* 513**,** 1-13.

YANG, Y., GEHRKE, S., IMAI, Y., HUANG, Z., OUYANG, Y., WANG, J. W., YANG, L., BEAL, M. F., VOGEL, H. & LU, B. 2006. Mitochondrial pathology and muscle and dopaminergic neuron degeneration caused by inactivation of Drosophila Pink1 is rescued by Parkin. *Proc Natl Acad Sci U S A,* 103**,** 10793-8.

YE, X., SUN, X., STAROVOYTOV, V. & CAI, Q. 2015. Parkin-Mediated Mitophagy in Mutant hAPP Neurons and Alzheimer's Disease Patient Brains. *Human molecular genetics*.

YOGEV, O., GOLDBERG, R., ANZI, S., YOGEV, O. & SHAULIAN, E. 2010. Jun proteins are starvation-regulated inhibitors of autophagy. *Cancer research,* 70**,** 2318-27.

YOULE, R. J. & NARENDRA, D. P. 2011. Mechanisms of mitophagy. *Nat Rev Mol Cell Biol,* 12**,** 9-14.

ZHANG, C., LEE, S., PENG, Y., BUNKER, E., GIAIME, E., SHEN, J., ZHOU, Z. & LIU, X. 2014a. PINK1 triggers autocatalytic activation of Parkin to specify cell fate decisions. *Curr Biol,* 24**,** 1854-65.

ZHANG, X. M., YIN, M. & ZHANG, M. H. 2014b. Cell-based assays for Parkinson's disease using differentiated human LUHMES cells. *Acta Pharmacol Sin,* 35**,** 945-56.

ZHU, J. H., GUO, F., SHELBURNE, J., WATKINS, S. & CHU, C. T. 2003. Localization of phosphorylated ERK/MAP kinases to mitochondria and autophagosomes in Lewy body diseases. *Brain pathology,* 13**,** 473-81.

ZHU, X., CASTELLANI, R. J., TAKEDA, A., NUNOMURA, A., ATWOOD, C. S., PERRY, G. & SMITH, M. A. 2001. Differential activation of neuronal ERK, JNK/SAPK and p38 in Alzheimer disease: the 'two hit' hypothesis. *Mech Ageing Dev,* 123**,** 39-46.

ZHU, X., LEE, H. G., PERRY, G. & SMITH, M. A. 2007. Alzheimer disease, the two-hit hypothesis: an update. *Biochim Biophys Acta,* 1772**,** 494-502.

ZIMPRICH, A., BENET-PAGES, A., STRUHAL, W., GRAF, E., ECK, S. H., OFFMAN, M. N., HAUBENBERGER, D., SPIELBERGER, S., SCHULTE, E. C., LICHTNER, P., ROSSLE, S. C., KLOPP, N., WOLF, E., SEPPI, K., PIRKER, W., PRESSLAUER, S., MOLLENHAUER, B., KATZENSCHLAGER, R., FOKI, T., HOTZY, C., REINTHALER, E., HARUTYUNYAN, A., KRALOVICS, R., PETERS, A., ZIMPRICH, F., BRUCKE, T., POEWE, W., AUFF, E., TRENKWALDER, C., ROST, B., RANSMAYR, G., WINKELMANN, J., MEITINGER, T. & STROM, T. M. 2011. A mutation in VPS35, encoding a subunit of the retromer complex, causes late-onset Parkinson disease. *Am J Hum Genet,* 89**,** 168-75.

ZIMPRICH, A., BISKUP, S., LEITNER, P., LICHTNER, P., FARRER, M., LINCOLN, S., KACHERGUS, J., HULIHAN, M., UITTI, R. J., CALNE, D. B., STOESSL, A. J., PFEIFFER, R. F., PATENGE, N., CARBAJAL, I. C., VIEREGGE, P., ASMUS, F., MULLER-MYHSOK, B., DICKSON, D. W., MEITINGER, T., STROM, T. M., WSZOLEK, Z. K. & GASSER, T. 2004a. Mutations in LRRK2 cause autosomal-dominant parkinsonism with pleomorphic pathology. *Neuron,* 44**,** 601-7.

ZIMPRICH, A., MULLER-MYHSOK, B., FARRER, M., LEITNER, P., SHARMA, M., HULIHAN, M., LOCKHART, P., STRONGOSKY, A., KACHERGUS, J., CALNE, D. B., STOESSL, J., UITTI, R. J., PFEIFFER, R. F., TRENKWALDER, C., HOMANN, N., OTT, E., WENZEL, K., ASMUS, F., HARDY, J., WSZOLEK, Z. & GASSER, T. 2004b. The PARK8 locus in autosomal dominant parkinsonism: confirmation of linkage and further delineation of the disease-containing interval. *Am J Hum Genet,* 74**,** 11-9.

ZIVIANI, E., TAO, R. N. & WHITWORTH, A. J. 2010. Drosophila parkin requires PINK1 for mitochondrial translocation and ubiquitinates mitofusin. *Proc Natl Acad Sci U S A,* 107**,** 5018-23.

APPENDICES

American Society for Cell Biology LICENSE TERMS AND CONDITIONS

Jun 03, 2016

This is a License Agreement between Thomas Ryan ("You") and American Society for Cell Biology ("American Society for Cell Biology") provided by Copyright Clearance Center ("CCC"). The license consists of your order details, the terms and conditions provided by American Society for Cell Biology, and the payment terms and conditions.

All payments must be made in full to CCC. For payment instructions, please see information listed at the bottom of this form.

License Number	3838160163395
License date	Mar 21, 2016
Licensed content publisher	American Society for Cell Biology
Licensed content title	MOLECULAR BIOLOGY OF THE CELL. ONLINE
Licensed content date	Dec 31, 1969
Type of Use	Thesis/Dissertation
Requestor type	Academic institution
Format	Print, Electronic
Portion	chart/graph/table/figure
Number of charts/graphs/tables/figures	1
Title or numeric reference of the portion(s)	Use of immunofluorescence images in figure 10. In results section of article.
Title of the article or chapter the portion is from	c-Fos activated phospholipid synthesis is required for neurite elongation in differentiating PC12 cells
Editor of portion(s)	n/a
Author of portion(s)	German A. Gil et al.
Volume of serial or monograph.	Vol. 15
Issue, if republishing an article from a serial	No. 4
Page range of the portion	1881-1894
Publication date of portion	April 2004
Rights for	Main product
Duration of use	Life of current and all future editions
Creation of copies for the disabled	no
With minor editing privileges	yes
For distribution to	U.K. and Commonwealth (excluding Canada)
In the following language(s)	Original language of publication
With incidental promotional use	no
The lifetime unit quantity of new product	Up to 499
Made available in the following markets	Education, e-thesis
Specified additional information	I request permission to use Figure 10 from Gil et al., 2004 in the introduction section of my PhD thesis.
The requesting person/organization is:	Thomas Ryan (PhD student - University of Leeds)
Order reference number	None
Author/Editor	Thomas Ryan
The standard identifier	PhD thesis
Title	Defining the early cellular response to mitochondrial stres: implications for Parkinson's
Publisher	University of Leeds
Expected publication date	Aug 2016
Estimated size (pages)	300
Total (may include CCC user fee)	0.00 USD

Appendix A: Copyright permission for Figure 1.6. Figure was adapted from Gil et al., 2004 and used in Chapter 1 of this thesis.

NATURE PUBLISHING GROUP LICENSE TERMS AND CONDITIONS

Jun 03, 2016

This is a License Agreement between Thomas Ryan ("You") and Nature Publishing Group ("Nature Publishing Group") provided by Copyright Clearance Center ("CCC"). The license consists of your order details, the terms and conditions provided by Nature Publishing Group, and the payment terms and conditions.

All payments must be made in full to CCC. For payment instructions, please see information listed at the bottom of this form.

License Number	3824251127120
License date	Mar 08, 2016
Licensed content publisher	Nature Publishing Group
Licensed content publication	Cell Death and Differentiation
Licensed content title	Parkin is transcriptionally regulated by ATF4: evidence for an interconnection between mitochondrial stress and ER stress
Licensed content author	L Bouman, A Schlierf, A K Lutz, J Shan, A Deinlein et al.
Licensed content date	Nov 26, 2010
Volume number	18
Issue number	5
Type of Use	reuse in a dissertation / thesis
Requestor type	academic/educational
Format	print and electronic
Portion	figures/tables/illustrations
Number of figures/tables/illustrations	1
High-res required	no
Figures	Figure 9
Author of this NPG article	no
Your reference number	None
Title of your thesis / dissertation	Defining the early cellular response to mitochondrial stress: implications for Parkinson's
Expected completion date	Aug 2016
Estimated size (number of pages)	280
Total	0.00 GBP

Appendix B: Copyright permission for Figure 1.14. Figure was adapted from Bouman et al., 2011 and used in Chapter 1 of this thesis.

siRNA SMARTpool	Target sequence	Dharmacon Gene ID	Catalogue number
JUN (c-JUN)	UGGAAACGACCUUCUAUGA	3725	M-003268-03-0005
	UAACGCAGCAGUUGCAAAC		
	GAGCGACCUUAUGGCUAC		
	AAGUCAUGAACCACGUUAA		
JUNB	GCAUCAAAGUGGAGCGCAA	3726	M-003269-01-0005
	UGGAAGACCAAGAGCGCAU		
	CAUACACAGCUACGGGAUA		
	CCAUCAACAUGGAAGACCA		
JUND	CGCUCAAGGACGAGCCACA	3627	M-003900-05-0005
	GAAACACCCUUCUACGGCG		
	CCGACGAGCUCACAGUUCC		
	CCGGCAGCAUGAUGAAGAA		
FOS (c-FOS)	GGGAUAGCCUCUCUUACUA	2352	M-003265-01-0005
	GAACAGUUAUCUCCAGAAG		
	GGAGACAGACCAACUAGAA		
	AGACCGAGCCCUUUGAUGA		
FOSB	GGAACGAAAUAAACUAGCA	2354	M-010086-03-0005
	GCUCAGCACCGGCUAAGGA		
	CCGGGAACGAAAUAAACUA		
	CGUGAGUGUGUGAGCGCUU		
FRA-1 (FOSL1)	GCUCAUCGCAAGAGUAGCA	8061	M-004341-04-0005
	GGACACAGGCAGUACCAGU		
	AGCGAGAGAUUGAGGAGCU		
	GCAGGCGGAGACUGACAAA		
FRA-2 (FOSL2)	GGCCCAGUGUGCAAGAUUA	2355	M-004110-00-0005
	GAAAUUCCGGGUAGAUAUG		
	GCUCACCGCAGAAGCAGUA		
	GCAGCUGUCUCCUGAAGAG		
PARK2 (PARKIN)	GGAGUGCAGUGCCGUAUUU	5071	M-003603-00-0005
	UCAAGGAGGUGGUUGCUAA		
	UUAAAGAGCUCCAUCACUU		
	GUAAAGAAGCGUACCAUGA		

Appendix C – Summary of siRNAs used in this thesis. All siRNAs were sourced from Dharmacon and used at a final concentration of 50nM for 48 hours prior to any experimental assay.

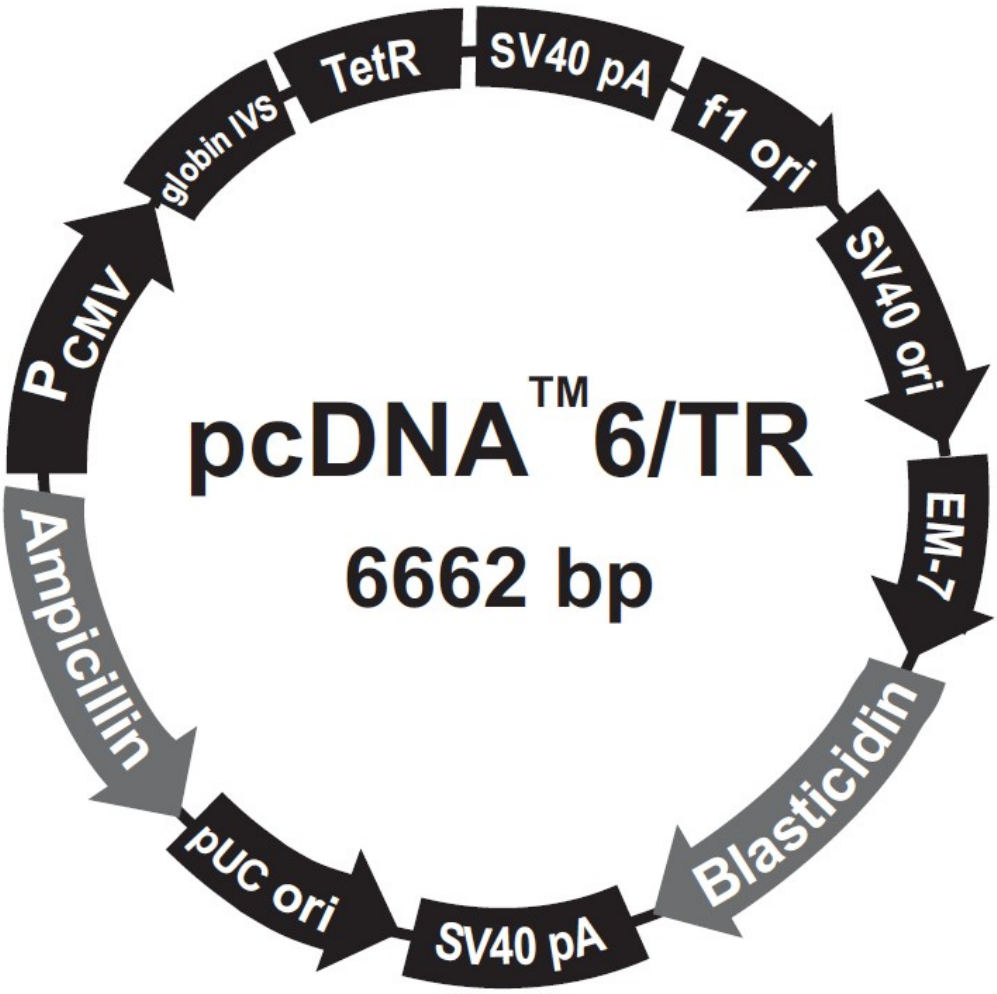

Appendix D: pcDNA6/TR vector containing the tetracycline repressor. The SH-TR host cell line was created by transfecting SH-SY5Y cells with a pcDNA6/TR vector purchased from Invitrogen using ExGen500 (Euromedex, France). These cells were kindly supplied by Dr. Buee (INSERM U422, IMPRT, Place de Verdun, France). This vector map was obtained from the Invitrogen website.

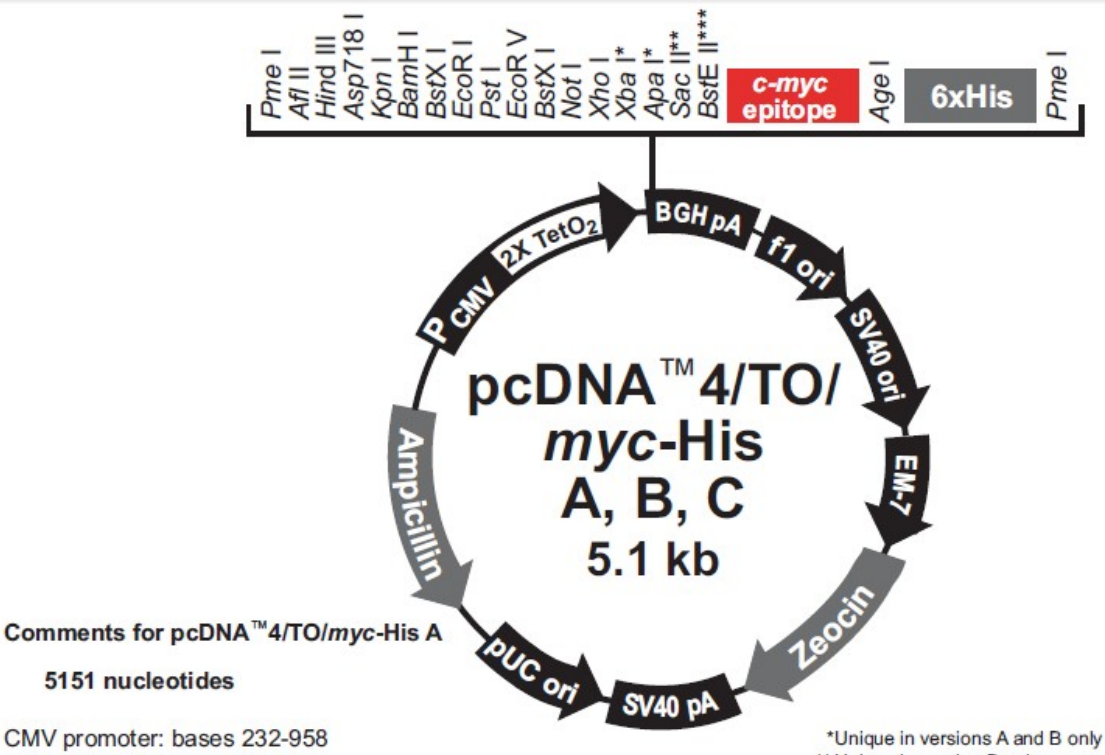

Comments for pcDNA™4/TO/*myc*-His A

5151 nucleotides

CMV promoter: bases 232-958
TATA box: bases 804-810
Tetracycline operator 2 (2X $TetO_2$) sequences: bases 820-859
CMV Forward priming site: bases 769-789
Multiple cloning site: bases 968-1069
c-myc epitope: bases 1073-1102
Polyhistidine (6xHis) tag: bases 1118-1135
BGH reverse priming site: bases 1158-1175
BGH polyadenylation sequence: bases 1164-1388
f1 origin: bases 1434-1862
SV40 promoter and origin: bases 1867-2211
EM-7 promoter: bases 2253-2319
Zeocin™ resistance gene: bases 2320-2694
SV40 early polyadenylation sequence: bases 2824-2954
pUC origin: bases 3337-4010 (complementary strand)
bla promoter: bases 5016-5114 (complementary strand)
Ampicillin (*bla*) resistance gene: bases 4155-5015 (complementary strand)

*Unique in versions A and B only
** Unique in version B only
***Unique in version C only

Appendix E: pcDNA™4/TO/*myc*-His A vector. This plasmid containing either WT or T240R Parkin cDNA was kindly supplied by Dr Phil Robinson. These were used to transfect SH-TR cells containing the pcDNA6/TR plasmid. This vector map was obtained from the Invitrogen website.

Find nuclei

- Channel = DAPI
- Method = B ('Common threshold' = 0.30 and 'Area' > 30μm^2
- Output population – Nuclei

Select population

- Population = Nuclei
- Method = Common Filters (remove border objects)
- Output population = Nuclei selected

Define Results

- Population: Nuclei selected
- Method = Standard Output (Nuclei – Nuclei selected) (Mean)

Appendix F: Columbus software algorithm for cell count analysis. Images captured using the Operetta microscope were analysed using these paarmeters in order to obtain accurate counts of cells from different treatment groups in Chapters 3, 4 and 5 of this thesis.

Find nuclei

- Channel = DAPI
- Method = C ('Common threshold' = 0.40 and 'Area' > 30μm^2
- Output population – Nuclei

Select population

- Population = Nuclei
- Method = Common Filters (remove border objects)
- Output population = Nuclei selected

Find cytoplasm

- Channel = DRAQ5
- Nuclei = Nuclei
- Method = D (Individual threshold = 0.15)

Calculate morphology properties

- Population = Nuclei
- Region = Cytoplasm
- Method = Standard (Area = μm^2)
- Output properties = Cytoplasm

Calculate morphology properties (2)

- Population = Nuclei
- Region = Cell
- Method = Standard (Area = μm^2)
- Output properties = Cell

Find spots

- Channel = Alexa 488
- Population = Nuclei
- Region = Cell
- Method = B ('Detection sensitivity' = 0.20, 'Splitting coefficient' = 0.500)
- Output population = Spots

Define results

- Method = Standard Output (Nuclei – Number of objects) (Object count)
  - Output name = Nuclei - Number of objects
- Method = Standard Output (Nuclei – Number of spots) (Mean)
  - Output name = Nuclei – Number of spots – Mean per well
- Method = Standard Output (Spots – Number of objects) (Object count)
  -Output name = Spots – Number of objects

Appendix G: Columbus software algorithm for calculating mitochondrial clustering. Images captured using the Operetta microscope were analysed using these paarmeters in order to obtain accurate counts of cells and mitochondrial 'spots' or 'clusters' from different treatment groups in Chapter 5 of this thesis. The average spots per cell for each individual well was then calculated.

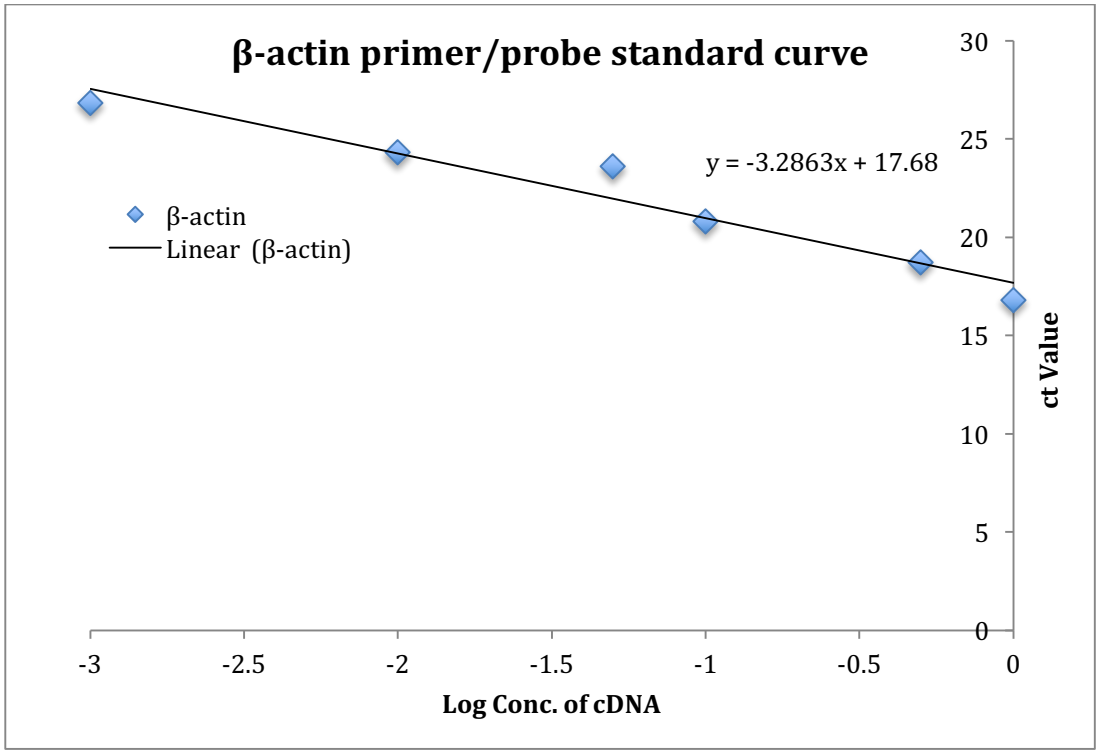

Appendix H: The amplification efficiency of the β-actin Taqman Gene Expression Assay primer/probe set. Each dilution of the template cDNA was performed in duplicate. Amplification efficiency was then calculated as described in the methods section of this thesis. This was performed for all genes assessed by qPCR.

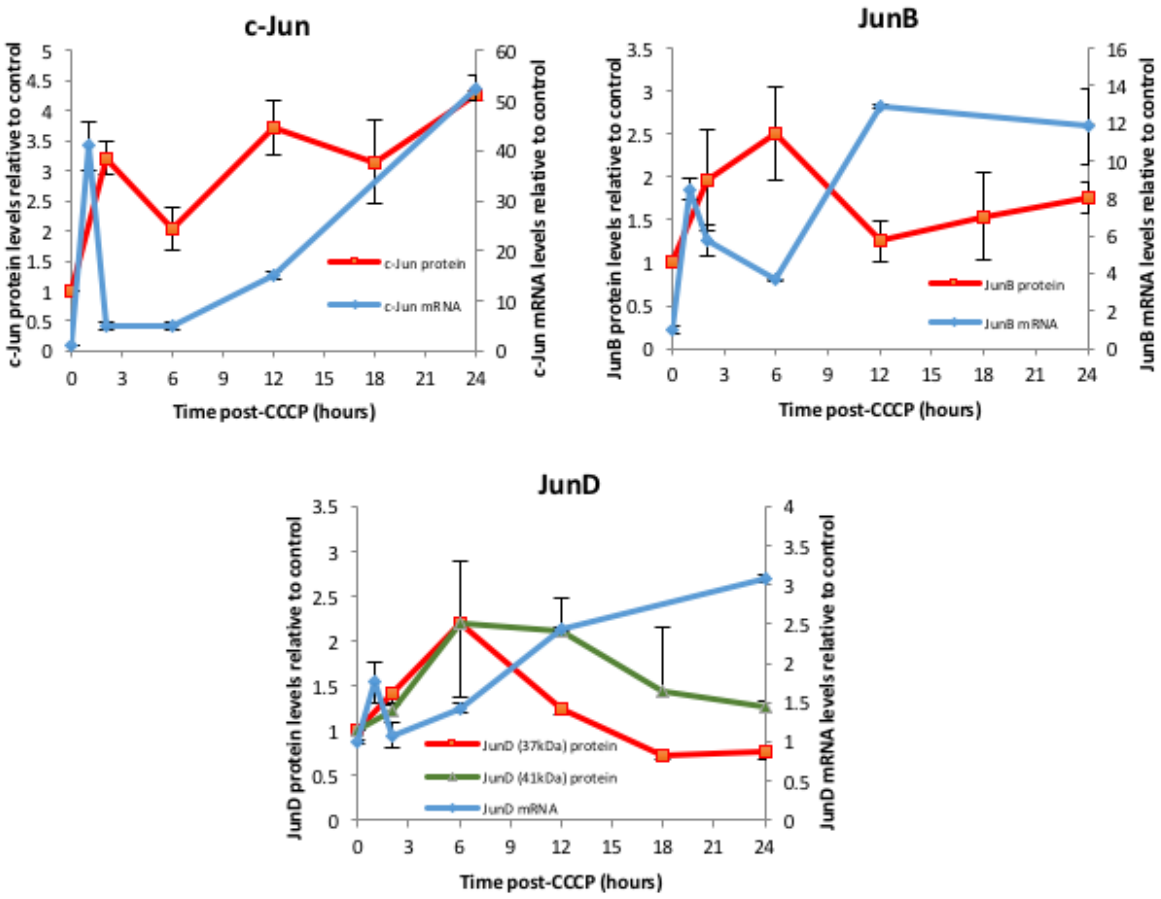

Appendix I: Combined mRNA and protein data for the Jun family transcription factors in response to 5μM CCCP. This is representative of data from undifferentiated WT SH-SY5Y cells. Protein levels are shown in red or green and mRNA levels shown in blue. Error bars represent SEM for protein and SD for mRNA. As two isoforms exist for JunD, negative SEM bars are used for the 37kDa isoform and positive SEM bars used for the 41kDa isoform.

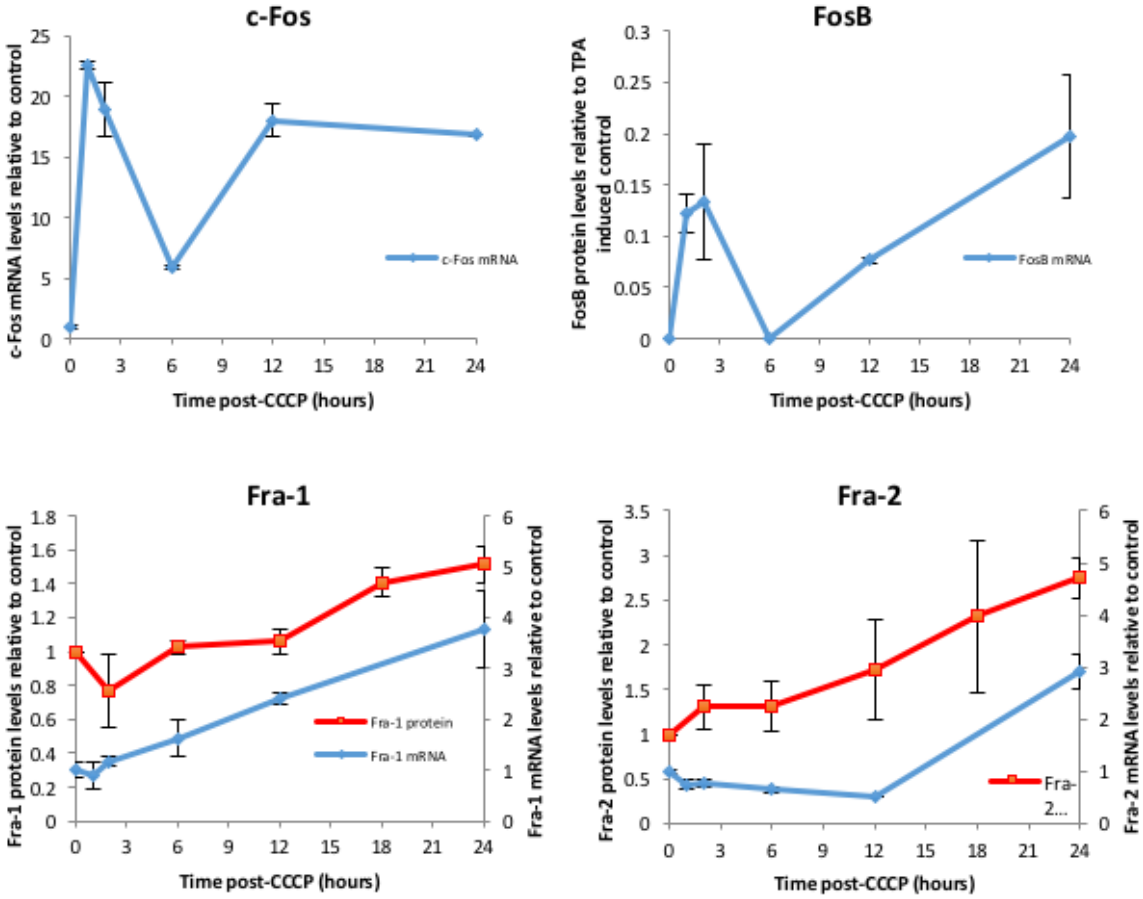

Appendix J: Combined mRNA and protein data for the Fos family transcription factors in response to 5μM CCCP. This is representative of data from undifferentiated WT SH-SY5Y cells. Protein levels are shown in red and mRNA levels shown in blue. Error bars represent SEM for protein and SD for mRNA. Protein levels were not detectable by western blotting for c-Fos and FosB, thus cannot be shown relative to the control upon mitochondrial uncoupling. Therefore, only mRNA expression is shown here.

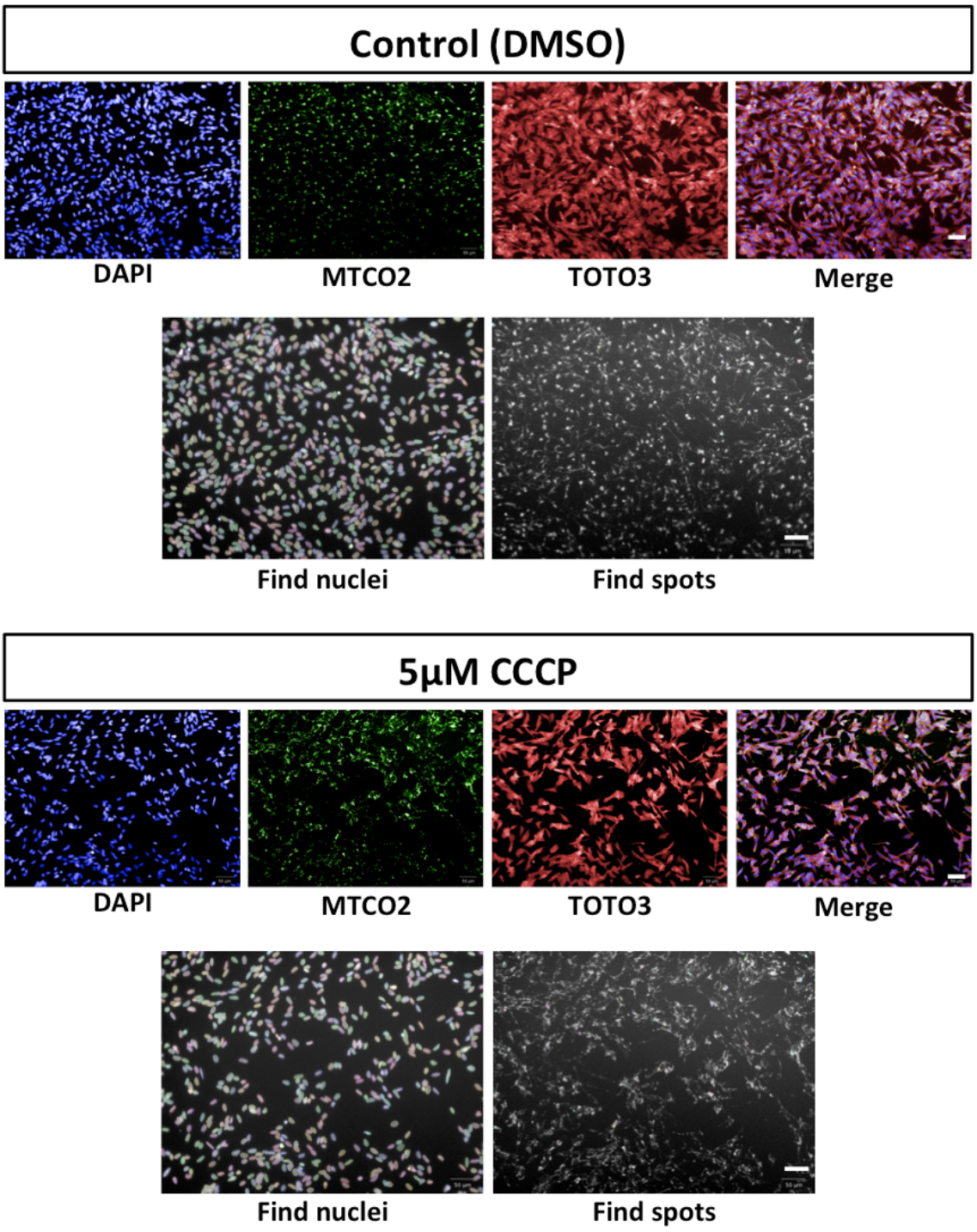

Appendix K: An example of Columbus software analysis of images captured using the Operetta system. Images were captured using the 20X lens. Columbus software calculated the number of mitochondrial spots (FITC channel) per nucleus (DAPI channel) for every well. Scale bar for both image sizes is 50µm.

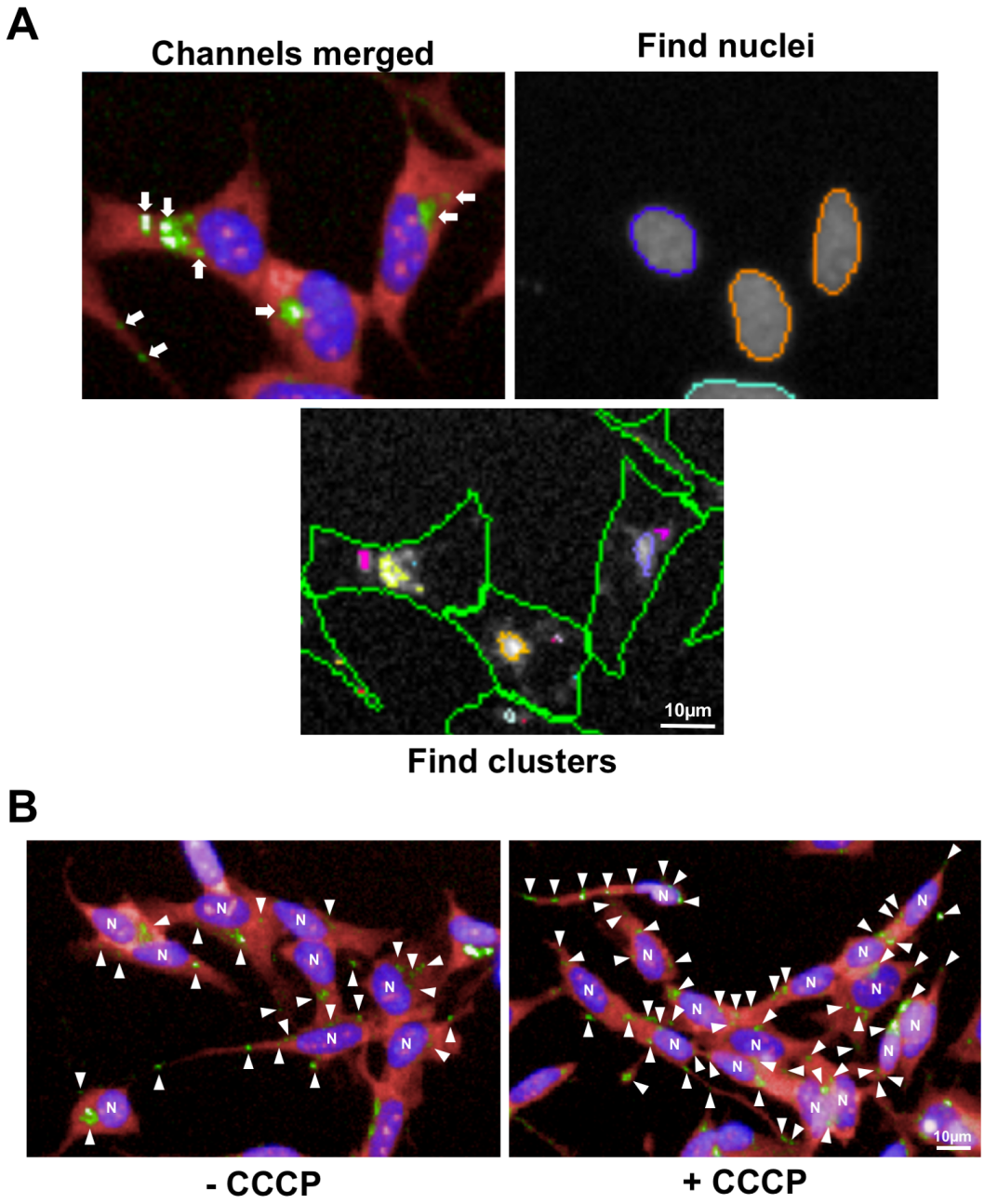

Appendix L: Mitochondrial clustering determined by eye and Columbus software. Pictures shown are enlarged from images captured at 20X magnification. (A) Columbus software separately analyses the DAPI and FITC/TOTO3 channels to count nuclei and determine clusters/cytoplasmic area, respectively. These are shown by different coloured lines around their edges. Arrows show an example of how mitochondrial clusters would be counted by eye. The sensitivity of Columbus allows for clusters to be counted that are not observed by eye through the merged image. (B) Example images of clustering. 'N' represents individual nuclei and arrowheads represent a single cluster counted. Only cells that are completely in view are counted. '– CCCP' (8 nuclei and 24 clusters = 3 clusters per cell) and '+ CCCP' (15 nuclei and 61 clusters = 4.1 clusters per cell) in differentiated SH-SY5Y cells.

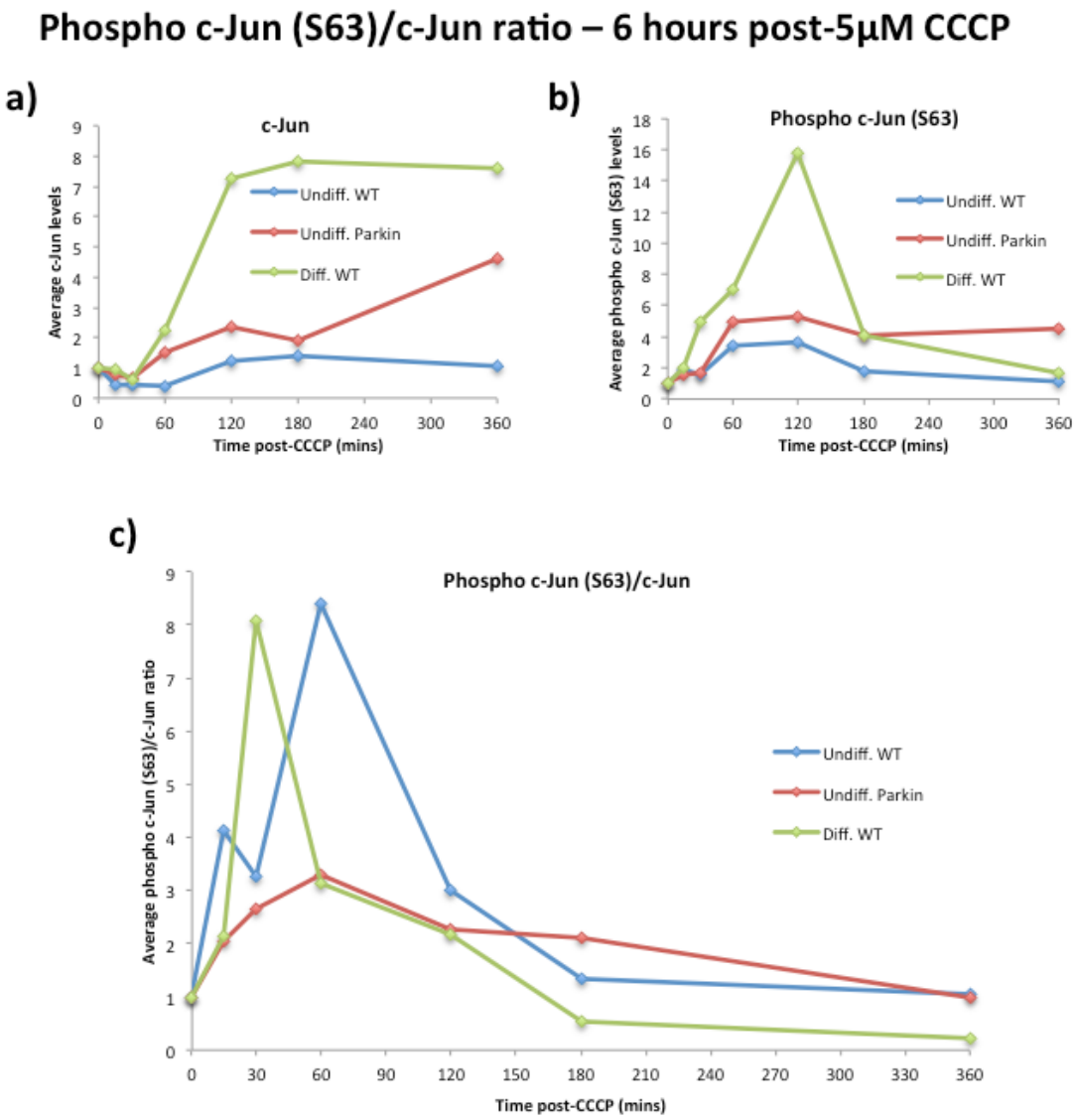

Appendix M: The modulation of c-Jun in SH-SY5Y cells over the first 6 hours of 5µM CCCP treatment. (a) The changes in total c-Jun protein levels. (b) The changes in c-Jun phosphorylation, (c) The phospho (S63)/total c-Jun ratio over the first 6 hours of CCCP exposure. Data obtained from western blot analysis initially shown in Chapters 4 and 5. Only average values are shown with no error bars in order to highlight the trend.

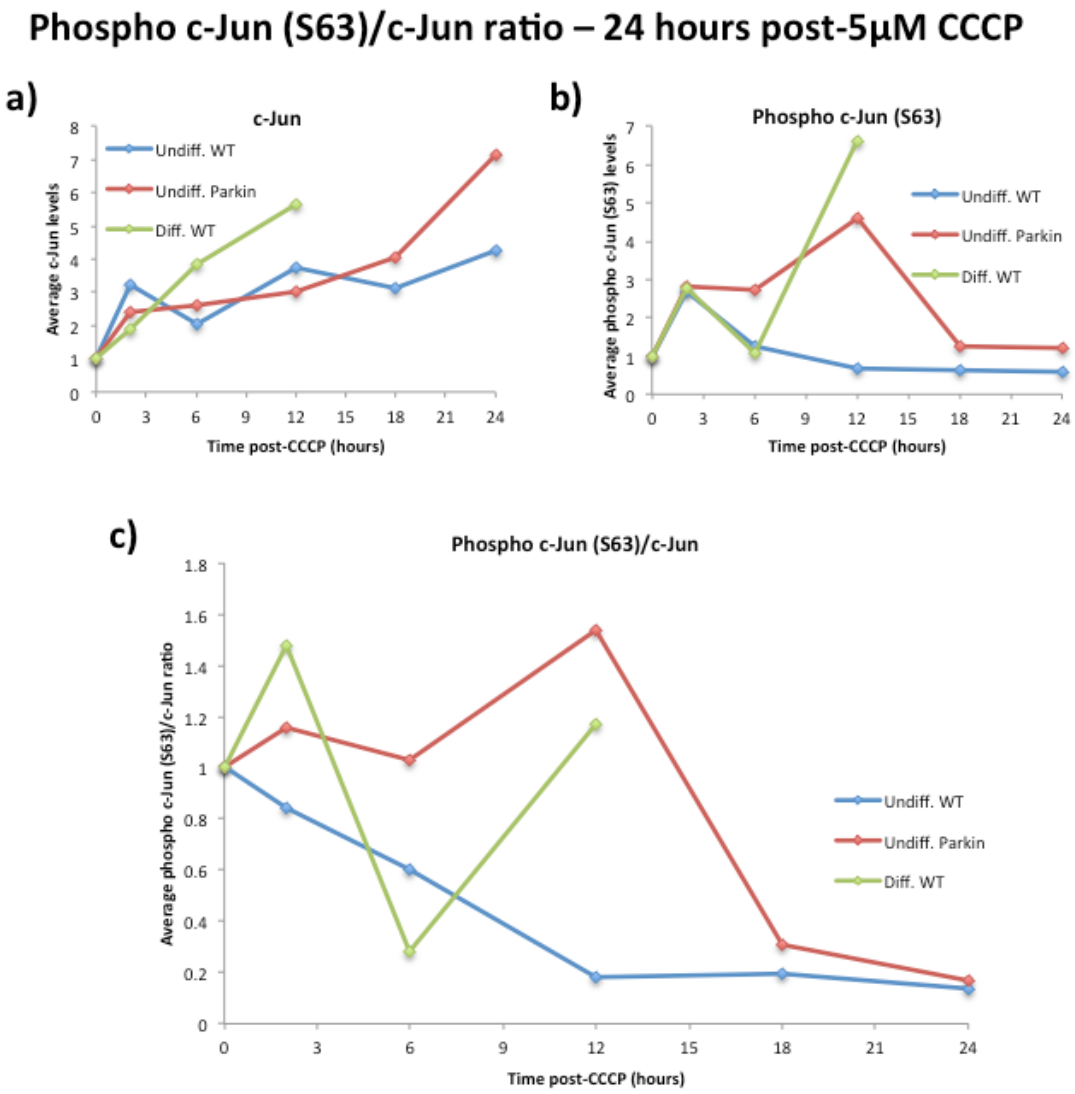

Appendix N: The modulation of c-Jun in SH-SY5Y cells over the 24 hours following 5µM CCCP treatment. (a) The changes in total c-Jun protein levels. (b) The changes in c-Jun phosphorylation, (c) The phospho (S63)/total c-Jun ratio over the first 24 hours of CCCP exposure. No extracts were analysed after the 12-hour time point for differentiated cells due to the high level of cell death induced by CCCP treatment. Data obtained from western blot analysis initially shown in Chapters 4 and 5. Only average values are shown with no error bars in order to highlight the trend.

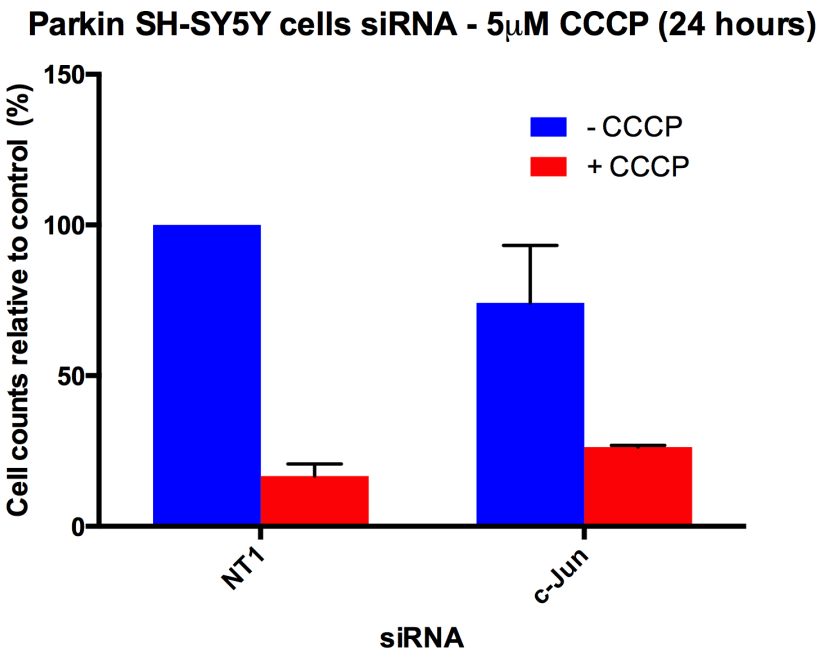

Appendix O: Knockdown of c-Jun in undifferentiated *PARKIN* overexpressing SH-SY5Y cells prior to mitochondrial uncoupling. Knockdown of c-Jun was performed in 96 well plates for 48 hours before treatment with 5μM CCCP (or DMSO) for 24 hours (n = 2). Cells were then fixed and stained with DAPI and images captured using the Operetta microscope. Images were analysed and cell counts obtained using Columbus software.